The Brain-Specific Alternatively Spliced Isoforms of Adapter Protein SH2B1 Regulate Energy Balance and Neuronal Morphology and Function

by

Jessica L. Cote

A dissertation submitted in partial fulfillment
of the requirements for the degree of
Doctor of Philosophy
(Neuroscience)
in the University of Michigan
2021

Doctoral Committee:

Professor Christin Carter-Su, Chair
Professor Roman J. Giger
Professor Martin G. Myers, Jr.
Professor Audrey F. Seasholtz
Professor Michael A. Sutton

Jessica Leigh Cote

cotejl@umich.edu

ORCID iD: 0000-0001-8967-2396

Acknowledgements

Countless people have supported me during my years as a graduate student. First and foremost, I would like to thank my mentor, Christy, who has been absolutely essential for my graduate career. Christy has taught me an immeasurable amount about how to design, carry out, and share high quality scientific research. Her wisdom regarding what constitutes good data and writing has been invaluable for my development as a scientist and communicator. Also, her love and enthusiasm for new data is contagious, and I hope to carry that with me as I embark on future endeavors. I am deeply grateful for the time and energy she poured into my training.

Thank you also to the other members of my thesis committee—Martin, Audrey, Roman, and Mike—who have offered invaluable feedback on my projects over the years. I am particularly grateful for Martin, who served as an unofficial secondary mentor for Chapter 2 of my dissertation. His insight and input were totally essential for the success of the project.

I would also like to thank members of the Carter-Su lab for their support and friendship. I am particularly grateful for Larry Argetsinger, Joel Cline, Ray Joe, and Anabel Flores who, especially during the early years, offered lots of guidance regarding protocols and experimental design. I owe a major thank you to Sarah Cain, who offered excellent administrative and tech support in the kindest manner. I also thank honorary lab member Amy Oakley, who, having started out as an afternoon walking buddy, has become a friend

and mentor. Thank you to these and other lab members who generated lots of laughter during stressful times.

I want to extend a special thank you to the students who worked with me for several years on my thesis projects: Paul Vander, Tahrim Choudhury, Seongbae Kong, Alex Bedard, and Lauren DeSantis. In addition to your scientific contributions, you all brought energy, motivation, and joy to the lab whenever we seemed to need it most. Thank you for taking a chance on me as your mentor. I am so proud of all of your accomplishments and look forward to seeing what the future holds for you.

I also want to thank members of the Yin/ Tong lab for their insight and conversation. Your feedback on my data and presentations was incredibly helpful. Lab meetings were somehow fun, especially before the pandemic. I will miss our discussions about science, travel, and good snacks.

I would like to acknowledge the Neuroscience Graduate Program and Program in Biomedical Sciences who made my time as a graduate student much smoother than it might have been otherwise. Thank you to Audrey, Ed, Rachel, and Valerie for lots of great advice, support, and conversations. Thank you to my NGP classmates for the comradery and fun times. Also, a major thank you to the classmates who organized many mentoring and outreach events with me.

Finally, I am extremely thankful for my wonderful friends and family who provided endless support and love from near and far during graduate school. To the original Ann Arbor crew, especially Veronica, Alyssa, Erin, Midhat, and Tracy, thank you for the game nights, climbing sessions, yoga hours, tennis mornings, and bar nights, and for making Ann Arbor feel like home. To Chrissy, thank you for the gym sessions, camping trips, and

general hilarity. To Olivia and Gaurav, thank you for the lovely dinners and walks. To the D&D crew, thank you for the fun and funny adventures. To Emily, thank you for the hours of thoughtful and inspiring conversation. To Maddie, Melissa, Steve, and Erik, thank you for the hilarious game nights. To Amanda and Moussa, thank you for everything—your smiles brightened so many of my days, especially during the bleak pandemic winter. To Nichola, Navneet, and Jess, I am so thankful for the visits, long phone calls, and continuous support. To Julia, I am forever grateful for our friendship and that you often seem to know me better than I know myself. To my boyfriend Parsa, thank you for your endless patience, love, and understanding. And of course, to my family, including my brother Chris, sister-in-law Hilary, and parents Dianne and Jim, thank you for your unending support during my long journey to get this degree.

Table of Contents

Acknowledgements ii

List of Figures vii

List of Tables x

Abstract xi

Chapter 1: Introduction 1

Monogenic Obesity 1

Adapter Protein SH2B1 8

SH2B family of adapter proteins 8

Alternatively spliced isoforms of SH2B1 8

SH2B1 variants and human obesity 15

Functions of SH2B1 isoforms—lessons from *in vivo* experiments 17

Functions of SH2B1 isoforms—lessons from *in vitro* experiments 21

Dissertation Summary 35

References 36

Chapter 2: Deletion of the Brain-Specific α and δ Isoforms of Adapter Protein SH2B1 Protect Mice from Obesity 45

Abstract 45

Introduction 47

Materials and Methods 49

Results 54

Discussion 81

Supplementary Material 86

Acknowledgements 108

References 111

Chapter 3: The Brain-Specific δ Isoform of SH2B1 Enhances the Morphological Complexity and Function of Cultured Neurons 115

Abstract 115

Introduction 117
Materials and Methods 121
Results 131
Discussion 158
Acknowledgements 167
Supplementary Materials 169
References 173
Chapter 4: Conclusions and Future Directions 179
Chapter Summary 179
Conclusions and Future Directions 180
How do SH2B1 isoforms regulate BDNF/TrkB activity in neurons? 180
What is the nucleolar function of SH2B1δ in neurons? 184
How do SH2B1 isoforms regulate neuronal synapses? 187
Do SH2B1 isoforms regulate other functions of primary hippocampal neurons? 192
Do SH2B1 isoforms regulate multiple neuron populations? 193
Do SH2B1 isoforms regulate activity of non-neuronal brain cells? 200
Do primary cultured neurons from other SH2B1 mouse models exhibit altered morphology and function? 205
Do physiological stressors and/or genetic mutations or variants regulate the SH2B1 isoform ratio? 207
Do external stimuli regulate the subcellular localization of SH2B1 isoforms? 209
Concluding Remarks 211
Acknowledgements 211
References 212

List of Figures

Figure 1.1. The leptin-melanocortin system 4

Figure 1.2. Four known SH2B1 isoforms 13

Figure 1.3. Alternative splicing of *SH2B1* 14

Figure 2.1. Generation and validation of αδKO mouse model. 57

Figure 2.2. Male αδKO mice fed standard chow exhibit reduced body weight, fat content, circulating leptin levels, adipose tissue weight, and liver weight. 61

Figure 2.3. Male αδKO mice fed standard chow exhibit decreased food consumption but normal energy expenditure. 64

Figure 2.4. Male αδKO mice are protected against diet-induced obesity 66

Figure 2.5. Older male αδKO mice exhibit improved glucose homeostasis 70

Figure 2.6. Young male αδKO mice (6-12 weeks old) exhibit normal glucose homeostasis 72

Figure 2.7. αδKO mice exhibit normal expression levels of leptin-regulated genes in the hypothalamus and normal sensitivity to exogenous leptin 75

Figure 2.8. Altered transcriptome in αδKO mice 78

Figure 2.9. Female KO mice fed standard chow exhibit reduced body weight, fat content, circulating leptin levels, adipose tissue weight, and liver weight 87

Figure 2.10. Female αδKO mice fed standard chow exhibit decreased food consumption but normal energy expenditure 89

Figure 2.11. Older female αδKO mice exhibit modestly improved glucose homeostasis. 91

Figure 2.12. Transcriptional changes in αδKO hypothalami are significantly associated with terms linked to microglial function 93

Figure 2.13. RNA-seq data analysis reveals potential novel transcripts of *Sh2b1* 95

Figure 2.14. RNA-seq reads from WT and αδKO hypothalami mapped to mouse *Sh2b1* Reference Sequence (RefSeq) 96

Figure 3.1. SH2B1δ localizes to the nucleolus and plasma membrane 120

Figure 3.2. SH2B1δ promotes NGF-stimulated signaling activities 134

Figure 3.3. SH2B1δ promotes NGF-stimulated gene expression 137

Figure 3.4. *Sh2b1* KO neurons exhibit decreased neurite outgrowth and complexity . 142

Figure 3.5. SH2B1 isoforms increase neurite outgrowth and/or complexity 146

Figure 3.6. Bipartite NLS in C-terminal tail is required for SH2B1δ to localize in nucleoli 150

Figure 3.7. The ability of SH2B1δ to localize to nucleoli and the plasma membrane appears to be required for SH2B1δ to increase neurite complexity 153

Figure 3.8. BDNF-induced expression of neuronal immediate early genes is partially dependent on SH2B1 activity 157

Figure 3.9. The ability of SH2B1δ to increase neurite complexity is altered by some human obesity-associated *SH2B1* variants 169

Figure 3.10. Deletion of SH2B1 isoforms does not appear to influence expression of genes associated with ribosomal biogenesis 170

Figure 3.11. BDNF treatment does not appear to influence the ability of SH2B1δ to increase neurite complexity 171

Figure 3.12. Scavenging endogenous BDNF with fusion protein TrkB-Fc does not appear to influence the ability of SH2B1δ to increase neurite complexity 172

Figure 4.1. SH2B1β or δ do not appear to influence gene expression associated with ribosomal biogenesis in PC12 cells 186

Figure 4.2. SH2B1β or SH2B1δ do not significantly alter NGF-stimulated gene expression of *Egr1* or *Arc* in PC12 cells 191

Figure 4.3. Endogenous SH2B1 localizes to the cytoplasm, plasma membrane, and nucleolus in cerebellar granule neurons 196

Figure 4.4. Cell-type specific expression of SH2B1 isoforms in neurons in P7 mouse hippocampus and prefrontal cortex 199

Figure 4.5. Cell-type specific expression of SH2B1 isoforms in P7 mouse cortex 202

Figure 4.6. Cell-type specific expression of SH2B1 isoforms in glial cells in P7 mouse hippocampus and prefrontal cortex 203

Figure 4.7. Morphology of primary hippocampal neurons from αδKO mice is largely similar to that of neurons from WT mice 206

Figure 4.8. Ratio of SH2B1 isoforms is similar between fed and fasted mice 208

Figure 4.9. Ratio of SH2B1 isoforms is similar between mice fed a normal chow or a HFD 208

Figure 4.10. Subcellular localization of endogenous SH2B1 after BDNF treatment and/or depolarization 210

List of Tables

Table 2.1. Primers for genotyping 97

Table 2.2. Primers for *Sh2b1*δ and β-*actin* cDNA 97

Table 2.3. TaqMan Gene Expression Assays from Applied Biosystems 97

Table 2.4. Genes with significantly increased expression in αδKO mice (sorted by % increase, largest to smallest) 98

Table 2.5. Genes with significantly decreased expression in αδKO mice (sorted by % decrease, largest to smallest) 99

Table 2.6. Oligos for guide RNAs 100

Table 2.7. Primers used to generate a vector encoding GFP-SH2B18c 100

Table 3.1. TaqMan Gene Expression Assays from Applied Biosystems 129

Table 4.1. Primers for qPCR using SYBR chemistry 186

Table 4.2. TaqMan Gene Expression Assays from Applied Biosystems 191

Abstract

Obesity currently afflicts over 750 million people worldwide and represents a major risk factor for diabetes, cardiovascular disease, and other health issues. Because few effective treatments for obesity exist, we need to better understand the molecular mechanisms underlying obesity to identify novel therapeutic targets. Monogenic obesity results from a variant or deficiency in a single gene. Humans with genetic mutations in the *SH2B1* gene display severe obesity and insulin resistance, the latter a hallmark symptom of diabetes. Mice lacking *Sh2b1* are similarly obese and insulin-resistant. SH2B1 is an adapter protein that is recruited to the receptors of multiple hormones and neurotrophic factors. In humans and mice, alternative splicing generates four known SH2B1 isoforms (α, β, γ, δ) that differ only in their C-terminal tails. SH2B1β and SH2B1γ are expressed in all tissues, whereas SH2B1α and SH2B1δ are expressed almost exclusively in brain tissue.

It was unknown how the different isoforms of SH2B1 contribute to SH2B1 regulation of energy balance and glucose homeostasis. Because the brain is the organ primarily responsible for regulating energy balance and both SH2B1α and SH2B1δ are expressed primarily in brain tissue, I investigated the contributions of the brain-specific isoforms of SH2B1 to energy balance and glucose metabolism. Using a novel mouse model, I demonstrate that deletion of SH2B1α and SH2B1δ suppresses appetite and body weight, and, indirectly, improves glucose control. My research suggests that the different

SH2B1 isoforms perform unique, non-redundant functions in the context of body weight regulation. Because deletion of SH2B1α and SH2B1δ protects mice from diet-induced obesity, my research presents potential targets for obesity therapeutics.

SH2B1 is thought to regulate body weight primarily through its activity in neurons. However, it was unknown how the different isoforms of SH2B1 regulate the morphology and function of neurons. I therefore investigated the contributions of all four SH2B1 isoforms, with a particular focus on the brain-specific δ isoform, to neuronal morphology and function. My results show that, unlike other SH2B1 isoforms that localize primarily to the cytoplasm and the plasma membrane, SH2B1δ localizes to the plasma membrane and the nucleolus of neurons and neuron-like PC12 cells. Nucleolar localization of SH2B1δ is directed by two highly basic regions that are unique to the C-terminal tail of SH2B1δ. Using PC12 cells, I demonstrate that SH2B1δ promotes neurotrophic factor-induced signaling events and gene expression. Using primary hippocampal neurons, I show that neurons lacking SH2B1 exhibit less outgrowth and complexity than control neurons and that SH2B1 is critical for BDNF-induced expression of two immediate early genes that serve important roles in synaptic plasticity. Reintroduction of each SH2B1 isoform into neurons lacking endogenous SH2B1 increases their neurite outgrowth and complexity, and SH2B1δ causes the most robust increase among all four isoforms. For SH2B1δ to maximally increase neurite outgrowth and complexity, it must have a functional SH2 domain and localize both to the nucleolus and plasma membrane. Thus, SH2B1 isoforms, and particularly the brain-specific δ isoform, enhance the development and/or maintenance of neurons and neuronal synapses.

To summarize, this dissertation advances our understanding of the functions of different isoforms of adapter protein SH2B1 in the context of body weight regulation and neuronal morphology and function. Thus, this work advances our knowledge of molecular components, at the whole-animal and cellular levels, underlying obesity.

Chapter 1:

Introduction

Monogenic Obesity

Obesity presents an immense threat to global health. Defined as excessive fat accumulation, obesity represents a major risk factor for type 2 diabetes, cardiovascular disease, hypertension, many cancers, and other health issues. According to recent estimates, obesity afflicts over 750 million people worldwide [1]. In the U.S., approximately 40% of adults and over 15% of youth are estimated to be obese [2]. Because rates of obesity continue to rise and few effective treatments for obesity exist, we need to better understand the molecular mechanisms underlying obesity and its sequelae to identify novel therapeutic targets.

Put simply, obesity arises when an individual's energy balance is disrupted such that energy intake exceeds energy expenditure. Excess energy is typically stored as triglyceride in adipose tissue, which leads to overweight and obesity [3]. Historically, obesity was thought to arise from lack of willpower. Research efforts from multiple laboratories over the past several decades have disintegrated this early assumption, instead demonstrating that energy balance is physiologically regulated by a complex collaboration

of multiple organs, hormones, and other signals [4]. The central nervous system is the primary director of this joint regulatory effort.

Individuals within the same environment have different susceptibilities to fat mass accumulation [5]. Thus, there are genetic factors contributing to some, if not all, cases of obesity. The first concrete evidence for genetic contribution to body weight emerged during the 1980s and 1990s with studies of twins and adopted children and parent-offspring relationships [6-10]. These studies indicated strong heritability of weight-related traits and encouraged researchers to further consider genetic components of body weight. Since these initial observations, our understanding of genetic contributions to human obesity has expanded immensely, due in large part to the Genetics of Obesity Study. Through its recruitment of over 7,500 obese patients, this Study has identified multiple different genes associated with severe obesity [11]. These findings in humans have been corroborated, and expanded upon, through murine models. Indeed, most phenotypes of humans with variants or deficiencies in these genes are mimicked by phenotypes of mice with targeted knockout or mutation of the same genes [12].

Monogenic obesity, resulting from a variant or deficiency in a single gene, usually presents during childhood and is typically driven by an inability of the individual to control their food intake [11]. Genes that can cause monogenic obesity include those that encode leptin, the leptin receptor (LepRb), proopiomelanocortin (POMC), the melanocortin 4 receptor (MC4R), brain-derived neurotrophic factor (BDNF), tropomyosin receptor kinase B (TrkB), and, the focus of this dissertation, adapter protein SH2B1. These genes encode components of the leptin-melanocortin system, which primarily acts within the

hypothalamus in the brain (Fig. 1.1). The main components of the system and their relationship to energy balance in humans and mice are described briefly below.

Research that aims to better understand the genetic drivers of obesity is of great importance for two major reasons. First, this research informs the development of therapeutics to treat patients with monogenic obesity. Impressively, recent efforts have been very fruitful in this regard: in 2020, the FDA approved IMCIVREE (setmelanotide), an MC4R agonist, for chronic weight management in adult and pediatric patients age six or older with obesity due to deficiency of POMC, LepRb, or proprotein convertase subtilisin/kexin type 1 (PCSK1), the latter being an enzyme that cleaves POMC. In Phase 3 clinical trials, 80% of patients with obesity due to POMC or PCSK1 deficiency, and 45.5% of patients with obesity due to LepR deficiency, achieved greater than 10% weight loss after one year of treatment [13]. Second, research into genetic components of obesity is important because it provides insight into critical molecular components and mechanisms that regulate energy balance in all humans. These findings could be used to design therapeutics for patients with polygenic or common obesity or, at the very least, improve our predictions of how different individuals will respond to interventional attempts (e.g., diet or exercise programs) to decrease their body weight.

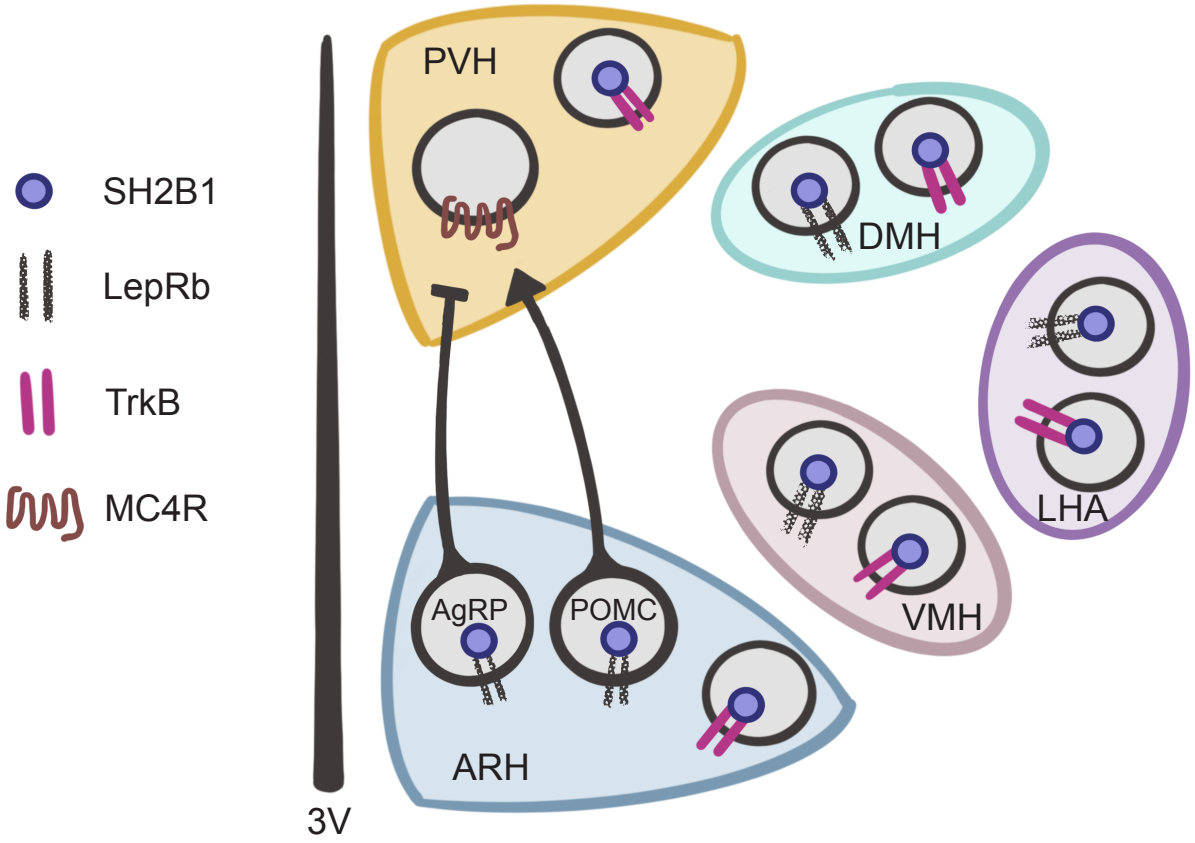

Figure 1.1. The leptin-melanocortin system

LepRb and TrkB are expressed on multiple hypothalamic nuclei. SH2B1 is thought to be recruited to LepRb and TrkB in all cells expressing these receptors. The arrowhead and "T" symbol at axon terminals of AgRP and POMC neurons demonstrate suppression and promotion of satiety, respectively, upon leptin binding to LepRb. Not all established neuronal projections and cell populations are shown. Some hypothalamic neurons co-express LepRb and TrkB [14]. 3V, third ventricle; PVH, paraventricular hypothalamic nucleus; VMH, ventromedial hypothalamic nucleus; LHA, lateral hypothalamic area; DMH, dorsomedial hypothalamic nucleus.

Leptin and LepRb

Leptin is secreted from white adipose tissue into the circulation in proportion to triglyceride stores [4]. Upon entering the central nervous system, leptin binds to and activates LepRb on specific subsets of neurons in the hypothalamus to signal the repletion of energy stores. Briefly, leptin action in the arcuate nucleus of the hypothalamus (ARH), on neurons expressing either POMC or agouti-related peptide and neuropeptide Y (AgRP/NPY), results in the promotion or suppression of satiety, respectively [15]. Intracellularly, leptin action at the long form of the leptin receptor, LepRb, triggers multiple signaling activities including activation of Janus kinase 2 (JAK2) and recruitment of SH2B1 [16-19]. Consistent with the appetite-suppressing effects of leptin, leptin-deficient humans and mice exhibit severe obesity and hyperphagia [20,21]. Humans and mice with LepRb deficiency similarly display severe hyperphagic obesity [22,23].

POMC

POMC is actively transcribed in a subpopulation of neurons whose cell bodies reside in the ARH. LepRb is relatively highly expressed in this POMC-expressing neuronal population and thus most POMC-expressing neurons are direct targets for leptin [24]. POMC expression is positively regulated by leptin. POMC is cleaved to yield multiple peptides including α melanocyte stimulating hormone (α-MSH). α-MSH, released from POMC-expressing neurons, binds to and activates MC4R on downstream neurons to suppress feeding and increase energy expenditure [24]. Humans with homozygous or compound heterozygous mutations in *POMC* show early-onset obesity and hyperphagia

[25,26]. Mice lacking all POMC-derived peptides exhibit hyperphagic obesity and decreased energy expenditure [24].

MC4R

MC4R is expressed in multiple hypothalamic sites including the PVH [27]. MC4R-expressing neurons in the PVH suppress appetite in response to the binding of its ligand α-MSH [28]. Humans with heterozygous mutations in *MC4R* exhibit obesity; subjects are hyperphagic but to a lesser degree than subjects with leptin deficiency [24]. Heterozygous mutations in *MC4R* are thought to be the most prevalent cause of monogenic obesity, having been identified in up to 6% of children with severe, early-onset obesity. Mice null for *Mc4r* exhibit obesity, hyperphagia, and decreased energy expenditure [24,29].

BDNF and TrkB

BDNF activity at TrkB is implicated in the regulation of energy balance [30]. BDNF is thought to contribute to the leptin-melanocortin pathway primarily downstream of MC4R [31]. The precise roles of BDNF and TrkB in energy regulation are yet to be determined, in part because the expression of both molecules is so widespread. Indeed, BDNF and TrkB are expressed in multiple hypothalamic and extrahypothalamic nuclei including the PVH, ventromedial nucleus of the hypothalamus (VMH), dorsomedial hypothalamus (DMH), lateral hypothalamus (LH), and the dorsal vagal complex in the hindbrain [30]. TrkB is also expressed in the ARH in neurons that do not express POMC or AgRP/NPY [32]. Consistent with BDNF suppression of appetite, humans deficient in BDNF [32-34] or TrkB [35] are severely obese and hyperphagic. Additionally, mice deficient in BDNF, globally or brain-

specifically, are obese and hyperphagic [36-38]. Hypomorphic mice that express TrkB at ~25% of normal levels also display hyperphagic obesity [32].

SH2B1

SH2B1 is an adapter protein that is recruited to multiple activated tyrosine kinases including JAK2 and TrkB. SH2B1 presumably contributes to the leptin-melanocortin pathway by mediating activity at LepRb/JAK2 and/or BDNF/TrkB complexes. Humans with inactivating mutations in *SH2B1*, and mice lacking SH2B1, are obese and hyperphagic [39-42]. See extensive overview of SH2B1 below.

Adapter Protein SH2B1

SH2B family of adapter proteins

Adapter proteins are signaling molecules that typically lack intrinsic enzymatic activity and instead facilitate interactions between other proteins. SH2B1 belongs to a family of adapter proteins that mediate cell signaling in response to a variety of hormones and growth factors. In addition to SH2B1, also known as SH2-B and PSM, the family includes SH2B2 and SH2B3, also known as APS and Lnk, respectively. All family members contain a dimerization domain, a pleckstrin homology (PH) domain, and a Src homology 2 (SH2) domain. SH2B1 and SH2B2 are able to form homo- and heterodimers, actions that are mediated by their dimerization domains [43-45]. SH2B3 does not heterodimerize with SH2B1 or SH2B2, presumably due to its different dimerization domain sequence [44]. The SH2 domains of all three family members bind to phosphorylated tyrosines in receptor tyrosine kinases or JAK proteins including JAK2, TrkB, and insulin receptors (InsR). SH2B1 is the only family member whose deletion results in obesity [46,47]. Deletion of either SH2B2 or SH2B3 disrupts immune function [48-51]. The SH2B family is evolutionarily conserved from insects through humans [52].

Alternatively spliced isoforms of SH2B1

SH2B1 encodes four known isoforms: α, β, γ, and δ (Fig. 1.2). The four isoforms are identical from amino acids 1 through 631 yet their C-terminal tails are unique. In human

tissue, SH2B1β and γ are expressed ubiquitously, whereas SH2B1α and δ are expressed almost exclusively in brain [41]. The sequences of the human isoforms have >90% similar identity to those found in mice and rats [53].

In addition to the dimerization domain, PH domain, and SH2 domain shared with SH2B2 and SH2B3, the N-terminus region of SH2B1, shared among the four known isoforms, contains proline-rich regions, a nuclear localization sequence (NLS), and a nuclear export sequence (NES). SH2B1α, β, and γ have each been shown to homodimerize via their dimerization domains, and SH2B1γ has been shown to heterodimerize with both SH2B1α and β via their dimerization domains [44]. While other combinations of these isoforms were not assessed in these assays, and SH2B1δ was not included at all, each isoform is presumably capable of dimerizing with each other isoform via their identical dimerization domains. The cellular function of the PH domain in SH2B1 is not fully understood; however, our lab recently observed that mutations in the PH domain alters the subcellular distribution of SH2B1β such that it accumulates in the nucleus rather than localizing to the plasma membrane and cytoplasm [40]. The SH2 domain in SH2B1 binds to phosphotyrosine motifs of binding partners [54,55].

The C-terminal tails of the four known SH2B1 isoforms differ in amino acid sequence and length (Fig. 1.2). The tails contain the following numbers of amino acids: α, 125; β, 39; γ, 51; and δ, 93. The C-terminal tail of SH2B1α has a unique tyrosine, Tyr753, whose phosphorylation dictates some cellular functions that are specific to this isoform [56]; some of these functions will be discussed below. The C-terminal tails of SH2B1β and γ do not contain recognizable domains or features. Yousaf and colleagues [53] identified two highly basic regions in the C-terminal tail of the δ isoform that closely

resemble nuclear localization sequence motifs, suggesting that SH2B1δ has three potential nuclear localization motifs.

In a steady state, SH2B1α [39,56], SH2B1β [39,56-58], and SH2B1γ (see Chapter 3) localize to the cytoplasm and plasma membrane. In the presence of nuclear export inhibitor leptomycin B (LMB), however, SH2B1β accumulates in the nucleus [39,56-58]. Thus, SH2B1β undergoes nucleocytoplasmic shuttling. The NLS (amino acids 147-198), NES (amino acids 224-233), and SH2 domain, all three of which are common to all SH2B1 isoforms, are required for SH2B1β to cycle through the nucleus [57,58]. Despite having the same NLS, NES, and SH2 domain as the β isoform, SH2B1α does not accumulate in the nucleus in the presence of LMB [39,56]. Mutation of Tyr753, specific to the C-terminal tail of SH2B1α, enables SH2B1α to translocate to the nucleus [56]. While the C-terminal tail of the δ isoform appears to contain two nuclear localization sequence motifs [53], the functionality of these motifs had not been tested before this work. In Chapter 3 of my dissertation, I assess the subcellular localization of SH2B1δ in PC12 cells. Furthermore, I investigate the subcellular localizations of all four known isoforms in primary hippocampal neurons.

The isoforms have been shown to perform some distinct cellular functions, which will be discussed in detail below. However, these observations are limited. Indeed, before this work, the functions of individual SH2B1 isoforms had not been investigated at the whole-animal level or in primary cultured neurons. To fill these gaps in knowledge, in Chapter 2, I investigate the contributions of the brain-specific α and δ isoforms to energy balance and glucose homeostasis. Additionally, in Chapter 3, I investigate the cellular

functions of the different isoforms in primary hippocampal neurons with a special focus on the brain-specific δ isoform.

The SH2B1 isoforms arise from alternative precursor mRNA (pre-mRNA) splicing. Alternative splicing mediates gene expression by selecting different combinations of exons in genes via their 5' or 3' splice sites and/or shifting the location of individual 5' or 3' splice sites. SH2B1 isoforms result from alternative splicing mechanisms that skip exon 9 and select an alternative 5' splice site within exon 8, resulting in altered reading frames (Fig. 1.3). The spliceosome, a large ribonucleoprotein complex, regulates the exclusion of introns and ligation of exons. Spliceosome activity can be regulated by a variety of factors including proteins that bind to the pre-mRNA and enhance or repress spliceosome assembly [59]. The factors that regulate *SH2B1* splicing have not yet been determined.

Alternative splicing creates an immense amount of proteomic diversity in the human body. Indeed, about 95% of all human multi-exon genes are estimated to be regulated by alternative splicing mechanisms [60]. Consistent with the brain-specific alternative splicing of *SH2B1*, the nervous system has been identified as a "hot spot" for alternative splicing [59,61-63]. This high prevalence of alternative splicing is thought to contribute to the immense functional complexity of the nervous system. Studies using recent advancements in experimental and computational technologies, such as novel RNA-sequencing analysis pipelines, have indicated that alternative splicing events within the nervous system are highly enriched in genes controlling neuronal architecture and synaptic interactions [61,64]. Specifically, alternative splicing events have been shown to be highly prevalent in genes that are involved in neurite outgrowth, cytoskeleton

reorganization, and aspects of synaptic formation and function including synaptogenesis, synaptic vesicle release, and postsynaptic scaffolding molecules [59,62,64].

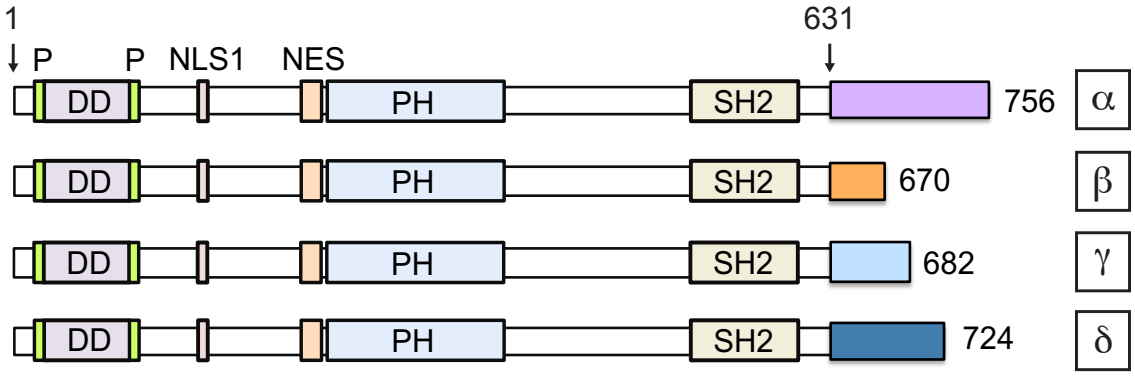

Figure 1.2. Four known SH2B1 isoforms

Isoform-specific C-terminal tails are noted in light purple, orange, light blue, and dark blue, respectively. Numbers indicate amino acids in mouse and human sequences. P, proline-rich domain; NLS, nuclear localization sequence; NES, nuclear export sequence; PH, pleckstrin homology domain; SH2, Src homology 2 domain. Figure is modified from Fig. 1A in Cote et al., 2021.

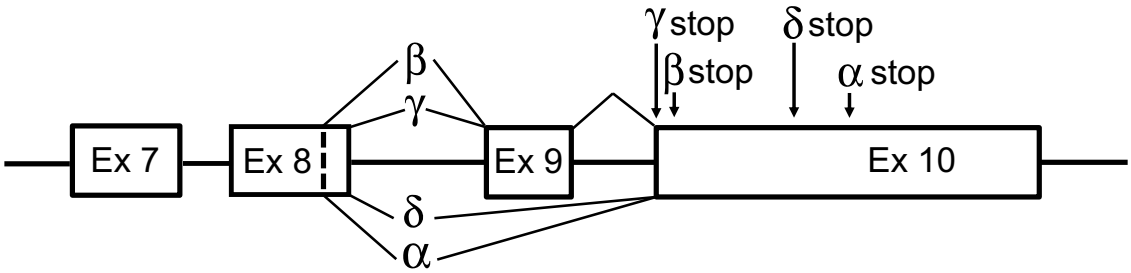

Figure 1.3. Alternative splicing of *SH2B1*

Schematic shows the region of *Sh2b1* that produces the four alternative splice variants. Four known isoforms are produced from the *Sh2b1* gene through alternative splicing. The splicing pattern that generates each isoform is indicated by lines above and below the gene structure labeled with each isoform names. The vertical dotted line in Exon 8 represents the splice site for the β and α isoforms. Stop codons for each isoform are labeled "stop". Ex, exon. Figure is modified from Fig. 1B in Cote et al., 2021.

SH2B1 variants and human obesity

The aforementioned Genetics of Obesity Study has identified 15 rare *SH2B1* variants in subjects with severe, early-onset obesity [39-41]. All identified subjects have heterozygous mutations in *SH2B1* except one who has a homozygous mutation (V695M) [39]. The variants appear to be equally prevalent in males and females. In addition to obesity, most subjects have been shown to exhibit hyperphagia, insulin resistance disproportionate for the level of obesity, reduced final height as adults, and neurobehavioral abnormalities including speech and language delay, learning difficulties, aggression, anxiety, social isolation, and hyperactivity and inattention [39-41]. Another mutation screen for *SH2B1* variants in a separate population of obese subjects, led by Volckmar and colleagues [65], identified five of the *SH2B1* variants identified by the Genetics of Obesity Study, along with two novel variants.

The rare *SH2B1* variants lie in multiple recognized regions/domains including the NLS and NES and the dimerization, PH, and SH2 domains, as well as in segments that do not contain recognized domains. While most identified variants are located in the first 631 amino acids shared by all isoforms, some are found in the unique C-terminal tails: Two variants have been found to solely affect the α isoform [39]; one has been found to affect both the α and δ isoforms [39]; one has been identified that is unique to the β isoform [40]; and one has been found to affect both the β and γ isoforms [65]. The individual with the β-specific variant presented with anxiety in addition to their obesity [40]. None of the individuals with the α and/or δ-specific variants were found to exhibit neurobehavioral abnormalities alongside their obesity [39].

Multiple genome-wide association studies (GWAS) have also associated *SH2B1* with obesity. The first of these studies, published in 2009 and 2010, examined associations between body mass index and single nucleotide polymorphisms (SNPs) in hundreds of thousands of individuals of European ancestry and found that variants at loci in *SH2B1* were associated with body mass index and other measures of obesity [66-68]. Since these initial publications, other GWAS studies have corroborated these findings by identifying *SH2B1* variants associated with obesity in other cohorts including Mexican [69], Chinese [70,71], Japanese [72], and African-American [73] populations.

Additionally, large rare deletions on chromosome 16p11.2, which encompasses the *SH2B1* gene, have been associated with severe, early-onset obesity [74]. Subjects carrying the *SH2B1*-containing deletion displayed hyperphagia, body fat levels matching those of LepRb-deficient patients, and insulin resistance disproportionate for the degree of obesity. Many of the deletion carriers also exhibited mild developmental delay. The nature of this assessment precluded any isoform-specific findings.

Functions of SH2B1 isoforms—lessons from *in vivo* experiments

Mice lacking all isoforms of SH2B1 (*Sh2b1* KO mice [KO mice]) exhibit severe obesity and hyperphagia [42,75]. Initial phenotyping studies by the Rui lab showed that the elevated body weight of KO mice is due primarily to increased fat mass, which is elevated in multiple adipose depots. KO mice also display increased energy expenditure [42], perhaps due to increased activity induced by altered behavior [76]. While heterozygous mice (*Sh2b1*$^{+/-}$ mice) do not display an obvious body weight phenotype while fed standard chow, they do exhibit an intermediate obesity phenotype when fed a high fat diet, suggesting that the obesity of mice deficient for *Sh2b1* is somewhat dosage-dependent [42].

An equivalent *Sh2b1* KO mouse model was developed independently by the Yoshimura group [77]. Similar to the Rui lab, they observed that KO mice had reduced body weight before 6 weeks of age. However, in contrast to the Rui lab's observation that KO mice progressively developed obesity after 7 weeks of age [42], the Yoshimura group noted that the size and weight of KO mice appeared similar to that of WT mice from 6 to 10 weeks of age [77]. This discrepancy may have resulted from differences in diets and environmental stress [42]. The Yoshimura lab also showed that male and female KO mice exhibited impaired fertility [77].

The Rui lab demonstrated that KO mice display insulin resistance and glucose intolerance, suggesting that KO have disrupted glucose homeostasis [78]. However, because this phenotype was observed in older mice with high fat mass, the apparent disruption in glucose homeostasis seen in KO mice is likely secondary to changes in adiposity. In fact, when Duan and colleagues tested younger mice with more normal fat

mass, they did not see much, if any, irregularity of glucose homeostasis by multiple measures [78].

Further analysis of KO mice suggested that SH2B1 regulates energy balance, at least in part, by modulating leptin signaling in the hypothalamus. For example, KO mice display increased plasma leptin prior to the onset of obesity, suggesting that decreased responsiveness to leptin could be a cause of their obesity [42]. Furthermore, KO mice exhibit attenuated leptin-induced inhibition of food intake and weight gain, increased hypothalamic expression of leptin-sensitive orexigenic genes *Npy* and *AgRP*, and decreased leptin-stimulated JAK2 activation and tyrosine phosphorylation of STAT3 and IRS2. While the gene expression data were collected from mice past the onset of obesity, the responses to leptin injections *in vivo* and *in vitro* were measured in mice at the cusp of the onset of obesity, suggesting that at least some of these apparent differences were not dependent on changes in adiposity but rather changes in leptin sensitivity itself.

Two recent publications by the Rui group have hinted at the possibility that SH2B1 may also regulate energy balance via leptin-independent mechanisms. In the first publication, Jiang and colleagues indicated that both global and neural-specific deletion of *Sh2b1* resulted in aggressive behavior [76]. In support of these findings, we too have observed aggressive behavior in our own colony of *Sh2b1* KO mice (unpublished observations). Because leptin-deficient mice do not exhibit aggressive behavior, the aggression of *Sh2b1*-deficient mice likely arises through leptin-independent means. Further, because mice with systemic or forebrain-specific deficiency (heterozygous) of *Bdnf* have been shown to develop aggressive traits [37,38], the aggressive phenotype of *Sh2b1*-deficient mice is suggestive of SH2B1 regulation of BDNF/TrkB activity. In their

second more recent publication, Jiang and colleagues demonstrated that deletion of *Sh2b1* specifically from LepRb-expressing cells (*Sh2b1*$^{\Delta LepRb}$ mice) resulted in obesity [79]. At first glance, these data support the theory that SH2B1 regulates body weight by leptin-dependent mechanisms. Upon further analysis, however, these same data also provide evidence for SH2B1 regulation of energy balance via leptin-independent means: The obesity of *Sh2b1*$^{\Delta LepRb}$ mice was much less severe than that of *Sh2b1* KO mice (~40 g vs. ~60 g in 19-week-old males), suggesting that SH2B1 must not regulate body weight solely through its activity in LepRb cells. Thus, SH2B1 appears to regulate energy balance through both leptin-dependent and -independent mechanisms. In Chapter 2 of my dissertation, I provide evidence for SH2B1 regulation of energy balance via leptin-independent mechanisms.

While the KO mouse model and its recent variations (e.g., *Sh2b1*$^{\Delta LepRb}$ mice) have offered great insight into how all SH2B1 isoforms, in combination, impact energy balance and glucose metabolism, they have not provided any information about how individual SH2B1 isoforms contribute to these processes. To date, very limited work has been done to assess isoform-specific contributions of SH2B1 to energy balance or glucose homeostasis. The only substantial isoform-specific finding from previous work involved the β isoform. In 2007, Ren and coworkers in the Rui lab demonstrated that a neuron-specific "restoration" of the β isoform of SH2B1 to approximately endogenous levels, achieved by expressing SH2B1β in KO mice using the neuron-specific enolase promoter, largely reversed the obesity and disruptions to glucose homeostasis and leptin sensitivity observed in KO mice [75]. These data impact our understanding of SH2B1 regulation of energy balance in two major ways. First, they suggest that SH2B1 activity in neurons, but

not other brain cells, is necessary for SH2B1 regulation of whole-animal metabolism. Second, they place the β isoform in the spotlight, suggesting that this isoform is partially, if not fully, responsible for SH2B1 regulation of energy balance. In Chapters 2, 3, and 4 of my dissertation, I present data that will encourage us and others to reconsider these previous findings and the assumptions they inspire.

Functions of SH2B1 isoforms—lessons from *in vitro* experiments

Previous investigations of the cellular functions of SH2B1 have predominantly centered around the β isoform. The functions of the α, γ, and δ isoforms have been assessed in a handful of studies. Thus, this section of the introduction will primarily focus on what is known about the function of SH2B1β and will address what is known about the function of the other isoforms when appropriate.

SH2B1 association with tyrosine kinases

SH2B1 has been shown to associate with multiple receptor tyrosine kinases including receptors for BDNF [76,80], nerve growth factor (NGF) [81], glial cell line-derived growth factor (GDNF) [82], insulin [55,83], insulin-like growth factor I [84], platelet-derived growth factor (PDGF) [85], and fibroblast growth factor (FGF) [86]. SH2B1 has also been shown to associate with the JAK family of cytoplasmic tyrosine kinases [54,87], which are activated in response to ligand binding to members of the cytokine family of receptors including receptors for leptin, growth hormone (GH), and prolactin. Many of these interactions were initially identified in yeast two-hybrid screens. The most relevant tyrosine kinases for this work, due to their association with regulation of energy balance and/or the development and maintenance of the nervous system, include JAK2 and receptors for insulin, BDNF, NGF, and GDNF. Because SH2B1 interacts with multiple tyrosine kinases that are heavily involved in these processes, it has been, and will continue to be, challenging to tease apart the contributions of SH2B1 activity associated with specific kinases.

SH2B1 interaction with the LepRb/JAK2 complex

Leptin stimulates activation of JAK2, which then autophosphorylates on Tyr813 [17]. SH2B1 binds via its SH2 domain to phospho-Tyr813 on JAK2 [17,44,88]; this action increases the catalytic activity of JAK2 and enhances activation of downstream signaling pathways including the STAT3 and PI 3-kinase (PI3K)/Akt pathways [17-19,54]. SH2B1α, β, γ, and δ have all been shown to interact with JAK2 [44,54] (B. Doctor and C. Carter-Su, unpublished data). Two models have been proposed for how SH2B1 enhances JAK2 activity. The first model [44] suggests that dimerization of SH2B1 leads to dimerization of associated JAK2, which, in turn, enhances JAK2 activity. The second model [89] posits that SH2B1 does not activate JAK2 as a consequence of dimerization, but rather induces or stabilizes an active conformation of JAK2. Interestingly, the N-terminal region of SH2B1 (amino acids 1-555), shared among all isoforms, also appears to bind to distinct sites (not Tyr813) on inactive JAK2 [18]. These additional interaction sites may serve to upregulate local concentration of SH2B1 around JAK2, perhaps facilitating a more rapid and robust signaling response to leptin action.

In addition to stimulating JAK2 activity, SH2B1 is thought to promote the formation of a complex containing itself, JAK2, and IRS proteins. Leptin stimulates tyrosine phosphorylation of insulin receptor substrate 1 (IRS1) and IRS2 to activate the PI3K/Akt pathway [90]. SH2B1β binds directly via its SH2 domain to both IRS1 and IRS2 and, upon leptin treatment enhances recruitment of IRS proteins to JAK2 [91]. These observations suggest that SH2B1β may mediate leptin stimulation of the PI3K/Akt pathway by enhancing the coupling of JAK2 and IRS proteins. SH2B1 also binds to other sites on IRS proteins via its PH domain-containing regions; this action does not require tyrosine

phosphorylation [91]. While the ability of SH2B1α, γ, or δ to bind IRS proteins has not yet been tested, all isoforms would be predicted to bind IRS proteins because of their identical SH2 and PH domains.

Consistent with the ability of SH2B1 to stimulate activation of JAK2 and tyrosine phosphorylation of IRS proteins, *Sh2b1* KO mice show decreased levels of leptin-stimulated activation of hypothalamic JAK2 [42]. In addition, leptin treatment failed to stimulate tyrosine phosphorylation of hypothalamic IRS2 in *Sh2b1* KO mice [42].

Unexpectedly, most human obesity-associated variants of SH2B1β did not disrupt the ability of SH2B1β to activate JAK2 or stimulate leptin- or insulin-stimulated tyrosine phosphorylation of IRS2 when tested in 293 cells transiently expressing GFP-SH2B1 and IRS2, and for leptin signaling, additionally stably expressing LepRb [41]. The only mutant that did disrupt the ability of SH2B1β to stimulate these signaling events was the F344LfsX20 mutant, which causes a frameshift that prevents translation of the SH2 domain [41]. The latter observations underscore the importance of the SH2 domain for SH2B1 stimulation of JAK2 and IRS proteins. Furthermore, they provide evidence for SH2B1 regulation of energy balance via leptin- and/or insulin-independent pathways.

SH2B1 interaction with insulin receptors

Insulin is primarily secreted from pancreatic β-cells in response to postprandial elevation of blood glucose levels. Insulin acts at insulin receptors (InsR) in multiple tissues including the brain to regulate energy balance and glucose homeostasis [92]. Insulin stimulates the binding of SH2B1 via its SH2 domain to InsR [55]. SH2B1 is thought to bind to phospho-Tyr1158, Tyr1162, and/or Tyr1163 within the InsR activation loop; this action promotes

tyrosine phosphorylation of SH2B1 [83,93,94]. All four isoforms increase InsR catalytic activity [95,96]. Interaction of SH2B1 and InsR increases InsR-dependent tyrosine phosphorylation of IRS proteins [96]. Consistent with these observations, both SH2B1β [96] and SH2B1α [97] protect against or delay dephosphorylation of IRS proteins, thereby enhancing insulin-stimulated tyrosyl phosphorylation of IRS proteins [78]. Furthermore, SH2B1β(R555E), a mutant with a defective SH2 domain, acts as a dominant negative to inhibit insulin signaling [78].

SH2B1 interaction with TrkA and TrkB

Neurotrophic factors, including NGF and BDNF, are a family of molecules that regulate proliferation, survival, migration, and differentiation of the nervous system. NGF and BDNF primarily bind to TrkA in the peripheral nervous system and TrkB in the central nervous system, respectively. The majority of research to date regarding interactions between Trk receptors and SH2B1 isoforms has focused on TrkA-SH2B1β interactions. NGF stimulates the binding of SH2B1β, via its SH2 domain, to TrkA in PC12 cells [98]. SH2B1β [98] and SH2B1γ[1] [45] positively regulate NGF-induced autophosphorylation of TrkA. NGF also promotes phosphorylation of SH2B1 on Ser/Thr residues [81]. The binding site of the SH2 domain of SH2B1 is predicted to reside within the activation loop of the Trk receptors [80,99,100]. Like NGF, BDNF similarly promotes SH2B1 binding to its receptor (TrkB) and stimulates tyrosine phosphorylation of SH2B1 [80,100,101]. However, unlike JAK2

[1] In Qian et al., 1998, the cDNA indicated as encoding SH2B1α was later discovered to encode SH2B1γ by sequencing analysis (communication with J. Cline and C. Carter-Su).

and InsR, TrkB kinase activity was reported not to be enhanced by SH2B1 [100]. Because SH2B1β interaction with Trk receptors occurs via its SH2 domain, all isoforms are predicted to interact with Trk receptors.

SH2B1β has been shown to enhance NGF- and BDNF-induced signaling events within three pathways: PLCγ, PI3K-Akt, and MEK-ERK. Specifically, SH2B1β enhances and prolongs NGF-induced phosphorylation of PLCγ at Tyr783 and Akt at Ser473 [56,101-103]. Some, but not all, studies have observed that SH2B1β modestly enhances NGF- and BDNF-induced phosphorylation of ERK1/2 at Thr202/Tyr204 [56,58,98,101,103]. In contrast to the β isoform, the α isoform has no effect on NGF-induced PLCγ phosphorylation and actually modestly inhibits NGF-induced phosphorylation of Akt and ERK1/2 [56]. However, mutation of Tyr753, specific to the C-terminal tail of SH2B1α, allows SH2B1α to enhance NGF-induced phosphorylation of PLCγ and Akt [56]. Mutational analysis suggests that TrkA phosphorylates Tyr753 [56]. Effects of SH2B1γ or δ on NGF-induced signaling events had not yet been tested before this work. In Chapter 3 of my dissertation, I assess the ability of SH2B1δ to enhance NGF-induced signaling events.

SH2B1 interaction with RET receptor

Like NGF and BDNF, GDNF is a neurotrophic factor. GDNF is thought to predominantly support the dopaminergic system in the central nervous system [104]. GDNF signals through a receptor complex consisting of the glycosylphosphatidylinositol-linked, ligand-binding GDNF family receptor α1 (GFRα1) and receptor tyrosine kinase RET [105,106]. GDNF stimulates the binding of SH2B1β via its SH2 domain to phospho-Tyr981 in RET receptor [82,107]. The SH2B1β-RET interaction increases RET kinase activity and

autophosphorylation [107]. Unlike its stimulatory effects on NGF- and BDNF-induced signaling events, SH2B1β does not appear to enhance GDNF-induced phosphorylation of ERK1/2 or Akt [82]. While SH2B1α, γ, or δ have not yet been tested in this context, all isoforms are presumed to bind to RET via their identical SH2 domain.

SH2B1 interaction with other non-receptor tyrosine kinases

In addition to its association with the JAK family of cytoplasmic tyrosine kinases, SH2B1 interacts with other non-receptor tyrosine kinases. For example, all four SH2B1 isoforms bind to Src via the SH2 and dimerization domains [108,109]. Also, SH2B1β, and presumably other isoforms, binds to Syk [110] and Fyn [109]. While not a focus of this work, these interactions are important to consider as they may contribute to the observed cellular effects of SH2B1 isoforms.

SH2B1 preferential binding between different tyrosine kinases

Many cells express multiple potential binding partners for SH2B1. For example, POMC and AgRP neurons in the ARH co-express LepRb/JAK2 and InsR [111]. To our knowledge, preferences for SH2B1 to associate with particular tyrosine kinases has only been tested once: In co-immunoprecipitation experiments in COS cells, the SH2 domain of SH2B1 was found to bind preferentially to JAK2 over InsR [94]. More experiments are needed to understand potential preferential binding of SH2B1 isoforms among tyrosine kinases that are co-expressed in different cell populations.

SH2B1 regulation of cellular responses associated with neuronal morphology and function

SH2B1 regulation of neuronal differentiation and maturation

Most investigations of SH2B1 regulation of neurotrophic factor-induced neurite outgrowth have been performed with PC12 cells. PC12 cells are derived from a pheochromocytoma of the rat adrenal medulla and have embryonic origin from the neural crest [112]. In response to NGF, PC12 cells cease proliferation and differentiate, acquiring neurites, analogous to axons and dendrites in neurons, and biochemical features that are similar to those of a true sympathetic neuron [112-115]. Indeed, NGF-treated PC12 cells are able to develop synapses with primary cultured neurons from rat cortex [116] and express neuron-specific genes [117]. PC12 cell neurite outgrowth is typically assessed by measuring the percent of cells expressing the plasmid of interest that have neurite outgrowths > 2 times the length of the cell body.

Multiple lines of evidences indicate that SH2B1 enhances neurotrophic factor-induced neurite outgrowth. First, knockdown of endogenous SH2B1 via shRNA decreased NGF-induced neurite outgrowth in PC12 cells by ~50% [58]. In agreement, SH2B1β, γ, and δ promote NGF-stimulated neuronal differentiation in PC12 cells [80,98] (M. Doche, J. Cote, P. Vander, C. Carter-Su, unpublished data). Mutational analysis showed that a defective SH2 domain [98] or mutated NES or NLS [57,58] prevents SH2B1β from enhancing NGF-stimulated neurite outgrowth in PC12 cells, suggesting that SH2B1 must be recruited to phosphotyrosines in tyrosine kinases and perform nucleocytoplasmic shuttling to enhance NGF-induced neurite outgrowth. Human obesity-associated variants

in SH2B1β also disrupt the ability of SH2B1β to enhance NGF-induced neurite outgrowth in PC12 cells [41]. In contrast to SH2B1β, γ, and δ, SH2B1α does not enhance NGF-stimulated neuronal differentiation in PC12 cells [39]. Furthermore, SH2B1α suppresses SH2B1β enhancement of neurite outgrowth in PC12 cells, an action that is dependent on the SH2B1α-specific Tyr753 [56].

The link between SH2B1 regulation of neurite outgrowth and signaling events is not well understood. It seems logical to predict that SH2B1 enhancement of neurotrophic factor-induced signaling events (e.g., phosphorylation of PLCγ, Akt, and/or ERK1/2) induces neurite outgrowth. However, while knockdown of endogenous SH2B1 or mutation of the SH2 domain or NLS in SH2B1β blocks NGF-stimulated neurite outgrowth in PC12 cells, these actions did not affect NGF-stimulated phosphorylation of TrkA, Akt, and/or ERK1/2 in the same cell line [58,98,102]. Thus, SH2B1β enhancement of NGF-dependent neurite outgrowth may not result from increased TrkA activation or an enhanced ability of TrkA to phosphorylate the substrates required to activate the Akt or ERK1/2 pathways. Instead, SH2B1β may enhance NGF-dependent neurite outgrowth through its actions at a point downstream of, or parallel to Akt and ERK1/2.

Because BDNF is strongly implicated in the regulation of energy balance [30], there has been abundant interest in understanding whether SH2B1 enhances BDNF-induced neurite outgrowth like it does NGF-induced neurite outgrowth. Given that PC12 cells do not express TrkB, Shih and colleagues [101] stably expressed TrkB in PC12 cells (PC12-TrkB cells) to study SH2B1 regulation of BDNF-induced neurite outgrowth using a cell line that is higher throughput than primary neurons. Upon knockdown of all SH2B1 isoforms via shRNA, PC12-TrkB cells exhibit decreased neurite outgrowth. Furthermore,

consistent with previous data, SH2B1β enhances neurite outgrowth in PC12-TrkB cells [101]. The SH2 domain of SH2B1β is required for this enhancement [101]. Thus, SH2B1β regulation of neurotrophic factor-induced neurite outgrowth appears to be consistent among at least two different neurotrophic factors: NGF and BDNF.

It is worth noting that selective pharmacological inhibitors of the MAPK or PI3K-Akt pathways completely (ERK1/2) or partially (Akt) abolished BDNF-induced, SH2B1β-enhanced neurite outgrowth [101]. These observations suggest that the MAPK and PI3K/Akt pathways are responsible, at least in part, for SH2B1β enhancement of neurite outgrowth. However, the pathways could be required but not sufficient to enhance neurite outgrowth. Whether these findings contradict the aforementioned predictions, which suggested that SH2B1β enhances neurotrophic factor-dependent neurite outgrowth at a point downstream of or parallel to ERK1/2 or Akt, is yet to be determined.

Consistent with its actions in PC12 cells, SH2B1 has been shown to be critical for neurite outgrowth in explants of sympathetic ganglia. Specifically, a mutant SH2B1β, lacking the N-terminus (amino acids 1-499) but containing the SH2 domain and C-terminal tail (amino acids 500-670), nearly eliminates axonal processes in the presence of NGF within explants of superior cervical ganglia prepared from embryonic day 18 (E18) rat embryos [80].

More recently, SH2B1 has also been shown to promote neurotrophic factor-induced outgrowth of axons and/or dendrites in primary cultured neurons. Knockdown of all SH2B1 isoforms via shRNA in day in vitro (DIV) 4 cortical [101] and hippocampal neurons [118], cultured from E18 rat embryos, decreases two features in neurons: the length of the longest neurite, typically reflective of axon length, and the number of endpoints,

representative of overall neurite branching. In agreement, SH2B1β increases the length of the longest neurite and number of endpoints in DIV 6 hippocampal neurons; the former enhancement by SH2B1β is increased by BDNF treatment but the latter is not [101]. Mutational analysis showed that the full SH2B1β sequence (amino acids 1-670) is necessary to maximally increase the number of primary neurites and endpoints of DIV 7 hippocampal neurons [118]. A truncated mutant excluding all sequence of SH2B1β except the SH2 domain and C-terminal tail (amino acids 505-670) severely disrupts the ability of SH2B1β to increase these measures, resulting in lower-than-control levels; various other truncations bring measures to control levels. Because the 505-670 truncation excludes a proline-rich region located between amino acids 397 and 505, the authors conclude that the proline-rich regions of SH2B1β are required to enhance neurite outgrowth [118]. Also, in DIV 7 cultured mesencephalic neurons from E14 rat embryos, which express RET receptor, SH2B1β increases the length of the longest neurite in the presence of GDNF [82]. The SH2 domain-deficient mutant SH2B1β(R555E) has the opposite effect, yielding neurites that are shorter than those of control cells.

All prior experiments investigating SH2B1 in primary hippocampal cultures were performed using the β isoform of SH2B1. This decision presumably arose in part from data suggesting that β is the primary isoform expressed in PC12 cells [102] and hippocampal neurons [118]. However, based on my personal experience with the assay used to measure isoform expression in hippocampal neurons [118], I have questioned the validity of the assumption that β is the predominant isoform in hippocampal neurons. Indeed, in Chapters 3 and 4 of my dissertation, I share new data that suggests that β is not the primary isoform expressed in hippocampal or cortical neurons.

SH2B1 regulation of gene expression

To identify SH2B1-regulated genes important for neuronal morphology and function, our lab [119] performed microarray analysis of control PC12 cells and PC12 cells stably overexpressing SH2B1β. Results indicated that SH2B1β enhances expression of a subset of NGF-induced genes including *Plaur*, *Mmp3*, *Mmp10*, and *FosL1*. uPAR (encoded by *Plaur*), MMP3, and MMP10 lie in the same protease cascade implicated in extracellular matrix degradation, cell motility, and neuronal differentiation [120,121]. Intriguingly, extracellular proteolysis has recently been shown to be a key factor in the plasticity of both glutamatergic excitatory synapses [122,123] and GABAergic inhibitory synapses [124]. *FosL1* is an immediate early gene that encodes a transcription factor thought to regulate a wave of late response genes [125] that, in turn, regulate cellular processes including dendritic growth, spine maturation, and synapse elimination [126]. Expression of these genes is reduced in PC12 cells stably expressing the SH2 domain-defective SH2B1β(R555E) mutant, suggesting that SH2B1β must be recruited to phosphotyrosines in tyrosine kinases to maximally enhance gene expression related to neuronal differentiation and maturation. Further assessment by our lab [58] suggested that SH2B1β requires both a functional NLS and NES, enabling nucleocytoplasmic shuttling, to maximally enhance expression of *Plaur*, *Mmp3*, and *Mmp10*; *FosL1* expression was not tested. Finally, because a distinct subset of NGF-induced genes is unaffected by SH2B1β or SH2B1β(R555E), our lab speculated that SH2B1β acts primarily downstream of TrkA to regulate gene expression involved in neuronal differentiation [119].

Our lab has also been interested in clarifying whether other SH2B1 isoforms are able to enhance the subset of NGF-induced genes whose expression is enhanced by

SH2B1β. Joe and colleagues [56] showed that SH2B1α is unable to enhance NGF-induced expression of *Plaur*, *Mmp3*, *Mmp10*, *or FosL1* in PC12 cells. However, in agreement with aforementioned observations, mutating a tyrosine specific to the α tail, Tyr753, enables SH2B1α to enhance the expression *Plaur*, *Mmp10*, and *FosL1*, but not *Mmp3*, to a statistically significant extent [56]. The effects of SH2B1γ have not yet been tested. In Chapter 3 of my dissertation, I assess the ability of SH2B1δ to regulate this subset of NGF-induced genes in PC12 cells. Additionally, in Chapters 2 and 3, I investigate whether SH2B1 isoforms regulate the transcriptome of the mouse hypothalamus and a subset of genes in primary hippocampal neurons.

SH2B1 regulation of the actin cytoskeleton and cell motility

Cytoskeletal dynamics are critical for the growth and maturation of a neuron, enabling it to transform from a simple sphere into a highly complex cell containing a cell body and multiple neurites of varying lengths. The cytoskeleton of a developing neuron is primarily composed of actin filaments and microtubules, both of which are regulated by myriad molecules and signals [127]. SH2B1 has been shown to regulate the actin cytoskeleton by multiple measures.

Our lab has provided insight into how SH2B1 regulates the actin cytoskeleton and cell motility. For example, SH2B1β not only localizes to broad weblike extensions known as membrane ruffles in 3T3-F442A fibroblasts, but also enhances membrane ruffling induced by GH and platelet-derived growth factor (PDGF) [128]. SH2 domain-deficient mutant SH2B1β(R555E) inhibits the GH- and PDGF-induced ruffling in these cells, suggesting recruitment of SH2B1β to phosphotyrosines in tyrosine kinases is necessary

for its effect. SH2B1β also promotes GH-induced cell motility in 3T3-F442A fibroblasts and 293T kidney epithelial-derived cells; the SH2 domain and N-terminal proline-rich region (amino acids 85-106) of SH2B1β are required for a maximal effect [129]. Furthermore, SH2B1β was found to bind via its N-terminal proline-rich region (amino acids 85-106) to Rac, a small GTPase implicated in membrane ruffling, lamellipodia formation, and cell motility; this binding does not require JAK2 or Rac activation [129]. In addition, SH2B1β localizes to focal adhesions in 3T3-F44TA fibroblasts and HeLa cells, suggesting that SH2B1β regulates cell motility via the attachment of the cell to the extracellular matrix [130]. Finally, SH2B1β interacts with talin, a cytoskeletal protein that links the cytoskeleton to the cell membrane [130]. The SH2 domain of SH2B1β is necessary and sufficient for localization of SH2B1β to focal adhesions, and necessary for maximal co-immunoprecipitation with talin [130].

Other groups have also made major contributions to our knowledge of how SH2B1β regulates the actin cytoskeleton and cell motility. The Ginty group [80] demonstrated that SH2B1γ binds via a proline-rich region (amino acids 384-504) to Grb2, a protein that has been deemed an important link between cellular signaling and the neuronal cytoskeleton [131,132]. Results from the Diakonova group [133] provided substantial evidence that SH2B1β has two actin-binding sites, amino acids 150-200 and 615-670, both of which are required for maximal GH- and prolactin-induced membrane ruffling in 3T3-F44TA fibroblasts. The weaker binding site of the two (amino acids 615-670) is partially located in the C-terminal tail unique to SH2B1β. SH2B1β was also found to cross-link actin filaments [133]. Additional work from the Diakonova lab [134] indicated that SH2B1β binds to actin-binding protein filamin A to regulate prolactin-dependent cytoskeletal

reorganization and cell motility. SH2B1β binds to filamin A via amino acids 200-260 [134], a region distinct from the two previously described actin-binding sites [133]. More recently, the Chen group [118] demonstrated that SH2B1β interacts via its N-terminal proline-rich regions with insulin receptor tyrosine kinase substrate p53 (IRSp53), an actin-binding protein that regulates the unbranched F-actin filament bundles in filopodia.

The aforementioned studies have led our lab and others to speculate that SH2B1β recruits Grb2, Rac, filamin A, IRSp53, and perhaps other proteins to activated receptor tyrosine kinases or activated membrane receptor/JAK complexes, positioning them to regulate the actin cytoskeleton. SH2B1β may also bind complexes of focal adhesion proteins, providing stability to facilitate regulation of cell motility. Because the majority of actin-related binding sites identified within SH2B1β lie within the shared region of SH2B1 isoforms, the other isoforms are predicted to interact with the same proteins. Involvement of SH2B1β, and perhaps other SH2B1 isoforms, in regulating the actin cytoskeleton has myriad implications for the development and maintenance of the nervous system. Indeed, in Chapters 2 and 3 of my dissertation, my interpretations of my data reflect upon the ability of SH2B1 to regulate the actin cytoskeleton.

Dissertation Summary

This dissertation examines how the different alternatively spliced isoforms of adapter protein SH2B1 contribute to the regulation of energy balance and neuronal morphology and function. In Chapter 2, I assess whether the brain-specific α and δ isoforms of SH2B1 regulate energy balance and glucose metabolism. Using a novel mouse model generated by CRISPR/Cas9 genome editing, I demonstrate that SH2B1α and/or SH2B1δ are critical determinants of appetite and body weight, and, indirectly, glucose control. My findings indicate that different SH2B1 isoforms perform different functions *in vivo.* In Chapter 3, I investigate the contributions of all four SH2B1 isoforms, with a particular focus on the brain-specific δ isoform, to neuronal morphology and function. Using PC12 cells and primary hippocampal neurons, I show that SH2B1δ exhibits a unique nucleolar subcellular localization. SH2B1δ promotes neurotrophic factor-induced signaling events and gene expression. Reintroduction of each SH2B1 isoform increases neurite outgrowth and complexity in neurons from mice lacking SH2B1, and SH2B1δ induces the largest increase. In Chapter 4, I build on my findings in Chapters 2 and 3 by sharing preliminary results from follow-up experiments, discussing other ongoing work, and proposing additional strategies for more future work. Collectively, this dissertation offers novel insight into functions of the alternatively spliced isoforms of SH2B1 in the context of nervous system control of body weight.

References

1. Collaboration, N.C.D.R.F. Worldwide trends in body-mass index, underweight, overweight, and obesity from 1975 to 2016: a pooled analysis of 2416 population-based measurement studies in 128.9 million children, adolescents, and adults. *Lancet* **390**, 2627-2642 (2017).
2. Hales, C.M., Fryar, C.D., Carroll, M.D., Freedman, D.S. & Ogden, C.L. Trends in Obesity and Severe Obesity Prevalence in US Youth and Adults by Sex and Age, 2007-2008 to 2015-2016. *Jama* **319**, 1723-1725 (2018).
3. Leibel, R.L. Energy in, energy out, and the effects of obesity-related genes. *N Engl J Med* **359**, 2603-2604 (2008).
4. Myers, M.G. & Leibel, R.L. Lessons From Rodent Models of Obesity. in *Endotext* (eds. Feingold, K.R., Anawalt, B., Boyce, A., Chrousos, G., Dungan, K., Grossman, A., . . . Wilson, D.P.) (South Dartmouth (MA), 2000).
5. Friedman, J.M. A war on obesity, not the obese. *Science* **299**, 856-858 (2003).
6. Stunkard, A.J., Foch, T.T. & Hrubec, Z. A twin study of human obesity. *Jama* **256**, 51-54 (1986).
7. Stunkard, A.J., Harris, J.R., Pedersen, N.L. & McClearn, G.E. The body-mass index of twins who have been reared apart. *N Engl J Med* **322**, 1483-1487 (1990).
8. Sorensen, T.I., Price, R.A., Stunkard, A.J. & Schulsinger, F. Genetics of obesity in adult adoptees and their biological siblings. *BMJ* **298**, 87-90 (1989).
9. Stunkard, A.J., Sorensen, T.I., Hanis, C., Teasdale, T.W., Chakraborty, R., Schull, W.J. & Schulsinger, F. An adoption study of human obesity. *N Engl J Med* **314**, 193-198 (1986).
10. Maes, H.H., Neale, M.C. & Eaves, L.J. Genetic and environmental factors in relative body weight and human adiposity. *Behavior genetics* **27**, 325-351 (1997).
11. Farooqi, I.S. Monogenic human obesity. *Front Horm Res* **36**, 1-11 (2008).
12. Yazdi, F.T., Clee, S.M. & Meyre, D. Obesity genetics in mouse and human: back and forth, and back again. *PeerJ* **3**, e856 (2015).
13. Clement, K., van den Akker, E., Argente, J., Bahm, A., Chung, W.K., Connors, H., . . . Investigators, L.P.T. Efficacy and safety of setmelanotide, an MC4R agonist, in individuals with severe obesity due to LEPR or POMC deficiency: single-arm, open-label, multicentre, phase 3 trials. *Lancet Diabetes Endocrinol* **8**, 960-970 (2020).
14. Liao, G.Y., Bouyer, K., Kamitakahara, A., Sahibzada, N., Wang, C.H., Rutlin, M., . . . Xu, B. Brain-derived neurotrophic factor is required for axonal growth of selective groups of neurons in the arcuate nucleus. *Molecular metabolism* **4**, 471-482 (2015).
15. Flak, J.N. & Myers, M.G., Jr. Minireview: CNS Mechanisms of Leptin Action. *Molecular endocrinology* **30**, 3-12 (2016).
16. Allison, M.B. & Myers, M.G., Jr. 20 years of leptin: connecting leptin signaling to biological function. *J Endocrinol* **223**, T25-35 (2014).
17. Li, Z., Zhou, Y., Carter-Su, C., Myers Jr., M.G. & Rui, L. SH2B1 enhances leptin signaling by both Janus kinase 2 Tyr^{813} phosphorylation-dependent and -independent mechanisms. *Mol. Endocrinol.* **21**, 2270-2281 (2007).

18. Rui, L., Gunter, D.R., Herrington, J. & Carter-Su, C. Differential binding to and regulation of JAK2 by the SH2 domain and N-terminal region of SH2-Bβ. *Mol. Cell. Biol.* **20**, 3168-3177 (2000).
19. Rui, L. & Carter-Su, C. Identification of SH2-Bβ as a potent cytoplasmic activator of the tyrosine kinase Janus kinase 2. *Proc. Nat. Acad. Sci. USA* **96**, 7172-7177 (1999).
20. Farooqi, I.S., Jebb, S.A., Langmack, G., Lawrence, E., Cheetham, C.H., Prentice, A.M., . . . O'Rahilly, S. Effects of recombinant leptin therapy in a child with congenital leptin deficiency. *N. Eng. J. Med.* **341**, 879-884 (1999).
21. Friedman, J.M. & Halaas, J.L. Leptin and the regulation of body weight in mammals. *Nature* **395**, 763-770 (1998).
22. Tartaglia, L.A., Dembski, M., Weng, X., Deng, N., Culpepper, J., Devos, R., . . . Deeds, J. Identification and expression cloning of a leptin receptor, OB-R. *Cell* **83**, 1263-1271 (1995).
23. Chua, S.C., Jr., Chung, W.K., Wu-Peng, X.S., Zhang, Y., Liu, S.M., Tartaglia, L. & Leibel, R.L. Phenotypes of mouse diabetes and rat fatty due to mutations in the OB (leptin) receptor. *Science* **271**, 994-996 (1996).
24. Coll, A.P., Farooqi, I.S., Challis, B.G., Yeo, G.S. & O'Rahilly, S. Proopiomelanocortin and energy balance: insights from human and murine genetics. *J. Clin. Endo. Metab.* **89**, 2557-2562 (2004).
25. Krude, H., Biebermann, H., Luck, W., Horn, R., Brabant, G. & Gruters, A. Severe early-onset obesity, adrenal insufficiency and red hair pigmentation caused by POMC mutations in humans. *Nat Genet* **19**, 155-157 (1998).
26. Krude, H., Biebermann, H., Schnabel, D., Tansek, M.Z., Theunissen, P., Mullis, P.E. & Gruters, A. Obesity due to proopiomelanocortin deficiency: three new cases and treatment trials with thyroid hormone and ACTH4-10. *J Clin Endocrinol Metab* **88**, 4633-4640 (2003).
27. Cone, R.D., Lu, D., Koppula, S., Vage, D.I., Klungland, H., Boston, B., . . . Kesterson, R.A. The melanocortin receptors: agonists, antagonists, and the hormonal control of pigmentation. *Recent Prog Horm Res* **51**, 287-317; discussion 318 (1996).
28. Shah, B.P., Vong, L., Olson, D.P., Koda, S., Krashes, M.J., Ye, C., . . . Lowell, B.B. MC4R-expressing glutamatergic neurons in the paraventricular hypothalamus regulate feeding and are synaptically connected to the parabrachial nucleus. *Proc Natl Acad Sci U S A* **111**, 13193-13198 (2014).
29. Huszar, D., Lynch, C.A., Fairchild-Huntress, V., Dunmore, J.H., Fang, Q., Berkemeier, L.R., . . . Lee, F. Targeted Disruption of the Melanocortin-4 Receptor Results in Obesity in Mice. *Cell* **88**, 131-141 (1997).
30. Rios, M. BDNF and the central control of feeding: accidental bystander or essential player? *Trends Neurosci.* **36**, 83-90 (2013).
31. Xu, B. & Xie, X. Neurotrophic factor control of satiety and body weight. *Nat Rev Neurosci* **17**, 282-292 (2016).
32. Xu, B., Goulding, E.H., Zang, K., Cepoi, D., Cone, R.D., Jones, K.R., . . . Reichardt, L.F. Brain-derived neurotrophic factor regulates energy balance downstream of melanocortin-4 receptor. *Nat Neurosci* **6**, 736-742 (2003).

33. Gray, J., Yeo, G.S., Cox, J.J., Morton, J., Adlam, A.L., Keogh, J.M., . . . Farooqi, I.S. Hyperphagia, severe obesity, impaired cognitive function, and hyperactivity associated with functional loss of one copy of the brain-derived neurotrophic factor (BDNF) gene. *Diabetes* **55**, 3366-3371 (2006).
34. Han, J.C., Liu, Q.R., Jones, M., Levinn, R.L., Menzie, C.M., Jefferson-George, K.S., . . . Yanovski, J.A. Brain-derived neurotrophic factor and obesity in the WAGR syndrome. *N. Engl. J. Med.* **359**, 918-927 (2008).
35. Yeo, G.S., Connie Hung, C.C., Rochford, J., Keogh, J., Gray, J., Sivaramakrishnan, S., . . . Farooqi, I.S. A de novo mutation affecting human TrkB associated with severe obesity and developmental delay. *Nat. Neurosci.* **7**, 1187-1189 (2004).
36. Kernie, S.G., Liebl, D.J. & Parada, L.F. BDNF regulates eating behavior and locomotor activity in mice. *EMBO J.* **19**, 1290-1300 (2000).
37. Lyons, W.E., Mamounas, L.A., Ricaurte, G.A., Coppola, V., Reid, S.W., Bora, S.H., . . . Tessarollo, L. Brain-derived neurotrophic factor-deficient mice develop aggressiveness and hyperphagia in conjunction with brain serotonergic abnormalities. *Proc. Nat. Acad. Sci. USA* **96**, 15239-15244 (1999).
38. Rios, M., Fan, G., Fekete, C., Kelly, J., Bates, B., Kuehn, R., . . . Jaenisch, R. Conditional deletion of brain-derived neurotrophic factor in the postnatal brain leads to obesity and hyperactivity. *Mol. Endocrinol.* **15**, 1748-1757 (2001).
39. Pearce, L.R., Joe, R., Doche, M.D., Su, H.W., Keogh, J.M., Henning, E., . . . Carter-Su, C. Functional characterisation of obesity-associated variants involving the alpha and beta isoforms of human SH2B1. *Endocrinology* **9**, 3219-3226 (2014).
40. Flores, A., Argetsinger, L.S., Stadler, L.K.J., Malaga, A.E., Vander, P.B., DeSantis, L.C., . . . Carter-Su, C. Crucial Role of the SH2B1 PH Domain for the Control of Energy Balance. *Diabetes* **68**, 2049-2062 (2019).
41. Doche, M.D., Bochukova, E.G., Su, H.W., Pearce, L., Keogh, J.M., Henning, E., . . . Farooqi, I.S. *SH2B1* mutations are associated with maladaptive behavior and obesity. *J. Clin. Invest.* **122**, 4732-4736 (2012).
42. Ren, D., Li, M., Duan, C. & Rui, L. Identification of SH2-B as a key regulator of leptin sensitivity, energy balance and body weight in mice. *Cell Metab.* **2**, 95-104 (2005).
43. Dhe-Paganon, S., Werner, E.D., Nishi, M., Hansen, L., Chi, Y.I. & Shoelson, S.E. A phenylalanine zipper mediates APS dimerization. *Nat. Struct. Mol. Biol.* **11**, 968-974 (2004).
44. Nishi, M., Werner, E.D., Oh, B.C., Frantz, J.D., Dhe-Paganon, S., Hansen, L., . . . Shoelson, S.E. Kinase activation through dimerization by human SH2-B. *Mol. Cell. Biol.* **25**, 2607-2621 (2005).
45. Qian, X. & Ginty, D.D. SH2-B and APS are multimeric adapters that augment TrkA signaling. *Mol. Cell. Biol.* **21**, 1613-1620 (2001).
46. Li, M., Ren, D., Iseki, M., Takaki, S. & Rui, L. Differential role of SH2-B and APS in regulating energy and glucose homeostasis. *Endocrinology* **147**, 2163-2170 (2006).
47. Mori, T., Suzuki-Yamazaki, N. & Takaki, S. Lnk/Sh2b3 Regulates Adipose Inflammation and Glucose Tolerance through Group 1 ILCs. *Cell Rep* **24**, 1830-1841 (2018).

48. Takaki, S. Sh2b3/Lnk family adaptor proteins in the regulation of lymphohematopoiesis. *Jpn. J. Clin. Immunol.* **31**, 440-447 (2008).
49. Takaki, S., Sauer, K., Iritani, B.M., Chien, S., Ebihara, Y., Tsuji, K., . . . Perlmutter, R.M. Control of B cell production by the adaptor protein lnk. *Immunity* **13**, 599-609 (2000).
50. Velazquez, L., Cheng, A.M., Fleming, H.E., Furlonger, C., Vesely, S., Bernstein, A., . . . Pawson, T. Cytokine signaling and hematopoietic homeostasis are disrupted in *Lnk*-deficient mice. *J. Exp. Med.* **195**, 1599-1611 (2002).
51. Yokouchi, M., Suzuki, R., Masuhara, M., Komiya, S., Inoue, A. & Yoshimura, A. Cloning and characterization of APS, an adaptor molecule containing PH and SH2 domains that is tyrosine phosphorylated upon B-cell receptor stimulation. *Oncogene* **15**, 7-15 (1997).
52. Song, W., Ren, D., Li, W., Jiang, L., Cho, K.W., Huang, P., . . . Rui, L. SH2B regulation of growth, metabolism, and longevity in both insects and mammals. *Cell Metab.* **11**, 427-437 (2010).
53. Yousaf, N., Deng, Y., Kang, Y. & Riedel, H. Four PSM/SH2-B alternative splice variants and their differential roles in mitogenesis. *J. Biol. Chem.* **276**, 40940-40948 (2001).
54. Rui, L., Mathews, L.S., Hotta, K., Gustafson, T.A. & Carter-Su, C. Identification of SH2-Bβ as a substrate of the tyrosine kinase JAK2 involved in growth hormone signaling. *Mol. Cell. Biol.* **17**, 6633-6644 (1997).
55. Riedel, H., Wang, J., Hansen, H. & Yousaf, N. PSM, an insulin-dependent, pro-rich, PH, SH2 domain containing partner of the insulin receptor. *J. Biochem.* **122**, 1105-1113 (1997).
56. Joe, R.M., Flores, A., Doche, M.E., Cline, J.M., Clutter, E.S., Vander, P.B., . . . Carter-Su, C. Phosphorylation of the Unique C-terminal Tail of the Alpha Isoform of the Scaffold Protein SH2B1 Controls the Ability of SH2B1alpha to Enhance Nerve Growth Factor Function. *Mol Cell Biol* (2017).
57. Chen, L. & Carter-Su, C. Adapter protein SH2-Bβ undergoes nucleocytoplasmic shuttling: implications for nerve growth factor induction of neuronal differentiation. *Mol. Cell. Biol.* **24**, 3633-3647 (2004).
58. Maures, T.J., Chen, L. & Carter-Su, C. Nucleocytoplasmic shuttling of the adapter protein SH2B1β (SH2-Bβ) is required for nerve growth factor (NGF)-dependent neurite outgrowth and enhancement of expression of a subset of NGF-responsive genes. *Mol. Endocrinol.* **23**, 1077-1091 (2009).
59. Li, Q., Lee, J.A. & Black, D.L. Neuronal regulation of alternative pre-mRNA splicing. *Nat Rev Neurosci* **8**, 819-831 (2007).
60. Wang, E.T., Sandberg, R., Luo, S., Khrebtukova, I., Zhang, L., Mayr, C., . . . Burge, C.B. Alternative isoform regulation in human tissue transcriptomes. *Nature* **456**, 470-476 (2008).
61. Raj, B. & Blencowe, B.J. Alternative Splicing in the Mammalian Nervous System: Recent Insights into Mechanisms and Functional Roles. *Neuron* **87**, 14-27 (2015).
62. Lipscombe, D. Neuronal proteins custom designed by alternative splicing. *Curr Opin Neurobiol* **15**, 358-363 (2005).
63. Tapial, J., Ha, K.C.H., Sterne-Weiler, T., Gohr, A., Braunschweig, U., Hermoso-Pulido, A., . . . Irimia, M. An atlas of alternative splicing profiles and functional

associations reveals new regulatory programs and genes that simultaneously express multiple major isoforms. *Genome Res* **27**, 1759-1768 (2017).
64. Furlanis, E., Traunmuller, L., Fucile, G. & Scheiffele, P. Landscape of ribosome-engaged transcript isoforms reveals extensive neuronal-cell-class-specific alternative splicing programs. *Nat Neurosci* **22**, 1709-1717 (2019).
65. Volckmar, A.L., Bolze, F., Jarick, I., Knoll, N., Scherag, A., Reinehr, T., . . . Hinney, A. Mutation screen in the GWAS derived obesity gene SH2B1 including functional analyses of detected variants. *BMC Med Genomics* **5**, 65 (2012).
66. Willer, C.J., Speliotes, E.K., Loos, R.J., Li, S., Lindgren, C.M., Heid, I.M., . . . Genetic Investigation of, A.T.C. Six new loci associated with body mass index highlight a neuronal influence on body weight regulation. *Nat. Genet.* **41**, 25-34 (2009).
67. Speliotes, E.K., Willer, C.J., Berndt, S.I., Monda, K.L., Thorleifsson, G., Jackson, A.U., . . . Loos, R.J. Association analyses of 249,796 individuals reveal 18 new loci associated with body mass index. *Nature Genetics* **42**, 937-948 (2010).
68. Thorleifsson, G., Walters, G.B., Gudbjartsson, D.F., Steinthorsdottir, V., Sulem, P., Helgadottir, A., . . . Stefansson, K. Genome-wide association yields new sequence variants at seven loci that associate with measures of obesity. *Nat. Genet.* **41**, 18-24 (2009).
69. León-Mimila P, V.-R.H., Villalobos-Comparán M, Villarreal-Molina T, Romero-Hidalgo S, López-Contreras B, Gutiérrez-Vidal R, Vega-Badillo J, Jacobo-Albavera L, Posadas-Romeros C, Canizalez-Román A, Río-Navarro BD, Campos-Pérez F, Acuña-Alonzo V, Aguilar-Salinas C, Canizales-Quinteros S. Contribution of common genetic variants to obesity and obesity-related traits in mexican children and adults. *PloS One* **8**, e70640 (2013).
70. Shi, J., Long J., Gao, YT., Lu, W, Cai, Q, Wen, W., Zheng, Y., Yu, K., Xiang, YB., Hu, FB., Zheng, W., Shu, XO. Evaluation of genetic susceptibility loci for obesity in Chinese women. *American Journal of Epidemiology* **172**, 244-254 (2010).
71. Ng, M.C., Tam, C.H., So, W.Y., Ho, J.S., Chan, A.W., Lee, H.M., . . . Ma, R.C. Implication of genetic variants near NEGR1, SEC16B, TMEM18, ETV5/DGKG, GNPDA2, LIN7C/BDNF, MTCH2, BCDIN3D/FAIM2, SH2B1, FTO, MC4R, and KCTD15 with obesity and type 2 diabetes in 7705 Chinese. *J Clin Endocrinol Metab* **95**, 2418-2425 (2010).
72. Takeuchi, F., Yamamoto, K., Katsuya, T., Nabika, T., Sugiyama, T., Fujioka, A., . . . Kato, N. Association of genetic variants for susceptibility to obesity with type 2 diabetes in Japanese individuals. *Diabetologia* **54**, 1350-1359 (2011).
73. Hester, J.M., Wing, M.R., Li, J., Palmer, N.D., Xu, J., Hicks, P.J., . . . Ng, M.C. Implication of European-derived adiposity loci in African Americans. *Int J Obes (Lond)* **36**, 465-473 (2012).
74. Bochukova, E.G., Huang, N., Keogh, J., Henning, E., Purmann, C., Blaszczyk, K., . . . Farooqi, I.S. Large, rare chromosomal deletions associated with severe early-onset obesity. *Nature* **463**, 666-670 (2010).
75. Ren, D., Zhou, Y., Morris, D., Li, M., Li, Z. & Rui, L. Neuronal SH2B1 is essential for controlling energy and glucose homeostasis. *J. Clin. Invest.* **117**, 397-406 (2007).

76. Jiang, L., Su, H., Keogh, J.M., Chen, Z., Henning, E., Wilkinson, P., . . . Rui, L. Neural deletion of Sh2b1 results in brain growth retardation and reactive aggression. *FASEB J* **32**, 1830-1840 (2018).
77. Ohtsuka, S., Takaki, S., Iseki, M., Miyoshi, K., Nakagata, N., Kataoka, Y., . . . Yoshimura, A. SH2-B is required for both male and female reproduction. *Mol. Cell. Biol.* **22**, 3066-3077 (2002).
78. Duan, C., Yang, H., White, M.F. & Rui, L. Disruption of SH2-B causes age-dependent insulin resistance and glucose intolerance. *Mol. Cell. Biol.* **24**, 7435-7443 (2004).
79. Jiang, L., Su, H., Wu, X., Shen, H., Kim, M.-H., Li, Y., . . . Rui, L. Leptin receptor-expressing neuron Sh2b1 supports sympathetic nervous system and protects against obesity and metabolic disease. *Nature communications* **11**, 1-13 (2020).
80. Qian, X., Riccio, A., Zhang, Y. & Ginty, D.D. Identification and characterization of novel substrates of Trk receptors in developing neurons. *Neuron* **21**, 1017-1029 (1998).
81. Rui, L., Herrington, J. & Carter-Su, C. SH2-B, a membrane-associated adapter, is phosphorylated on multiple serines/threonines in response to nerve growth factor by kinases within the MEK/ERK cascade. *J. Biol. Chem.* **274**, 26485-26492 (1999).
82. Zhang, Y., Zhu, W., Wang, Y.G., Liu, X.J., Jiao, L., Liu, X., . . . He, C. Interaction of SH2-Bβ with RET is involved in signaling of GDNF-induced neurite outgrowth. *J. Cell. Sci.* **119**, 1666-1676 (2006).
83. Nelms, K., O'Neill, T.J., Li, S., Hubbard, S.R., Gustafson, T.A. & Paul, W.E. Alternative splicing, gene localization, and binding of SH2-B to the insulin receptor kinase domain. *Mammalian Genome* **10**, 1160-1167 (1999).
84. Wang, J. & Riedel, H. Insulin-like growth factor-I receptor and insulin receptor association with a Src homology-2 domain-containing putative adapter. *J. Biol. Chem.* **273**, 3136-3139 (1998).
85. Rui, L. & Carter-Su, C. Platelet-derived growth factor (PDGF) stimulates the association of SH2-Bβ with PDGF receptor and phosphorylation of SH2-Bβ. *J. Biol. Chem.* **273**, 21239-21245 (1998).
86. Kong, M., Wang, C.S. & Donoghue, D.J. Interaction of fibroblast growth factor receptor 3 and the adapter protein SH2-B. *J. Biol. Chem.* **277**, 15962-15970 (2002).
87. O'Brien, K.B., O'Shea, J.J. & Carter-Su, C. SH2-B family members differentially regulate JAK family tyrosine kinases. *J. Biol. Chem.* **277**, 8673-8681 (2002).
88. Kurzer, J.H., Argetsinger, L.S., Zhou, Y.-J., Kouadio, J.-L., O'Shea, J.J. & Carter-Su, C. Tyrosine 813 is a site of JAK2 autophosphorylation critical for activation of JAK2 by SH2-Bβ. *Mol. Cell. Biol.* **24**, 4557-4570 (2004).
89. Kurzer, J.H., Saharinen, P., Silvennoinen, O. & Carter-Su, C. Binding of SH2-B family members within a potential negative regulatory region maintains JAK2 in an active state. *Mol. Cell. Biol.* **26**, 6381-6394 (2006).
90. Morris, D.L. & Rui, L. Recent advances in understanding leptin signaling and leptin resistance. *Am. J. Physiol. Endocrinol. Metab.* **297**, E1247-E1259 (2009).
91. Duan, C., Li, M. & Rui, L. SH2-B promotes insulin receptor substrate 1 (IRS1)- and IRS2-mediated activation of the phosphatidylinositol 3-kinase pathway in response to leptin. *J. Biol. Chem.* **279**, 43684-43691 (2004).

92. Dodd, G.T. & Tiganis, T. Insulin action in the brain: Roles in energy and glucose homeostasis. *Journal of neuroendocrinology* **29**(2017).
93. Kotani, K., Wilden, P. & Pillay, T.S. SH2-Bα is an insulin-receptor adapter protein and substrate that interacts with the activation loop of the insulin-receptor kinase. *Biochem. J.* **335**, 103-109 (1998).
94. Hu, J. & Hubbard, S.R. Structural basis for phosphotyrosine recognition by the Src homology-2 domains of the adapter proteins SH2-B and APS. *J. Mol. Biol.* **361**, 69-79 (2006).
95. Zhang, M., Deng, Y., Tandon, R., Bai, C. & Riedel, H. Essential role of PSM/SH2-B variants in insulin receptor catalytic activation and the resulting cellular responses. *J. Cell. Biochem.* **103**, 162-181 (2008).
96. Morris, D.L., Cho, K.W., Zhou, Y. & Rui, L. SH2B1 enhances insulin sensitivity by both stimulating the insulin receptor and inhibiting tyrosine dephosphorylation of insulin receptor substrate proteins. *Diabetes* **58**, 2039-2047 (2009).
97. Ahmed, Z. & Pillay, T.S. Adapter protein with a pleckstrin homology (PH) and an Src homology 2 (SH2) domain (APS) and SH2-B enhance insulin-receptor autophosphorylation, extracellular-signal-regulated kinase and phosphoinositide 3-kinase-dependent signalling. *Biochem. J.* **371**, 405-412 (2003).
98. Rui, L., Herrington, J. & Carter-Su, C. SH2-B is required for nerve growth factor-induced neuronal differentiation. *J. Biol. Chem.* **274**, 10590-10594 (1999).
99. Koch, A., Mancini, A., Stefan, M., Niedenthal, R., Niemann, H. & Tamura, T. Direct interaction of nerve growth factor receptor, TrkA, with non-receptor tyrosine kinase, c-Abl, through the activation loop. *FEBS Lett.* **469**, 72-76 (2000).
100. Suzuki, K., Mizutani, M., Hitomi, Y., Kizaki, T., Ohno, H., Ishida, H., . . . Koizumi, S. Association of SH2-B to phosphorylated tyrosine residues in the activation loop of TrkB. *Res. Commun. Mol. Pathol. Pharmacol.* **111**, 27-39 (2002).
101. Shih, C.H., Chen, C.J. & Chen, L. New function of the adaptor protein SH2B1 in brain-derived neurotrophic factor-induced neurite outgrowth. *PloS one* **8**, e79619 (2013).
102. Wang, X., Chen, L., Maures, T.J., Herrington, J. & Carter-Su, C. SH2-B is a positive regulator of nerve growth factor-mediated activation of the Akt/Forkhead pathway in PC12 cells. *J. Biol. Chem.* **279**, 133-141 (2004).
103. Wang, T.C., Chiu, H., Chang, Y.J., Hsu, T.Y., Chiu, I.M. & Chen, L. The adaptor protein SH2B3 (Lnk) negatively regulates neurite outgrowth of PC12 cells and cortical neurons. *PloS one* **6**, e26433 (2011).
104. Lin, L.F., Doherty, D.H., Lile, J.D., Bektesh, S. & Collins, F. GDNF: a glial cell line-derived neurotrophic factor for midbrain dopaminergic neurons. *Science* **260**, 1130-1132 (1993).
105. Treanor, J.J., Goodman, L., de Sauvage, F., Stone, D.M., Poulsen, K.T., Beck, C.D., . . . Rosenthal, A. Characterization of a multicomponent receptor for GDNF. *Nature* **382**, 80-83 (1996).
106. Trupp, M., Arenas, E., Fainzilber, M., Nilsson, A.S., Sieber, B.A., Grigoriou, M., . . . Arumae, U. Functional receptor for GDNF encoded by the c-ret proto-oncogene. *Nature* **381**, 785-789 (1996).

107. Donatello, S., Fiorino, A., Degl'Innocenti, D., Alberti, L., Miranda, C., Gorla, L., . . . Borrello, M.G. SH2B1β adaptor is a key enhancer of RET tyrosine kinase signaling. *Oncogene* **26**, 6546-6559 (2007).
108. Zhang, M., Deng, Y. & Riedel, H. PSM/SH2B1 splice variants: critical role in src catalytic activation and the resulting STAT3s-mediated mitogenic response. *J. Cell. Biochem.* **104**, 105-118 (2008).
109. Yang, P., Whelan, R.J., Mao, Y., Lee, A.W., Carter-Su, C. & Kennedy, R.T. Multiplexed detection of protein-peptide interaction and inhibition using capillary electrophoresis. *Anal. Chem.* **79**, 1690-1695 (2007).
110. Osborne, M.A., Dalton, S. & Kochan, J.P. The Yeast Tribrid System - Genetic Detection of *trans*-phosphorylated ITAM-SH2-Interactions. *BioTechnology* **13**, 1474-1478 (1995).
111. Myers Jr., M.G. & Olson, D.P. Central nervous system control of metabolism. *Nature* **491**, 357-363 (2012).
112. Greene, L.A. & Tischler, A.S. Establishment of a noradrenergic clonal line of rat adrenal pheochromocytoma cells which respond to nerve growth factor. *Proc. Nat. Acad. Sci. USA* **73**, 2424-2428 (1976).
113. Klein, R., Jing, S., Nanduri, V., O-Rourke, E. & Barbacid, M. The trk proto-oncogene encodes a receptor for nerve growth factor. *Cell* **65**, 189-197 (1991).
114. Loeb, D.M., Maragos, J., Martin-Zanca, D., Chao, M.V., Parada, L.F. & Greene, L.A. The *trk* proto-oncogene rescues NGF responsiveness in mutant NGF-nonresponsive PC12 cell lines. *Cell* **66**, 961-966 (1991).
115. Kaplan, D.R., Hempstead, B., Martin-Zanca, D., Chao, M. & Parada, L.F. The *trk* proto-oncogene product: a signal transducing receptor for nerve growth factor. *Science* **252**, 554-558 (1991).
116. Zhou, T., Xu, B., Que, H., Lin, Q., Lv, S. & Liu, S. Neurons derived from PC12 cells have the potential to develop synapses with primary neurons from rat cortex. *Acta Neurobiol. Exp. (Wars)* **66**, 105-112 (2006).
117. Fujita, K., Lazarovici, P. & Guroff, G. Regulation of the differentiation of PC12 pheochromocytoma cells. *Environ. Health Perspect.* **80**, 127-142 (1989).
118. Chen, C.J., Shih, C.H., Chang, Y.J., Hong, S.J., Li, T.N., Wang, L.H. & Chen, L. SH2B1 and IRSp53 proteins promote the formation of dendrites and dendritic branches. *J Biol Chem* **290**, 6010-6021 (2015).
119. Chen, L., Maures, T.J., Jin, H., Huo, J.S., Rabbani, S.A., Schwartz, J. & Carter-Su, C. SH2B1β (SH2-Bβ) enhances expression of a subset of nerve growth factor-regulated genes important for neuronal differentiation including genes encoding uPAR and MMP3/10. *Mol. Endocrinol.* **22**, 454-476 (2008).
120. Basbaum, C.B. & Werb, Z. Focalized proteolysis: spatial and temporal regulation of extracellular matrix degradation at the cell surface. *Curr. Opin. Cell Biol.* **8**, 731-738 (1996).
121. Ossowski, L. & Aguirre-Ghiso, J.A. Urokinase receptor and integrin partnership: coordination of signaling for cell adhesion, migration and growth. *Curr. Opin. Cell Biol.* **12**, 613-620 (2000).
122. Nagappan-Chettiar, S., Johnson-Venkatesh, E.M. & Umemori, H. Activity-dependent proteolytic cleavage of cell adhesion molecules regulates excitatory synaptic development and function. *Neurosci Res* **116**, 60-69 (2017).

123. Sonderegger, P. & Matsumoto-Miyai, K. Activity-controlled proteolytic cleavage at the synapse. *Trends in neurosciences* **37**, 413-423 (2014).
124. Wiera, G., Lebida, K., Lech, A.M., Brzdak, P., Van Hove, I., De Groef, L., . . . Mozrzymas, J.W. Long-term plasticity of inhibitory synapses in the hippocampus and spatial learning depends on matrix metalloproteinase 3. *Cell Mol Life Sci* (2020).
125. Yap, E.L. & Greenberg, M.E. Activity-Regulated Transcription: Bridging the Gap between Neural Activity and Behavior. *Neuron* **100**, 330-348 (2018).
126. West, A.E. & Greenberg, M.E. Neuronal activity-regulated gene transcription in synapse development and cognitive function. *Cold Spring Harb Perspect Biol* **3**(2011).
127. Menon, S. & Gupton, S. Recent advances in branching mechanisms underlying neuronal morphogenesis. *F1000Res* **7**(2018).
128. Herrington, J., Diakonova, M., Rui, L., Gunter, D.R. & Carter-Su, C. SH2-B is required for growth hormone-induced actin reorganization. *J. Biol. Chem.* **275**, 13126-13133 (2000).
129. Diakonova, M., Gunter, D.R., Herrington, J. & Carter-Su, C. SH2-Bβ is a Rac-binding protein that regulates cell motility. *J. Biol. Chem.* **277**, 10669-10677 (2002).
130. Lanning, N.J., Su, H.W., Argetsinger, L.S. & Carter-Su, C. Identification of SH2B1β as a focal adhesion protein that regulates focal adhesion size and number. *J. Cell Sci.* **124**, 3095-3105 (2011).
131. Lim, R.W. & Halpain, S. Regulated association of microtubule-associated protein 2 (MAP2) with Src and Grb2: evidence for MAP2 as a scaffolding protein. *J Biol Chem* **275**, 20578-20587 (2000).
132. Reynolds, C.H., Garwood, C.J., Wray, S., Price, C., Kellie, S., Perera, T., . . . Anderton, B.H. Phosphorylation regulates tau interactions with Src homology 3 domains of phosphatidylinositol 3-kinase, phospholipase Cgamma1, Grb2, and Src family kinases. *J Biol Chem* **283**, 18177-18186 (2008).
133. Rider, L., Tao, J., Snyder, S., Brinley, B., Lu, J. & Diakonova, M. Adapter protein SH2B1β cross-links actin filaments and regulates actin cytoskeleton. *Mol. Endocrinol.* **23**, 1065-1076 (2009).
134. Rider, L. & Diakonova, M. Adapter protein SH2B1β binds filamin A to regulate prolactin-dependent cytoskeletal reorganization and cell motility. *Mol. Endocrinol.* **25**, 1231-1243 (2011).

Chapter 2:

Deletion of the Brain-Specific α and δ Isoforms of Adapter Protein SH2B1 Protect Mice from Obesity

Abstract

Mice lacking SH2B1 and humans with inactivating mutations of SH2B1 display severe obesity and insulin resistance. SH2B1 is an adapter protein that is recruited to the receptors of multiple hormones and neurotrophic factors. Of the four known alternatively-spliced SH2B1 isoforms, SH2B1β and SH2B1γ exhibit ubiquitous expression, whereas SH2B1α and SH2B1δ are essentially restricted to the brain. To understand the roles for SH2B1α and SH2B1δ in energy balance and glucose metabolism, we generated mice lacking these brain-specific isoforms (αδKO mice). αδKO mice exhibit decreased food intake, protection from weight gain on standard and high fat diets, and an adiposity-dependent improvement in glucose homeostasis. SH2B1 has been suggested to impact energy balance via the modulation of leptin action. However, αδKO mice exhibit leptin sensitivity that is similar to that of wild-type mice by multiple measures. Thus, decreasing the abundance of SH2B1α and/or SH2B1δ relative to the other SH2B1 isoforms likely shifts energy balance towards a lean phenotype via a primarily leptin-independent

mechanism. Our findings suggest that the different alternatively-spliced isoforms of SH2B1 perform different functions *in vivo*.

Note: This chapter has been published in *Diabetes* (2021; 70 (2): 400-414) as “Deletion of the Brain-Specific α and δ Isoforms of Adapter Protein SH2B1 Protects Mice from Obesity” by Jessica L. Cote, Lawrence S. Argetsinger, Anabel Flores, Alan C. Rupp, Joel M. Cline, Lauren C. DeSantis, Alexander H. Bedard, Devika P. Bagchi, Paul B. Vander, Abrielle M., Cacciaglia, Erik S. Clutter, Gowri Chandrashekar, Ormond A. MacDougald, Martin G. Myers Jr., and Christin Carter-Su.

https://doi.org/10.2337/db20-0687.

Introduction

Human mutations in *SH2B1* are associated with severe, early-onset obesity, hyperphagia, and often disproportionately high insulin resistance [1-3]. Similarly, mice null for *Sh2b1* (*Sh2b1* KO mice) exhibit hyperphagic obesity and impaired glucose homeostasis [4,5]. Reintroduction of SH2B1β into neurons in *Sh2b1* KO mice largely restores normal body weight and glucose homeostasis [6], suggesting the importance of neuronal SH2B1 for metabolic control. SH2B1 is an adapter protein that regulates responses to multiple hormones and neurotrophic factors that regulate the nervous system. For example, SH2B1 binds to and modulates the activity of the tyrosine kinase JAK2, which forms a complex with several cytokine family receptors including the leptin receptor (LepRb). SH2B1 also binds to and modulates actions of the insulin receptor; TrkA and TrkB, receptors for nerve growth factor (NGF) and brain-derived neurotrophic factor (BDNF) respectively; and RET, a co-receptor for glial cell line-derived neurotrophic factor (GDNF) and growth/differentiation factor-15 (GDF-15) [7,8]. When activated, these kinases recruit SH2B1 via its SH2 domain. SH2B1 then facilitates a variety of cellular responses, including changes in the actin cytoskeleton and gene expression [9-11]. Consistent with SH2B1's involvement in neurotrophic factor signaling and energy balance and the importance of neurons for appetite control, SH2B1 promotes outgrowth of dendrites and/or axons of cultured primary neurons [12-14] and neurite outgrowth and neuron-specific gene expression in PC12 cells [9,15,16]. Hence, SH2B1 influences both structural and functional aspects of the nervous system.

Previous work suggests that SH2B1 contributes to energy balance by modulating LepRb/JAK2 activity [7]. Leptin, secreted primarily from white adipose tissue (WAT) in

approximate proportion to triacylglycerol content, signals the repletion of energy stores to the brain [17]. Normal leptin concentrations indicate an adequate fat supply and thus suppress hunger and allow for energy use; conversely, low leptin levels signal low fat stores and thus increase hunger and conserve existing energy stores [17]. Consistent with SH2B1 enhancing leptin signaling, *Sh2b1* KO mice exhibit reduced leptin-induced inhibition of food intake and weight gain and dysregulated control of hypothalamic leptin-sensitive gene expression [4,6].

Alternative splicing yields four previously-described SH2B1 isoforms—α, β, γ, and δ—which differ only in their C-terminal tails (Fig. 2.1A-B). In humans, SH2B1β and γ are expressed ubiquitously, whereas SH2B1α and δ are restricted almost exclusively to the brain [1]. *In vitro* studies indicate that some SH2B1 isoforms possess unique cellular properties. For example, while SH2B1β and γ promote neurite outgrowth in PC12 cells [9,15,16], SH2B1α does not, and even inhibits the ability of SH2B1β to do so [2,18]. However, before this work, functions of the various SH2B1 isoforms had not been assessed *in vivo.* Because both SH2B1α and δ exhibit the unique characteristic of being expressed almost exclusively in the brain, the central regulator of metabolism, we investigated the combined contributions of these two brain-specific SH2B1 isoforms to energy balance and glucose homeostasis. Our results not only suggest that SH2B1α and/or δ are critical regulators of body weight, but also that the different alternatively-spliced SH2B1 isoforms perform different functions *in vivo.*

Materials and Methods

Animal care

Mice were housed in ventilated cages (~22°C) on a 12-hour light/dark cycle (~6_{AM}-6_{PM}) in a pathogen-free animal facility at the University of Michigan. Food and water were available *ad libitum* except as noted. Experimental mice were fed a standard chow (9% fat, #5058; LabDiet) or a high fat diet (HFD) (60% fat, #D1249; Research Diets). Experiments were approved by the University of Michigan Institutional Animal Care & Use Committee.

Mouse model, genotyping, and breeding

CRISPR/Cas9 editing was used to delete regions in *Sh2b1* required for expression of SH2B1α and δ (*Sh2b1*$^{DEL\alpha\delta}$). RNA guides were selected as described previously [19]. A 4 kb donor template was designed to juxtapose exon 9 of *Sh2b1*, the sequence in exon 10 that contains the β/γ stop codons, and the region of exon 10 downstream of the α stop codon (Fig. 2.1B). Each guide/donor package was injected into C57BL/6J x SJL F2 oocytes, which were implanted into C57BL/6J x SJL F2 mice (University of Michigan Transgenic Animal Model Core). Founders were backcrossed against C57BL/6J mice. See details in Supplemental Material.

Genomic DNA was isolated from tails prior to weaning and diagnostic fragments were amplified by PCR using Taq polymerase and two primer sets (Supplementary Material Table 2.1). *Sh2b1*$^{DEL\alpha\delta/+}$ ($\alpha\delta$HET) mice were backcrossed to C57BL/6J mice for

3-5 generations. Non-sibling αδHET mice were bred to produce experimental mice. Experimenters were blind to genotypes. Mice were re-genotyped after harvest.

Body weight, food intake, body composition, and energy expenditure

Body weight was assessed weekly. Food intake was monitored once or twice weekly (details in Supplemental Material). Body composition was measured using NMR (Minispec LF90II; Bruker Scientific). Oxygen consumption (VO_2), carbon dioxide production (VCO_2), and spontaneous locomotor activity were monitored by the Comprehensive Lab Animal Monitoring System (CLAMS; Columbus Instruments) (Michigan Mouse Metabolic Phenotyping Center) as described previously [3].

Blood samples

Blood was collected between 9_{AM} and 11_{AM} (glucose, insulin) or 10_{AM} and 2_{PM} (leptin). Glucose levels were measured via tail-vein bleeding and Bayer Contour glucometer. Insulin and leptin levels in tail-vein blood or terminal trunk blood were measured using Crystal Chem ELISA kits for Mouse Insulin (#90080) or Leptin (#90030).

Glucose and insulin tolerance tests

Mice were subjected to a 5-to-6-hour morning fast followed by intraperitoneal (i.p.) injection of D-glucose or human insulin. Blood glucose levels were measured as described above.

Leptin sensitivity

Mice were i.p. injected twice daily (6_{AM}, 6_{PM}) with vehicle (PBS, pH 7.4) (days 1-3, 7-8) or recombinant mouse leptin (days 4-6).

Tissue harvest and histology

Mice were anesthetized by isoflurane between 10_{AM} and 2_{PM}, decapitated, and terminal blood was collected. Tissues were dissected, weighed, and fixed in 10% neutral buffered formalin and stored (4°C) for histology, or cryopreserved in liquid nitrogen and stored (-80°C) for RNA or protein extraction. Hypothalami (3 mm cubes) were dissected from the ventral diencephalon immediately caudal to the optic chiasm using a coronal brain matrix. Other brain sections were dissected under a dissecting microscope. Fixed liver tissue was paraffin-embedded, sectioned (5 μm thickness), stained with hematoxylin & eosin, and imaged, as previously described [20].

RNA isolation, PCR, and qPCR

RNA was isolated from frozen tissue using QIAGEN RNeasy Mini Kits (#74104, #74804). RNA was reverse-transcribed into cDNA using TaqMan Reverse Transcription Reagents (Fig. 2.1E) or iScript cDNA Synthesis Kit (Figs. 2.1C, 2.7A and Supplementary Material Fig. 2.12A). Taq polymerase was then used for PCR reactions in Fig. 2.1E (primers listed in Supplementary Material Table 2.2). Relative mRNA levels of *Sh2b1* isoforms and leptin-regulated genes were determined using TaqMan Gene Expression Assays (details in Supplementary Material Table 2.3 and Supplementary Material).

RNA-seq

RNA samples had integrity numbers ≥ 7.5. cDNA library preparation and sequencing were performed by the University of Michigan DNA Sequencing Core. See Supplemental Material for details of preparation and analyses.

Plasmids

cDNAs encoding mouse GFP-SH2B1α (GenBank accession #AF421138) [18] and rat GFP-SH2B1β (accession #NM_001048180) [15] were described previously. cDNA encoding mouse GFP-SH2B18c was created from cDNA encoding mouse GFP-SH2B1γ (accession #NM_011363.3) (details in Supplemental Material).

PC12 cell neurite outgrowth assay

PC12 cells (ATCC) were grown and treated and neurite outgrowth experiments were completed as described previously [18] with modifications described in Supplemental Material.

Immunoblotting

Frozen tissues were lysed and homogenized using a glass Dounce homogenizer containing lysis buffer, described previously [3]. PC12 cells were transfected and lysed as described previously [18]. Equal amounts of protein were immunoblotted with antibody to SH2B1 (#sc-136065; Santa Cruz), β-tubulin (#sc-55529; Santa Cruz), or ERK1/2 (#4695S; Cell Signaling) as described previously [3] with modifications in Supplemental

Material. Expression levels of SH2B1 isoforms in Fig. 2.1I were quantified using Li-Cor Image Studio Lite (version 5.2.5).

Statistics for phenotyping data

Statistics were performed using GraphPad Prism or the R programming language with CalR [21], a custom package for analysis of indirect calorimetry using analysis of covariance (ANCOVA). Body weights were compared by two-way repeated measures ANOVA with Dunnett's or Sidak's multiple comparisons tests. Cumulative food intake was analyzed by linear regression. All other comparisons were analyzed by one-way ANOVA with Dunnett's multiple comparisons test or two-tailed Student's t-test. $P < 0.05$ was considered significant.

Data and Resource Availability

The data generated during this study are available in the GEO repository, GSE145202, or available from the corresponding author upon reasonable request. The mouse model generated during this study is available from the corresponding author upon reasonable request.

Results

Generation of mice lacking SH2B1α and δ

Exon skipping and an alternative donor site produce four *Sh2b1* splice variants (Fig. 2.1B) [22,23]. Consistent with the human tissue expression profile of *SH2B1* mRNA [1], we detected substantial *Sh2b1*α and δ mRNA in mouse brain tissue, including hypothalamus, cortex, and cerebellum, but little to none in peripheral tissues including gonadal WAT (gWAT), liver, and testes; all of these tissues contained *Sh2b1*β and γ mRNA (Fig. 2.1C).

To gain insight into the importance of *Sh2b1* splicing in the brain and the contributions of the brain-specific SH2B1α and δ isoforms to metabolism *in vivo*, we used CRISPR/Cas9 to generate mice lacking SH2B1α/δ (Fig. 2.1B). Genotyping (Fig. 2.1D) and DNA sequencing (data not shown) of founder animals and their progeny identified mice containing correctly-edited *Sh2b1*$^{DEL\alpha\delta}$ alleles. αδHET intercrosses produced pups with *Sh2b1* genotypes at the expected Mendelian ratio (data not shown). PCR confirmed the absence of *Sh2b1*δ mRNA in brain tissue from *Sh2b1*$^{DEL\alpha\delta\,/\,DEL\alpha\delta}$ (αδKO) mice (Fig. 2.1E). Additionally, RNA-seq confirmed the absence of *Sh2b1*α/δ transcripts in αδKO hypothalami and the presence of similar levels of *Sh2b1*β/γ transcripts in *Sh2b1*$^{+/+}$ (wild-type, WT) and αδKO hypothalami (Fig. 2.1F). We confirmed the absence of SH2B1α/δ proteins, and the continued presence of SH2B1β/γ proteins, in αδKO brain lysates (Fig. 2.1G). As expected, only β/γ isoforms were detected in liver tissue from WT and αδKO mice (Fig. 2.1H). SH2B1β/γ protein levels were similar between WT and αδKO mice in liver tissue (Fig. 2.1H) and between WT, αδKO, and αδHET mice in brain tissue (Fig.

2.1G, 2.1I), whereas SH2B1α/δ protein levels were decreased by about 40% in αδHET compared to WT brain lysates (Fig. 2.1I). Thus, αδKO mice exhibit the predicted isoform-specific ablation of SH2B1α/δ, and αδHET mice exhibit reduced SH2B1α/δ, without compensatory alterations in expression of SH2B1β/γ isoforms.

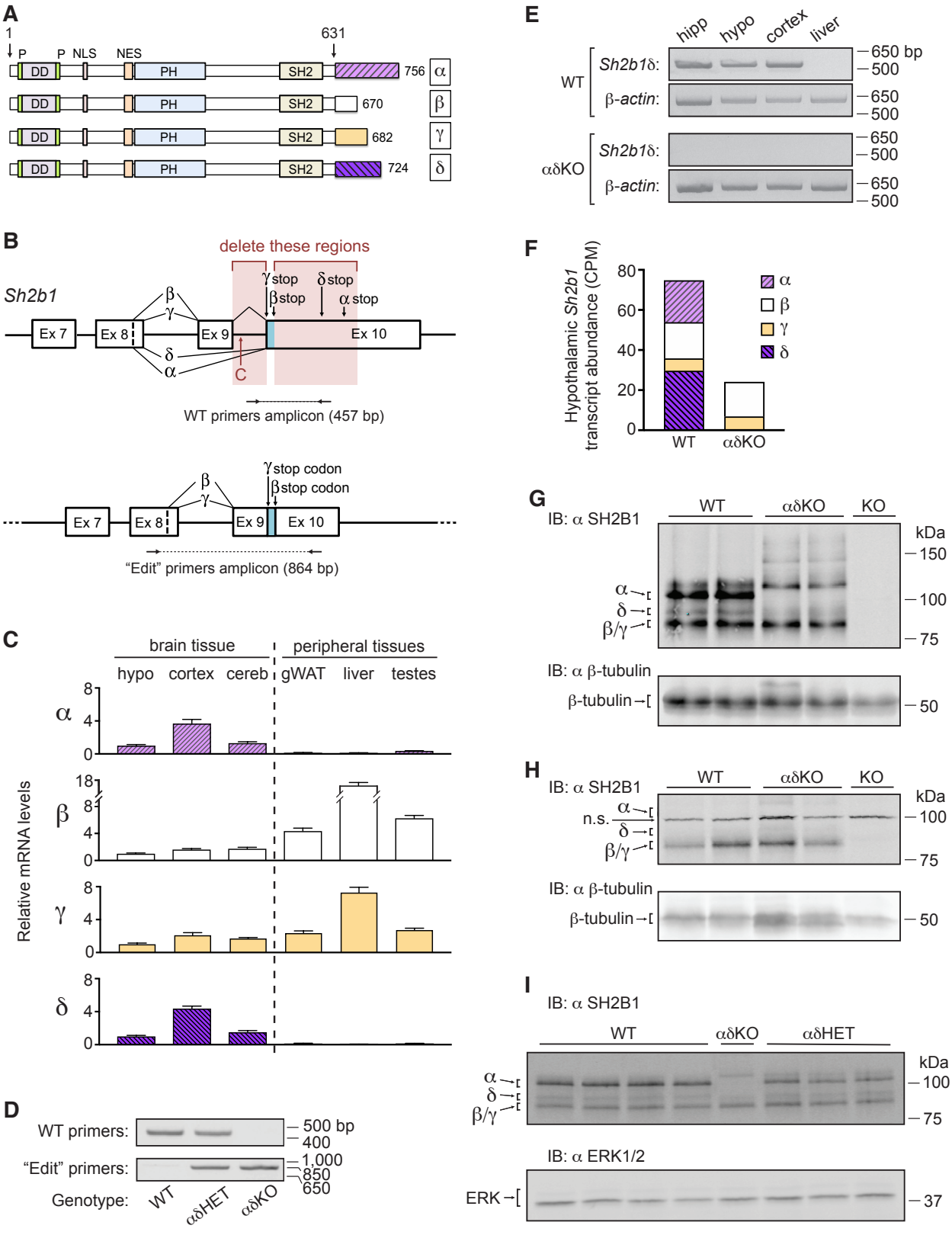
A
1
631
P
P NLS
NES
DD
PH
SH2
756 α
670 β
682 γ
724 δ
B
delete these regions
Sh2b1
γ stop
δ stop
β stop
α stop
Ex 7
Ex 8
Ex 9
Ex 10
C
WT primers amplicon (457 bp)
γ stop codon
β stop codon
"Edit" primers amplicon (864 bp)
C
brain tissue
peripheral tissues
hypo cortex cereb gWAT liver testes
Relative mRNA levels
D
WT primers:
"Edit" primers:
Genotype:
WT
αδHET
αδKO
500 bp
400
1,000
850
650
E
hipp hypo cortex liver
WT
Sh2b1δ:
β-actin:
αδKO
650 bp
500
F
Hypothalamic Sh2b1 transcript abundance (CPM)
WT
αδKO
G
IB: α SH2B1
WT
αδKO
KO
kDa
150
100
75
IB: α β-tubulin
β-tubulin
50
H
IB: α SH2B1
n.s.
IB: α β-tubulin
I
IB: α SH2B1
WT
αδKO
αδHET
IB: α ERK1/2
ERK
37

Figure 2.1. Generation and validation of αδKO mouse model

(A) Schematic of SH2B1α, β, γ, and δ. Isoform-specific C-terminal tails are noted in light purple (diagonally striped), white, yellow, and dark purple (diagonally striped), respectively. Numbers indicate amino acids in mouse and human sequences. P, proline-rich domain; DD, dimerization domain; NLS, nuclear localization sequence; NES, nuclear export sequence; PH, pleckstrin homology domain; SH2, Src homology 2 domain. **(B)** Top: Schematic shows strategy for deletion of SH2B1α and δ within the region of *Sh2b1* that produces the four alternative splice variants. The pink-shaded regions were targeted for deletion whereas the blue-shaded segment was retained. Stop codons are labeled "stop". Cas9 cut site is indicated by "C". Locations of WT genotyping primers are indicated by horizontal arrows beneath the schematic. Bottom: Schematic depicts donor template for homology-directed repair. Locations of "edit" genotyping primers are indicated by horizontal arrows beneath the schematic. Ex, exon. **(C)** RNA was isolated from brain and peripheral tissues of 10-to-12-week-old male WT mice fed standard chow. Transcript levels for *Sh2b1*α, β, γ, and δ were measured by qPCR (n = 4-8 mice/tissue type/isoform). For each isoform, tissue expression levels were normalized to expression in the hypothalamus. Hypo, hypothalamus; cereb, cerebellum; gWAT, gonadal white adipose tissue. **(D)** Genomic DNA was purified and analyzed by PCR using WT and "edit" primers. The migration of DNA standards is shown on the right. Bp, base pair. **(E)** RNA was isolated from brain and liver of WT and αδKO adult male mice and assessed in the same gel for the presence of *Sh2b1*δ or β-*actin* (control). The migration of DNA standards is shown on the right. Hipp, hippocampus; hypo, hypothalamus; bp, base pair. **(F)** RNA was isolated from hypothalami of 10-to-12-week-old male mice and analyzed by RNA-seq. Transcript abundance of *Sh2b1*α, β, γ, and δ was predicted by StringTie analysis using both annotated and previously unannotated transcripts (n: WT = 9; αδKO = 12). Proteins in **(G)** whole brain and **(H)** liver tissue lysates from WT, αδKO, and *Sh2b1* KO adult male mice were immunoblotted with antibody to SH2B1 (α SH2B1) or to β-tubulin (α β-tubulin). The migration of molecular weight standards is shown on the right. The expected migration of the different isoforms (and in **H**, a non-specific band) is indicated on the left. (**I**) Proteins in whole brain lysates from WT, αδKO, and αδHET 10-to-12-week-old female mice were immunoblotted with antibody to SH2B1 (α SH2B1) or to ERK1/2 (α ERK1/2). The migration of molecular weight standards is shown on the right. The expected migration of the different isoforms is indicated on the left. IB, immunoblot; kDa, kilodaltons; n.s., non-specific band. Data are means ± SEM.

Reduced SH2B1α and δ decreases body weight and adiposity in mice

To determine whether SH2B1α/δ influence energy balance, we fed male and female αδKO, αδHET, and WT littermates standard chow and measured their body weight weekly. Both male and female αδKO mice appeared thinner and weighed considerably less than WT littermates by 8 weeks of age (males) (Fig. 2.2A-B) or 20 weeks of age (females) (Supplementary Material Fig. 2.9A). Body weight of male and female αδHET mice did not diverge from that of controls before 25 weeks; however, the weight of αδHET males was significantly decreased compared to controls at 38-42 weeks (Fig. 2.2C, Supplementary Material Fig. 2.9B).

While αδKO males exhibited slightly decreased body length and lean mass, these measures were not different from those of sex-matched WT littermates for αδKO females or αδHET mice of either sex (Fig. 2.2D-E, Supplementary Material Fig. 2.9C-D), suggesting that differences in overall body size were unlikely to have mediated the decreased body weight of αδKO mice. Indeed, compared to controls, fat mass was decreased in male and female αδKO and male αδHET mice (Fig. 2.2F, Supplementary Material Fig. 2.9E). Additionally, percent lean mass was increased and percent fat was decreased in αδKO mice of both sexes (Fig. 2.2G-H, Supplementary Material Fig. 2.9F-G). Similarly, leptin concentrations and adipose tissue weights were decreased in αδKO mice of both sexes (Fig. 2.2I-J, Supplementary Material Fig. 2.9H-I). Thus, while body length was slightly decreased in αδKO males compared to controls, the major effect across sexes was of decreased adiposity in αδKO mice. αδKO liver weight was also decreased compared to controls, which may reflect a decrease in triacylglycerol content

(as for animals on HFD, see below) because the mass of other tissues (e.g., brain mass) was unchanged (Fig. 2.2J, Supplementary Material Fig. 2.9I). Furthermore, the decreased body weight and fat mass of αδHET males compared to controls suggests that reduced expression of SH2B1α/δ associated with haploinsufficiency of SH2B1α/δ in males is sufficient to impact body weight and adiposity.

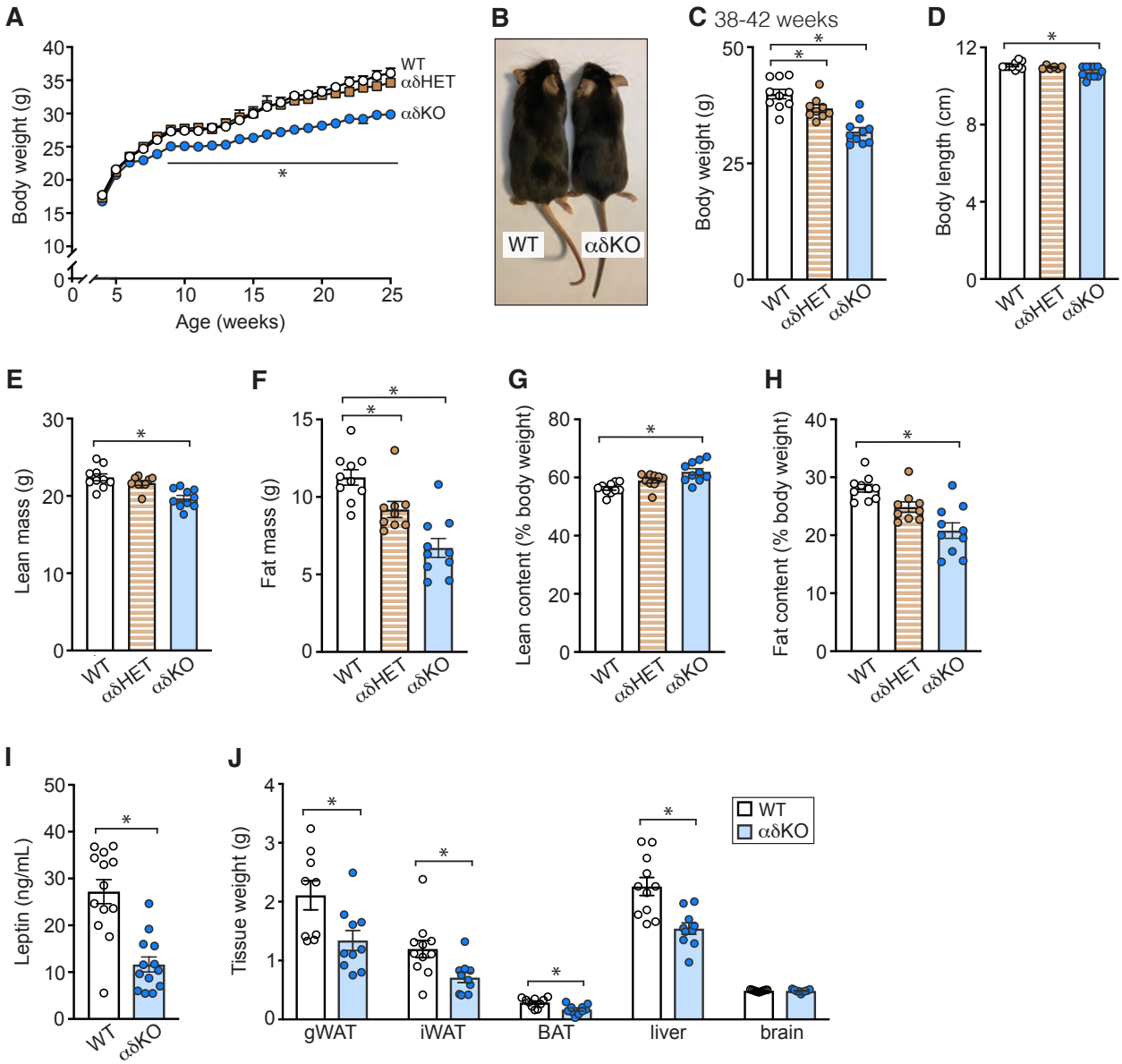
A
Body weight (g)
Age (weeks)
WT
αδHET
αδKO
B
WT
αδKO
C 38-42 weeks
Body weight (g)
D
Body length (cm)
E
Lean mass (g)
F
Fat mass (g)
G
Lean content (% body weight)
H
Fat content (% body weight)
I
Leptin (ng/mL)
J
Tissue weight (g)
gWAT
iWAT
BAT
liver
brain

Figure 2.2. Male αδKO mice fed standard chow exhibit reduced body weight, fat content, circulating leptin levels, adipose tissue weight, and liver weight

Male αδKO mice fed standard chow exhibit reduced body weight, fat content, circulating leptin levels, adipose tissue weight, and liver weight. **(A)** Body weight was measured weekly from 4 to 25 weeks (n: WT = 9-13; αδHET = 8-11; αδKO = 6-10). **(B)** Representative 36-week-old WT and αδKO mice. **(C)** Body weight was measured between 38-42 weeks of age (n: WT = 10; αδHET = 9; αδKO = 10). **(D)** Body length was measured from nose to anus in 38-to-42-week-old mice (n: WT = 10; αδHET = 6; αδKO = 11). **(E-H)** Body composition of 38-to-42-week-old mice was analyzed by NMR between 9_{AM}-11_{AM} (n: WT = 10; αδHET = 9; αδKO = 10). **(I)** Blood was collected from 38-to-42-week-old mice fed *ad libitum*, and serum leptin levels were measured by ELISA (n: WT = 13; αδKO = 13). **(J)** Tissues of 38-to-42-week-old mice were dissected and weighed (n: WT = 9-11; αδKO = 10). gWAT, gonadal white adipose tissue; iWAT, inguinal white adipose tissue; BAT, brown adipose tissue. See Supplementary Material Fig. 2.9 for corresponding data from female mice. **Statistics**: **A**, two-way repeated measures ANOVA (weeks 7 to 25); **C-H**, one-way ANOVA; **I-J**, unpaired, two-tailed Student's t-test. * $P < 0.05$. Data are means ± SEM.

αδKO mice exhibit reduced food intake but normal energy expenditure

To determine whether the decreased body weight of αδKO mice resulted from reduced caloric intake, increased energy expenditure, or both, we measured weekly food intake of αδKO and WT littermates when their body weights were diverging. Male (Fig. 2.3A-B) and female (Supplementary Material Fig. 2.10A) αδKO mice consumed less food than controls. We observed no statistically significant alteration in food intake in αδHET versus control mice, consistent with the minor alteration in their body weight. Metabolic cages revealed no differences by genotype in VO_2, respiratory exchange ratio (RER), or locomotor activity (Fig. 2.3C-F, Supplementary Material Fig. 2.10B-E). There were also no differences by genotype in VO_2, VCO_2, or energy expenditure when body weight, lean mass, or fat mass were taken into account as covariates in the ANCOVA. These data suggest that the decreased weight of chow-fed αδKO mice results primarily from decreased caloric intake.

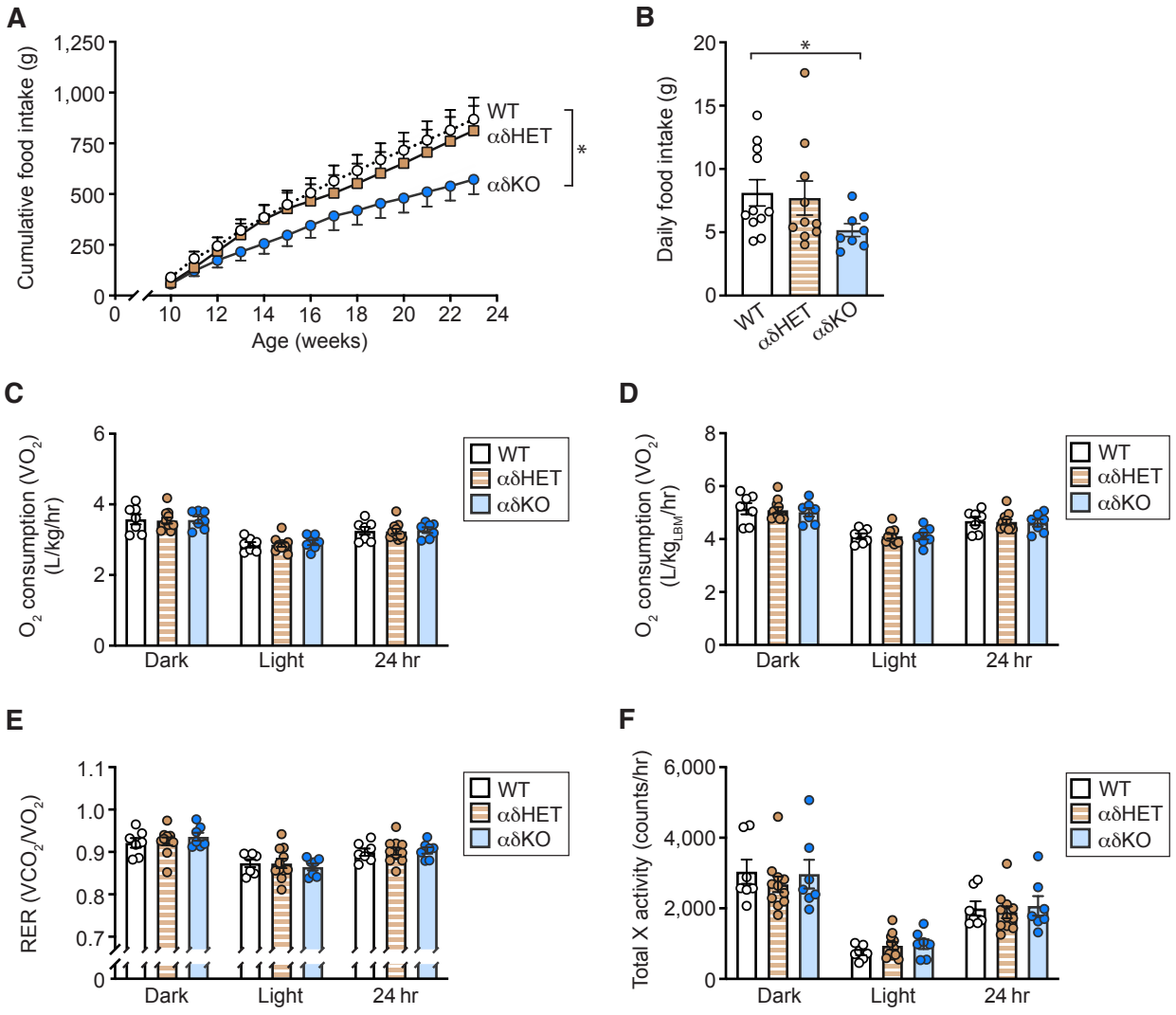
A
Cumulative food intake (g)
1,250
1,000
750
500
250
0
0
10
12
14
16
18
20
22
24
Age (weeks)
WT
αδHET
αδKO
*
B
Daily food intake (g)
20
15
10
5
0
*
WT
αδHET
αδKO
C
O2 consumption (VO2) (L/kg/hr)
6
4
2
0
Dark
Light
24 hr
WT
αδHET
αδKO
D
O2 consumption (VO2) (L/kgLBM/hr)
8
6
4
2
0
Dark
Light
24 hr
WT
αδHET
αδKO
E
RER (VCO2/VO2)
1.1
1.0
0.9
0.8
0.7
0
Dark
Light
24 hr
WT
αδHET
αδKO
F
Total X activity (counts/hr)
6,000
4,000
2,000
0
Dark
Light
24 hr
WT
αδHET
αδKO

Figure 2.3. Male αδKO mice fed standard chow exhibit decreased food consumption but normal energy expenditure

(A) Food intake was measured weekly from 10 to 23 weeks (n: WT = 11; αδHET = 10; αδKO = 8). (**B**) Average daily food intake during final 10 weeks of measurements shown in **A** (n: WT = 11; αδHET = 10; αδKO = 8). **(C-F)** Energy expenditure was measured in 10-to-12-week-old mice by CLAMS (n: WT = 7; αδHET = 11; αδKO = 7). Parameters included: **(C)** oxygen consumption corrected for total body weight or **(D)** lean body mass; **(E)** respiratory exchange ratio (RER); and **(F)** total motor activity in the X dimension. RER was calculated as VCO_2/VO_2. The final 24 hours of recordings are presented. See Supplementary Material Fig. 2.10 for corresponding data from female mice. **Statistics: A**, linear regression analysis (weeks 10 to 23); **B-F**, one-way ANOVA. * $P < 0.05$. Data are means ± SEM.

Protection from diet-induced obesity (DIO) in αδKO mice

To determine whether removal of SH2B1α/δ affords protection from DIO, we challenged αδKO and WT littermates with a HFD. Males were used because of their enhanced susceptibility to DIO relative to females [24,25]. HFD-fed αδKO mice gained significantly less weight than controls (Fig. 2.4A). In fact, their body weight remained near to or below that of chow-fed WT mice for the entire study (compare to Fig. 2.2A). HFD-fed αδKO mice consumed similar amounts of food as controls (Fig. 2.4B-C). The finding that the body weight of HFD-fed αδKO mice was reduced but their food intake was normal suggests that they expended more energy than controls. Body composition measurements revealed that, as for chow-fed mice, the decreased body weight of HFD-fed αδKO mice resulted primarily from decreased fat mass (Fig. 2.4D-G). While leptin levels were highly variable and not significantly different by genotype, they trended lower in αδKO mice (Fig. 2.4H). Similar to chow-fed animals, HFD-fed αδKO mice exhibited reduced weight of inguinal WAT and liver (Fig. 2.4I). Histological analysis of liver tissue detected less lipid in livers of HFD-fed αδKO mice compared to controls, suggesting that decreased steatosis may underlie the lower weight of αδKO livers (Fig. 2.4J).

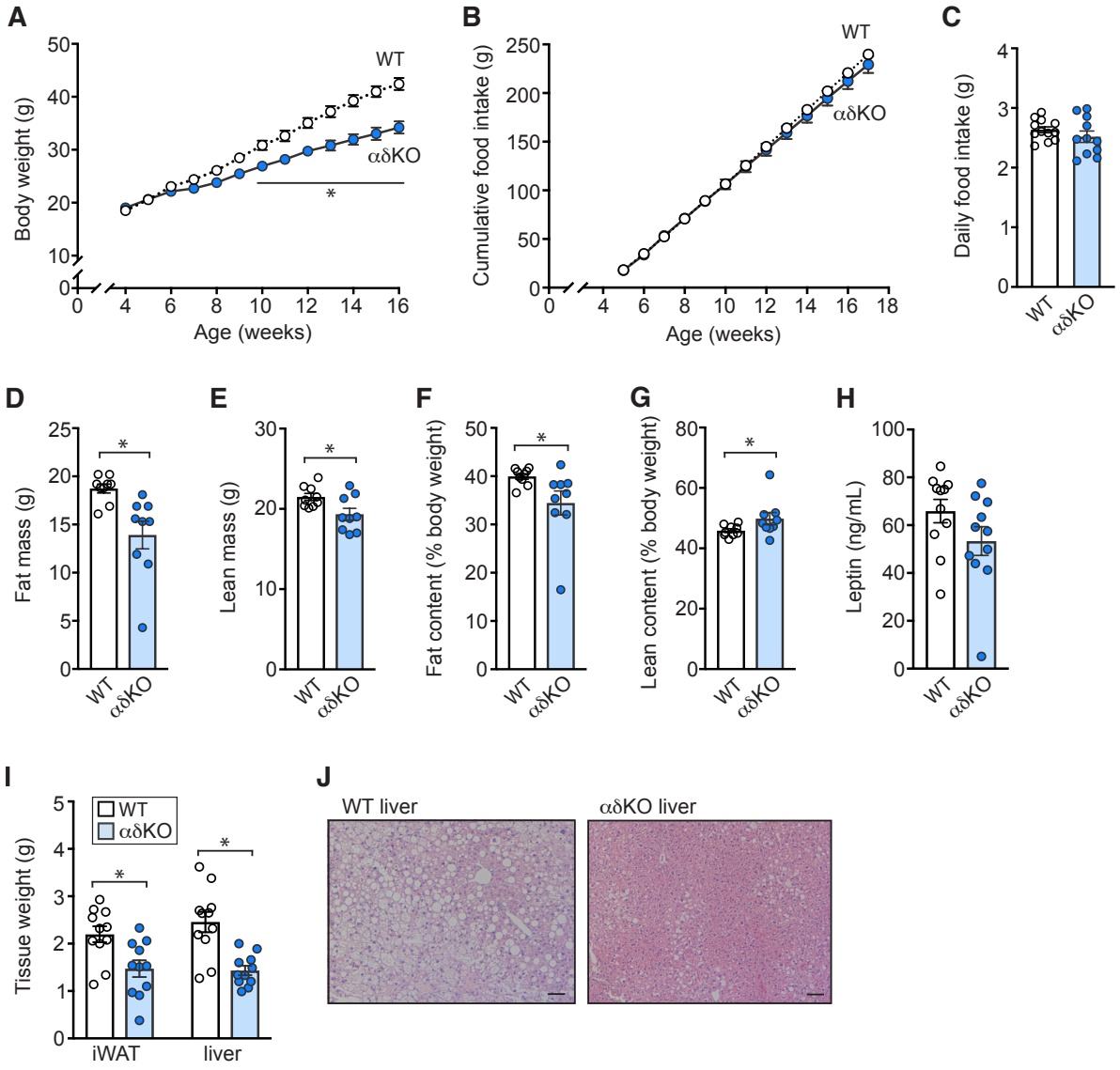

Figure 2.4. Male αδKO mice are protected against diet-induced obesity

(A) Body weight was measured weekly from 4 to 16 weeks (n: WT = 12-13; αδKO = 11-12). **(B)** Cumulative food intake was measured twice weekly from 5 to 17 weeks (n: WT = 12; αδKO = 11). (**C**) Average daily food intake during the 12 weeks of measurements shown in **B** (n: WT = 12; αδKO = 11). **(D-G)** Body composition was analyzed in 21-to-23-week-old mice by NMR between 9_{AM}-11_{AM} (n: WT = 9; αδKO = 9). **(H)** Blood was collected from 21-to-23-week-old mice fed *ad libitum*, and serum leptin levels were measured by ELISA (n: WT = 11; αδKO = 11). **(I)** Tissues of 21-to-23-week-old mice were dissected and weighed (n: WT = 11; αδKO = 11). iWAT, inguinal white adipose tissue. **(J)** Liver tissues from 21-to-23-week-old mice were paraffin-embedded and stained with hematoxylin and eosin. Images are representative of indicated genotypes (n, livers imaged: WT = 3; αδKO = 5). Scale bar = 50 μm. **Statistics**: **A**, two-way repeated measures ANOVA (weeks 4 to 16); **B,** linear regression analysis (weeks 5 to 17); **C-I**, unpaired, two-tailed Student's t-test. * $P < 0.05$. Data are means ± SEM.

Adiposity-dependent improvements in glucose metabolism in αδKO mice

To determine whether deletion of SH2B1α/δ impacts glucose metabolism, we first measured glucose and insulin in *ad libitum*-fed or overnight-fasted αδKO and WT mice (22-27 weeks old). Fed αδKO males displayed normal blood glucose levels but low insulin concentrations (Fig. 2.5A-B). When fasted, αδKO males exhibited low blood glucose and insulin concentrations (Fig. 2.5C-D). Glucose and insulin tolerance tests revealed improved glucose tolerance in 28-to-32-week-old chow-fed αδKO males (Fig. 2.5E-F) and improved glucose tolerance and insulin sensitivity in 18-to-20-week-old HFD-fed αδKO males (Fig. 2.5G-H). In chow-fed αδKO females, parameters of glucose metabolism were unchanged except that their insulin concentrations were decreased in the fed state (Supplementary Material Fig. 2.11A-F). Thus, αδKO mice generally exhibit improved glucose tolerance and insulin responsiveness compared to their more obese littermate controls.

Together with the improved glucose homeostasis in the lean αδKO males, the relatively normal glucose metabolism in αδKO females, which exhibit a more modest reduction in body weight, suggested that alterations in glucose homeostasis in αδKO mice might not result directly from the lack of SH2B1α/δ, but rather from decreased adiposity. We therefore assessed glucose homeostasis in young, 10-to-12-week-old chow-fed male αδKO mice, when their fat content was similar to that of controls (Fig. 2.6A). Their decreased leptin levels (Fig. 2.6B) suggested that some differences in adiposity were beginning to develop. We observed no differences by genotype in glucose or insulin concentrations, nor glucose tolerance or insulin sensitivity in these young animals (Fig. 2.6C-H). Thus, the improved glucose homeostasis observed in older αδKO mice is likely

to be secondary to their reduced adiposity, rather than the result of any direct effect of removal of SH2B1α/δ.

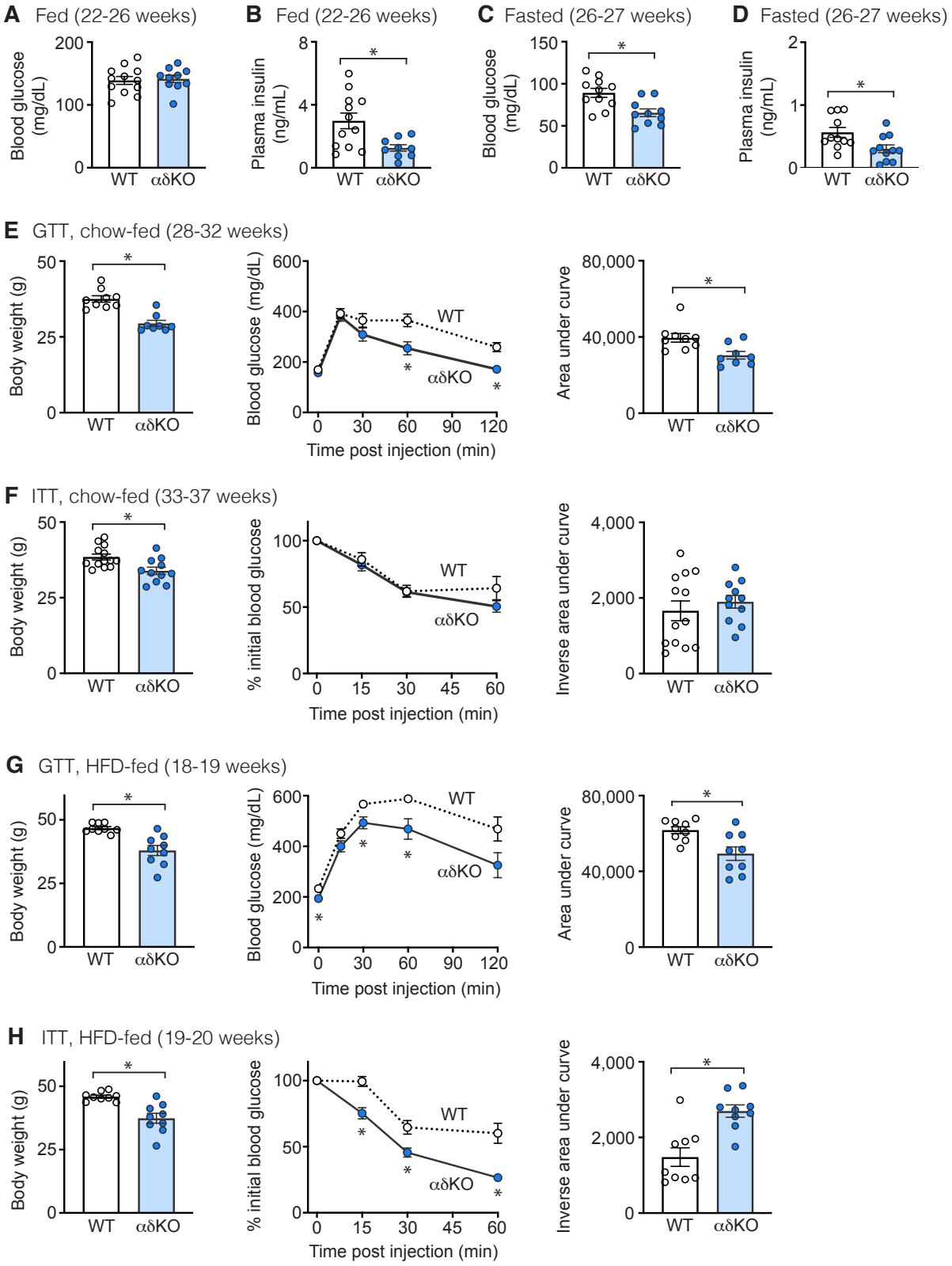
A Fed (22-26 weeks)
Blood glucose (mg/dL)
200
100
0
WT
αδKO
B Fed (22-26 weeks)
Plasma insulin (ng/mL)
8
4
0
*
WT
αδKO
C Fasted (26-27 weeks)
Blood glucose (mg/dL)
150
100
50
0
*
WT
αδKO
D Fasted (26-27 weeks)
Plasma insulin (ng/mL)
2
1
0
*
WT
αδKO
E GTT, chow-fed (28-32 weeks)
Body weight (g)
50
25
0
*
WT
αδKO
Blood glucose (mg/dL)
600
400
200
0
WT
αδKO
*
0
30
60
90
120
Time post injection (min)
Area under curve
80,000
40,000
0
*
WT
αδKO
F ITT, chow-fed (33-37 weeks)
Body weight (g)
50
25
0
*
WT
αδKO
% initial blood glucose
100
50
0
WT
αδKO
0
15
30
45
60
Time post injection (min)
Inverse area under curve
4,000
2,000
0
WT
αδKO
G GTT, HFD-fed (18-19 weeks)
Body weight (g)
50
25
0
*
WT
αδKO
Blood glucose (mg/dL)
600
400
200
0
WT
αδKO
*
0
30
60
90
120
Time post injection (min)
Area under curve
80,000
40,000
0
*
WT
αδKO
H ITT, HFD-fed (19-20 weeks)
Body weight (g)
50
25
0
*
WT
αδKO
% initial blood glucose
100
50
0
WT
αδKO
0
15
30
45
60
Time post injection (min)
Inverse area under curve
4,000
2,000
0
*
WT
αδKO

Figure 2.5. Older male αδKO mice exhibit improved glucose homeostasis

Blood was collected from 22-to-26-week-old mice fed chow *ad libitum* and **(A)** blood glucose levels were measured by glucometer (n: WT = 12; αδKO = 10) and **(B)** plasma insulin levels were measured by ELISA (n: WT = 12; αδKO = 9). Blood was collected from 26-to-27-week-old chow-fed mice fasted overnight (16 hours) and **(C)** blood glucose levels were measured by glucometer (n: WT = 11; αδKO = 10) and **(D)** plasma insulin levels were measured by ELISA (n: WT = 11; αδKO = 11). **(E)** Glucose tolerance tests (GTT) were performed on 28-to-32-week-old chow-fed mice (i.p. glucose, 2 g/kg) (n: WT = 9; αδKO = 8). Area under the curve for each animal was calculated using a baseline of y = 0. **(F)** Insulin tolerance tests (ITT) were performed on 33-to-37-week-old chow-fed mice (i.p. insulin, 1 unit/kg) (n: WT = 13; αδKO = 11). Data are reported as % initial blood glucose values. Inverse area under the curve for each animal was calculated using a baseline of y = 100. **(G)** GTTs were performed on 18-to-19-week-old HFD-fed mice (i.p. glucose, 2 g/kg) (n: WT = 9; αδKO = 9). Area under the curve for each animal was calculated using a baseline of y = 0. **(H)** ITTs were performed on 19-to-20-week-old HFD-fed mice (i.p. insulin, 1 unit/kg) (n: WT = 9; αδKO = 9). Data are reported as % initial blood glucose values. Inverse area under the curve for each animal was calculated using a baseline of y = 100. **E-H**, Body weights corresponding to each experiment are shown. See Supplementary Material Fig. 2.11 for corresponding data from females. **Statistics**: **A-H**, unpaired, two-tailed Student's t-test. * $P < 0.05$. Data are means ± SEM.

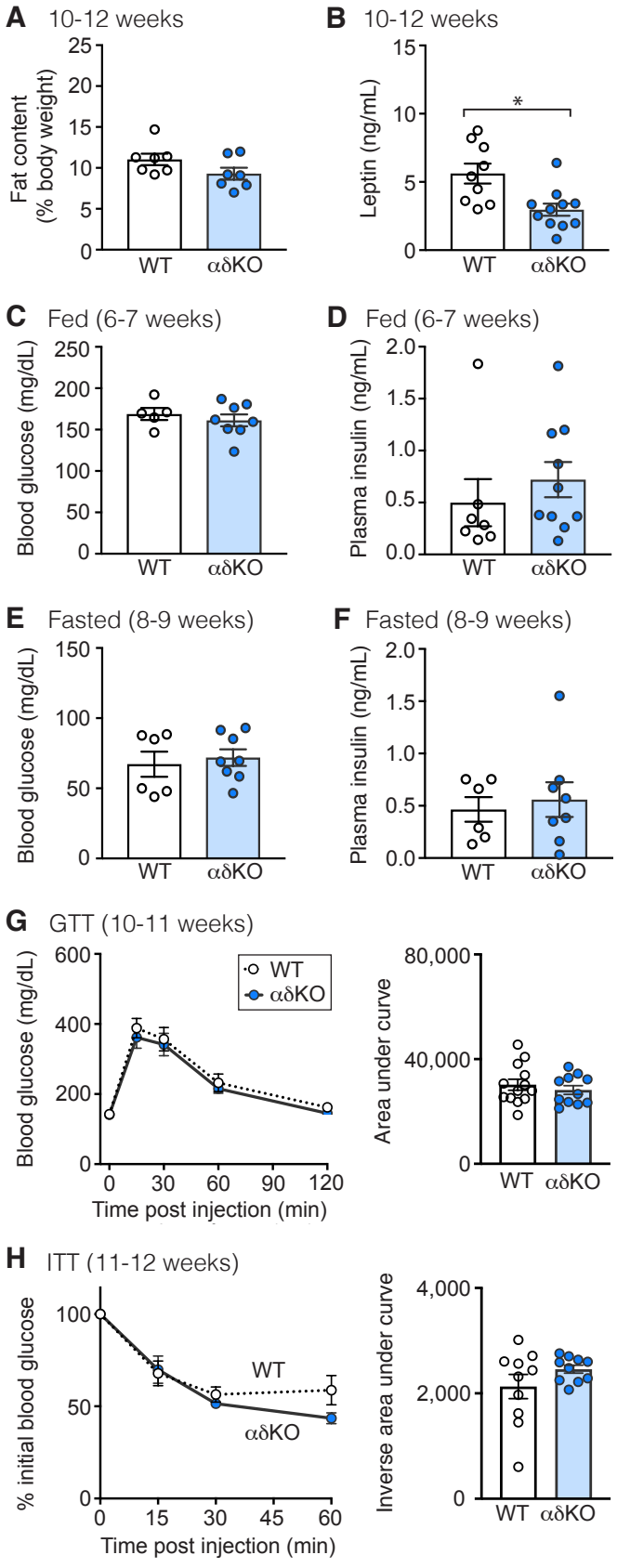
A
10-12 weeks
Fat content (% body weight)
25
20
15
10
5
0
WT
αδKO
B
10-12 weeks
Leptin (ng/mL)
15
10
5
0
*
WT
αδKO
C
Fed (6-7 weeks)
Blood glucose (mg/dL)
250
200
150
100
50
0
WT
αδKO
D
Fed (6-7 weeks)
Plasma insulin (ng/mL)
2.0
1.5
1.0
0.5
0.0
WT
αδKO
E
Fasted (8-9 weeks)
Blood glucose (mg/dL)
150
100
50
0
WT
αδKO
F
Fasted (8-9 weeks)
Plasma insulin (ng/mL)
2.0
1.5
1.0
0.5
0.0
WT
αδKO
G
GTT (10-11 weeks)
Blood glucose (mg/dL)
600
400
200
0
WT
αδKO
0
30
60
90
120
Time post injection (min)
Area under curve
80,000
40,000
0
WT
αδKO
H
ITT (11-12 weeks)
% initial blood glucose
100
50
0
WT
αδKO
0
15
30
45
60
Time post injection (min)
Inverse area under curve
4,000
2,000
0
WT
αδKO

Figure 2.6. Young male αδKO mice (6-12 weeks old) exhibit normal glucose homeostasis

(A) Fat content was analyzed by NMR in 10-to-12-week-old mice (n: WT = 7; αδKO = 7). **(B)** Blood was collected from 10-to-12-week-old mice fed *ad libitum* and serum leptin levels were measured by ELISA (n: WT = 9; αδKO = 11). Blood was collected from 6-to-7-week-old mice fed *ad libitum* and **(C)** blood glucose levels were measured by glucometer (n: WT = 5; αδKO = 8) and **(D)** plasma insulin levels were measured by ELISA (n: WT = 7; αδKO = 10). Blood was collected from 8-to-9-week-old mice fasted overnight (16 hours) and **(E)** blood glucose levels were measured by glucometer (n: WT = 6; αδKO = 8) and **(F)** plasma insulin levels were measured by ELISA (n: WT = 6; αδKO = 8). **(G)** Glucose tolerance tests (GTT) were performed on 10-to-11-week-old-mice (i.p. glucose, 2 g/kg) (n: WT = 13; αδKO = 11). Area under the curve for each animal was calculated using a baseline of y = 0. **(H)** Insulin tolerance tests (ITT) were performed on 11-to-12-week-old mice (i.p. insulin, 1 unit/kg) (n: WT = 10; αδKO = 10). Data are reported as % initial blood glucose values. Inverse area under the curve for each animal was calculated using a baseline of y = 100. **Statistics**: **A-H**, unpaired, two-tailed Student's t-test. * $P < 0.05$. Data are means ± SEM.

Normal leptin sensitivity in αδKO mice

Because SH2B1 modulates leptin signaling and SH2B1α/δ expression is restricted to the brain, the site of leptin action on food intake and energy balance, we examined the possibility that increased leptin signaling might underlie the leanness of αδKO mice. The arcuate nucleus of the hypothalamus is a primary target for leptin [26,27]. Leptin action in the arcuate nucleus inhibits the expression of appetite-stimulating neuropeptides agouti-related peptide (AgRP) and neuropeptide Y (NPY) and promotes the expression of appetite-suppressing neuropeptides proopiomelanocortin (POMC) and cocaine- and amphetamine-regulated transcript (CART) [28]. Leptin also regulates the expression of other genes in LepRb-expressing cells in the hypothalamus [29]. We measured expression of eight relevant leptin-regulated, protein-encoding genes (*Agrp*, *Npy*, *Pomc*, *Cartpt*, *Asb4*, *Irf9*, *Ghrh*, *Serpina3n*) in αδKO and WT hypothalami using qPCR. To avoid potential confounding by differences in adiposity and/or circulating leptin levels, which would impact leptin action, we assessed young, 10-to-12-week-old male mice. We found no differences by genotype in expression of these genes (Fig. 2.7A).

To more directly test the effects of SH2B1α/δ on leptin sensitivity, we examined the responses of 6-week-old αδKO and WT mice to low-dose leptin injections. We have previously used this assay to identify increased leptin sensitivity in other mouse lines [3,30,31]. At this age, there was no difference in circulating leptin levels between αδKO and WT littermates (Fig. 2.7B). We observed no difference by genotype in rate of weight loss or food intake reduction (Fig. 2.7C-D) in response to leptin treatment. In conjunction with the WT-like expression levels of leptin-responsive genes in αδKO hypothalami, these

results suggest that removal of SH2B1α/δ does not alter leptin action, but rather protects mice from obesity primarily via leptin-independent mechanisms.

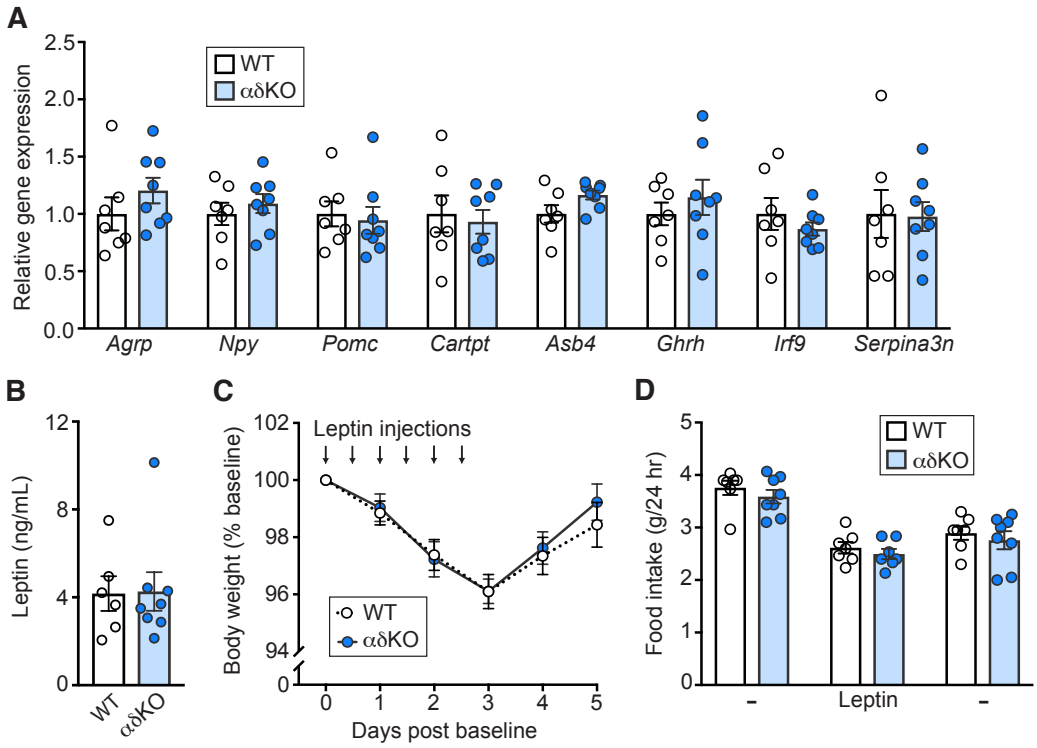

Figure 2.7. αδKO mice exhibit normal expression levels of leptin-regulated genes in the hypothalamus and normal sensitivity to exogenous leptin

(A) RNA was isolated from hypothalami of 10-to-12-week-old male mice. Expression levels of leptin-responsive genes were measured by qPCR (n: WT = 7; αδKO = 8). αδKO results were normalized to the average relative expression obtained for WT samples. **(B)** Blood was collected from 6-week-old male mice fed *ad libitum* and plasma leptin levels were measured by ELISA (n: WT = 6; αδKO = 8). **(C)** Body weight and **(D)** food intake were measured before, during, and after leptin injections (i.p., vehicle (-) or 1 mg/kg of leptin diluted in vehicle) in 6-week-old mice (n: WT = 7; αδKO = 8). Average values from days 1-3 served as baseline. **Statistics**: **A-D**, no significant differences by unpaired, two-tailed Student's t-test. Data are means ± SEM.

Altered transcriptome in αδKO hypothalami

To gain additional insight into mechanisms underlying the leanness of αδKO mice, we examined the impact of deleting SH2B1α/δ on hypothalamic gene expression using RNA-seq. Given that WT and αδKO mice had similar fat content at the time of hypothalamic dissection (Fig. 2.6A), changes in gene expression were expected to be adiposity-independent. The combined expression of all *Sh2b1* transcripts annotated in the Ensembl mouse genome was substantially decreased in αδKO mice, as predicted (Supplementary Material Fig. 2.13B). RNA-seq identified 59 additional genes that exhibited statistically significant differential regulation by genotype. Of these, 29 were up-regulated and 30 were down-regulated in αδKO mice (Supplementary Material Tables 2.4 and 2.5, Fig. 2.8A). qPCR analysis validated the gene expression changes of a representative sample (*Slc5a11*, *C1qa*, *Gsg1l*, *Kdm8*) of the up- and down-regulated genes identified by RNA-seq (Supplementary Material Fig. 2.12A).

We compared the hypothalamic transcriptional changes that we observed in αδKO mice with published results from leptin-treated mice [29]. There was no correlation between datasets, neither among all genes that were differentially expressed, nor among the genes that were statistically significantly regulated (Fig. 2.8B-C). These results provide further evidence that removal of SH2B1α/δ protects mice from obesity via leptin-independent mechanisms.

Interestingly, Gene Ontology (GO) revealed that changes in the transcriptional profile of hypothalamic tissue from αδKO mice were significantly associated with several genes linked to microglial function (Supplementary Material Fig. 2.12B). Similarly, querying MouseMine revealed that many of the mouse phenotypes that significantly

associate with differentially expressed genes in αδKO mice were related to microglia (Supplementary Material Fig. 2.12C). Also, comparison with a previously-published mouse hypothalamic single-cell RNA-seq dataset that contained expression profiles for all hypothalamic cell types including neurons, microglia, and macrophages [32] indicated that most of the genes with statistically significant differential regulation in αδKO hypothalami were predominantly expressed in microglia and/or macrophages (Supplementary Material Fig. 2.12D). In addition, *Sh2b1* was expressed in all hypothalamic cell types including neurons, microglia, and macrophages [32]. These findings provide evidence that deletion of SH2B1α/δ impacts hypothalamic microglial function. Interestingly, most of the microglia-related genes (*C1qa*, *C1qb*, *Cx3cr1*, *Grn*, *Trem2*, *Tyrobp*) that exhibited statistically significantly up-regulated expression in our dataset have been previously identified as contributors to complement-mediated synaptic pruning [33-37], presenting the possibility that SH2B1α/δ may regulate structural changes at synapses. The ability of SH2B1α/δ to regulate structural changes at synapses would be consistent with previous *in vitro* findings that SH2B1 regulates the actin cytoskeleton [10,11,14].

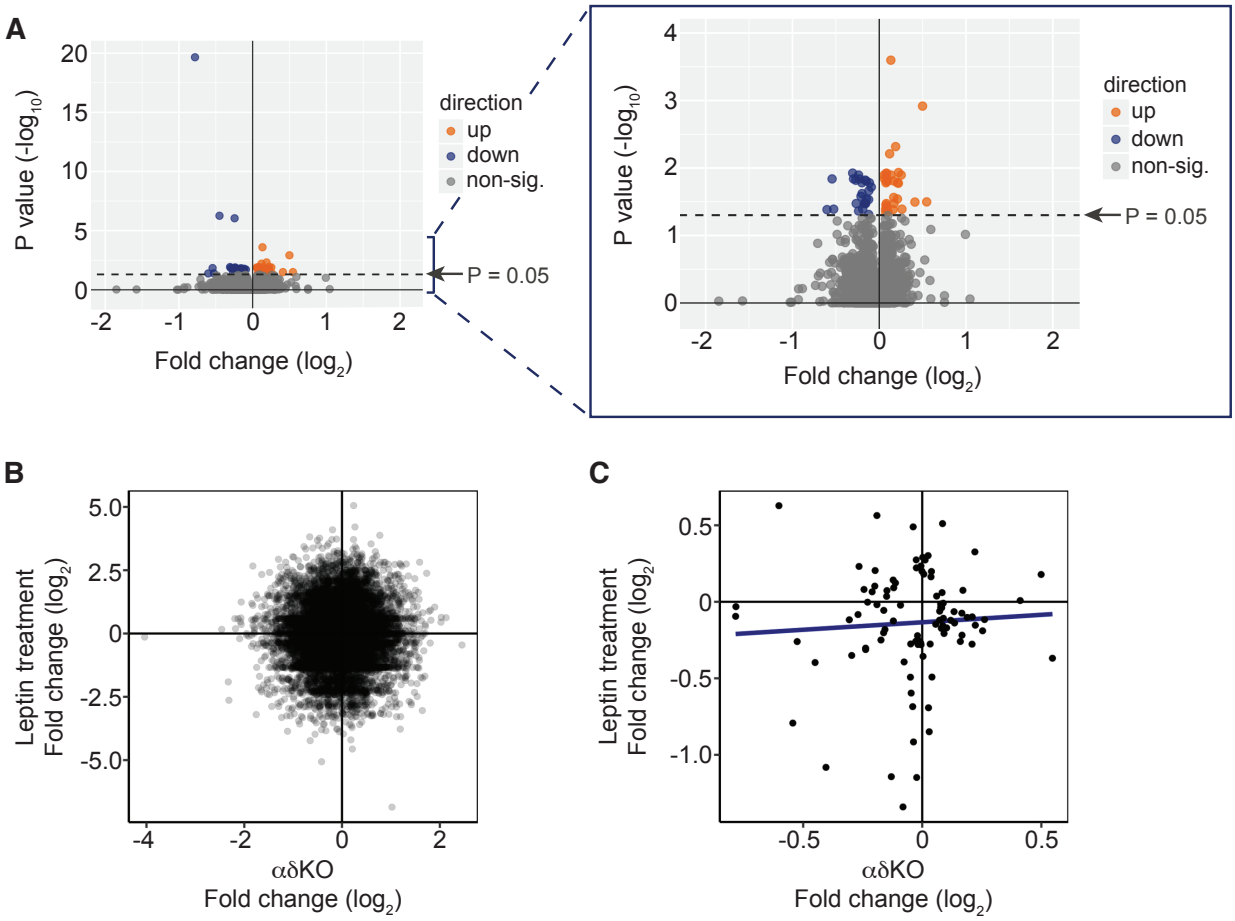

Figure 2.8. Altered transcriptome in αδKO mice

(A) mRNA was isolated from hypothalami of 10-to-12-week-old male mice and analyzed by RNA-seq (n: WT = 9; αδKO = 12). Left: volcano plot depicts differentially expressed genes. Genes located above the dotted horizontal line are significantly ($P < 0.05$) up-regulated (orange dots, $x > 0$) or significantly downregulated (dark blue dots, $x < 0$) in αδKO mice. Genes located below the line (gray dots) are not significantly regulated ($P \geq 0.05$). *Sh2b1* is not shown. Right: enlargement of graph on left. Non-sig., non-significant. **(B)** Scatterplot compares differentially expressed genes from hypothalami of αδKO and leptin-treated mice ($r = 0.003$; $p = 0.616$). **(C)** Scatterplot compares genes with statistically significant differential regulation between hypothalami of αδKO and leptin-treated mice ($r = 0.061$; $p = 0.56$). See Supplementary Material Figs. 2.12-2.14 for additional analyses of RNA-seq data. **Statistics**: **A**-**C**, see Supplemental Materials.

Novel *Sh2b1* transcripts may exist

A byproduct of our RNA-seq analysis was greater insight into *Sh2b1* transcripts. Our initial quantification of *Sh2b1* transcripts using StringTie included only transcripts that had previously been annotated in the Ensembl mouse genome (Supplementary Material Fig. 2.13A). However, this analysis suggested that almost no mRNA encoding SH2B1α was detected in WT hypothalami (Supplementary Material Fig. 2.13B), which contradicted our qPCR data (Fig. 2.1C). We reanalyzed the data to include previously-unannotated transcripts. This analysis revealed six potential novel *Sh2b1* transcripts in WT mice (Supplementary Material Fig. 2.13A). Inclusion of unannotated alongside annotated transcripts provided a more accurate measurement of *Sh2b1* transcript abundance (Supplementary Material Fig. 2.13C). This revised sum of RNA-seq transcripts more closely matches total *Sh2b1* gene expression measured by qPCR (Supplementary Material Fig. 2.13D).

While four of six potential novel (unannotated) *Sh2b1* transcripts are slight variations of known transcripts, the remaining two differ notably from known transcripts in that their 8th intron is not spliced out (Supplementary Material Figs. 2.13A, 2.14). We named these predicted transcripts "*Sh2b1*8c" for their unique 8th exon.

*Sh2b1*8c mRNA contains an in-frame stop codon located 263 base pairs downstream of exon 8 and is predicted to be targeted for nonsense-mediated decay [38]. Regardless, to examine potential expression of *Sh2b1*8c-encoded proteins, we generated a GFP-SH2B18c expression vector and transfected it into PC12 cells. GFP-SH2B18c migrated at its predicted molecular size on SDS-PAGE gels (Supplementary Material Fig. 2.13E) and enhanced neurite outgrowth to a similar extent as SH2B1β

(Supplementary Material Fig. 2.13F), suggesting that if it were expressed, it might function similarly to SH2B1β or γ. However, αδKO brain lysates showed no increase in SH2B1 protein migrating at the expected size of SH2B18c on SDS-PAGE gels (Supplementary Material Fig. 2.13E), despite the increased *Sh2b1*8c mRNA in these mice. Thus, when combined with our prediction that the *Sh2b1*8c transcripts would be targeted for nonsense-mediated decay, this lack of an appropriately migrating band makes it unlikely that *Sh2b1*8c transcripts contributed to the αδKO phenotype.

Discussion

Here we create a novel mouse model that lacks two isoforms of adapter protein SH2B1, α and δ, both of which are expressed almost exclusively in brain tissue. We demonstrate that αδKO mice gain less weight than controls and are protected against DIO. The decreased body weight of the chow-fed αδKO mice results primarily from suppressed food intake. Additionally, the αδKO mice exhibit adiposity-dependent improvements in glucose homeostasis. Thus, SH2B1α and/or δ are critical determinants of energy balance and, indirectly, glucose homeostasis.

Most isoform-specific knockout models exhibit phenotypes that are similar yet less severe than animals with the complete knockout [39]. Thus, given the obesity of *Sh2b1* KO mice, the simplest prediction for mice lacking two of four known SH2B1 isoforms would be an overweight phenotype. However, αδKO mice, lacking two of four known SH2B1 isoforms, and approximately half the normal SH2B1 brain protein content, are underweight. These findings suggest that the different SH2B1 isoforms make non-redundant, even opposing, contributions to the regulation of energy balance. Furthermore, normal expression of SH2B1β/γ is not sufficient to maintain normal energy balance, suggesting that the ratio of SH2B1 isoforms must be carefully titrated for the body to appropriately balance its energy. We investigated if altering the ratio of the isoforms could be a defense against famine or over-eating. However, preliminary studies indicated that the ratios of the various isoforms do not appear to be regulated by a 24-hour fast or a HFD (data not shown). Nevertheless, our finding that in the brain WT mice have a high ratio of SH2B1α/δ to β/γ protein levels, αδHET mice have a medium ratio,

and αδKO mice have a ratio of zero, suggests that the lower the ratio of SH2B1α/δ to β/γ, the stronger the resistance to weight gain. Therefore, we propose that manipulating the ratio of SH2B1 isoforms, perhaps by identifying molecular targets that could be modified to alter *SH2B1* splicing activity or disrupt the expression of SH2B1α/δ specifically, may serve as the basis for new obesity therapeutics. It is also possible that other physiological stressors and/or genetic variants or mutations may impact the *SH2B1* isoform ratio and, as a consequence, energy balance.

The lean phenotype of αδKO mice is consistent with known cellular actions of the individual SH2B1 isoforms. Specifically, in PC12 cells, SH2B1α was shown to inhibit SH2B1β enhancement of NGF-induced neurite outgrowth by a process that appears to be dependent on NGF-induced phosphorylation of a specific tyrosine unique to the C-terminus of SH2B1α [18]. Thus, the simplest explanation of the αδKO phenotype is that in these mice, removal of SH2B1α enhances the activity of SH2B1β, and presumably γ, to enhance the actions of neurotrophic factor receptors known to recruit SH2B1 isoforms. One can envision that the competing actions of SH2B1 isoforms enable the highly specialized fine-tuning between neurite outgrowth versus retraction that is required for the formation and maintenance of the neuronal synapses that are needed to properly regulate energy balance. Cells in non-brain tissues may not have a need for such specialized fine-tuning, perhaps explaining why the α isoform evolved almost exclusively in the brain. Indeed, in a variety of assays in other non-brain cell types, in response to a variety of ligands, SH2B1α functions similarly to SH2B1β/γ [1,40,41]. Whether SH2B1δ also has unique functions relevant to the brain is not yet known. Unfortunately, it was not possible to parse the individual contributions of SH2B1α or δ by deleting either isoform

individually because of the *Sh2b1* gene structure. However, based on protein levels detected by western blotting, the α isoform is present at much higher levels than the δ isoform, suggesting that removal of the α isoform may make the major contribution to the αδKO phenotype.

Which brain cells might be driving the αδKO phenotype? Despite prior evidence suggesting that SH2B1 contributes to energy balance by modulating LepRb/JAK2 signaling [7], our data suggest that deletion of SH2B1α/δ does not alter cellular responses to leptin. Our RNA-seq data suggest that removal of SH2B1α/δ has the greatest impact on genes associated with cells of the immune system, including microglia. These are the first results to our knowledge that associate SH2B1 isoforms with microglial functions, and thus highlight a novel focal point for follow-up studies. Microglia could contribute to the αδKO phenotype via complement-mediated synaptic pruning of appetite-regulating neuronal synapses. In fact, most of the microglia-related genes within our significantly differentially-regulated gene set (*C1qa, C1qb, Cx3cr1, Grn, Trem2, Tyrobp*) have been identified as contributors to complement-mediated synaptic pruning [33-37]. Whether the lack of SH2B1α/δ affects microglia function directly or indirectly, perhaps via neurons, remains to be determined.

Given the ability of SH2B1 to enhance signaling of neurotrophic factors and affect neuronal architecture, the αδKO phenotype could also be a consequence, at least in part, of altered neuronal activity. BDNF-sensitive neurons are attractive candidates for neurons affected in αδKO mice. BDNF and TrkB are critical regulators of metabolism [42]. BDNF/TrkB activity is important for many neuronal processes that contribute to energy balance, including regulation of mature neural circuits through structural changes of

dendritic spines at excitatory synapses. SH2B1β has been shown to enhance BDNF-induced neurite outgrowth of PC12 cells, regulate the actin cytoskeleton, and interact with actin-binding protein IRSp53 in primary cultured neurons to regulate the formation of dendritic filopodia—the small membranous protrusions that often develop into dendritic spines [10,11,13,14]. Thus, SH2B1 isoforms could collectively fine-tune appetite-regulating neuronal synapses by mediating cytoskeletal rearrangement within dendritic spines of TrkB-expressing neurons, and perhaps the synaptic pruning carried out by microglia. In αδKO mice, we would predict that up-regulated SH2B1β/γ activity would increase cytoskeletal rearrangement, and thereby improve communication between appetite-regulating neurons to decrease appetite. Consistent with our hypothesis that activity downstream of TrkB is up-regulated in αδKO hypothalami, administration of BDNF into various hypothalamic nuclei in mice reduces food intake and weight gain [43]. Future experiments will be necessary to clarify whether TrkB or other receptor tyrosine kinases have altered activity in αδKO mice. Additional work will also be required to fully understand why the lean phenotype of αδKO mice appears to have arisen through distinct physiological mechanisms when mice were fed normal chow versus a HFD.

Alternative splicing generates much of the molecular and cellular diversity that exists, spatially and temporally, in the brain [44,45]. However, alternative splicing is delicately regulated and has been shown to go awry. Indeed, prior studies have linked alternative splicing aberrations to neurological disorders [46] and metabolic dysregulation [47,48]. Our work is unique in that it presents alternative splicing not as a potential cause for disease, but rather as an opportunity to treat disease. In other words, regardless of the exact cellular mechanisms involved, the bottom line of this report is that disrupting brain-specific

alternative splicing of *Sh2b1* to delete SH2B1α/δ generates mice that are resistant to weight gain and seemingly healthy otherwise.

To summarize, our findings advance our understanding in four major ways. First, while removal of all SH2B1 isoforms induces obesity in mice [4], we show that deletion of the brain-specific SH2B1α/δ isoforms has the opposite effect, offering protection against obesity. Thus, for the first time, our data demonstrate unique, non-redundant functions of SH2B1 isoforms *in vivo.* Second, these results indicate that disrupting the alternative splicing of *Sh2b1* to delete the α and δ isoforms protects against weight gain, presenting a potential target for obesity therapeutics. Third, our research suggests that the α and δ isoforms of SH2B1 regulate energy homeostasis primarily via leptin-independent mechanisms. Fourth, our RNA-seq dataset suggests potential cellular mechanisms by which isoforms of SH2B1 control energy balance—perhaps by refining synapses between appetite-regulating neurons in the hypothalamus. Together, these findings highlight the importance of alternative splicing in regulating brain function relevant to energy balance and illuminate several novel pathways that researchers might follow to gain more information about the mechanism(s) by which SH2B1 isoforms work together to regulate body weight.

Supplementary Material

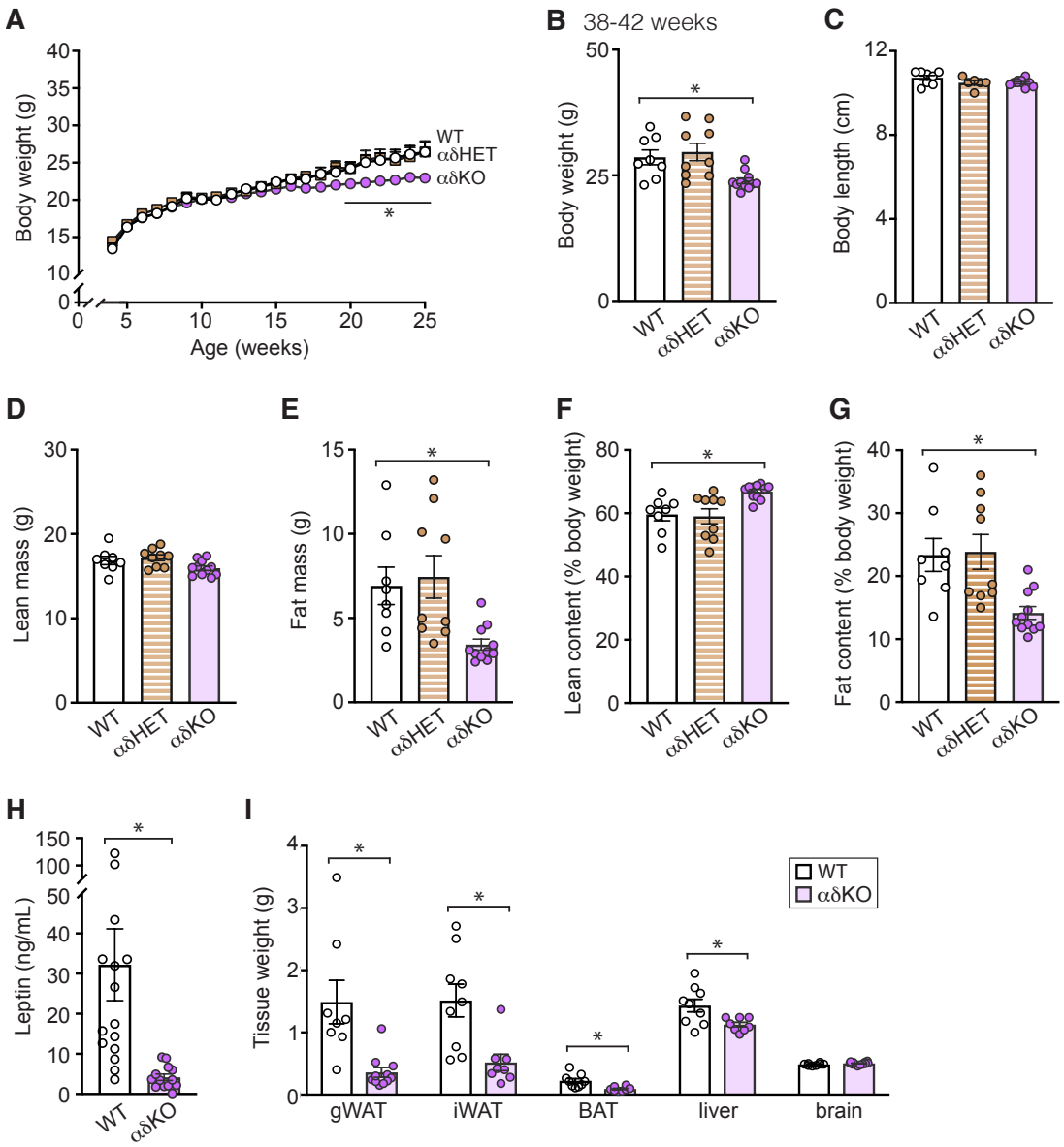

Figure 2.9. Female KO mice fed standard chow exhibit reduced body weight, fat content, circulating leptin levels, adipose tissue weight, and liver weight

(A) Body weight was measured weekly from 4 to 25 weeks (n: WT = 6-8; αδHET = 7-9; αδKO = 11-13). **(B)** Body weight was measured between 38 and 42 weeks of age (n: WT = 8; αδHET = 9; αδKO = 11). (**C**) Body length was measured from nose to anus in 38-to-42-week-old mice (n: WT = 8; αδHET = 6; αδKO = 10). **(D-G)** Body composition of 38-to-42-week-old mice was analyzed by NMR between $9{:}00_{AM}$ and $11{:}00_{AM}$ (n: WT = 8; αδHET = 9; αδKO = 11). **(H)** Blood was collected from 38-to-42-week-old mice fed *ad libitum*, and serum leptin levels were measured by ELISA (n: WT = 15; αδKO = 13). **(I)** Tissues of 38-to-42-week-old mice were dissected and weighed (n: WT = 8-10; αδKO = 8-12). gWAT, gonadal white adipose tissue; iWAT, inguinal white adipose tissue; BAT, brown adipose tissue. **Statistics: A**, two-way repeated measures ANOVA (weeks 7 to 25); **B-G**, one-way ANOVA; **H-I**, unpaired, two-tailed Student t test. * $P < 0.05$. Data are means ± SEM.

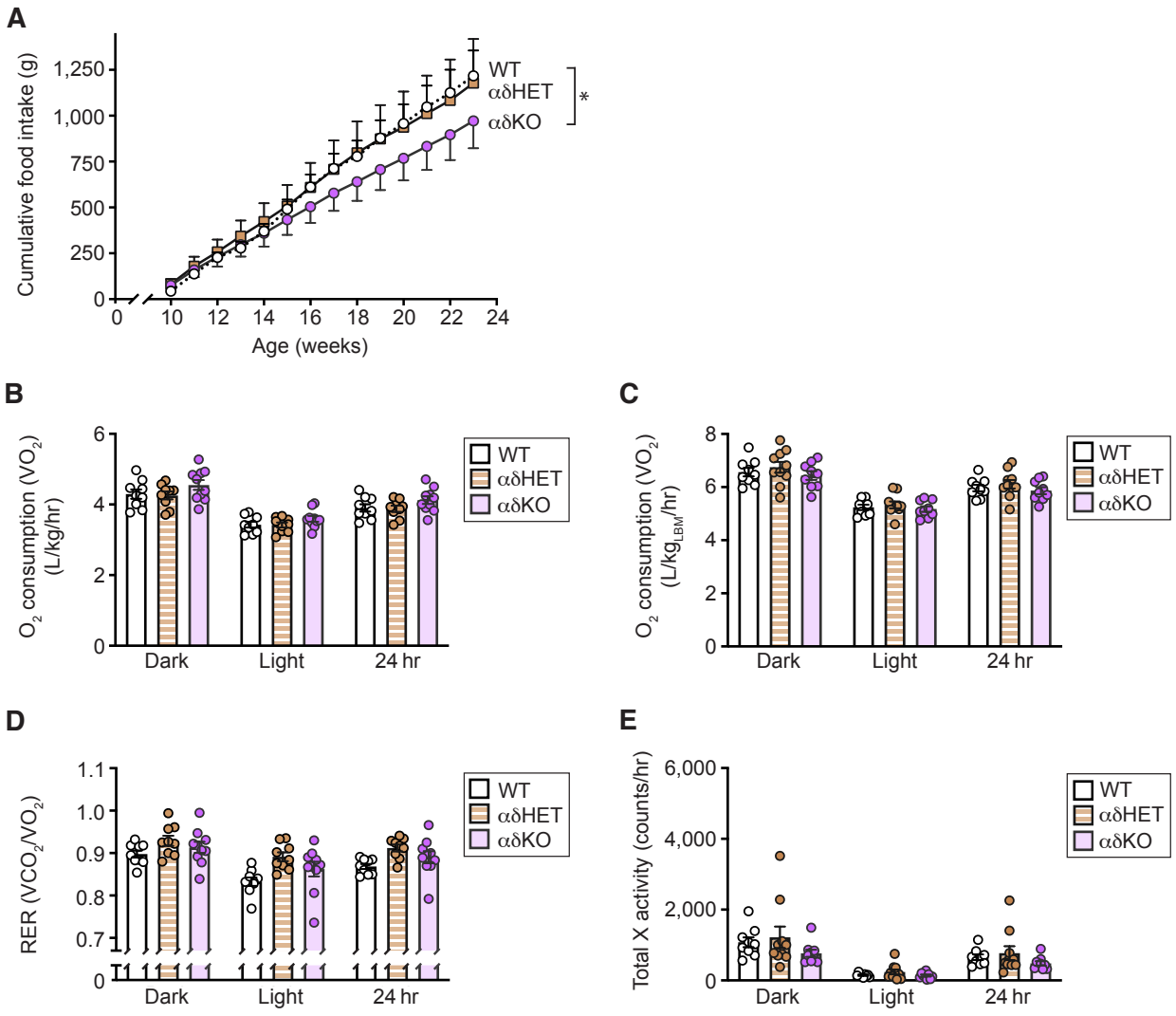
A
Cumulative food intake (g)
1,250
1,000
750
500
250
0
0
10
12
14
16
18
20
22
24
Age (weeks)
WT
αδHET
αδKO
*
B
O2 consumption (VO2) (L/kg/hr)
6
4
2
0
Dark
Light
24 hr
WT
αδHET
αδKO
C
O2 consumption (VO2) (L/kgLBM/hr)
8
6
4
2
0
Dark
Light
24 hr
WT
αδHET
αδKO
D
RER (VCO2/VO2)
1.1
1.0
0.9
0.8
0.7
0
Dark
Light
24 hr
WT
αδHET
αδKO
E
Total X activity (counts/hr)
6,000
4,000
2,000
0
Dark
Light
24 hr
WT
αδHET
αδKO

Figure 2.10. Female αδKO mice fed standard chow exhibit decreased food consumption but normal energy expenditure

(A) Food intake was measured weekly from 10 to 23 weeks (n: WT = 7; αδHET = 8; αδKO = 11). **(B-E)** Energy expenditure was measured in 10-to-12-week-old mice by CLAMS (n: WT = 9; αδHET = 10; αδKO = 9). Parameters included: **(B)** oxygen consumption corrected for total body weight or **(C)** lean body mass (LBM); **(D)** respiratory exchange ratio (RER); and **(E)** total motor activity in the X dimension. RER was calculated as VCO_2/VO_2. The final 24 hours of recordings are presented. **Statistics: A**, linear regression analysis (weeks 10 to 23); **B-E**, one-way ANOVA. * $P < 0.05$. Data are means ± SEM.

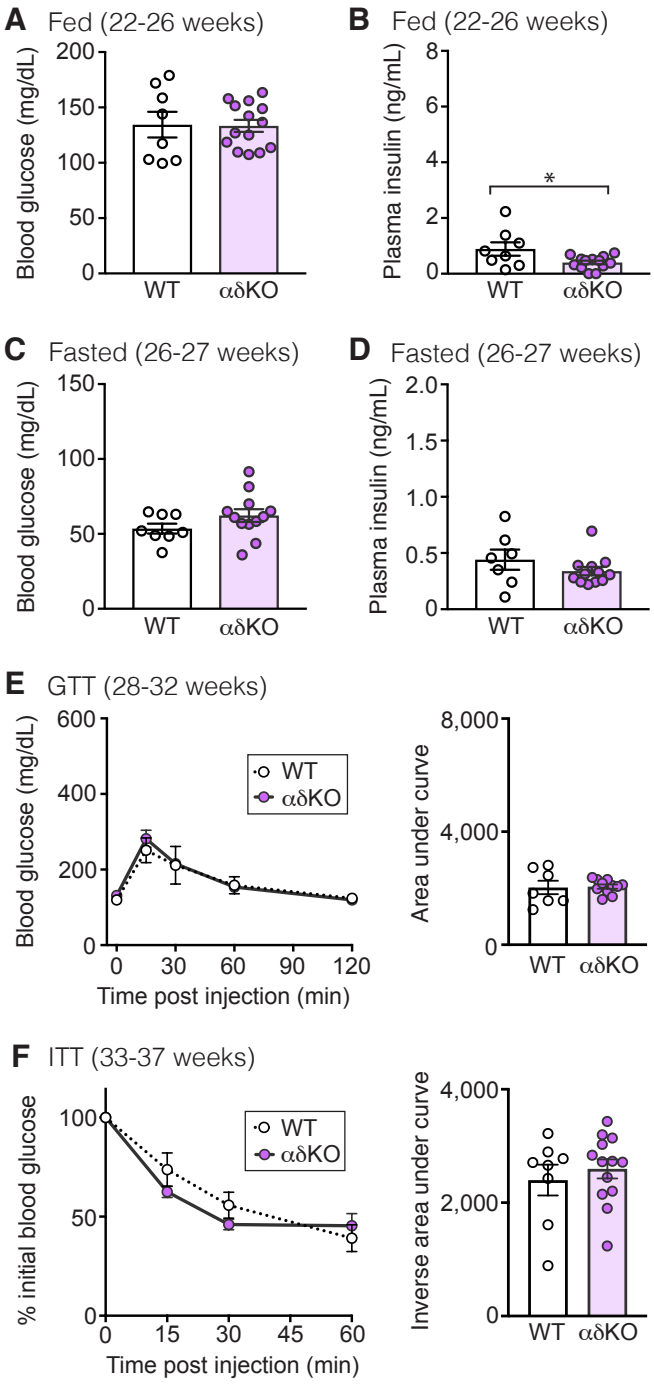
A Fed (22-26 weeks)
Blood glucose (mg/dL)
200
150
100
50
0
WT
αδKO
B Fed (22-26 weeks)
Plasma insulin (ng/mL)
8
6
4
2
0
*
WT
αδKO
C Fasted (26-27 weeks)
Blood glucose (mg/dL)
150
100
50
0
WT
αδKO
D Fasted (26-27 weeks)
Plasma insulin (ng/mL)
2.0
1.5
1.0
0.5
0
WT
αδKO
E GTT (28-32 weeks)
Blood glucose (mg/dL)
600
400
200
0
WT
αδKO
0
30
60
90
120
Time post injection (min)
Area under curve
8,000
4,000
0
WT
αδKO
F ITT (33-37 weeks)
% initial blood glucose
100
50
0
WT
αδKO
0
15
30
45
60
Time post injection (min)
Inverse area under curve
4,000
2,000
0
WT
αδKO

Figure 2.11. Older female αδKO mice exhibit modestly improved glucose homeostasis

Blood was collected from 22-to-26-week-old mice fed *ad libitum* and **(A)** blood glucose levels were measured by glucometer (n: WT = 8; αδKO = 14) and **(B)** plasma insulin levels were measured by ELISA (n: WT = 8; αδKO = 13). Blood was collected from 26-to-27-week-old mice fasted overnight (16 hours) and **(C)** blood glucose levels were measured by glucometer (n: WT = 8; αδKO = 12) and **(D)** plasma insulin levels were measured by ELISA (n: WT = 8; αδKO = 12). **(E)** Glucose tolerance tests (GTTs) were performed on 28-to-32-week-old-mice following i.p. injection with glucose (2 g/kg) (n: WT = 7; αδKO = 11). Area under the curve for each animal was calculated using a baseline of y = 0. **(F)** Insulin tolerance tests (ITTs) were performed on 33-to-37-week-old mice following i.p. injection with insulin (1 unit/kg) (n: WT = 8; αδKO = 13). Data are reported as % initial blood glucose values. Inverse area under the curve for each animal was calculated using a baseline of y = 100. **Statistics**: **A-F**, unpaired, two-tailed Student t test. * $P < 0.05$. Data are means ± SEM.

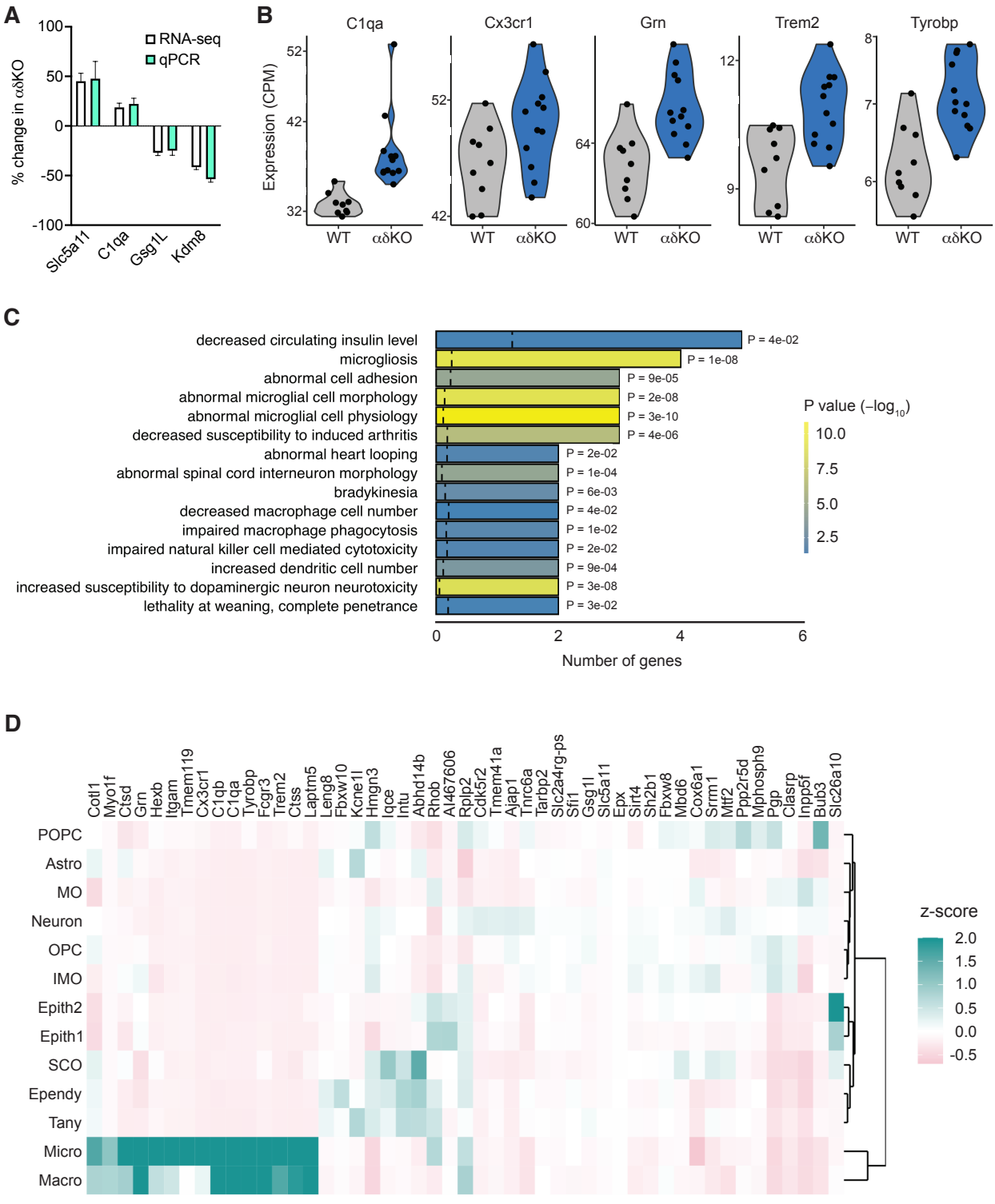
A
% change in αδKO
RNA-seq
qPCR
Slc5a11
C1qa
Gsg1L
Kdm8
B
C1qa
Cx3cr1
Grn
Trem2
Tyrobp
Expression (CPM)
WT
αδKO
C
decreased circulating insulin level
microgliosis
abnormal cell adhesion
abnormal microglial cell morphology
abnormal microglial cell physiology
decreased susceptibility to induced arthritis
abnormal heart looping
abnormal spinal cord interneuron morphology
bradykinesia
decreased macrophage cell number
impaired macrophage phagocytosis
impaired natural killer cell mediated cytotoxicity
increased dendritic cell number
increased susceptibility to dopaminergic neuron neurotoxicity
lethality at weaning, complete penetrance
P = 4e-02
P = 1e-08
P = 9e-05
P = 2e-08
P = 3e-10
P = 4e-06
P = 2e-02
P = 1e-04
P = 6e-03
P = 4e-02
P = 1e-02
P = 2e-02
P = 9e-04
P = 3e-08
P = 3e-02
P value (–log10)
Number of genes
D
POPC
Astro
MO
Neuron
OPC
IMO
Epith2
Epith1
SCO
Ependy
Tany
Micro
Macro
z-score

Figure 2.12. Transcriptional changes in αδKO hypothalami are significantly associated with terms linked to microglial function

(A) mRNA analyzed by RNA-seq was assessed by qPCR for expression levels of indicated genes (n: 4 animals per genotype). Graph depicts the % change in gene expression in αδKO compared to WT mice. **(B)** Violin plots depict expression of genes identified by Gene Ontology analysis. CPM, counts per million. **(C)** Bar graph displays mouse phenotypes that significantly associate with genes that have statistically significant differential expression in αδKO mice. The dashed vertical line on each bar corresponds to the frequency of finding that phenotype associated with all genes. **(D)** Heat map depicts cell type-specific expression of genes with statistically significant differential regulation in αδKO mice. POPC, proliferating oligodendrocyte precursor cell; Astro, astrocyte; MO, myelinating oligodendrocyte; OPC, oligodendrocyte precursor cell; IMO, immature myelinating oligodendrocyte; Epith, epithelial cell; SCO, subcommissural organ cells; Ependy, ependymocyte; Tany, tanycyte; Micro, microglia; Macro, macrophages. **Statistics**: **B**-**D**, see Supplementary Materials. Data are means.

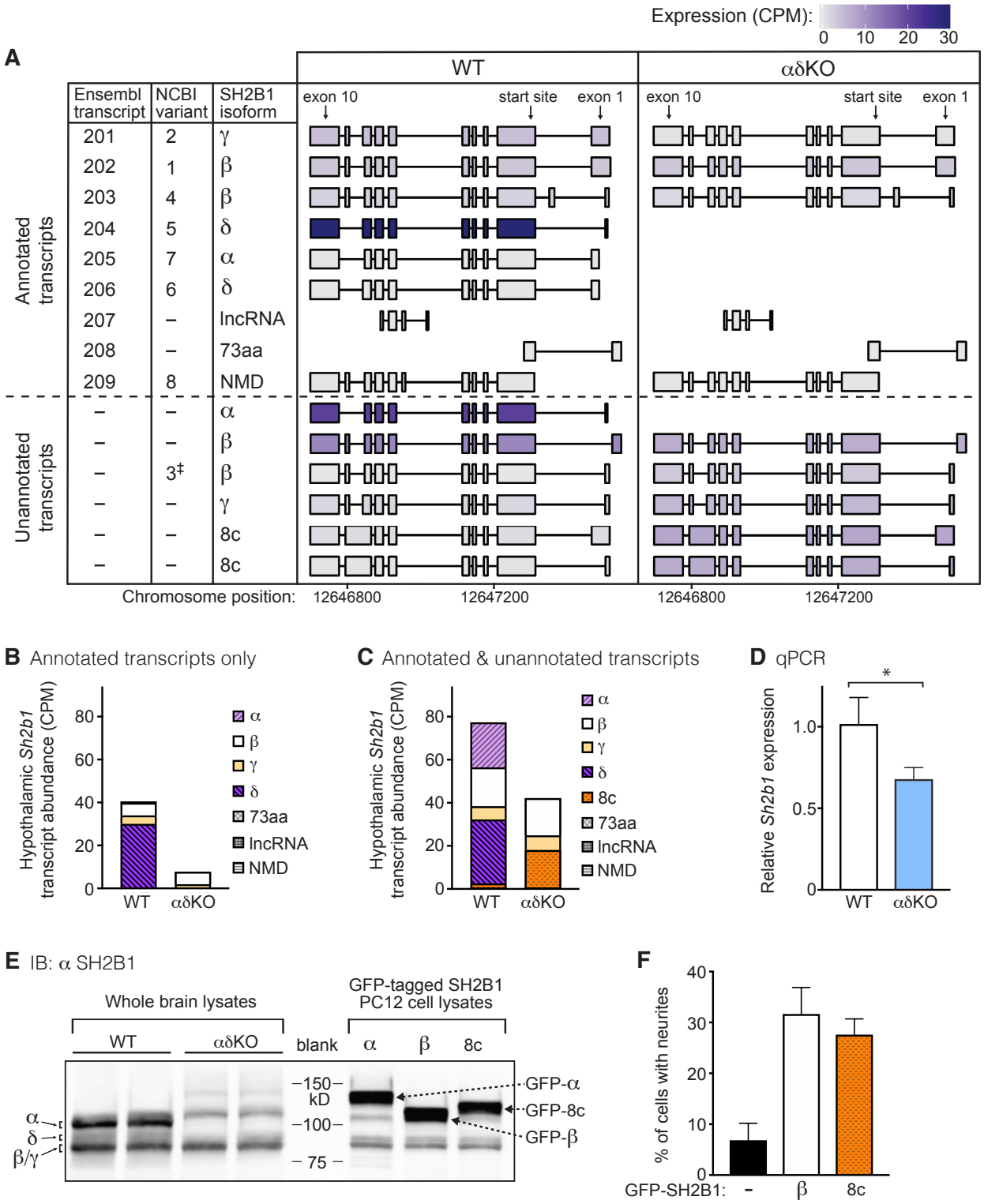
A
Expression (CPM):
0 10 20 30
WT
αδKO
Ensembl transcript
NCBI variant
SH2B1 isoform
exon 10
start site
exon 1
Annotated transcripts
Unannotated transcripts
201 2 γ
202 1 β
203 4 β
204 5 δ
205 7 α
206 6 δ
207 – lncRNA
208 – 73aa
209 8 NMD
– – α
– – β
– 3‡ β
– – γ
– – 8c
– – 8c
Chromosome position: 12646800 12647200
B Annotated transcripts only
Hypothalamic Sh2b1 transcript abundance (CPM)
α β γ δ 73aa lncRNA NMD
WT αδKO
C Annotated & unannotated transcripts
Hypothalamic Sh2b1 transcript abundance (CPM)
α β γ δ 8c 73aa lncRNA NMD
WT αδKO
D qPCR
Relative Sh2b1 expression
*
WT αδKO
E IB: α SH2B1
Whole brain lysates
GFP-tagged SH2B1 PC12 cell lysates
WT αδKO blank α β 8c
α
δ
β/γ
150 kD
100
75
GFP-α
GFP-8c
GFP-β
F
% of cells with neurites
GFP-SH2B1: - β 8c

Figure 2.13. RNA-seq data analysis reveals potential novel transcripts of *Sh2b1*

(A) Schematic of *Sh2b1* transcripts and their expression levels in hypothalami of 10-to-12-week-old male mice as identified by RNA-seq (n: WT = 9; αδKO = 12). The dotted horizontal line separates annotated (top) versus unannotated (bottom) Ensembl transcripts. *Sh2b1*8c transcripts have an extended 8th exon. Validated NCBI variant numbers are listed. ‡ SH2B1 isoform assignment based on transcript schematic. CPM, counts per million; lncRNA, long non-coding RNA; aa, amino acids; NMD, nonsense-mediated decay. **(B)** *Sh2b1* transcript abundance was calculated by RNA-seq data analysis using annotated Ensembl transcripts only or **(C)** both annotated and unannotated Ensembl transcripts. Data for α, β, γ, and δ transcripts in **C** are the same as in Figure 2.1F. **(D)** Levels of total *Sh2b1* mRNA were measured by qPCR using an aliquot of the same hypothalamic RNA as in Fig. 2.8A (n: WT = 9; αδKO = 12). **(E)** Proteins in brain tissue homogenates from WT and αδKO adult male mice and lysates of PC12 cells expressing GFP-tagged SH2B1α, β, or 8c were immunoblotted with antibody to SH2B1 (α SH2B1). The migration of molecular weight standards is shown in the center of the blot. The expected migration of the different isoforms is indicated on the left (endogenous) and right (GFP-tagged). IB, immunoblot. **(F)** PC12 cells transiently expressing GFP (-), GFP-SH2B1β (β), or GFP-SH2B18c (8c) were treated with 25 ng/mL NGF for 2 days, at which point neurite outgrowth was assessed. GFP-positive cells were scored for the presence of neurites at least 2 times the length of the cell body (n: 3 experiments, 200-300 cells/condition/experiment). **Statistics**: **D**, unpaired, two-tailed Student t test. * $P < 0.05$. Data are means ± SEM.

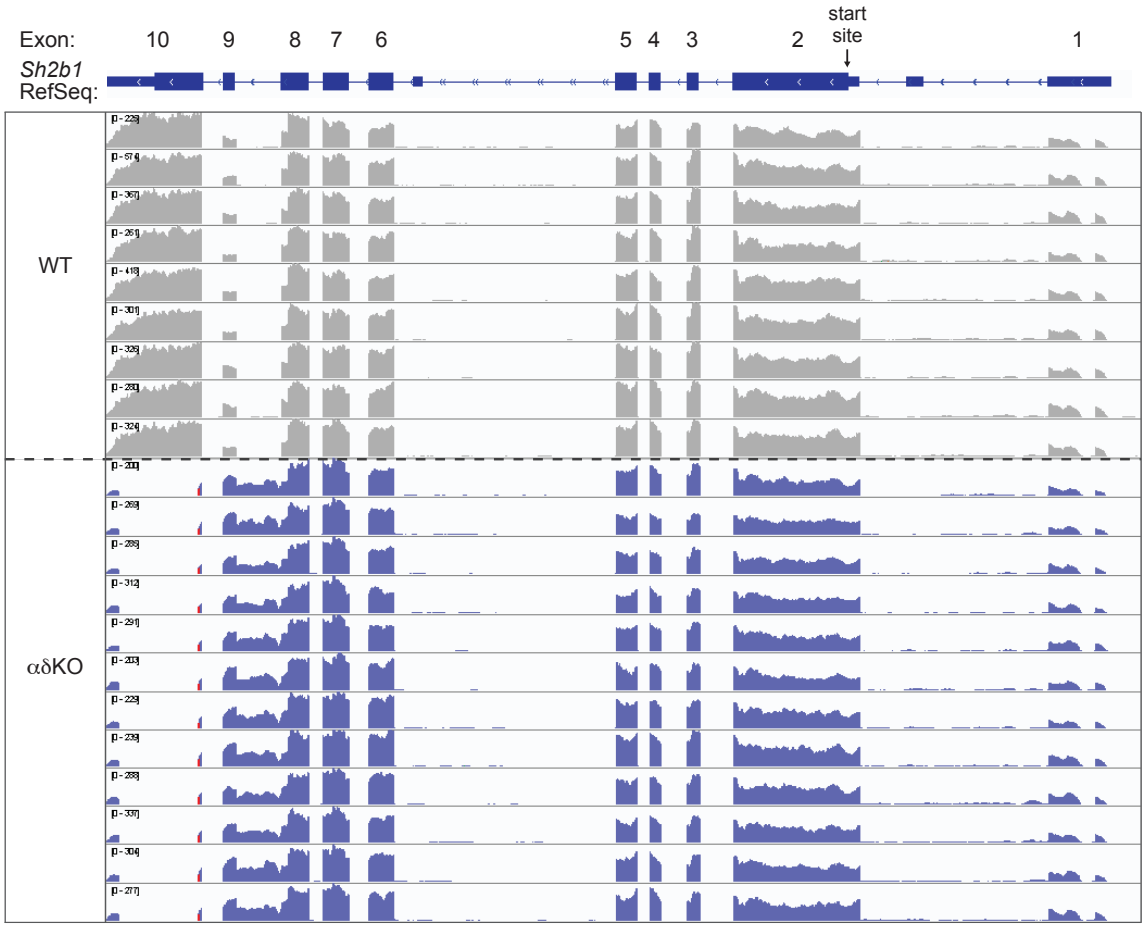

Figure 2.14. RNA-seq reads from WT and αδKO hypothalami mapped to mouse *Sh2b1* Reference Sequence (RefSeq)

In the *Sh2b1* RefSeq schematic at the top of the figure, blue rectangles represent exons; non-coding regions have less height than coding regions. The height of the reads tracks from individual WT (light gray) and αδKO mice (dark blue) depicts the level of mRNA expression at each nucleotide of the RefSeq for each mouse. Note that αδKO reads tracks are lacking expression for most of exon 10 as expected. However, additional expression is present between exons 8 and 9, which was unexpected and corresponds to the predicted *Sh2b1*8c transcripts (Supplementary Material Fig. 2.13). Numbers in brackets on the left side of each track (e.g., [0-225]) are the range of expression values for that track.

Table 2.1. Primers for genotyping

Primer	Direction	Sequence (5' → 3')
WT	Forward	CAAAGGGGAGGTCACCATAAGAACTCAC
WT	Reverse	GTGGGCAGGTATCTCACACAAATGAGTA
Edit	Forward	GGGAATGTGCAGAACTGGACCCA
Edit	Reverse	GCGAGTGACTGTGTAACGGAGCA

Table 2.2. Primers for *Sh2b1*δ and β-*actin* cDNA

Primer	Direction	Sequence (5' → 3')
*Sh2b1*δ	Forward	GTGCACCCAAGAAGTGAGAAC
*Sh2b1*δ	Reverse	CTTGTACCAACATACACACCCTTG
β-*actin*	Forward	CGTCTGGACCTGGCTGGCCGGGACC
β-*actin*	Reverse	CTAGAAGCATTTGCGGTGGACGATG

Table 2.3. TaqMan Gene Expression Assays from Applied Biosystems

Gene	TaqMan Gene Expression Assay
Agrp	Mm00475829_g1
Asb4	Mm00480830_m1
C1qa	Mm00432142_m1
Cartpt	Mm04210469_m1
Ghrh	Mm00439100_m1
Gsg1l	Mm01278519_m1
Irf9	Mm00492679_m1
Kdm8	Mm00513079_m1
Pomc	Mm00435874_m1
Npy	Mm00445771_m1
Serpina3n	Mm00776439_m1
*Sh2b1*α	Mm01275190_m1
*Sh2b1*β	Mm01163373_g1
*Sh2b1*γ	Mm00488153_m1
*Sh2b1*δ	Mm01163374_m1
Slc5a11	Mm00461434_m1
36b4 (reference gene)	Mm00725448_s1
Gapdh (reference gene)	Mm99999915_g1
Tbp (reference gene)	Mm01277042_m1

Table 2.4. Genes with significantly increased expression in αδKO mice (sorted by % increase, largest to smallest)

Gene name	Gene product	Average CPM		% increase in αδKO	P value
		WT	αδKO		
Slc5a11	Solute carrier family 5 (sodium/glucose cotransporter), member 11 (a.k.a. KST1, SMIT2)	1.663	2.413	45.087	0.0318
AI467606	Expressed sequence AI467606	3.974	5.599	40.882	0.0012
Myo1f	Myosin IF (unconventional)	2.428	3.185	31.195	0.0320
C1qa	Complement component 1, q subcomponent, α polypeptide	32.498	38.561	18.658	0.0127
Itgam	Integrin α M (a.k.a. CD11b/CD18, CR3, CR3α, Mac-1, Mac-1α)	4.279	5.033	17.613	0.0407
Ctss	Cathepsin S	49.920	58.084	16.355	0.0117
Fcgr3	Fc receptor, IgG, low affinity III (a.k.a. CD16)	7.314	8.459	15.648	0.0168
Tyrobp	TYRO protein tyrosine kinase binding protein (a.k.a. DAP12, KARAP)	6.190	7.141	15.370	0.0288
C1qb	Complement component 1, q subcomponent, β polypeptide	39.367	45.255	14.957	0.0048
Trem2	Triggering receptor expressed on myeloid cells 2 (a.k.a. TREM2a, TREM2b, TREM2c)	9.441	10.832	14.732	0.0166
Tmem41a	Transmembrane protein 41a	19.207	21.883	13.936	0.0155
Kcne1l	Potassium voltage-gated channel, Isk-related family, member 1-like, pseudogene (a.k.a. MINK, KCNE5)	10.386	11.626	11.943	0.0337
Laptm5	Lysosomal-associated protein transmembrane 5 (a.k.a. E3)	27.053	30.221	11.708	0.0273
Tmem119	Transmembrane protein 119 (a.k.a. OBIF)	19.186	21.245	10.732	0.0413
Pgp	Phosphoglycolate phosphatase (a.k.a AUM, G3PP)	64.349	70.578	9.680	2.53E-04
Cx3cr1	Chemokine (C-X3-C motif) receptor 1	46.008	49.929	8.521	0.0127
Hexb	Hexosaminidase B	98.714	106.838	8.230	0.0062
Ajap1	Adherens junction associated protein 1	44.643	47.881	7.252	0.0443
Cox6a1	Cytochrome c oxidase subunit 6A1	166.605	178.519	7.151	0.0145
Ppp2r5d	Protein phosphatase 2, regulatory subunit B', δ (a.k.a. B'δ, TEG-271)	131.952	140.590	6.546	0.0407
Ctsd	Cathepsin D (a.k.a. CD, CatD)	143.229	152.248	6.297	0.0381
Cdk5r2	Cyclin-dependent kinase 5, regulatory subunit 2 (p39)	199.699	212.086	6.203	0.0159
Rplp2	Ribosomal protein, large P2	97.732	103.728	6.135	0.0159
Abhd17a	αβ hydrolase domain containing 17A (a.k.a. FAM108A)	96.430	102.187	5.971	0.0121
Grn	Progranulin (a.k.a. GP88, PEPI, PCDGF)	62.386	65.965	5.736	0.0336
Gpat4	Glycerol-3-phosphate acyltransferase 4 (a.k.a. AGPAT6, TSARG7)	107.142	113.061	5.525	0.0166
Cotl1	Coactosin-like 1 (Dictyostelium) (a.k.a. CLP)	73.903	77.760	5.218	0.0119
Rhob	Ras homolog family member B (a.k.a. ARH6, ARHB)	390.237	409.486	4.933	0.0449
Inpp5f	Inositol polyphosphate-5-phosphatase F (a.ka. SAC2)	181.284	189.614	4.595	0.0145
Fbxw8	F-box and WD-40 domain protein 8 (a.k.a. FBW6, FBW8, FBX29, FBXO29)	66.920	69.887	4.435	0.0354
Map7d1	MAP7 domain containing 1 (a.k.a. RPRC1, PARCC1, MTAP7D1)	341.982	354.815	3.752	0.0127

CPM, counts per million

Table 2.5. Genes with significantly decreased expression in αδKO mice (sorted by % decrease, largest to smallest)

Gene name	Gene product	Average CPM		% decrease in αδKO	P value
		WT	αδKO		
Kdm8	Lysine (K)-specific demethylase 8 (a.k.a. JMJD5)	5.606	3.277	-41.546	2.23E-20
Epx	Eosinophil peroxidase (a.k.a. EPO)	1.271	0.842	-33.792	0.0414
Slc26a10	Solute carrier family 26, member 10	2.566	1.789	-30.264	0.0145
Fbxw10	F-box and WD-40 domain protein 10 (a.k.a FBW10, HREP, SM25H2, SM2SH2)	1.268	0.900	-29.027	0.0407
Gsg1l	Germ cell-specific gene 1-like	44.831	32.760	-26.926	5.52E-07
Slc2a4rg-ps	Slc2a4 regulator, pseudogene	6.401	5.206	-18.662	0.0119
Gm15446		18.392	15.394	-16.305	0.0336
C78859	Expressed sequence C78859, long non-coding RNA	8.953	7.497	-16.259	0.0145
Bub3	BUB3 mitotic checkpoint protein	85.535	71.881	-15.963	9.00E-07
Sfi1	SFI1 centrin binding protein	15.313	13.211	-13.727	0.0145
Leng8	Leukocyte receptor cluster (LRC) member 8	135.504	117.415	-13.349	0.0434
Mbd6	Methyl-CpG binding domain protein 6	34.378	29.797	-13.327	0.0127
Intu	Inturned planar cell polarity protein (a.k.a. PDZD6, PDZK6)	9.416	8.162	-13.316	0.0240
Sirt4	Sirtuin 4	13.946	12.167	-12.762	0.0407
Mir124a-1hg	Mir124-1 host gene (non-protein coding)	46.598	40.709	-12.639	0.0152
Uvssa	UV stimulated scaffold protein A	10.853	9.535	-12.141	0.0263
Rsrp1	Arginine/serine rich protein 1	221.905	198.823	-10.402	0.0166
Abhd14b	αβ hydrolase domain containing 14b	16.624	14.957	-10.026	0.0151
Tarbp2	TARBP2, RISC loading complex RNA binding subunit (a.k.a. PrBP)	15.433	13.893	-9.975	0.0337
Clasrp	CLK4-associating serine/arginine rich protein (a.k.a. CLASP, SFRS16, SRSF16, SWAP2)	54.974	49.735	-9.531	0.0337
Zfp512b	Zinc finger protein 512B (a.k.a. ZNF512b)	52.156	47.248	-9.410	0.0337
Mtf2	Metal response element binding transcription factor 2 (a.k.a M96, PCL2)	28.200	25.661	-9.002	0.0288
Mphosph9	M-phase phosphoprotein 9 (a.k.a. MPP9)	17.364	15.892	-8.476	0.0155
Hmgn3	High mobility group nucleosomal binding domain 3 (a.k.a. TRIP7)	28.740	26.527	-7.700	0.0293
Iqce	IQ motif containing E	32.067	29.635	-7.582	0.0218
Kmt2b	Lysine (K)-specific methyltransferase 2B (a.k.a. MLL2, WBP7)	64.157	59.958	-6.544	0.0489
Tnrc6a	Trinucleotide repeat containing 6a (a.k.a. GW182)	121.310	113.487	-6.449	0.0166
Srrm1	Serine/arginine repetitive matrix 1 (a.k.a. SRM160)	108.441	101.786	-6.137	0.0192

CPM, counts per million

Table 2.6. Oligos for guide RNAs

Guide	Nucleotide	Strand	Sequence (5' → 3') *
C	7203-7222	1	AAACccgcccatgattcatcttcc
C	7203-7222	2	CACCggaagatgaatcatgggcgg
D	8024-8043	1	AAACaacccaaccaagggtgagggC
D	8024-8043	2	CACCGccctcacccttggttgggtt

* The capitalized nucleotides correspond to the recognition sites for the Bbs1 restriction enzymes. The lowercase nucleotides correspond to the guide sequences.

Table 2.7. Primers used to generate a vector encoding GFP-SH2B18c

Primer	Direction	Sequence (5' → 3')
AarI	Forward	GCTGACGGATCCCACCTGCGCTTG TCACTAAATGAG
HindIII (reverse complement)	Reverse	GGATCCGTCAGCAAGCTTTCAGGC CATGAATCCCCCAAAAGG

Animal care

Mice were weaned at 3 weeks of age. Mice were fed standard chow or a HFD starting at 3 or 4 weeks of age, respectively. Mice included in standard chow experiments were individually housed at 5 weeks of age (leptin sensitivity experiments, Fig. 2.7B-D) or 9 weeks of age (all other experiments). Mice included in HFD experiments were individually housed at 4 weeks of age. Breeders were fed a standard chow containing 6.5% fat (#5008; LabDiet) or 9% fat (#5058; LabDiet). When fed *ad libitum*, mice were housed in cages with corncob bedding (Bed-o'Cobs ¼", #4B; The Andersons). When fasted, mice were temporarily housed in cages with corn-free natural soft cellulose bedding (Comfort Bedding; BioFresh) to prevent them from eating the bedding and thus disrupting their fasting.

Generation of αδKO mice

The reverse complement of the genomic *Sh2b1* sequence in C57BL/6J mice (GenBank accession #NC_000073, GRCm38) was used when designing CRISPR reagents. The selected guides were designed to direct Cas9 to cut close to the ends of the desired deleted regions (Fig. 2.1B, top) and have a low likelihood of off-target binding. Two sets of RNA guides, C and D, were selected. Guide D is located 3' of the α stop codon at the 3' end of the deleted region. Guide C was used alone or Guides C and D were used together. The guides were expressed using the pX330 vector [19,49], which contains a chimeric guide RNA expression cassette and an hSpCas9 expression cassette. Sense and anti-sense oligos (Supplementary Material Table 2.6) corresponding to either Guide C or Guides C and D were annealed and subcloned between the two Bbs1 sites in the

pX330 vector. The resulting construct was expressed in DH5α cells. Colonies were selected, DNA isolated, and the sequence verified in the region of the inserted guide sequence. The pX330 plasmid containing the guide sequence and the Zero blunt TOPO vector containing the donor template were purified as previously described [3].

The guide(s) and donor template were tested in blastocysts of C57BL/6J x SJL F2 mice. Sequencing of DNA from blastocysts showed that 6 of 20 blastocysts (30%) injected with Guide C and 16 of 30 blastocysts (53%) injected with both Guides C and D contained the correctly edited *Sh2b1* sequence. Of the 17 pups born from mice implanted with oocytes injected with Guide C, 3 (18%) contained the correctly edited *Sh2b1* sequence and 14 were WT. Of the 58 pups born from mice implanted with oocytes injected with both Guides C and D, 7 (12%) contained the correctly edited sequence, 2 had insertions/deletions, and 52 were WT. DNA sequencing revealed germline transmission from all founders. All experiments were performed using progeny of one founder generated from Guide C.

Body weight and food intake

Body weight was assessed starting at 4 weeks of age. Food intake was determined weekly starting at 10 weeks of age for standard chow experiments or twice weekly starting at 5 weeks of age for the HFD experiment. Food intake was determined by weighing the food remaining in the cage and subtracting the value from the weight of the food initially added to the hopper. Following determination of food intake, old food was removed and fresh food was added. Mice were excluded from food intake data analysis if one or more weekly measurement was missing and/or they were identified as outliers by the following

rule: their final cumulative food intake value was greater than two standard deviations from the mean. This quantitative identification of outliers matched with qualitative notes from individuals blinded to mouse genotypes that identified “extreme nibblers”—mice that ground food pellets into powder and spread it around their cage, making it difficult to accurately measure their food intake.

Glucose tolerance tests

When HFD-fed mice were subjected to glucose tolerance tests, six WT mice reached the maximum value of the glucometer range (600 mg/dL) at one or more time points. As a result, the average WT curve depicted (Fig. 2.5G) is lower than it would be if the meter had a higher maximum value.

qPCR

Before reverse transcription, RNA quality was confirmed using a Nanodrop spectrophotometer. qPCR was performed with an Eppendorf Realplex2 using Mastercycler software and PCR parameters recommended by Applied Biosystems. Three reference genes (*36b4, Gapdh, Tbp*) were used for all assays. All cDNA samples were analyzed in triplicate and a non-template control was included for each gene of interest. Cycle threshold (Ct) values were normalized to the geometric mean of the Ct values of the reference genes, as in Vandesompele et al. [50]. The expression of the reference genes did not differ between the control and experimental samples (data not shown).

RNA-seq and data analysis

RNA samples were treated with DNase I. RNA was assessed for quality using Agilent 4200 TapeStation. RNA samples were enriched for mRNA transcripts using NEBNext Poly(A) mRNA Magnetic Isolation Module (#E7490; New England BioLabs). cDNA libraries were prepared from mRNA using NEBNext Ultra II Directional RNA Library Prep Kit for Illumina (#E7760; New England BioLabs). Libraries were assessed for quality and quantity using Agilent TapeStation and qPCR by KAPA Library Quantification Kit for Illumina Platforms (#KK4835; Kapa Biosystems). Libraries were sequenced on the Illumina NovaSeq 6000 S4 Flow Cell for 200 cycles with 100 base pair paired-end reads.

FASTQ files were inspected using FastQC 0.11.7 [51] to ensure quality reads. Fastq_quality_filter (from the fastx_toolkit 0.0.14) [52] was used to remove data with Phred score < 20. Reads that made it through filtering were then aligned to the genome using STAR 2.5.3a_modified [53] and mouse genome GRCm38 (version 92). Count tables were generated using STAR with flag --quantMode GeneCounts. Count tables were analyzed in R 3.5.2 [54] and another round of quality control was performed. Samples were inspected for library size (all samples had > 20 million mapped reads), downregulation of *Sh2b1* in $\alpha\delta$KO samples, and dimension reduction for detection of batch effects. RNA samples were prepared in multiple batches, which were accounted for in the analysis. Differential expression of genes was determined using DESeq2 1.22.2 [55]. GO analysis was performed using PANTHER DB [56]. *Sh2b1* transcripts were assembled using Ensembl annotation (version 92) [57]. Novel *Sh2b1* transcripts were identified using StringTie 1.3.6 [58]. WT and $\alpha\delta$KO samples were merged during StringTie analysis. Read sequences misaligned by StringTie were excluded from further analysis. Misalignments were

identified by their robust outlier quality (e.g., all samples of the same genotype measured 0 counts per million except one sample, which measured 11 counts per million). Statistics for differential gene expression and GO analysis were calculated using the default parameters of DESeq2 and PANTHER DB, respectively. $P < 0.05$ was considered significant. Differentially expressed genes were visualized using ggplot2 3.3.0 [59] in RStudio [60].

To identify phenotype enrichment of differentially expressed genes, the differentially expressed genes were used to query the MouseMine database through the python Application Programming Interface (http://www.mousemine.org/mousemine/). The associated phenotype corresponds to the MouseMine category "ontologyTerm.name". To determine significant enrichment, all protein-coding genes for which a P value was measured by DESeq2 were fed into the same MouseMine query. Enrichment significance of phenotypes in differentially expressed genes versus all genes was determined using prop.test() in R 3.6.3. P values were corrected for multiple comparisons using the Benjamini-Hochberg method.

To determine cell type enrichment of differentially expressed genes, data from GSE87544 was downloaded from GEO as a count matrix (GSE87544_Merged_17samples_14437cells_count.txt.gz) and metadata (GSE87544_1443737Cells.SVM.cluster.identity.renamed.csv.gz). Data were imported into R and analyzed with Seurat 3.1.5 [61,62]. Count data was scaled with NormalizeData() followed by ScaleData(), then averaged by cell type as defined by the GSE87544 metadata. Heatmap and dendrogram were plotted with ggplot2 3.3.0 and ggdendro 0.1-20.

Plasmid expressing GFP-SH2B18c

The genomic sequence of *Sh2b1* between the end of exon 8 and the start of exon 9 (nt 6658-7181) was isolated from a pCR-Blunt II-TOPO vector (Invitrogen) containing a segment of genomic *Sh2b1* sequence corresponding to nt 4579-8807 using primers containing the AarI or the HindIII restriction sites (primers listed in Supplementary Material Table 2.7) and PfuUltra High-Fidelity DNA Polymerase (#600380; Agilent). cDNA encoding mouse SH2B1γ [23] was subcloned into pEGFPC1 (Clontech). The resulting vector encoding GFP-SH2B1γ was then cleaved with the AarI and HindII restriction sites and the novel PCR product (*Sh2b1* nt 6658-7181) was inserted into the GFP-SH2B1γ vector. The sequence was confirmed by the University of Michigan DNA Sequencing Core.

PC12 cell neurite outgrowth assay

PC12 cells were plated in tissue culture dishes coated with rat tail type I collagen (#354236; Corning) in RPMI 1640 (#A10491-01; Gibco) supplemented with 10% horse serum (HS) (#16050114; Gibco) and 5% fetal bovine serum (FBS) (#S11150; Atlanta Biologicals). For the neurite outgrowth assay, PC12 cells were plated in 6-well collagen-coated plates and transiently transfected with the indicated construct for 24 hours using Lipofectamine LTX (#15338030; Invitrogen). Cells were treated with 25 ng/mL mouse NGF 2.5S (BT.5025; Envigo) in RPMI 1640 medium containing 2% HS and 1% FBS. After 2 days, GFP-positive cells were visualized by fluorescence microscopy (20X or 40X objective, Nikon Eclipse TE200) and scored for the presence of neurites $\geq$ 2 times the

length of the cell body. N: 3 experiments (300 cells per condition counted in 1st replicate; 200 cells per condition counted in 2nd and 3rd replicates).

Immunoblotting

Blots were incubated overnight at 4°C with mouse monoclonal antibody to SH2B1 (1:1,000) (#sc-136065; Santa Cruz) or β-tubulin (1:1,000) (#sc-55529; Santa Cruz) or ERK1/2 (1:1,000) (#4695S; Cell Signaling) in 10 mM Tris, 150 mM NaCl, pH 7.4, 0.1% Tween 20, and 3% ovalbumin from chicken egg white, followed by IRDye-800CW goat anti-mouse IgG secondary antibody (1:20,000) (#926-32210; Li-Cor) for 1 hour at room temperature.

Acknowledgements

We thank Drs. Ray Joe, Lei Yin, Xin (Tony) Tong, and Deqiang Zhang for their feedback on experimental design and data analysis, and Sarah Cain for her administrative assistance. We thank Drs. Miriam Meisler, Carey Lumeng, and Malcolm Low for helpful discussions, Dr. Liangyou Rui for the gift of the *Sh2b1* KO strain, and Dr. Heimo Riedel (West Virginia University) for the cDNA encoding SH2B1γ. We acknowledge the Michigan Diabetes Research Center Molecular Genomics Core and Dr. Thomas Saunders, Galina Gavrilina, and Dr. Wanda Filipiak of the University of Michigan Transgenic Animal Model Core for help generating the $\alpha\delta$KO mouse model. We thank MedImmune for the gift of recombinant mouse leptin.

Funding

This research was supported by National Institutes of Health grants R01-DK-054222 and R01-DK-107730 (to C.C.-S.), R01-DK-056731 (to M.G.M.), and R01-DK-062876 and R01-DK-092759 (to O.A.M.). J.L.C. was supported by a National Science Foundation Graduate Research Fellowship and a Rackham Predoctoral Fellowship from the Horace H. Rackham School of Graduate Studies at the University of Michigan. A.F. was supported by predoctoral fellowships from the Rackham School of Graduate Studies at the University of Michigan (Rackham Merit Fellowship), Systems and Integrative Biology Training Program (NIH T32-GM-008322), and the Howard Hughes Medical Institute (Gilliam Fellowship for Advanced Study). L.C.D. was supported by an Endocrine Society Summer Research Fellowship and an American Physiological Society Undergraduate Summer Research Fellowship. D.P.B. was supported by predoctoral fellowships from the

Medical Scientist Training Program (NIH T32-GM-007863), Training Program for Organogenesis (NIH T32-HD-007605), and Rackham School of Graduate Studies at the University of Michigan (Rackham Merit Fellowship), and a Tylenol Future Care Scholarship. Mouse body composition and CLAMS studies were partially supported by the Michigan Diabetes Research Center (NIH P30-DK-020572), Michigan Nutrition Obesity Research Center (NIH P30-DK-089503), and Michigan Mouse Metabolic Phenotyping Center (NIH U2C-DK-110678). Generation of the CRISPR mice was partially supported by the Michigan Diabetes Research Center Molecular Genomics Core (NIH P30-DK-020572).

Author Contributions

J.L.C. directed and conducted experiments and prepared the manuscript including all figures. L.S.A. and A.F. designed and generated the $\alpha\delta$KO mice. J.L.C., L.S.A., O.A.M., M.G.M., and C.C.-S. developed the concepts and hypotheses, designed the experiments, and interpreted the data. L.S.A., O.A.M., M.G.M., and C.C.-S. made revisions to the manuscript. A.C.R. performed the initial bioinformatic analysis of RNA-seq data and generated plots for Supplementary Material Figs. 2.12B-D, 2.13A, and 2.14. J.M.C. performed qPCR assays (Figs. 2.1C, 2.7A and Supplementary Material Figs. 2.12A, 2.13D), ran western blots (Fig. 2.1G-H and Supplementary Material Fig. 2.13E), and made the construct encoding GFP-SH2B18c (Supplementary Material Fig. 2.13E). L.C.D. and A.H.B. assisted with body weight and food intake studies, blood sample collections, harvests, and genotyping. D.P.B. prepared and imaged liver samples (Fig. 2.4J). P.B.V. performed neurite outgrowth experiments (Supplementary Material Fig. 2.13F). A.M.C.

and E.S.C. assisted with genotyping and mouse colony maintenance. G.C. assisted with body weight studies and genotyping. All authors reviewed and approved the final content.

References

1. Doche, M.D., Bochukova, E.G., Su, H.W., Pearce, L., Keogh, J.M., Henning, E., . . . Farooqi, I.S. *SH2B1* mutations are associated with maladaptive behavior and obesity. *J. Clin. Invest.* **122**, 4732-4736 (2012).
2. Pearce, L.R., Joe, R., Doche, M.D., Su, H.W., Keogh, J.M., Henning, E., . . . Carter-Su, C. Functional characterisation of obesity-associated variants involving the alpha and beta isoforms of human SH2B1. *Endocrinology* **9**, 3219-3226 (2014).
3. Flores, A., Argetsinger, L.S., Stadler, L.K.J., Malaga, A.E., Vander, P.B., DeSantis, L.C., . . . Carter-Su, C. Crucial Role of the SH2B1 PH Domain for the Control of Energy Balance. *Diabetes* **68**, 2049-2062 (2019).
4. Ren, D., Li, M., Duan, C. & Rui, L. Identification of SH2-B as a key regulator of leptin sensitivity, energy balance and body weight in mice. *Cell Metab.* **2**, 95-104 (2005).
5. Duan, C., Yang, H., White, M.F. & Rui, L. Disruption of SH2-B causes age-dependent insulin resistance and glucose intolerance. *Mol. Cell. Biol.* **24**, 7435-7443 (2004).
6. Ren, D., Zhou, Y., Morris, D., Li, M., Li, Z. & Rui, L. Neuronal SH2B1 is essential for controlling energy and glucose homeostasis. *J. Clin. Invest.* **117**, 397-406 (2007).
7. Rui, L. SH2B1 regulation of energy balance, body weight, and glucose metabolism. *World J Diabetes* **5**, 511-526 (2014).
8. Emmerson, P.J., Wang, F., Du, Y., Liu, Q., Pickard, R.T., Gonciarz, M.D., . . . Wu, X. The metabolic effects of GDF15 are mediated by the orphan receptor GFRAL. *Nat Med* **23**, 1215-1219 (2017).
9. Chen, L., Maures, T.J., Jin, H., Huo, J.S., Rabbani, S.A., Schwartz, J. & Carter-Su, C. SH2B1β (SH2-Bβ) enhances expression of a subset of nerve growth factor-regulated genes important for neuronal differentiation including genes encoding uPAR and MMP3/10. *Mol. Endocrinol.* **22**, 454-476 (2008).
10. Diakonova, M., Gunter, D.R., Herrington, J. & Carter-Su, C. SH2-Bβ is a Rac-binding protein that regulates cell motility. *J. Biol. Chem.* **277**, 10669-10677 (2002).
11. Rider, L., Tao, J., Snyder, S., Brinley, B., Lu, J. & Diakonova, M. Adapter protein SH2B1β cross-links actin filaments and regulates actin cytoskeleton. *Mol. Endocrinol.* **23**, 1065-1076 (2009).
12. Zhang, Y., Zhu, W., Wang, Y.G., Liu, X.J., Jiao, L., Liu, X., . . . He, C. Interaction of SH2-Bβ with RET is involved in signaling of GDNF-induced neurite outgrowth. *J. Cell. Sci.* **119**, 1666-1676 (2006).
13. Shih, C.H., Chen, C.J. & Chen, L. New function of the adaptor protein SH2B1 in brain-derived neurotrophic factor-induced neurite outgrowth. *PloS one* **8**, e79619 (2013).
14. Chen, C.J., Shih, C.H., Chang, Y.J., Hong, S.J., Li, T.N., Wang, L.H. & Chen, L. SH2B1 and IRSp53 proteins promote the formation of dendrites and dendritic branches. *J Biol Chem* **290**, 6010-6021 (2015).
15. Rui, L., Herrington, J. & Carter-Su, C. SH2-B is required for nerve growth factor-induced neuronal differentiation. *J. Biol. Chem.* **274**, 10590-10594 (1999).

16. Qian, X., Riccio, A., Zhang, Y. & Ginty, D.D. Identification and characterization of novel substrates of Trk receptors in developing neurons. *Neuron* **21**, 1017-1029 (1998).
17. Myers, M.G. & Leibel, R.L. Lessons From Rodent Models of Obesity. in *Endotext* (eds. Feingold, K.R., Anawalt, B., Boyce, A., Chrousos, G., Dungan, K., Grossman, A., . . . Wilson, D.P.) (South Dartmouth (MA), 2000).
18. Joe, R.M., Flores, A., Doche, M.E., Cline, J.M., Clutter, E.S., Vander, P.B., . . . Carter-Su, C. Phosphorylation of the Unique C-terminal Tail of the Alpha Isoform of the Scaffold Protein SH2B1 Controls the Ability of SH2B1alpha to Enhance Nerve Growth Factor Function. *Mol Cell Biol* (2017).
19. Ran, F.A., Hsu, P.D., Wright, J., Agarwala, V., Scott, D.A. & Zhang, F. Genome engineering using the CRISPR-Cas9 system. *Nat. Protoc.* **8**, 2281-2308 (2013).
20. Parlee, S.D., Lentz, S.I., Mori, H. & MacDougald, O.A. Quantifying size and number of adipocytes in adipose tissue. *Methods Enzymol* **537**, 93-122 (2014).
21. Mina, A.I., LeClair, R.A., LeClair, K.B., Cohen, D.E., Lantier, L. & Banks, A.S. CalR: A Web-Based Analysis Tool for Indirect Calorimetry Experiments. *Cell Metab* **28**, 656-666 e651 (2018).
22. Nelms, K., O'Neill, T.J., Li, S., Hubbard, S.R., Gustafson, T.A. & Paul, W.E. Alternative splicing, gene localization, and binding of SH2-B to the insulin receptor kinase domain. *Mammalian Genome* **10**, 1160-1167 (1999).
23. Yousaf, N., Deng, Y., Kang, Y. & Riedel, H. Four PSM/SH2-B alternative splice variants and their differential roles in mitogenesis. *J. Biol. Chem.* **276**, 40940-40948 (2001).
24. Tortoriello, D.V., McMinn, J. & Chua, S.C. Dietary-induced obesity and hypothalamic infertility in female DBA/2J mice. *Endocrinology* **145**, 1238-1247 (2004).
25. Yang, Y., Smith, D.L., Jr., Keating, K.D., Allison, D.B. & Nagy, T.R. Variations in body weight, food intake and body composition after long-term high-fat diet feeding in C57BL/6J mice. *Obesity (Silver Spring)* **22**, 2147-2155 (2014).
26. Patterson, C.M., Leshan, R.L., Jones, J.C. & Myers Jr., M.G. Molecular mapping of mouse brain regions innervated by leptin receptor-expressing cells. *Devl. Brain Res.* **1378**, 18-28 (2011).
27. Scott, M.M., Lachey, J.L., Sternson, S.M., Lee, C.E., Elias, C.F., Friedman, J.M. & Elmquist, J.K. Leptin targets in the mouse brain. *J Comp Neurol* **514**, 518-532 (2009).
28. Flak, J.N. & Myers, M.G., Jr. Minireview: CNS Mechanisms of Leptin Action. *Molecular endocrinology* **30**, 3-12 (2016).
29. Allison, M.B., Pan, W., MacKenzie, A., Patterson, C., Shah, K., Barnes, T., . . . Myers, M.G., Jr. Defining the Transcriptional Targets of Leptin Reveals a Role for Atf3 in Leptin Action. *Diabetes* **67**, 1093-1104 (2018).
30. Bjornholm, M., Munzberg, H., Leshan, R.L., Villanueva, E.C., Bates, S.H., Louis, G.W., . . . Myers, M.G., Jr. Mice lacking inhibitory leptin receptor signals are lean with normal endocrine function. *J Clin Invest* **117**, 1354-1360 (2007).
31. Rupp, A.C., Allison, M.B., Jones, J.C., Patterson, C.M., Faber, C.L., Bozadjieva, N., . . . Myers, M.G., Jr. Specific subpopulations of hypothalamic leptin receptor-

expressing neurons mediate the effects of early developmental leptin receptor deletion on energy balance. *Molecular metabolism* **14**, 130-138 (2018).
32. Chen, R., Wu, X., Jiang, L. & Zhang, Y. Single-Cell RNA-Seq Reveals Hypothalamic Cell Diversity. *Cell Rep* **18**, 3227-3241 (2017).
33. Filipello, F., Morini, R., Corradini, I., Zerbi, V., Canzi, A., Michalski, B., . . . Matteoli, M. The Microglial Innate Immune Receptor TREM2 Is Required for Synapse Elimination and Normal Brain Connectivity. *Immunity* **48**, 979-991 e978 (2018).
34. Hoshiko, M., Arnoux, I., Avignone, E., Yamamoto, N. & Audinat, E. Deficiency of the microglial receptor CX3CR1 impairs postnatal functional development of thalamocortical synapses in the barrel cortex. *J Neurosci* **32**, 15106-15111 (2012).
35. Paolicelli, R.C., Bolasco, G., Pagani, F., Maggi, L., Scianni, M., Panzanelli, P., . . . Gross, C.T. Synaptic pruning by microglia is necessary for normal brain development. *Science* **333**, 1456-1458 (2011).
36. Zhang, B., Gaiteri, C., Bodea, L.G., Wang, Z., McElwee, J., Podtelezhnikov, A.A., . . . Emilsson, V. Integrated systems approach identifies genetic nodes and networks in late-onset Alzheimer's disease. *Cell* **153**, 707-720 (2013).
37. Stevens, B., Allen, N.J., Vazquez, L.E., Howell, G.R., Christopherson, K.S., Nouri, N., . . . Barres, B.A. The classical complement cascade mediates CNS synapse elimination. *Cell* **131**, 1164-1178 (2007).
38. Popp, M.W. & Maquat, L.E. Leveraging Rules of Nonsense-Mediated mRNA Decay for Genome Engineering and Personalized Medicine. *Cell* **165**, 1319-1322 (2016).
39. Moroy, T. & Heyd, F. The impact of alternative splicing in vivo: mouse models show the way. *RNA* **13**, 1155-1171 (2007).
40. Zhang, M., Deng, Y. & Riedel, H. PSM/SH2B1 splice variants: critical role in src catalytic activation and the resulting STAT3s-mediated mitogenic response. *J. Cell. Biochem.* **104**, 105-118 (2008).
41. Zhang, M., Deng, Y., Tandon, R., Bai, C. & Riedel, H. Essential role of PSM/SH2-B variants in insulin receptor catalytic activation and the resulting cellular responses. *J. Cell. Biochem.* **103**, 162-181 (2008).
42. Rios, M. BDNF and the central control of feeding: accidental bystander or essential player? *Trends Neurosci.* **36**, 83-90 (2013).
43. Noble, E.E., Billington, C.J., Kotz, C.M. & Wang, C. The lighter side of BDNF. *Am. J. Physiol. Regul. Integr. Comp. Physiol.* **300**, R1053-R1069 (2011).
44. Lipscombe, D. Neuronal proteins custom designed by alternative splicing. *Curr Opin Neurobiol* **15**, 358-363 (2005).
45. Li, Q., Lee, J.A. & Black, D.L. Neuronal regulation of alternative pre-mRNA splicing. *Nat Rev Neurosci* **8**, 819-831 (2007).
46. Licatalosi, D.D. & Darnell, R.B. Splicing regulation in neurologic disease. *Neuron* **52**, 93-101 (2006).
47. Kaminska, D. & Pihlajamaki, J. Regulation of alternative splicing in obesity and weight loss. *Adipocyte* **2**, 143-147 (2013).
48. Wong, C.M., Xu, L. & Yau, M.Y. Alternative mRNA Splicing in the Pathogenesis of Obesity. *Int J Mol Sci* **19**(2018).

49. Ran, F.A., Hsu, P.D., Lin, C.Y., Gootenberg, J.S., Konermann, S., Trevino, A.E., . . . Zhang, F. Double nicking by RNA-guided CRISPR Cas9 for enhanced genome editing specificity. *Cell* **154**, 1380-1389 (2013).
50. Vandesompele, J., De Preter, K., Pattyn, F., Poppe, B., Van Roy, N., De Paepe, A. & Speleman, F. Accurate normalization of real-time quantitative RT-PCR data by geometric averaging of multiple internal control genes. *Genome Biol* **3**, research0034.0031-0034.0011 (2002).
51. Andrews, S. FastQC: A Quality Control Tool for High Throughput Sequence Data. (2010).
52. Hannon, G.J. FASTX-Toolkit. (2010).
53. Dobin, A., Davis, C.A., Schlesinger, F., Drenkow, J., Zaleski, C., Jha, S., . . . Gingeras, T.R. STAR: ultrafast universal RNA-seq aligner. *Bioinformatics* **29**, 15-21 (2013).
54. Team, R.C. R: A language and environment for statistical computing. *R Foundation for Statistical Computing, Vienna, Austria* (2017).
55. Love, M.I., Huber, W. & Anders, S. Moderated estimation of fold change and dispersion for RNA-seq data with DESeq2. *Genome Biol* **15**, 550 (2014).
56. Thomas, P.D., Campbell, M.J., Kejariwal, A., Mi, H., Karlak, B., Daverman, R., . . . Narechania, A. PANTHER: a library of protein families and subfamilies indexed by function. *Genome Res* **13**, 2129-2141 (2003).
57. Cunningham, F., Achuthan, P., Akanni, W., Allen, J., Amode, M.R., Armean, I.M., . . . Flicek, P. Ensembl 2019. *Nucleic Acids Res* **47**, D745-D751 (2019).
58. Pertea, M., Pertea, G.M., Antonescu, C.M., Chang, T.C., Mendell, J.T. & Salzberg, S.L. StringTie enables improved reconstruction of a transcriptome from RNA-seq reads. *Nat Biotechnol* **33**, 290-295 (2015).
59. Wickham, H. ggplot2: Elegant Graphics for Data Analysis. *Springer-Verlag New York (book)* (2009).
60. Team, R. RStudio: Integrated Development for R. RStudio, Inc., Boston, MA. (2015).
61. Stuart, T., Butler, A., Hoffman, P., Hafemeister, C., Papalexi, E., Mauck, W.M., 3rd, . . . Satija, R. Comprehensive Integration of Single-Cell Data. *Cell* **177**, 1888-1902 e1821 (2019).
62. Butler, A., Hoffman, P., Smibert, P., Papalexi, E. & Satija, R. Integrating single-cell transcriptomic data across different conditions, technologies, and species. *Nat Biotechnol* **36**, 411-420 (2018).

Chapter 3:

The Brain-Specific δ Isoform of SH2B1 Enhances the Morphological Complexity and Function of Cultured Neurons

Abstract

Adapter protein SH2B1 is recruited to multiple neurotrophic factor receptors including receptors for nerve growth factor (NGF) and brain-derived neurotrophic factor (BDNF). Alternative splicing produces four previously described SH2B1 isoforms (α, β, γ, δ) that differ only in their C-terminal tails. SH2B1β and SH2B1γ are expressed ubiquitously, whereas SH2B1α and SH2B1δ exhibit brain-specific expression. SH2B1β, but not SH2B1α, enhances neurotrophic factor-induced gene expression and neurite outgrowth in PC12 cells and/or primary hippocampal neurons. Here we demonstrate how the unique C-terminal tail of the brain-specific δ isoform of SH2B1 modulates SH2B1 function in PC12 cells and primary hippocampal neurons. We show that SH2B1δ localizes to the nucleolus and plasma membrane in both cell types. A bipartite nucleolar localization sequence in the C-terminal tail of SH2B1δ is required for SH2B1δ to localize to the nucleolus. SH2B1δ enhances neurotrophic factor-induced signaling events and gene expression in PC12 cells. Primary hippocampal neurons harvested from mice null for *Sh2b1* (*Sh2b1* KO mice) exhibit decreased neurite length and complexity. Hippocampal

neurons from *Sh2b1* KO mice exhibit decreased BDNF-induced expression of key synapse-regulating immediate early genes *Egr1* and *Arc*. Re-introduction of each SH2B1 isoform into hippocampal neurons from *Sh2b1* KO mice increases neurite complexity to some degree; SH2B1δ induces the most robust effect. Nucleolar and plasma membrane localization and a functional SH2 domain are required for SH2B1δ to increase neurite complexity. Together, these findings suggest that SH2B1 isoforms are important for proper development and/or maintenance of individual neurons and neuronal synapses. These results also suggest that the unique C-terminal tail of the brain-specific δ isoform of SH2B1 enables SH2B1 to increase neurite outgrowth and complexity in neurons by, at least in part, localizing to the nucleolus.

Note: This chapter is being prepared for submission as a manuscript titled "The Brain-Specific δ Isoform of Adapter Protein SH2B1 Enhances the Morphological Complexity and Function of Cultured Neurons" by Jessica L. Cote, Paul B. Vander, Michael Ellis, Joel M. Cline, Michael E. Doche, Travis J. Maures, Tahrim A. Choudhury, Seongbae Kong, Olivia Klaft, Lawrence S. Argetsinger, and Christin Carter-Su.

Introduction

The neurotrophin family of growth factors make critical contributions to the development and maintenance of the nervous system. Their actions regulate neuronal structure and function both globally, through changes in gene expression, and locally, through modifications to the cytoskeleton [1]. The neurotrophin family consists of nerve growth factor (NGF), brain-derived neurotrophic factor (BDNF), neurotrophin-3, and neurotrophin-4/5. Of these, NGF and BDNF are the primary regulators of peripheral and central nervous system development, respectively [2]. NGF and BDNF bind their respective receptor tyrosine kinases, TrkA and TrkB, to activate and induce autophosphorylation of these receptors, which initiates recruitment of signaling proteins and subsequent downstream activities [3,4].

SH2B1 is a signaling adapter protein that is recruited to phosphotyrosines in activated tyrosine kinase receptors including TrkA and TrkB [5]. From these activated receptors, SH2B1 stimulates and propagates downstream signaling events [6-9] and enhances gene expression [8,10,11] and reorganization of the actin cytoskeleton [12-16]. Indeed, knockdown of SH2B1 reduces neurotrophin-induced gene expression [10] in PC12 cells as well as neurite outgrowth and/or branching in PC12 cells [9,10] and primary neurons [9,14]. Human and mouse studies indicate that disruption or deletion of SH2B1 disturbs mechanisms that regulate feeding and social behaviors. Humans with inactivating mutations in *SH2B1* develop severe, early-onset obesity from over-eating and many have disproportionate insulin resistance for their level of obesity [17-19]. Some also display developmental delay, aggressive behavior, and/or social isolation [17-19]. Mice null for *Sh2b1* (*Sh2b1* KO mice [KO mice]) similarly exhibit obesity, insulin resistance, and

aggression [20-22]. While earlier work [20] provided evidence that SH2B1 regulates energy balance, at least in part, by modulating leptin signaling, more recent work [22-24] suggests that some isoforms of SH2B1 may regulate energy balance through leptin-independent means. Because BDNF/TrkB activity is strongly implicated in the regulation of energy balance [25] and SH2B1 is recruited to activated TrkB, SH2B1 may regulate energy balance, at least in part, by modulating TrkB signaling. This possibility underscores the need to better understand how SH2B1 modulates the activity of the Trk receptors at the cellular level.

Alternative splicing generates four unique SH2B1 isoforms: α, β, γ, and δ [26,27]. In humans and rodents, these isoforms share 631 amino acids and differ only in their C-terminal tails (Fig. 3.1A). SH2B1β and SH2B1γ are expressed ubiquitously, whereas SH2B1α and SH2B1δ are expressed almost exclusively in brain tissue [17]. In a steady state, SH2B1α [8,18], β [8,11,18,28], and γ localize to the cytoplasm and plasma membrane. While the C-terminal tail of SH2B1α contains a unique tyrosine (Tyr753) whose phosphorylation dictates some isoform-specific functions [8], the C-terminal tails of SH2B1β and γ do not contain recognizable domains or features. The C-terminal tail of SH2B1δ contains two highly basic regions [27] but its subcellular localization had not been determined previously. SH2B1β and/or γ, but not SH2B1α, enhance NGF-induced signaling events [6-8], gene expression [8,10,11], and neurite outgrowth in PC12 cells [8,11,29,30]. SH2B1β enhances BDNF-induced signaling events and neurite outgrowth and branching in primary neurons [9,14,31]. The ability of the unique C-terminal tail of SH2B1δ to modulate SH2B1 regulation of neurotrophin-induced cellular activities had not been investigated previously.

Specific SH2B1 isoforms have been implicated in SH2B1 regulation of energy balance. For example, reintroduction of SH2B1β into neurons of KO mice via the neuron-specific enolase promoter results in mice of normal, rather than high, body weight [32]. Additionally, our lab recently demonstrated that deletion of the brain-specific α and δ isoforms of SH2B1 results in a lean mouse that eats less food than its control littermates [23]. Together, these results suggest not only that the α, β, and/or δ isoforms contribute to SH2B1 regulation of energy balance, but also that the different SH2B1 isoforms perform different functions *in vivo*. These findings highlight the need to better understand how the different isoforms, particularly the less studied δ isoform, function in the context of neurotrophin-induced cellular activities.

Here we investigate cellular actions of the brain-specific δ isoform of adapter protein SH2B1. We report that SH2B1δ localizes to the nucleolus. The nucleolar localization of SH2B1δ requires two highly basic regions in its unique C-terminal tail. SH2B1δ promotes NGF-induced signaling events and gene expression in PC12 cells. Primary hippocampal neurons from KO mice exhibit decreased neurite outgrowth and arborization and the expression of BDNF-induced, synapse-related immediate early genes. While reintroduction of each SH2B1 isoform into neurons from KO mice enhances their outgrowth and arborization, SH2B1δ has the greatest impact. SH2B1δ must localize to the nucleolus and plasma membrane to maximally increase neurite complexity in hippocampal neurons. Together, these data suggest that the unique C-terminal tail of SH2B1δ modulates SH2B1 regulation of neuronal development by, at least in part, its ability to target SH2B1 to the nucleolus.

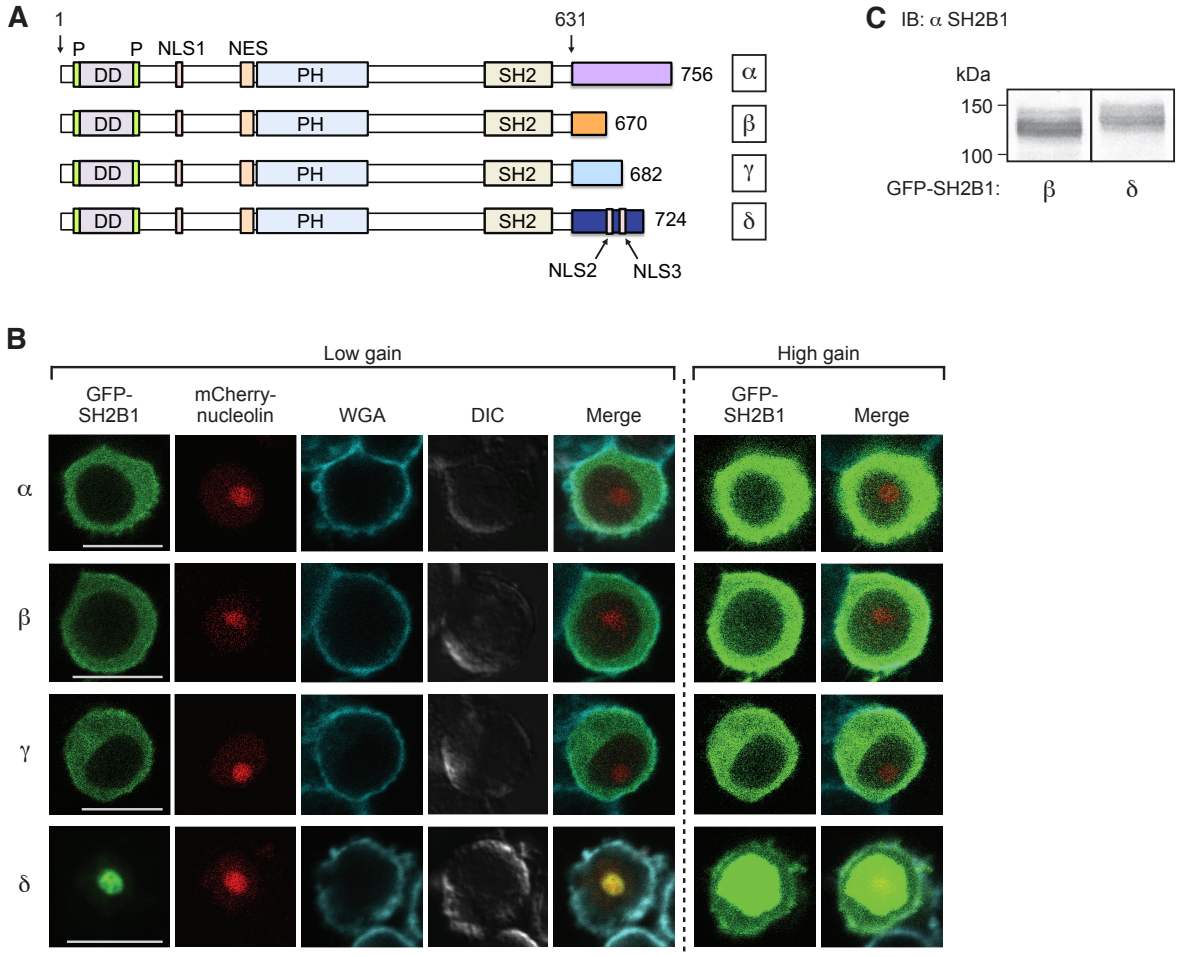

Figure 3.1. SH2B1δ localizes to the nucleolus and plasma membrane

(A) Schematic of SH2B1α, β, γ, and δ, modified from Cote et al., 2021. Isoform-specific C-terminal tails are noted in purple, orange, light blue, and dark blue, respectively. Numbers indicate amino acids in mouse and human sequences. P, proline-rich region; DD, dimerization domain; NLS, nuclear localization sequence; NES, nuclear export sequence, PH, pleckstrin homology domain; SH2, Src homology 2 domain. **(B)** PC12 cells transiently co-expressing GFP-tagged SH2B1 isoforms and mCherry-tagged nucleolin were stained with Alexa Fluor 488-conjugated wheat germ agglutinin (WGA) and imaged using live-cell confocal microscopy. Left 5 panels: low gain. Right 2 panels: high gain. Images are representative; depicted localizations of SH2B1 isoforms were observed in at least 20 cells per isoform. DIC, differential interference contrast. Scale bar = 10 μm. **(C)** Proteins in cell lysates from PC12 cells transiently expressing GFP-tagged SH2B1β or SH2B1δ were immunoblotted with antibody to SH2B1 (α SH2B1). The migration of molecular weight standards is shown on the left.

Materials and Methods

Antibodies

Primary antibodies: Mouse monoclonal antibody to SH2B1 (sc-136065) (1:1,000) was obtained from Santa Cruz. Rabbit polyclonal antibody to GFP (632592) (1:2,000) was obtained from Clontech. Rabbit polyclonal antibody to PSD-95 (AB9708) (1:1,000) was obtained from Sigma-Aldrich. Chicken polyclonal antibody to GFP (AB_2307313) (1:500) was obtained from Aves Labs. The following antibodies were obtained from Cell Signaling: rabbit polyclonal antibodies to PLCγ (2822S) (1:1,000), phospho-PLCγ (Y783) (2821S) (1:500), and doubly phosphorylated ERK1/2 (T202/Y204) (9101S) (1:1,000); rabbit monoclonal antibody to phospho-AKT (S473) (4058L) (1:1,000); and mouse monoclonal antibodies to AKT (2920S) (1:2,000) and ERK1/2 (4696S) (1:2,000).

Secondary antibodies: Goat anti-chicken IgY Alexa Fluor 488 (A-11039) was obtained from Invitrogen. The following infrared dye conjugated secondary antibodies were obtained from Li-Cor Biosciences: goat anti-rabbit IgG 680RD (926-68071) (1:15,000) and goat anti-mouse IgG 680LT (926-68020) (1:15,000), 680RD (926-68070) (1:15,000), and 800CW (926-32210) (1:20,000).

Plasmids

cDNAs encoding mouse GFP-SH2B1α (GenBank accession #AF421138) [8] and rat GFP-SH2B1β (GenBank accession #NM_001048180) [33] were described previously. cDNA encoding mouse SH2B1γ (GenBank accession #NM_01136.3) and SH2B1δ (GenBank accession #AF_380422) [27] (from Dr. Heimo Riedel, West Virginia University) were

subcloned into pEGFPC1 (Clontech). cDNA encoding mouse GFP-SH2B1β (GenBank accession #NM_001081459.2) was created from cDNA encoding mouse GFP-SH2B1γ (GenBank accession #NM_011363.3). Briefly, nucleotides 6659-6711 of mouse genomic *Sh2b1* (NC_000073), corresponding to the γ/δ-specific portion of exon 8, were removed using the QuikChange II site-directed mutagenesis kit (200521; Agilent). Nucleotides 7358-7376 that lie beyond the stop codon of SH2B1γ in exon 10 but encode the last four amino acids and stop codon (TEHLP*) of SH2B1β, were inserted into the vector. Mutations were introduced into SH2B1δ using site-directed mutagenesis. cDNA encoding mCherry-tagged human nucleolin (GenBank accession #NM_005381.2) was created from cDNA encoding GFP-tagged human nucleolin (plasmid 28176, Addgene) using AgeI and BsrGI restriction enzymes. All sequences were confirmed by the University of Michigan DNA Sequencing Core or Eurofin Genomics.

PC12 cell culture and transfection

PC12 cells (CRL-1721; ATCC) were grown on 10 cm tissue culture dishes (0877222; Corning) coated with rat tail type I collagen (354236; Corning) and maintained at 37°C with 5% CO_2 in normal growth medium (RPMI 1640; A10491-01; Life Technologies) supplemented with 10% horse serum (HS) (16050-122; Gibco) and 5% fetal bovine serum (FBS) (S11150; Atlanta Biologicals). PC12 cells were transiently transfected using Lipofectamine LTX. PC12 cell lines stably expressing GFP, GFP-SH2B1β, or GFP-SH2B1δ were prepared and maintained as described previously [8]. Prior to experiments requiring NGF stimulation, PC12 cells were incubated overnight in deprivation medium

(RPMI 1640 containing 1% bovine serum albumin [BSA] [7500804; Proliant Biologicals]). Recently thawed stocks of PC12 cells were periodically tested for mycoplasma.

Animal care and models

Mice (*Mus musculus*) were housed in ventilated cages (~22°C) on a 12-hour light/dark cycle (~6_{AM}/6_{PM}) in a pathogen-free animal facility at the University of Michigan. Food and water were available *ad libitum*. Breeders were given standard chow containing 6.5% fat (5008; LabDiet) or 9% fat (5058; LabDiet). The previously-described *Sh2b1* KO mouse strain [21] was obtained from Dr. Liangyou Rui (University of Michigan). C57BL/6J mice (000664) were obtained from The Jackson Laboratory. Experiments were approved by the University of Michigan Institutional Animal Care & Use Committee.

Primary hippocampal neuron culture

Hippocampal neuron cultures were prepared from male and/or female mouse neonates from C57BL/6J x C57BL/6J breeding pairs (Figs. 3.4A and 3.5A) or *Sh2b1*$^{+/-}$ x *Sh2b1*$^{+/-}$ breeding pairs (all other figures) on postnatal day 0, 1, or 2. Day of neuron plating was considered DIV 0. Hippocampi were dissected in ice-cold dissociation medium (DM) (1 M Na_2SO_4, 0.5 M K_2SO_4, 1 M $MgCl_2$, 1 M $CaCl_2$, 1 M HEPES, 2.5 M glucose, pH 7.4) under a stereo microscope (SZ51; Olympus). Isolated hippocampi were treated with papain (pH 7.4) (LK003178; Worthington Biochemical) for 30 minutes at 37°C, washed first with DM supplemented with 10% FBS, and then washed with normal DM. Papain was activated with L-cysteine (C7352; Sigma-Aldrich) before use. Hippocampi were dissociated in neuron growth medium (Neurobasal Plus medium [A3582901; Gibco], 2% B-27 Plus

[A3582801; Gibco], 1% penicillin/streptomycin [pen/strep] [15140-122; Gibco]) by triturating the tissue 10-20 times using a 5 mL serological pipette set to high speed. Cell suspension was placed on ice for 3 minutes and centrifuged at 600 x *g* for 5 minutes at 4°C. Pelleted cells were resuspended in neuron growth medium and plated onto glass coverslips as detailed below. Cultures were maintained at 37°C in 5% CO_2 in neuron growth medium.

Live-cell confocal imaging and analysis

Prior to live-cell imaging, PC12 cells were grown overnight on 35 mm poly-D-lysine-coated glass bottom dishes (P35GC-1.5-15-C; MatTek Life Sciences) and then transiently transfected with the indicated constructs. Live cells were imaged in Ringer's buffer (10 mM HEPES, 155 mM NaCl, 2 mM $CaCl_2$, 5 mM KCl, 1 mM $MgCl_2.6H_2O$, 10 mM $NaH_2PO_4.H_2O$, 10 mM glucose, pH 7.2) using a 60X water immersion objective on a Nikon A1 laser-scanning confocal microscope (Nikon Instruments) and Nikon NIS-Elements software (Microscopy, Imaging, and Cellular Physiology Core of the Michigan Diabetes Research Center). The plasma membrane was labeled with wheat germ agglutinin (WGA) Alexa Fluor 647 conjugate (W32466; Invitrogen). Focal planes were chosen to allow for maximum visualization of nucleoli and the plasma membrane, and each cell was imaged at both low and high gain by adjusting the voltage to the photomultiplier tubes on the microscope. The relative levels of GFP-SH2B1 in the nucleoli, nucleus, cytoplasm, and plasma membrane were assessed by a researcher blinded to the experimental conditions: Levels were "bright" if visible at low gain, "dim" if visible at high gain but not at low gain, or "absent" if not visible at high gain. Sample size (20-30 cells/condition) was

determined from our previous work [8]. Cells were excluded from analysis if they exhibited unusually high or low levels of expression or were dead or unhealthy (<10% of cells).

Hippocampal neurons (90,000 cells/dish) were plated onto 35 mm glass bottom dishes (P35G-1.5-14-C; MatTek Life Sciences), which had been coated with poly-D-lysine (A3890401; Gibco) prior to plating. Neurons were transfected using Lipofectamine 3000 (L3000-008; Invitrogen) and 1 ug total of the indicated cDNAs. Live neurons were imaged using 40X and 60X water immersion objectives on a Nikon A1 laser-scanning confocal microscope. Focal planes were chosen to maximize visualization of the nucleus or neurites.

Analysis of neuronal architecture

Hippocampal neurons (90,000 cells/coverslip) were plated onto glass coverslips pre-coated with poly-D-lysine (GG-15-PDL; Neuvitro Corporation) and laminin (L2020-1MG; Sigma-Aldrich). Neurons were transfected on DIV 4 using Lipofectamine 3000 and 1 ug total of the indicated cDNAs. Live neurons were imaged on DIV 5 using 10X and 20X objectives on a fluorescent microscope (Eclipse TE200; Nikon Instruments). Neurites were traced and Sholl analysis was performed using the semi-automated Simple Neurite Tracer plugin for FIJI 2. A subset of neuron images were selected for analysis from a larger depository of images using a random number generator. Sample size (> 25 neurons/condition) was determined from preliminary data analysis (data not shown) and consultation with Biostatistical Services of the Michigan Diabetes Research Center. Researchers taking and tracing images were blinded to experimental conditions. Neurons were excluded from all further analysis if their measurements were greater than 3 standard deviations from the mean for any of the following parameters: number of

endpoints, total neurite length, length of the longest neurite, maximum number of intersections, or maximum distance.

Immunoblotting

PC12 cells were treated and lysed as previously described [8] using ice-cold modified L-RIPA buffer (20 mM Tris, 150 mM NaCl, 1% Triton X-100, 1 mM EGTA, 1 mM EDTA, pH 7.4) supplemented with 20 mM NaF, 1 mM Na_3VO_4, and protease inhibitors (1 mM phenylmethylsulfonyl fluoride [PMSF], 10 ug/mL aprotinin, 10 ug/mL leupeptin). Hippocampal neurons (200,000 cells/coverslip) were plated as described for analysis of neuronal architecture. Neurons were washed with Hank's Basic Salt Solution or phosphate buffered saline (PBS) (10mM $NaPO_4$, 140 mM NaCl, pH 7.4) and lysed using ice-cold modified L-RIPA buffer supplemented with 50 mM β-glycerophosphate, 1 mM Na_3VO_4, and protease inhibitor cocktail (1:100) (P8340; Sigma-Aldrich). Cell lysates were centrifuged at 15,000 x *g* for 15 minutes at 4°C. Protein concentration of the supernatant was measured using the DC Protein Assay (5000116; Bio-Rad).

Equal amounts of proteins were resolved using 4-15% precast Criterion Tris-HCl protein gels (3450027; Bio-Rad) and transferred to low-fluorescence PVDF membranes (1620264; Bio-Rad). Blots were blocked for 1 hour at room temperature in blocking buffer (10 mM Tris, 150 mM NaCl, pH 7.4, 0.1% Tween 20, 3% BSA). Blots were incubated with primary antibody diluted in blocking buffer overnight at 4°C followed by secondary antibody diluted in blocking buffer for 1 hour at room temperature. Bands were visualized using the Odyssey infrared imaging system (Li-Cor Biosciences) and quantified using Image Studio Lite 5.2.

Immunocytochemistry

Hippocampal neurons (90,000 cells/coverslip) were plated onto glass coverslips pre-coated with poly-D-lysine. Cultures were fixed using 4% paraformaldehyde (15710; Electron Microscopy Sciences) for 20 minutes at room temperature and permeabilized using 0.3% Triton X-100 in ICC blocking buffer (PBS containing 1% BSA). Following 30 minutes in ICC blocking buffer, cells were incubated with primary antibody for one hour at room temperature or overnight at 4°C. Cultures were incubated with secondary antibody for one or two hours at room temperature. Coverslips were mounted on glass microscope slides (22-035813; Fisherbrand) using ProLong Gold Antifade Mountant (P10144; Invitrogen) and stored at 4°C. Cells were imaged using a Nikon A1 laser-scanning confocal microscope or Eclipse TE200 fluorescent microscope.

RNA isolation and qPCR

PC12 cells were treated and relative mRNA levels of *Plaur*, *Mmp3*, *Mmp10*, and *FosL1* were determined as described previously [8]. Hippocampal neurons (200,000 cells/coverslip) were plated as described above for analysis of neuronal architecture and RNA isolated on the indicated DIV using the RNeasy Mini Kit (74104; QIAGEN). RNA quality was confirmed using a Nanodrop spectrophotometer before RNA was reverse-transcribed using iScript cDNA Synthesis Kit (1708891; Bio-Rad). Relative mRNA levels were determined using TaqMan Gene Expression Assays (ThermoFisher Scientific) (Table 3.1). qPCR was performed with an Eppendorf Realplex2 using Mastercycler software and PCR parameters recommended by Applied Biosystems. All cDNA samples

were analyzed in triplicate and a non-template control was included for each gene of interest. Cycle threshold (Ct) values were normalized to the geometric mean of the Ct values of three reference genes (*36b4*, *Gapdh*, *Tbp*) as previously described [34]. Expression of the reference genes did not differ between control and experimental samples (data not shown).

Table 3.1. TaqMan Gene Expression Assays from Applied Biosystems

Gene	Species	TaqMan Gene Expression Assay
Sh2b1	Mouse	Mm01137783_m1
*Sh2b1*α	Mouse	Mm01275190_m1
*Sh2b1*β	Mouse	Mm01163373_g1
*Sh2b1*γ	Mouse	Mm00488153_m1
*Sh2b1*δ	Mouse	Mm01163374_m1
Ubtf	Mouse	Mm00456972_m1
Fbl	Mouse	Mm02601599_gH
Ncl	Mouse	Mm01290591_m1
Npm1	Mouse	Mm02391781_g1
Arc	Mouse	Mm00479619_g1
Egr1	Mouse	Mm00656724_m1
36b4 (reference gene)	Mouse	Mm007725448_s1
Gapdh (reference gene)	Mouse	Mm99999915_g1
Tbp (reference gene)	Mouse	Mm01277042_m1

Statistical analyses

Statistics were performed using GraphPad Prism 8 or 9. Sholl analysis results were compared by two-way repeated measures ANOVA with Dunnett's or Sidak's multiple comparisons tests. All other comparisons were analyzed by one-way ANOVA with Dunnett's multiple comparisons test or two-tailed Student's t-test. For qPCR experiments, relative mRNA expression levels were normalized to those measured in NGF-treated GFP-SH2B1β-expressing PC12 cells (Fig. 3.3) or BDNF-treated WT hippocampal neurons (Figs. 3.8 and 3.10). Data are mean values ± standard error of the mean. $P < 0.05$ was considered significant.

Results

Subcellular localization and molecular weight of SH2B1δ

Each of the four SH2B1 isoforms has a unique C-terminal tail (Fig. 3.1A). The C-terminal tail in SH2B1δ contains two highly basic regions that match the canonical sequence for nuclear localization motifs [27]. We refer to these regions as NLS2 and NLS3. To gain insight into the impact of the unique C-terminal tail of SH2B1δ on SH2B1 function, we first examined whether SH2B1δ localizes similarly to the other known SH2B1 isoforms. We transiently expressed GFP-tagged SH2B1α, β, γ, or δ in PC12 cells and imaged their steady-state subcellular localizations using live-cell confocal microscopy. Consistent with our previous results [8,18,35], SH2B1α and β localized primarily in the cytoplasm and at the plasma membrane (Fig. 3.1B). SH2B1γ localized similarly. However, in contrast to the other three isoforms, SH2B1δ localized primarily to nucleoli. SH2B1δ also localized to the plasma membrane, which was observed at an increased photomultiplier gain level.

We next tested whether the δ isoform of SH2B1 was expressed at levels similar to that of the well-studied β isoform. We transiently transfected equal amounts of cDNA encoding either GFP-SH2B1β or GFP-SH2B1δ into PC12 cells and subjected protein lysates to immunoblotting with antibody to SH2B1 (α SH2B1). Consistent with our previous observations [8,36], GFP-SH2B1β migrated as a ~120 kDa protein (Fig. 3.1C). As expected based on its longer amino acid sequence (Fig. 3.1A), GFP-SH2B1δ migrated as a slightly larger protein, ~125 kDa (Fig. 3.1C). The two proteins were expressed to similar extents.

SH2B1δ enhances neurotrophic factor-induced signaling events

The binding of neurotrophic factors NGF and BDNF to their respective Trk receptors activates and induces autophosphorylation of these receptors. This activity enables signaling proteins, including SH2B1, to be recruited via their SH2 and/or PTB domains to phosphotyrosines in these receptors. Three major signaling pathways are induced by NGF and BDNF binding to their Trk receptors: MAPK/ERK, PI3K/Akt, and PLCγ. Our lab and/or others have previously shown that SH2B1β enhances and prolongs NGF- and BDNF-induced phosphorylation of PLCγ at Tyr783 and Akt at Ser473 in PC12 cells [6-9]. Some, but not all, studies have observed that SH2B1β modestly enhances NGF- and BDNF-induced phosphorylation of ERK1/2 at Thr202/Tyr204 in PC12 cells [6-9,11,29]. All three signaling pathways may contribute to neurite outgrowth [37-40].

Given that SH2B1β and SH2B1δ localize to distinct subcellular compartments (Fig. 3.1B), we wondered whether SH2B1δ would, like SH2B1β, enhance neurotrophic factor-induced signaling events. We stably expressed GFP, GFP-SH2B1β, or GFP-SH2B1δ in PC12 cells, stimulated the cells with NGF (25 ng/mL) for 0, 10, or 60 minutes, and subjected cell lysates to immunoblotting to determine phosphorylation of activating amino acids in PLCγ, Akt, and ERK1/2. Consistent with previous results [6,8,41], SH2B1β promoted prolonged phosphorylation of PLCγ (Fig. 3.2A-B) and rapid phosphorylation of Akt (Fig. 3.2A,C). SH2B1β did not have a statistically significant impact on the phosphorylation of ERK1/2 (Fig. 3.2A,D). Similar to SH2B1β, SH2B1δ promoted prolonged phosphorylation of PLCγ (Fig. 3.2A-B) and rapid phosphorylation of Akt (Fig. 3.2A,C). SH2B1δ also promoted prolonged phosphorylation of Akt (Fig. 3.2A,C) and rapid phosphorylation of ERK1/2 (Fig. 3.2A,D).

Whether SH2B1δ is more effective at promoting NGF-induced signaling events than SH2B1β is unclear. Probing the cell lysates for GFP indicated that GFP-SH2B1δ was expressed at lower levels than GFP-SH2B1β (Fig. 3.2A). Because SH2B1δ enhanced signaling activity to a similar extent as SH2B1β despite its apparent reduced protein expression, SH2B1δ may have been a more potent promoter of NGF-induced signaling activity than SH2B1β. However, while this difference was present in protein expression level, GFP-SH2B1β and GFP-SH2B1δ mRNA were expressed at equal levels as assessed by quantitative RT-PCR (qPCR) using GFP-targeted primers (data not shown). Regardless of the relative protein levels of SH2B1β and SH2B1δ, our results indicate that SH2B1δ, localizing primarily to nucleoli, enhances several neurotrophic factor-induced signaling events to an extent similar to, or even greater than, SH2B1β.

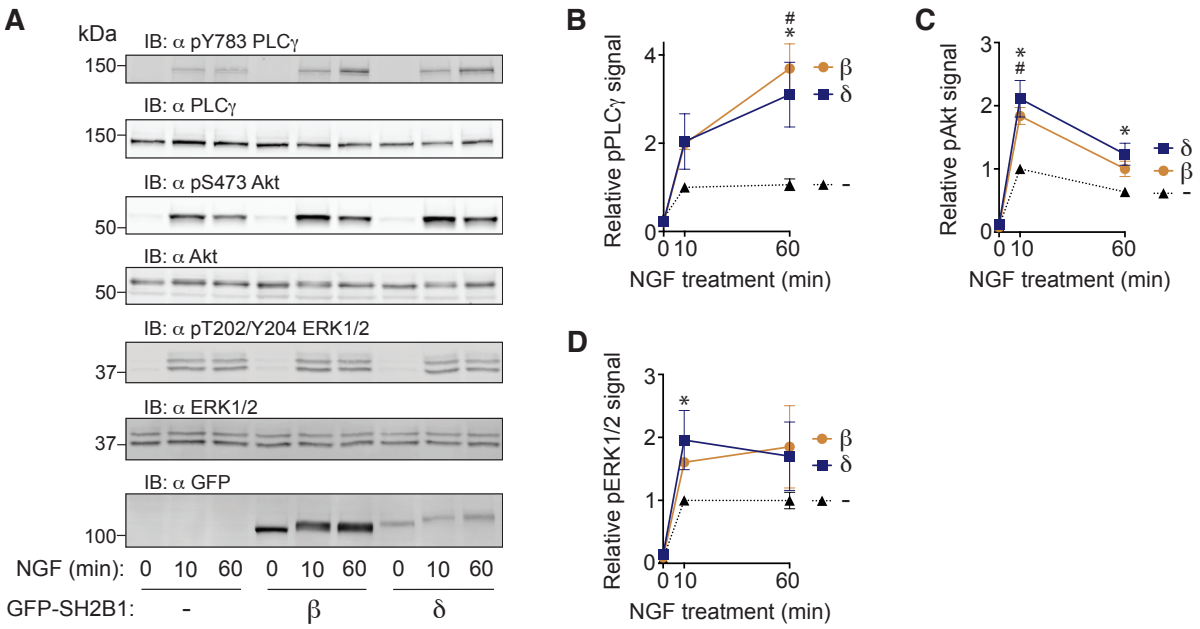

Figure 3.2. SH2B1δ promotes NGF-stimulated signaling activities

(A) Serum-starved PC12 cells stably expressing GFP or GFP-tagged SH2B1β or SH2B1δ were stimulated with 25 ng/mL NGF for 0, 10, or 60 minutes. Proteins in cell lysates were immunoblotted with the indicated antibodies. The migration of molecular weight standards is shown on the left. **(B-D)** Quantification of representative western blots in **A** plus 2 additional sets of western blots, each set performed using distinct biological replicates. Relative signals of the indicated phosphorylated proteins were normalized to the signal for GFP-expressing cells stimulated with NGF for 10 minutes. Data are means ± SEM. **Statistics: B-D**, one-way ANOVA at 10 and 60 minutes followed by Tukey's multiple comparisons test. # denotes GFP vs. GFP-SH2B1β and * denotes GFP vs. GFP-SH2B1δ. For # and *, $P < 0.05$.

SH2B1δ enhances neurotrophic factor-dependent gene expression

We demonstrated previously that SH2B1β enhances the expression of a subset of NGF-responsive genes important for neuronal differentiation [10]. These genes include plasminogen activator urokinase receptor (*Plaur*), matrix metalloproteinases 3 and 10 (*Mmp3*, *Mmp10*), and Fos-related antigen 1 (*FosL1*). *Plaur,* encoding urokinase plasminogen activator receptor (uPAR), is an early response gene critical for NGF-induced neurite outgrowth in PC12 cells [42], differentiation of cultured mouse dorsal root ganglia neurons [43], and migration of mouse cortical interneurons *in vivo* [44]. Matrix metalloproteases, such as MMP3 and MMP10, are critical for the degradation of the extracellular matrix that precedes the extension of axons and dendrites from the neuronal cell body (e.g., soma) [45]. uPAR, MMP3, and MMP10 are members of a protease cascade implicated in extracellular matrix degradation, neuronal differentiation, and cell motility [46,47]. *FosL1*, an immediate early response gene, encodes a transcription factor thought to regulate a wave of late response genes [48] that encode proteins that mediate multiple morphological processes including dendritic growth, spine maturation, and synapse elimination [49].

Because the subcellular localization of SH2B1δ differs greatly from that of SH2B1β, we wondered if SH2B1δ would, like SH2B1β, be capable of enhancing expression of these NGF-responsive genes. We stably expressed GFP, GFP-SH2B1β, or GFP-SH2B1δ in PC12 cells, stimulated the cells with NGF (100 ng/mL) for 6 hours, and measured the expression of *Plaur*, *Mmp3*, *Mmp10*, and *FosL1* using qPCR. Consistent with previous results, SH2B1β greatly increased the NGF-induced expression of all four genes (Fig. 3.3A-D). SH2B1δ also greatly enhanced the NGF-induced

expression of all four genes, although SH2B1δ enhanced the expression of all four genes to a lesser extent than SH2B1β. Thus, despite localizing primarily to nucleoli, SH2B1δ increases neurotrophic factor-induced gene expression, although to a somewhat lesser extent than SH2B1β.

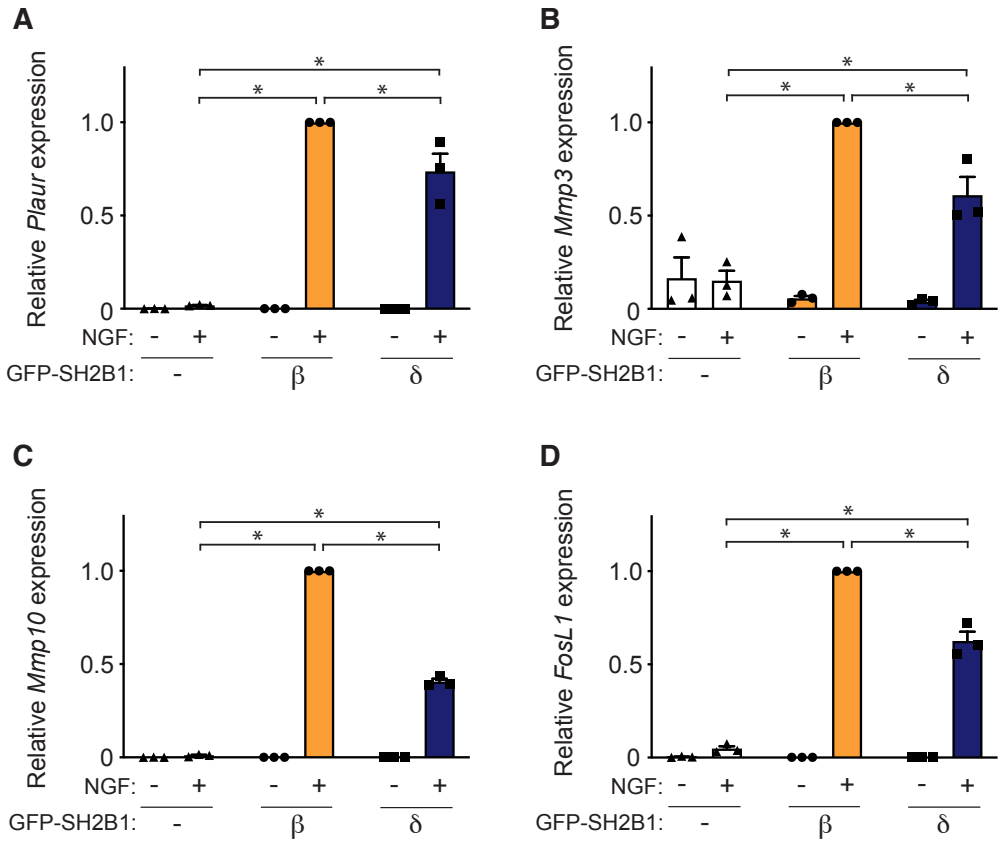

Figure 3.3. SH2B1δ promotes NGF-stimulated gene expression

PC12 cells stably expressing GFP or GFP-tagged SH2B1β or SH2B1δ were treated with or without NGF (100 ng/mL for 6 hours). RNA was isolated and relative expression levels of **(A)** *Plaur,* **(B)** *Mmp3,* **(C)** *Mmp10*, and **(D)** *FosL1* were measured by qPCR. Expression of the genes of interest was normalized to the geometric mean of the expression levels of reference genes *36b4*, *Cyclophilin A*, and *Hprt*. Data were normalized to values obtained for GFP-SH2B1β-expressing cells treated with NGF. Means are from 3 separate experiments, each using distinct biological samples. Data are means ± SEM. **Statistics**: **A-D**, repeated measures one-way ANOVA on NGF-treated samples followed by Holm-Sidak's multiple comparisons test. * $P < 0.05$.

Sh2b1 KO neurons exhibit reduced neurite outgrowth and complexity

The lengths and branching patterns of axons and dendrites affect the ability of individual neurons to reach and make appropriate connections with other neurons at synapses. Because SH2B1δ increases expression of multiple neurotrophic factor-induced genes that are important for the outgrowth of axons and dendrites (e.g., neurites) (Fig. 3.3) and promotes several neurotrophic factor-induced signaling events that are associated with neurite outgrowth (Fig. 3.2), we hypothesized that SH2B1δ would promote neurite outgrowth and complexity. We therefore assessed the effects of SH2B1δ on neurite outgrowth and complexity of primary cultured hippocampal neurons. Given their large size and ability to develop complex branching patterns, these cultured neurons offer valuable opportunities to study neurite outgrowth in great detail. Whereas PC12 cells express TrkA and are responsive to NGF, hippocampal neurons predominantly express TrkB and are most responsive to BDNF, including the BDNF that they produce endogenously. The mechanism by which SH2B1 is recruited to TrkA and TrkB and the resulting signal transduction activities are thought to be very similar. Indeed, consistent with SH2B1β enhancement of NGF-induced phosphorylation of PLCγ, Akt, and ERK1/2 in PC12 cells, SH2B1β also enhances BDNF-induced phosphorylation of PLCγ, Akt, and ERK1/2 in PC12 cells stably expressing TrkB [9].

We first analyzed the overall impact of all SH2B1 isoforms on neurite outgrowth and complexity by assessing cultured primary hippocampal neurons from neonates that lacked all SH2B1 isoforms. Using qPCR, we established that *Sh2b1* mRNA was expressed in hippocampal neuron cultures from WT mice on day *in vitro* (DIV) 2, 5, 8, and 14, and its expression level increased significantly between DIV 2 and 14 (Fig. 3.4A).

We also confirmed that neither *Sh2b1* mRNA nor SH2B1 protein was present in neuron cultures from KO mice (data not shown). To understand how SH2B1 isoforms influence the growth of young neurons, we transiently transfected cDNA encoding GFP into WT and KO neurons on DIV 4 to facilitate visualization of neurons and their neurites. We then imaged individual GFP-positive neurons at DIV 5 using live-cell fluorescent microscopy (Fig. 3.4B). We traced these images using Simple Neurite Tracer in FIJI and measured the following parameters: 1) the number of endpoints, representative of overall neurite complexity; 2) the total neurite length, representative of overall neurite outgrowth; and 3) the length of the longest neurite, typically representative of axonal outgrowth. KO neurons exhibited decreased measures of all three parameters (Fig. 3.4C-E).

To gain additional insight into the impact of SH2B1 isoforms on neurite outgrowth and complexity, we compared the images of WT and KO neurons using Sholl analysis, a computerized algorithm that evaluates the complexity and reach of a neuron's axon and dendrites by placing concentric circles of incremental radii centered around the soma and measuring the number of neurites that intersect each circle (Sholl 1953). Changes in the number of intersections close to the soma are typically indicative of changes in dendritic complexity, whereas those farther away from the soma are typically indicative of changes in axonal complexity. Consistent with our results obtained via neurite tracing, Sholl analysis demonstrated that KO neurons exhibited significantly fewer intersections compared to WT neurons at multiple distances close to the soma (distances between 18 and 112 μm), suggesting that KO neurons have decreased dendritic arborization (Fig. 3.4F). Sholl analysis also revealed that KO neurons display decreased maximum number of intersections (Fig. 3.4G), indicative of decreased dendritic complexity, and decreased

maximum distance (Fig. 3.4H), typically indicative of decreased axonal outgrowth. These results are consistent with previous observations in which knockdown of SH2B1 using shRNA in primary cultured cortical neurons inhibited neurite outgrowth and branching [9].

Because KO neurons appeared to exhibit decreased dendritic complexity, we predicted that they would have reduced expression of synaptic proteins. We immunoblotted cell lysates from WT and KO neuron cultures to measure expression levels of postsynaptic density (PSD) 95 protein, a key synaptic protein that localizes to the PSD within dendritic spines. We measured PSD-95 levels at DIV 8, when synapses are beginning to form, and at DIV 13, when synapses are mostly formed. PSD-95 expression levels trended downward in KO neurons at both time points, although statistical significance was not reached (Fig. 3.4I).

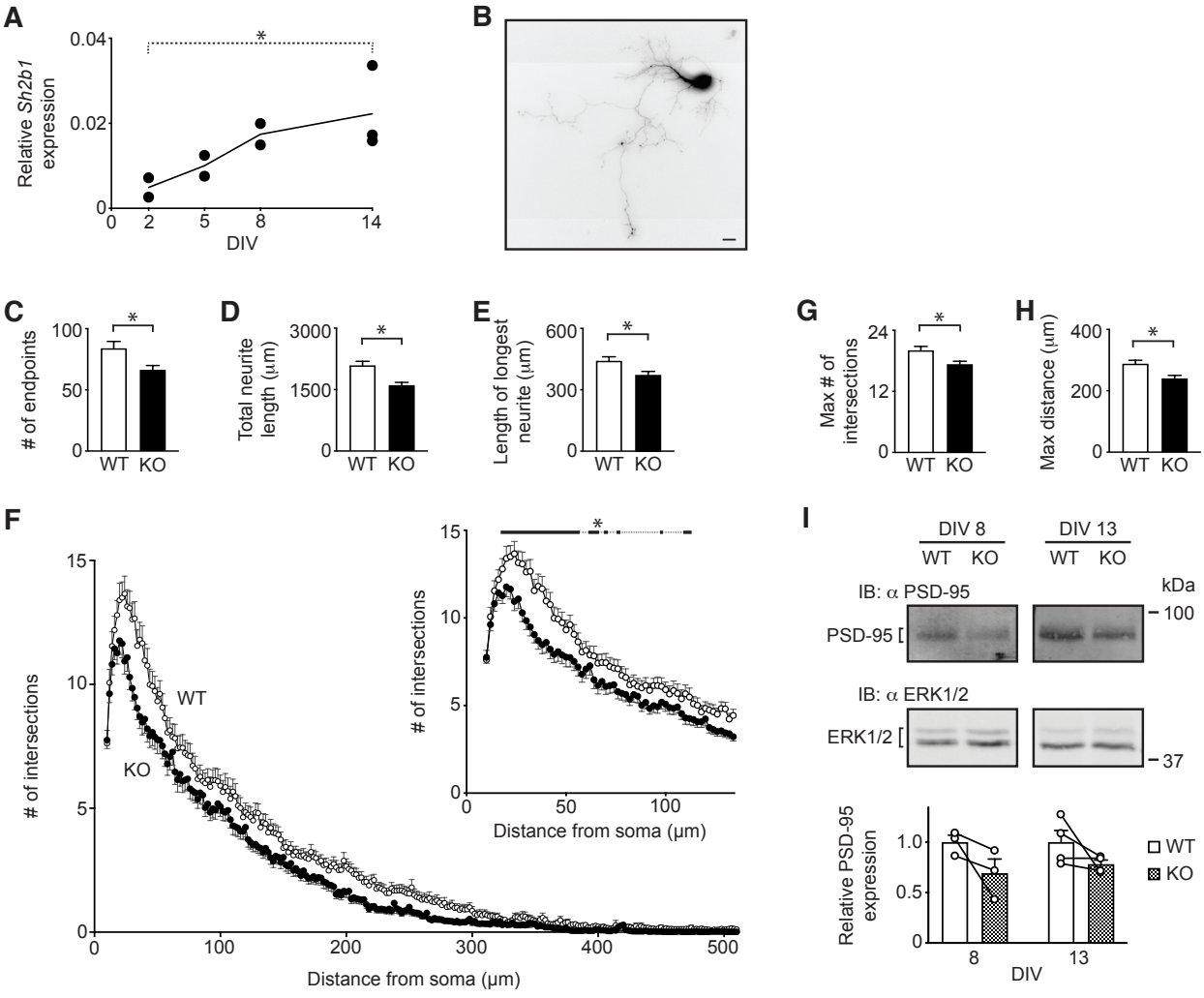
A
Relative Sh2b1 expression
0.04
0.02
0
0 2 5 8 14
DIV
*
B
C
# of endpoints
100
50
0
WT KO
*
D
Total neurite length (μm)
3000
1500
0
WT KO
*
E
Length of longest neurite (μm)
600
300
0
WT KO
*
G
Max # of intersections
24
12
0
WT KO
*
H
Max distance (μm)
400
200
0
WT KO
*
F
# of intersections
15
10
5
0
0 100 200 300 400 500
Distance from soma (μm)
WT
KO
# of intersections
15
10
5
0
0 50 100
Distance from soma (μm)
*
I
DIV 8
DIV 13
WT KO WT KO
kDa
IB: α PSD-95
PSD-95 [
100
IB: α ERK1/2
ERK1/2 [
37
Relative PSD-95 expression
1.0
0.5
0
8 13
DIV
WT
KO

Figure 3.4. *Sh2b1* KO neurons exhibit decreased neurite outgrowth and complexity

(A) RNA was isolated from cultured primary hippocampal neurons from WT mice on the indicated DIV. Relative levels of *Sh2b1* mRNA expression were measured by qPCR. Expression of *Sh2b1* was normalized to the geometric mean of the expression levels of reference genes *36b4*, *Gapdh*, and *Tbp*. *N*, biological replicates: DIV 2, 5, 8 = 2; DIV 14 = 3. **(B)** Representative hippocampal neuron from WT mouse transiently expressing GFP on DIV 4 and imaged on DIV 5 using live-cell fluorescent microscopy. Image inverted. Scale bar = 20 μm. **(C-E)** Indicated parameters were measured using Simple Neurite Tracer on images of primary hippocampal neurons that were prepared as in **C**. *N*, individual neurons (from 7 distinct experiments): WT = 92; KO = 89. **(F)** Sholl analysis was performed on neuron images used in **C-E.** Inset: subset of data in **F**, distances of 0-130 μm from soma. **(G-H)** Indicated parameters were obtained via Sholl analysis, which was performed on images used in **C-E**. **(I)** Proteins in cell lysates prepared from cultured primary hippocampal neurons on DIV 8 and DIV 13 were immunoblotted with antibodies to PSD-95 (α PSD-95) or to ERK1/2 (α ERK1/2). The migration of molecular weight standards is shown on the right. Four western blots per time point were quantified. PSD-95 signal was normalized to ERK1/2 signal at each time point. IB, immunoblot. **Statistics: A**, unpaired, one-tailed Student's t test; **C-E, G-H**, unpaired, one-tailed Student's t-test; **F, inset**, two-way repeated measures ANOVA followed by Dunnett's multiple comparisons test, significance indicated by thick black line above graph; **I**, paired, one-tailed Student's t-test. * $P < 0.05$. Data are means ± SEM.

SH2B1δ increases neurite outgrowth and complexity

Because deletion of all SH2B1 isoforms decreased neurite outgrowth and complexity in hippocampal neurons, we investigated the influence of each individual SH2B1 isoform on these parameters. We first determined that mRNA of each SH2B1 isoform was expressed in WT hippocampal neuron cultures on DIV 2, 5, 8, and 14 (Fig. 3.5A). Assuming similar efficiencies among the different TaqMan assays [50], these data suggest that the α isoform is the most highly expressed SH2B1 isoform in primary hippocampal neuron cultures, followed by β and δ, and lastly γ. The expression level of the α isoform increased significantly between DIV 2 and 14; the expression levels of SH2B1β and δ also appeared to increase over time, although these did not achieve statistical significance.

To understand how each SH2B1 isoform influences neurite outgrowth and complexity in developing neurons, we transiently transfected KO neurons on DIV 5 with cDNA encoding GFP or GFP-tagged SH2B1α, β, γ, or δ. We co-expressed mCherry to ensure that neurites were equally visible for all transfected neurons. Using fluorescent microscopy of neurons fixed on DIV 6 and stained with antibody to GFP (α GFP), we observed that all four isoforms were expressed within the soma and throughout neurites (Fig. 3.5B, top panels) (γ not shown). Using live-cell confocal microscopy of DIV 6 neurons, we confirmed that SH2B1α, β, and δ localized to the same subcellular compartments in hippocampal neurons (Fig. 3.5B, middle panels) as in PC12 cells (Fig. 3.1B). Indeed, SH2B1α and β localized primarily in the cytoplasm and plasma membrane, whereas SH2B1δ localized primarily in nucleoli with some in the plasma membrane. Additionally, all four isoforms appeared to be expressed within microstructures protruding from dendritic shafts (Fig. 3.5B, lower panels) (γ not shown). Given that these neurons

were relatively immature (DIV 6), these microstructures were likely filopodia, some of which would have presumably developed into dendritic spines [51].

To analyze the effects of individual SH2B1 isoforms on hippocampal neuronal morphology, we imaged individual GFP-positive neurons on DIV 5 using live-cell fluorescent microscopy and analyzed their morphology as described above. Neurite tracing demonstrated that SH2B1δ robustly increased the number of endpoints and total neurite length compared to the GFP control (Fig. 3.5C-D). SH2B1α and β also increased the number of endpoints (Fig. 3.5C). None of the SH2B1 isoforms significantly impacted the length of the longest neurite (Fig. 3.5E). Sholl analysis indicated that SH2B1δ greatly increased neurite complexity at multiple distances near the soma, between 10 and 124 μm away (Fig. 3.5F). SH2B1α, β, and γ also increased neurite complexity near the soma, although these increases were less pronounced and occurred at fewer distances compared to the SH2B1δ-induced enhancement. Sholl analysis also indicated that SH2B1δ, but not the other isoforms, significantly increased the maximum number of intersections (Fig. 3.5G). None of the isoforms impacted the maximum distance measured by Sholl's concentric circles (Fig. 3.5H). Collectively, these data suggest that, whereas SH2B1α, β, and γ are capable of increasing some aspects of neurite complexity, SH2B1δ has the unique ability to greatly increase both neurite complexity and outgrowth. Given that neurons expressing SH2B1δ exhibited increased complexity near the soma and increased total neurite length yet their reach went unchanged, SH2B1δ likely impacts the outgrowth and complexity of dendrites, not the axon.

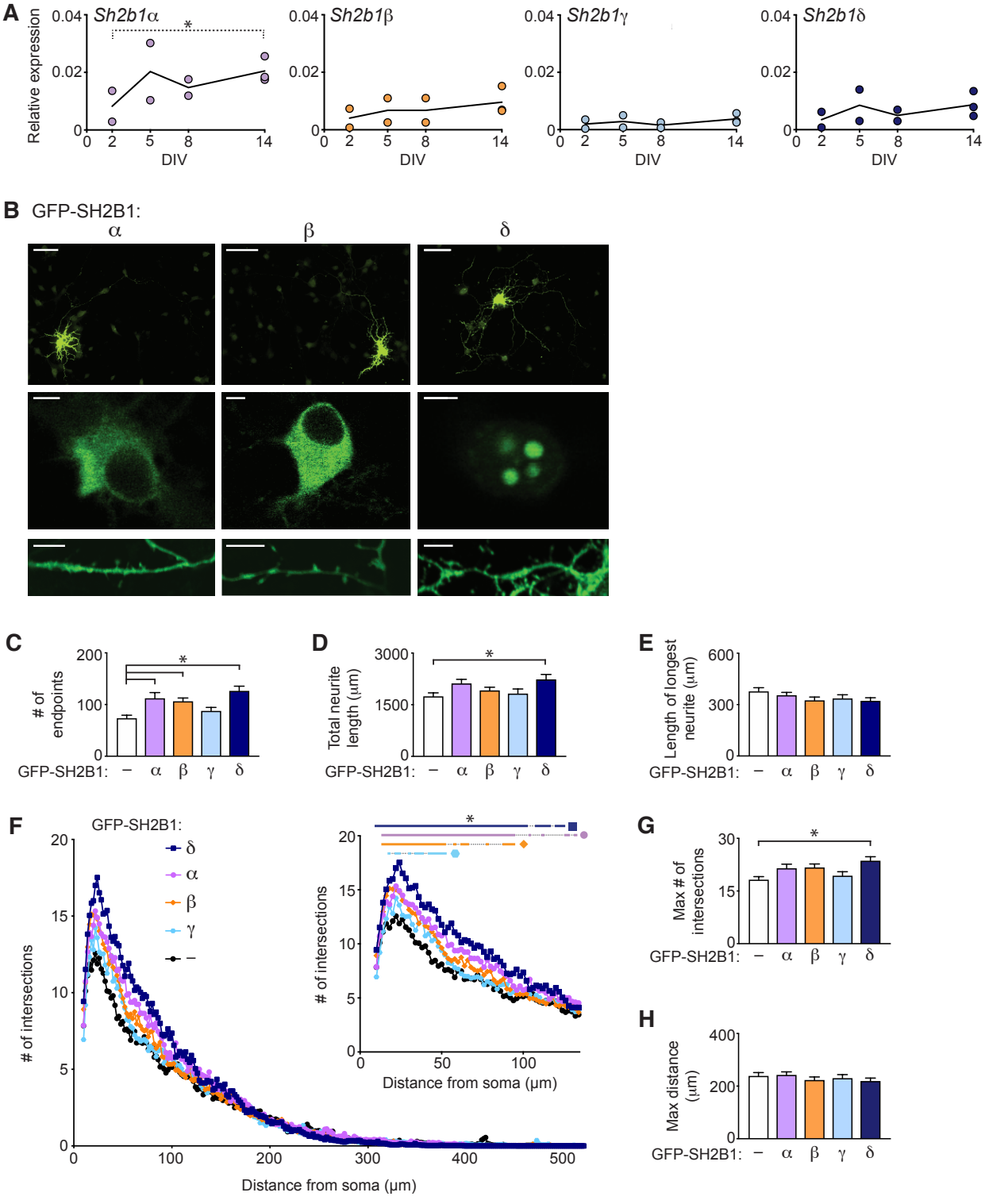
A
Sh2b1α
Sh2b1β
Sh2b1γ
Sh2b1δ
Relative expression
0.04
0.02
0
0 2 5 8 14
DIV
*
B
GFP-SH2B1:
α
β
δ
C
# of endpoints
200
100
0
GFP-SH2B1: – α β γ δ
D
Total neurite length (μm)
3000
1500
0
E
Length of longest neurite (μm)
600
300
F
GFP-SH2B1:
δ
α
β
γ
–
# of intersections
Distance from soma (μm)
0 100 200 300 400 500
0 50 100
G
Max # of intersections
30
15
H
Max distance (μm)
400
200

Figure 3.5. SH2B1 isoforms increase neurite outgrowth and/or complexity

(A) RNA was isolated from primary hippocampal neuron cultures from WT mice on the indicated DIV. Relative levels of the indicated *Sh2b1* isoform mRNA were measured by qPCR and normalized to the geometric mean of the expression levels of reference genes *36b4*, *Gapdh*, and *Tbp*. *N*, biological replicates: DIV 2, 5, 8 = 2; DIV 14 = 3. **(B)** Cultured hippocampal neurons from KO mice were transiently transfected with cDNAs encoding the indicated GFP-tagged SH2B1 isoform on DIV 5 and imaged on DIV 6 using fluorescent microscopy of fixed neurons stained with antibody to GFP (α GFP) (upper and lower panels) or live-cell confocal microscopy (middle panels). Scale bars: upper panels = 50 μm; middle and lower panels = 5 μm. **(C-E)** Indicated parameters were measured using Simple Neurite Tracer on images of primary hippocampal neurons from KO mice transiently expressing GFP-tagged SH2B1 isoforms. Neurons were transfected on DIV 4 and imaged on DIV 5 using fluorescent microscopy. *N*, individual neurons (from 3 distinct experiments): GFP = 44; GFP-SH2B1α = 45; GFP-SH2B1β = 48; GFP-SH2B1γ = 46; GFP-SH2B1δ = 44. **(F)** Sholl analysis was performed on neuron images used in **C-E**. Inset: subset of data in **F**, distances of 0-130 μm from soma. **(G-H)** Indicated parameters were obtained via Sholl analysis, which was performed on images used in **C-E**. Data are means $\pm$ SEM. **Statistics: A**, unpaired, one-tailed Student's t test; **C-E, G-H**, one-way ANOVA followed by Dunnett's multiple comparisons test; **F, inset**, two-way repeated measures ANOVA followed by Dunnett's multiple comparisons test, significance indicated by thick lines above graph. * $P < 0.05$.

Bipartite nuclear localization sequence in C-terminal tail in SH2B1δ is required for SH2B1δ to localize to nucleoli

Because SH2B1δ induced the most robust increase of neurite outgrowth and complexity in primary hippocampal neurons of the four known SH2B1 isoforms (Fig. 3.5), and SH2B1δ is the only known SH2B1 isoform targeted to nucleoli (Fig. 3.1), we questioned whether nucleolar localization contributes to the ability of SH2B1 to increase neurite outgrowth and complexity. We first identified the sequence(s) of SH2B1δ that are required for its nucleolar localization. Using a nucleolar localization sequence detector, we discovered that the segment encompassing NLS2 and NLS3 (amino acids 666-711) is predicted to localize the protein to the nucleolus (Fig. 3.6A) [52]. Additionally, the SH2B1δ tail contains a serine/tryptophan-rich segment (amino acids 708-718) [27] and stretches of aromatic amino acids such as tryptophans have been implicated in targeting nuclear proteins to the nucleolus [53-55]. We therefore tested whether one or both of these NLSs or the tryptophan-rich segment is required for SH2B1δ to localize to nucleoli. We mutated NLS2 and NLS3, either individually or in combination, by changing four basic amino acid residues in each NLS to non-polar alanine or glycine (Fig. 3.6A). We also truncated the sequence of SH2B1δ after amino acid 712 (W712X) to delete a stretch containing 4 tryptophans. We transiently expressed the GFP-tagged SH2B1δ mutants in PC12 cells and, using live-cell confocal microscopy, imaged and assessed their subcellular localization (Fig. 3.6B-C). Mutating either NLS2 or NLS3 alone caused SH2B1δ to localize more strongly in the nucleus and at the plasma membrane. However, mutating NLS2 and NLS3 simultaneously (NLS2+3) caused SH2B1δ to be excluded from nucleoli and localize primarily at the plasma membrane. The W712X truncation did not affect the ability of

SH2B1δ to localize in nucleoli. However, surprisingly, it prevented SH2B1δ from localizing to the plasma membrane.

All SH2B1 isoforms share a nuclear localization sequence, NLS1, and nuclear export sequence (Figs. 3.1A and 3.6A). NLS1 has been shown previously to both localize SH2B1β to the plasma membrane and enable it to cycle through the nucleus [35]. We therefore tested whether mutating NLS1 in SH2B1δ would impact the ability of SH2B1δ to localize to nucleoli or the plasma membrane. Mutating NLS1 did not affect the ability of SH2B1δ to localize to nucleoli, presumably because it has additional NLSs in its unique C-terminal tail, but it did prevent SH2B1δ from localizing to the plasma membrane (Fig. 3.6B-C).

Thus, for SH2B1δ to localize in nucleoli, either NLS2 or NLS3 must be functional. For SH2B1δ to localize at the plasma membrane, NLS1 and the tryptophan-rich segment of the C-terminal tail, amino acids 712-724, must be intact.

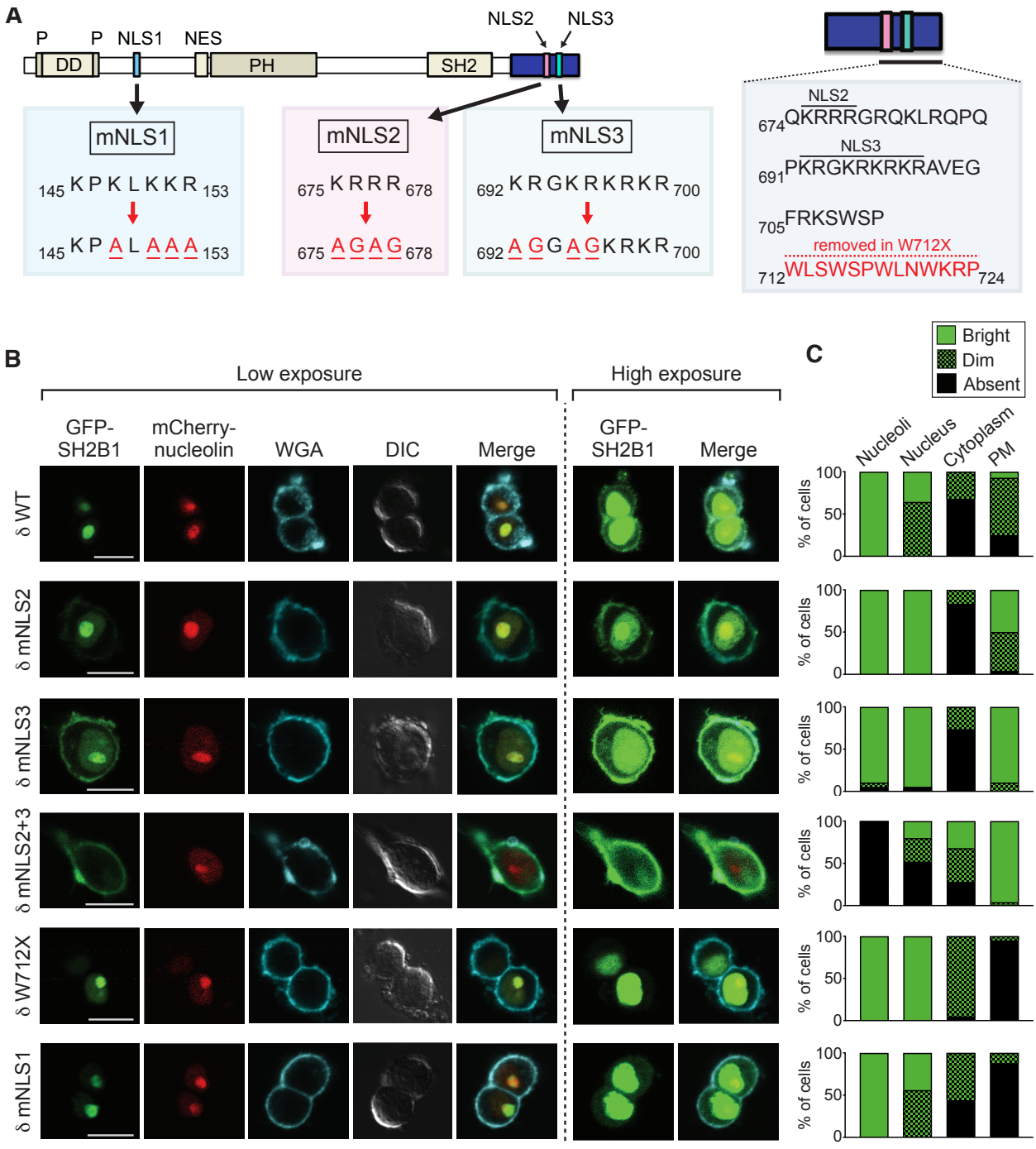
A
P
P
NLS1
NES
NLS2
NLS3
DD
PH
SH2
mNLS1
145 K P K L K K R 153
145 K P A L A A A 153
mNLS2
675 K R R R 678
675 A G A G 678
mNLS3
692 K R G K R K R K R 700
692 A G G A G K R K R 700
NLS2
674QKRRRGRQKLRQPQ
NLS3
691PKRGKRKRKRAVEG
705FRKSWSP
removed in W712X
712WLSWSPWLNWKRP724
B
Low exposure
High exposure
GFP-SH2B1
mCherry-nucleolin
WGA
DIC
Merge
GFP-SH2B1
Merge
δ WT
δ mNLS2
δ mNLS3
δ mNLS2+3
δ W712X
δ mNLS1
C
Bright
Dim
Absent
Nucleoli
Nucleus
Cytoplasm
PM
% of cells
100
50
0

Figure 3.6. Bipartite NLS in C-terminal tail is required for SH2B1δ to localize in nucleoli

(A) Schematic of SH2B1δ with mutations and truncation denoted in boxes below schematic. Red font and/or underline indicates mutation or removal of amino acids. mNLS, mutated NLS. **(B)** PC12 cells transiently co-expressing the indicated GFP-tagged SH2B1δ mutant and mCherry-tagged nucleolin were stained with Alexa Fluor 467-conjugated WGA and imaged using live-cell confocal microscopy. Left 5 panels: low photomultiplier gain. Right 2 panels: high photomultiplier gain. Images are representative; depicted localizations of SH2B1 isoforms were observed in at least 20 cells per isoform. WGA, wheat germ agglutinin; DIC, differential interference contrast. Scale bar = 10 μm. **(C)** Subcellular localization of the indicated SH2B1δ mutants observed in representative images in **B** and additional images. Bright, dim, and absent refer to the intensity of the signal in a particular cellular compartment: bright = seen with low gain; dim = seen only with high gain; absent = not seen. *N*, individual cells (from 2 or 3 separate experiments): δ(WT) = 28; δ(mNLS2) = 24; δ(mNLS3) = 19; δ(mNLS2+3) = 25; δ(W712X) = 20; δ(mNLS1) = 25. PM, plasma membrane. Data are means.

SH2B1δ localization to nucleoli and the plasma membrane appears to be required for SH2B1δ to increase neurite complexity

To determine whether SH2B1δ localization to nucleoli affects neurite outgrowth and complexity in hippocampal neurons, we tested the effect of different SH2B1δ mutants (Fig. 3.7A) with distinct subcellular localization profiles (Fig. 3.6) on neurite outgrowth and complexity. We transiently transfected cDNAs encoding GFP-tagged SH2B1δ mutants into neurons from *Sh2b1* KO mice on DIV 4. We imaged individual GFP-positive neurons on DIV 5 and analyzed their architecture as described above. Neurite tracing demonstrated that, consistent with our previous results (Fig. 3.5C), SH2B1δ(WT) greatly increased the number of endpoints compared to the GFP control (Fig. 3.7B). Mutating NLS2+3 in SH2B1δ significantly disrupted the ability of SH2B1δ to increase the number of endpoints. In fact, mutating NLS2+3 returned the number of endpoints to the level of the GFP control. Truncating W712X or mutating NLS1 in SH2B1δ also appeared to disrupt the ability of SH2B1δ to increase the number of endpoints, although statistical significance was not achieved for these mutants. Consistent with our previous results (Fig. 3.5D), SH2B1δ(WT) greatly increased the total neurite length (Fig. 3.7C). Mutating NLS2+3 or NLS1 or truncating W712X in SH2B1δ did not alter the ability of SH2B1δ to increase total neurite length. SH2B1δ(WT) did not alter the length of the longest neurite, nor did any of the mutations alter the length of the longest neurite from SH2B1δ(WT) levels (Fig. 3.7D).

Consistent with our previous results (Fig. 3.5F), Sholl analysis indicated that SH2B1δ(WT) greatly increased the number of intersections close to the soma (Fig. 3.7E). Mutating NLS2+3 in SH2B1δ significantly reduced the ability of SH2B1δ to increase this

neurite complexity. At multiple distances between 50 and 100 μm from the soma, mutating NLS2+3 brought the number of intersections down to the GFP level. Truncating W712X or mutating NLS1 in SH2B1δ more modestly disrupted the ability of SH2B1δ to increase the number of intersections, resulting in multiple statistically significant decreases between 18 and 120 μm or 8 and 72 μm, respectively, from the soma.

To gain additional insight into the sequences required for SH2B1δ to increase neurite outgrowth and complexity, we mutated arginine 555 to glutamate (R555E) in SH2B1δ, which disrupts the SH2 domain such that SH2B1 is unable to be recruited to phosphotyrosines in tyrosine kinases [29,56]. Mutating R555E did not alter the subcellular localization of SH2B1δ; like SH2B1δ(WT), this mutant localized in nucleoli and at the plasma membrane (data not shown). However, mutating R555E in SH2B1δ reduced the ability of SH2B1δ to increase the number of endpoints (Fig. 3.7B), total neurite length (Fig. 3.7C), and number of intersections at multiple distances between 12 and 122 μm from the soma (Fig. 3.7E). Similar to mutating NLS2+3, mutating R555E in SH2B1δ brought the number of intersections down to the GFP level at multiple distances from the soma. In conjunction with the data above, these results suggest that SH2B1δ needs to localize to both nucleoli and the plasma membrane to increase dendritic complexity to its fullest extent. SH2B1δ recruitment to phosphotyrosines in tyrosine kinases appears to be required for SH2B1δ to fully increase dendritic outgrowth and complexity.

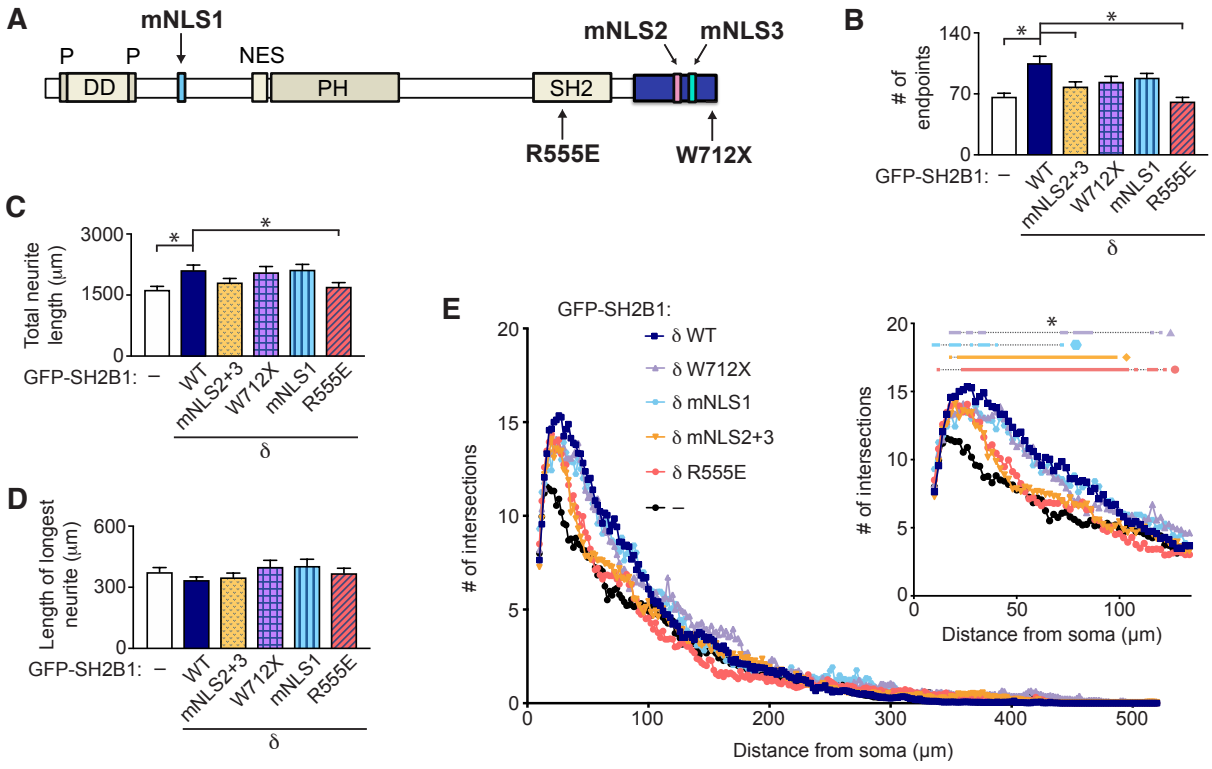

Figure 3.7. The ability of SH2B1δ to localize to nucleoli and the plasma membrane appears to be required for SH2B1δ to increase neurite complexity

(A) Schematic of SH2B1δ showing locations of mutations. **(B-D)** Indicated parameters were measured using Simple Neurite Tracer on images of primary hippocampal neurons from KO mice that were transiently expressing GFP (-), GFP-SH2B1δ(WT), or GFP-SH2B1δ with the indicated mutant. Neurons were transfected on DIV 4 and imaged on DIV 5 using fluorescent microscopy. *N*, individual neurons from 3 distinct experiments: GFP = 49; GFP-SH2B1δ(WT) = 58; GFP-SH2B1δ(mNLS2+3) = 41; GFP-SH2B1δ(W712X) = 28; GFP-SH2B1δ(mNLS1) = 27; GFP-SH2B1δ(R555E) = 34. **(E)** Sholl analysis was performed on neuron images used in **B-D**. Inset: subset of data in **E**, distances of 0-130 μm from soma. **Statistics: B-D**, one-way ANOVA followed by Dunnett's multiple comparisons test; **E, inset**, two-way repeated measures ANOVA followed by Dunnett's multiple comparisons test, significance indicated by thick lines above graph. * $P < 0.05$. Data are means ± SEM.

We next tested whether five previously identified human obesity-associated SH2B1 variants (P90H, P322S, A484T, T546A, R680C) (Supplementary Material Fig. 3.9A) would disrupt the ability of SH2B1δ to increase neurite outgrowth and complexity [17-19]. These variants exhibited subcellular localizations similar to that of SH2B1δ(WT) in PC12 cells (data not shown). The obesity-associated variants did not impact the ability of SH2B1δ to increase neurite outgrowth or complexity as assessed by neurite tracing (Supplementary Material Fig. 3.9B-D). However, these variants did impact, to varying degrees, the ability of SH2B1δ to increase neurite complexity as assessed by Sholl analysis (Supplementary Material Fig. 3.9E). The P322S variant, located in the PH domain, and the T546A variant, located in the SH2 domain, notably disrupted the ability of SH2B1δ to increase the number of intersections close to the soma. The P90H variant, located in a proline-rich region, and the A484T variant, located in a region of the protein without recognized domains, only barely disrupted the ability of SH2B1δ to increase the number of intersections. Interestingly, the R680C variant, located in the unique C-terminal tail of SH2B1δ, had the opposite effect from the other variants, enhancing the ability of SH2B1δ to increase the number of intersections close to the soma. These data suggest that human obesity-associated variants of SH2B1 located in the PH and SH2 domains and the unique C-terminal tail of SH2B1δ impact the ability of SH2B1δ to increase dendritic complexity.

SH2B1 does not appear to influence gene expression associated with ribosomal biogenesis

Because the double mutation of NLS2 and NLS3 in SH2B1δ, which prevented the protein from localizing to nucleoli (Fig. 3.6B), greatly reduced the ability of SH2B1δ to increase neurite complexity in primary hippocampal neurons (Fig. 3.7), we concluded that the ability of SH2B1δ to localize to nucleoli appeared to be required for it to maximally increase neurite complexity. Previous work suggested that BDNF increases ribosomal biogenesis [57], a prominent function of nucleoli, and that this BDNF-induced ribosomal biogenesis promotes neurite complexity [58]. Thus, we hypothesized that SH2B1δ increases neurite complexity by promoting BDNF-induced ribosomal biogenesis in nucleoli. We therefore compared expression levels of *45S pre-rRNA*, a marker of ribosomal biogenesis, in WT vs. KO neuronal cultures treated with or without BDNF (50 ng/mL for 1 hour), predicting that deletion of all SH2B1 isoforms, including SH2B1δ, would disrupt ribosomal biogenesis. We also measured expression levels of *18S rRNA*, *Ubtf*, which encodes a transcription factor of ribosomal genes, and *Ncl*, *Fbl*, and *B23/Npl*, which encode key proteins for pre-ribosomal RNA processing and assembly of pre-ribosomal particles [59,60]. Surprisingly, there were no differences in the expression levels of any of these genes by genotype or BDNF treatment (Supplementary Material Fig. 3.10A-F), suggesting that SH2B1 isoforms do not increase neurite complexity by upregulating gene expression associated with ribosomal biogenesis.

BDNF-induced expression of neuronal immediate early genes *Egr1* and *Arc* is partially dependent on SH2B1

Because deletion of all SH2B1 isoforms reduced neurite complexity and tended to reduce expression of the key synaptic protein PSD-95 in hippocampal neurons (Fig. 3.4), we hypothesized that deletion of SH2B1 would reduce expression of genes associated with the function of neuronal synapses in hippocampal neurons. Additionally, despite not detecting any impact of BDNF activity on SH2B1δ-induced increase in neurite complexity (Supplementary Material Figs. 3.11 and 3.12), we considered that a more sensitive assay such as qPCR might detect BDNF regulation of SH2B1δ activity in the context of neuronal function. We therefore tested whether deletion of all SH2B1 isoforms would reduce the expression of two immediate early genes important for synaptic function [61,62] whose expression is induced by BDNF [63-65]: early growth response 1 (*Egr1)* and activity-regulated cytoskeleton-associated gene (*Arc)*. As expected, BDNF treatment greatly increased expression levels of *Egr1* and *Arc* in WT neurons (Fig. 3.8A-B). However, in neurons lacking SH2B1, the BDNF-induced enhancement of the expression of these two genes was markedly decreased. These results suggest that SH2B1 is critical for the well-documented BDNF-induced expression of immediate early genes *Egr1* and *Arc*.

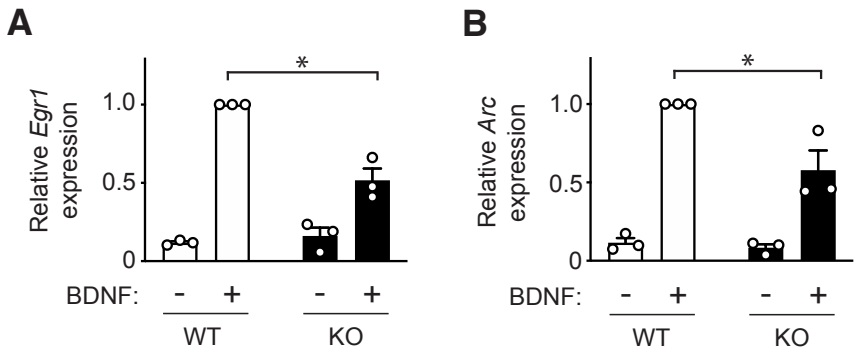

Figure 3.8. BDNF-induced expression of neuronal immediate early genes is partially dependent on SH2B1 activity

Primary hippocampal neuron cultures from WT or KO mice were treated on DIV 5 with or without BDNF (50 ng/mL for 1 hour). RNA was isolated and relative expression levels of **(A)** *Egr1* and **(B)** *Arc* were measured by qPCR. Expression of these genes was normalized to the geometric mean of the expression of reference genes *36b4*, *Gapdh*, and *Tbp*. Data were normalized to values obtained for WT cells treated with BDNF. *N*, biological replicates = 3. Data are means ± SEM. **Statistics: A-B**, one-tailed, paired Student's t test. * $P < 0.05$.

Discussion

Here we demonstrate that the brain-specific δ isoform of adapter protein SH2B1 is the only SH2B1 isoform that localizes to the nucleolus. SH2B1δ enhances NGF-induced signaling activity and gene expression in PC12 cells, both of which are thought to contribute to neurite outgrowth. Indeed, while primary hippocampal neurons lacking endogenous SH2B1 exhibit decreased neurite outgrowth and complexity, reintroduction of each SH2B1 isoform increases neurite outgrowth and/or complexity, and the δ isoform increases these parameters more potently than the other isoforms.

The unique nucleolar localization of SH2B1δ distinguishes it not only from other SH2B1 isoforms but also from most other proteins. Only 7% of all human proteins have been experimentally identified in the nucleolus [66,67]. Of those, only 47 are seen both at the plasma membrane and the nucleolus. Yousaf and colleagues [27] previously identified two highly basic regions and a tryptophan-rich segment within the unique C-terminal tail of SH2B1δ and suggested that these sequences may target the isoform to the nucleus. However, no one had determined where SH2B1δ localized in cells nor the contributions of these sequences to its localization. Our mutational analysis indicated that SH2B1δ requires both highly basic regions in its unique C-terminal tail (NLS2, NLS3) to localize to the nucleolus. Our mutational analysis also revealed that, like SH2B1β [11], SH2B1δ requires a functional NLS1 to localize to the plasma membrane. Surprisingly, SH2B1δ also requires the tryptophan-rich segment (amino acids 712-724) in its C-terminal tail to localize to the plasma membrane. With these specialized sequences intact, SH2B1δ may shuttle between the plasma membrane and the nucleolus.

Neurotrophin-induced expression of *Plaur*, *Mmp3*, *Mmp10*, and *FosL1*, along with neurotrophin-induced phosphorylation of PLCγ, Akt, and ERK1/2, is implicated in neurite outgrowth in PC12 cells. Thus, given that we and others have now shown that SH2B1β [29], γ [30], and/or δ (this paper) promote at least some of these neurotrophic factor-induced signaling events (SH2B1β, γ, δ) and increases in gene expression (SH2B1β, δ), it was not surprising that deletion of all SH2B1 isoforms inhibited neurite outgrowth and arborization in primary hippocampal neurons. Indeed, this observation is consistent with previous reports that reduction of SH2B1 levels using shRNA suppresses neurite outgrowth and/or branching in PC12 cells [11] and primary cortical [9] and hippocampal neuron cultures [14]. Our extensive morphological analyses showing that neurons from *Sh2b1* KO mice exhibit decreased number of endpoints, neurite lengths, and number of neurite segments at multiple distances from the soma suggest that deletion of all SH2B1 isoforms suppresses axon length and arborization of both proximal and distal dendrites in neurons. Reintroduction of each individual SH2B1 isoform appeared to increase arborization of proximal dendrites but not arborization of distal dendrites or arborization or length of the axon, suggesting that interaction among different SH2B1 isoforms may be necessary to enhance length or complexity of axons and/or distal dendrites. The ability of SH2B1β to increase neurite complexity in primary neurons is consistent with previous overexpression studies [9,14]. While each of the four isoforms increases neurite outgrowth and complexity in primary hippocampal neurons to some degree, the δ isoform outperforms the other isoforms in its ability to do so. Thus, the shared region of SH2B1 may facilitate a baseline ability for the isoforms to perform a specific cellular function related to neurite outgrowth, and their unique C-terminal tails may make them more or less fit for the task. For example,

because most motifs/sites required for SH2B1β to enhance actin cytoskeleton-related activity (e.g., enhance growth hormone-induced membrane ruffling and cell motility, cross-link actin filaments, or bind to actin-related proteins including Rac, Grb2, and IRSp53) are located in the shared N-terminus of SH2B1 [12-16,30], all four isoforms may promote rearrangement of the actin cytoskeleton in neurons and their C-terminal tails may dictate the extent to which they are able to do so.

We showed previously [10] that SH2B1β enhances expression of a subset of NGF-induced genes in PC12 cells including *Plaur*, *Mmp3*, *Mmp10*, and *FosL1*. Here we demonstrate that SH2B1δ also promotes NGF-stimulated expression of these genes. However, SH2B1β appeared to increase the expression of all four genes to a greater extent than SH2B1δ. The simplest explanation for these differences is that the δ isoform was not expressed as highly as the β isoform in our stable PC12 cell lines, as suggested by western blotting. If one assesses gene expression normalized to amount of GFP-SH2B1 isoform expressed, SH2B1δ is found to be more effective than SH2B1β. Another possibility is that both isoforms stimulated gene expression to similar extents but with slightly different time courses. A third possibility is that the β isoform actually increases the expression of this particular subset of genes to a greater extent than the δ isoform. The latter scenario would contribute to the growing list of instances in which different SH2B1 isoforms are "tailored" to perform different functions [8,23,27,68,69]. Because SH2B1β and δ enhance NGF-stimulated signaling activities to similar extents, differing abilities of these two isoforms to enhance NGF-induced expression of *Plaur*, *Mmp3*, *Mmp10*, and *FosL1* would suggest that cellular activities of SH2B1 other than those driven by Akt,

PLCγ, and ERK signaling pathways contribute to SH2B1 enhancement of this gene expression.

Our investigation of the ability of SH2B1δ mutants with different subcellular distributions to enhance hippocampal neurite complexity suggests that SH2B1δ must localize to the nucleolus and plasma membrane and have a functional SH2 domain to maximally increase neurite complexity. The need for SH2B1δ to localize to the plasma membrane and have a functional SH2 domain to enhance neurite complexity is consistent with SH2B1δ being recruited to activated Trk receptors at the plasma membrane. Indeed, we showed not only that stable expression of SH2B1δ promotes NGF-induced gene expression in PC12 cells, but also that BDNF-induced gene expression is greatly impaired in primary hippocampal neurons from KO mice. If SH2B1δ localizes to the plasma membrane only to bind to phosphorylated tyrosines in activated receptor tyrosine kinases, and if SH2B1δ binds to phosphorylated tyrosines in activated tyrosine kinases only at the plasma membrane, one would predict that mutations disrupting the ability of SH2B1δ to perform either activity would give identical results. However, these mutations gave different results: Disruption of the SH2 domain in SH2B1δ via the R555E mutant resulted in a more dramatic morphological change in hippocampal neuron architecture, greatly reducing the ability of SH2B1δ to increase the number of endpoints and number of intersections of both proximal and distal neurites (reaching ~120 μm from the soma). Despite the inability of SH2B1 isoforms with the R555E mutation to bind to phosphotyrosines in tyrosine kinases [29,56], SH2B1δ(R555E) still localizes to the plasma membrane. In contrast, removal of SH2B1δ from the plasma membrane via the W712X or mNLS1 mutations induced a lesser morphological change in hippocampal neuron

architecture, only reducing the ability of SH2B1δ to increase the number of intersections for the most proximal neurites (reaching <50 μm from the soma). The effects of the W712X and mNLS1 mutations were nearly identical. The simplest interpretation of this apparent discrepancy is that the W712X and mNLS1 mutants did not completely prevent plasma membrane localization of SH2B1δ, allowing enough protein to access the plasma membrane for recruitment to phosphotyrosines in activated TrkB in some cells. Indeed, in a small percentage (<10%) of the PC12 cells expressing SH2B1δ(W712X) or SH2B1δ(mNLS1), SH2B1δ was found at the plasma membrane. While constitutive localization at the plasma membrane via the NLS1 may enhance the ability of SH2B1 to bind Trk receptors, SH2B1δ binding to TrkB may only require levels of SH2B1δ at the plasma membrane small enough or transient enough to escape detection when looking at the steady state. In addition to binding via its SH2 domain to phosphotyrosines in receptor tyrosine kinases at the plasma membrane, SH2B1δ may bind via its SH2 domain to phosphotyrosines in tyrosine kinases located elsewhere in the cell (e.g., on internalized receptor tyrosine kinases or non-receptor tyrosine kinases) to increase neurite outgrowth and arborization.

Despite the inability of SH2B1 isoforms with the R555E mutation to bind to phosphotyrosines in tyrosine kinases [29,56], SH2B1δ(R555E) was still able to increase neurite complexity to some degree compared to neurons from *Sh2b1* KO mice expressing GFP control. Thus, SH2B1δ must increase neurite complexity, at least in part, through mechanisms that are independent of its recruitment to activated tyrosine kinases. One possibility is that SH2B1δ facilitates rearrangement of actin filaments that form proximal dendrites, even in the absence of tyrosine kinase activity. Previous work suggests that

SH2B1 may promote actin cytoskeleton rearrangement by SH2 domain-independent means: The binding of SH2B1β to Rac, a small GTPase implicated in membrane ruffling, lamellipodia formation, and cell motility, in 293T cells does not require the presence of tyrosine kinase JAK2 [13].

Consistent with the ability of all SH2B1 isoforms to enhance neurite complexity in hippocampal neurons, we present substantial evidence that SH2B1 isoforms, including SH2B1δ, are important for synaptic function in neurons. First, the ability of SH2B1β [8,10,11] and δ to promote NGF-induced expression of *Plaur*, *Mmp3*, and *Mmp3* in PC12 cells has strong implications for a role of SH2B1 in synaptic plasticity: extracellular proteolysis, to which these genes contribute, has been shown to be important for plasticity of both glutamatergic excitatory synapses [70,71] and GABAergic inhibitory synapses [72]. Second, we found that SH2B1 was critical for BDNF-induced expression of immediate early genes *Egr1* and *Arc* in hippocampal neurons. Immediate early genes contribute to a rapid and dynamic response to neuronal activity that, directly or indirectly, can cause lasting change within the cell. *Egr1* is a regulatory transcription factor that broadly influences neuronal function by regulating the expression of multiple “downstream” genes involved in a variety of neuronal processes including synaptic plasticity [61]. Indeed, EGR1 triggers the transcription of *Arc* following synaptic activation [73], although *Arc* can also be regulated independently of EGR1 [64]. Within minutes of its transcription, *Arc* mRNA is transported through the cytoplasm to dendrites [74,75]. Both *Arc* mRNA and protein accumulate in dendrites following synaptic activity [76,77]. Consistent with previous work demonstrating that SH2B1 promotes actin cytoskeleton rearrangement and cell motility [12-15,33], ARC protein is a critical enhancer of actin cytoskeleton rearrangement in dendritic spines [78].

ARC also facilitates AMPA receptor endocytosis within the postsynaptic compartment [79,80]. Both *Egr1* and *Arc* have been shown to be critical for synaptic plasticity, long-term potentiation, and memory consolidation [61,62]. Taken together, this work suggests that SH2B1 is a critical component of neurotrophin-induced gene expression associated with neuronal synapses. Future studies will be necessary to clarify whether all or only some SH2B1 isoforms contribute to SH2B1 regulation of this gene expression. Additional work will also be required to determine whether SH2B1 promotes synapse-related gene expression in all, or only some, neurons.

We predicted that SH2B1δ increases neurite complexity, at least in part, by upregulating BDNF-induced ribosomal biogenesis. However, our assessment of BDNF-induced expression of genes associated with ribosomal biogenesis in neurons from WT and *Sh2b1* KO mice suggest otherwise. It is possible that our experimental conditions simply did not detect the regulatory relationship. Indeed, in contrast with Gomes and colleagues [57], we did not observe an increase in *45S pre-rRNA* expression levels in primary neuron cultures from WT mice following BDNF treatment. This apparent discrepancy may have arisen from different source materials: Gomes and colleagues [57] used rat cortical neurons whereas we used mouse hippocampal neurons. Perhaps the use of embryonic rather than postnatal mouse neurons, the former having been shown to be more sensitive to BDNF [81], would allow us to detect not only BDNF-induced gene expression associated with ribosomal biogenesis, but also its enhancement by SH2B1. It is conceivable, too, that SH2B1δ does not promote ribosomal biogenesis, but rather enhances one or more of the myriad other nucleolar functions [82,83]. For example, SH2B1δ may transport other proteins to the nucleolus for sequestration. Preliminary data indicate

that SH2B1δ is able to take SH2B1β or a cytoplasmically localized, N-terminally truncated form of the cytoskeletal protein β-spectrin to nucleoli (T. Maures, L. Mancour, C. Carter-Su, unpublished data). Alternatively, SH2B1δ may serve as a scaffold protein that facilitates the formation of multiprotein complexes in the nucleolus [84]. Future experiments will be necessary to clarify the precise role of SH2B1δ in neuronal nucleoli.

Human subjects and mouse models indicate that disruption or deletion of SH2B1 negatively affects feeding and social behaviors. Because the brain is the major regulator of energy balance, SH2B1δ is expressed almost exclusively in brain tissue [17], deletion of SH2B1α and δ decreases body weight in mice [23], and SH2B1δ enhances neuronal complexity and function, we predict that SH2B1δ promotes the development and maintenance of neuronal circuitry governing energy balance. Previous results indicated that human obesity-associated mutations decreased the ability of SH2B1β [17,18] and SH2B1δ (data not shown) to enhance neurite outgrowth in PC12 cells. Thus, we tested the impact of obesity-associated mutations on the ability of SH2B1δ to increase neurite outgrowth and complexity in hippocampal neurons. Some obesity-associated mutations (P90H, P322S, T546A) significantly impaired the ability of SH2B1δ to increase complexity of proximal neurites, whereas one obesity-associated mutation (R680C) actually enhanced it. The nominal disruption from the A484T variant is consistent with our previous observation that this variant did not affect the ability of SH2B1β to enhance NGF-induced neurite outgrowth in PC12 cells [18]. Thus, SH2B1 isoforms, particularly SH2B1δ, may increase neuronal outgrowth and/or complexity important for the development and maintenance of appetite-regulating neuronal networks. However, because deletion of SH2B1α and δ decreased body weight in mice [23], we acknowledge that overexpression

of SH2B1δ, and thus increased neurite outgrowth and complexity, could lead to negative consequences for body weight regulation.

The current work advances our understanding of cellular actions of SH2B1 isoforms. We demonstrate that the unique C-terminal tail of SH2B1δ facilitates its subcellular localization to the nucleolus. SH2B1δ promotes neurotrophin-stimulated signaling events and gene expression in PC12 cells and enhances neurite outgrowth and arborization in neurotrophin-responsive primary hippocampal neurons. We also demonstrate that SH2B1 isoforms are critical regulators not only of neuronal architecture, but also gene expression associated with neuronal synapses. Together, these findings provide novel insight into the cellular functions of the SH2B1 isoforms, and in particular the brain-specific δ isoform, in the context of nervous system development.

Acknowledgements

We thank Drs. Lei Yin, Xin (Tony) Tong, Deqiang Zhang, Michael Sutton, and Roman Giger (University of Michigan) for their feedback on experimental design and data analysis, and Sarah Cain for her administrative assistance. We thank Cynthia Carruthers, Christian Althaus, and Dr. Rafi Kohen (University of Michigan) for their assistance with hippocampal neuron protocols and Dr. Liangyou Rui (University of Michigan) for the gift of the *Sh2b1* KO mouse strain. We acknowledge Dr. Stephen Lentz and the Michigan Diabetes Research Center Imaging Laboratory for assistance with confocal imaging.

Funding

This research was supported by National Institutes of Health grants R01-DK-054222 and R01-DK-107730 (to C.C.-S.). J.L.C. was supported by a National Science Foundation Graduate Research Fellowship and a Rackham Predoctoral Fellowship from the Horace H. Rackham School of Graduate Studies at the University of Michigan. T.J.M. was supported by a Rackham Predoctoral Fellowship from the Horace H. Rackham School of Graduate Studies at the University of Michigan. T.A.C. was supported by the Sean Low Undergraduate Summer Research Opportunity from the University of Michigan Neuroscience Graduate Program. Imaging studies were partially supported by the Michigan Diabetes Research Center (NIH P30-DK-020572).

Author Contributions

J.L.C. directed and conducted experiments and prepared the manuscript. P.V., M.E., and J.M.C. dissociated and plated primary neurons. P.V. imaged primary neurons for

morphology experiments, analyzed the resulting images, and ran the western blot in Fig. 3.1C. M.E. performed live-cell confocal microscopy (Figs. 3.1B, 3.5B middle panels, and 3.6B) and performed signaling experiments (Fig. 3.2A). J.M.C. performed qPCR experiments (Figs. 3.3 and 3.8 and Supplemental Material Fig. 3.10). M.D. performed preliminary experiments for Figs. 3.2 and 3.3. T.J.M. performed site-directed mutagenesis for SH2B1δ mutants (Figs. 3.6 and 3.7). T.C.C., S.K., and O.K. analyzed morphology of primary neurons. J.L.C. and C.C.-S. developed the concepts and hypotheses, designed the experiments, and interpreted the data. C.C.-S. made revisions to the manuscript.

Supplementary Materials

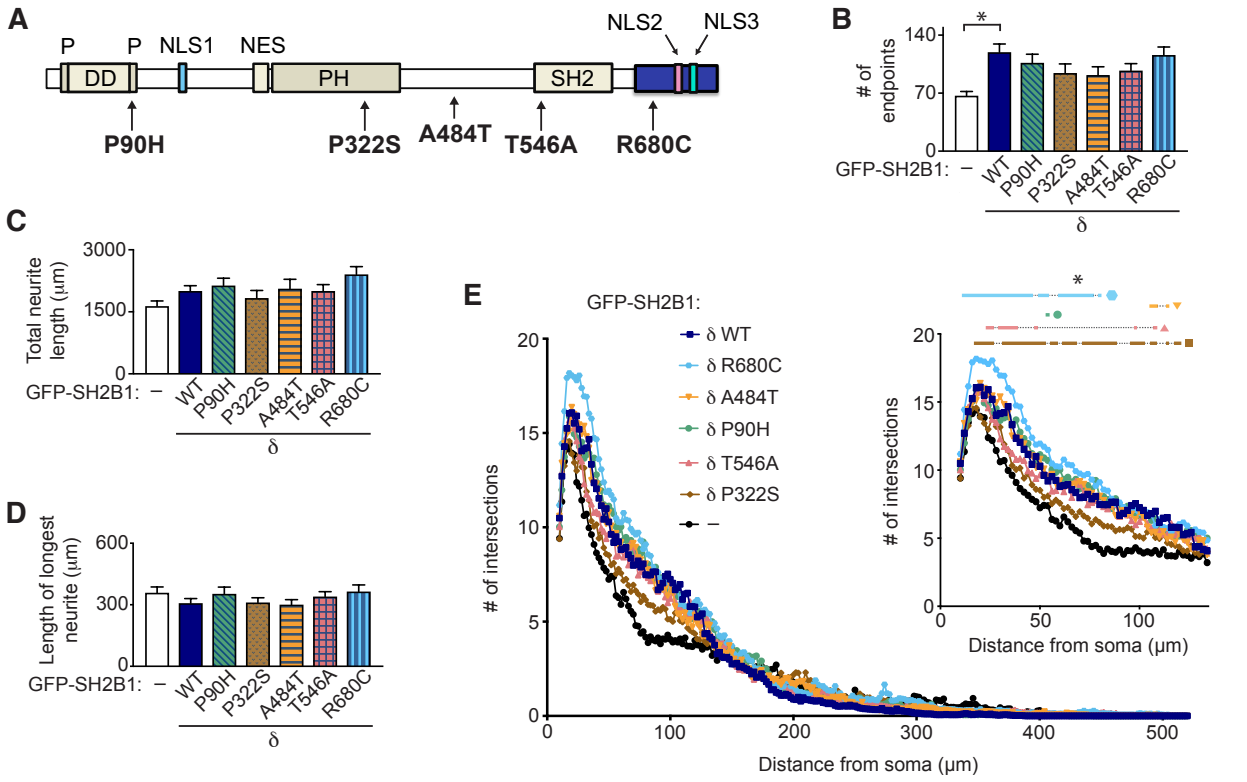

Figure 3.9. The ability of SH2B1δ to increase neurite complexity is altered by some human obesity-associated *SH2B1* variants

(A) Schematic of SH2B1δ showing locations of human obesity-associated variants. **(B-D)** Indicated parameters were measured using Simple Neurite Tracer on images of primary hippocampal neurons from KO mice that were transiently expressing GFP (-), GFP-SH2B1δ(WT), or GFP-SH2B1δ with the indicated obesity-associated variant. Neurons were transfected on DIV 4 and imaged on DIV 5 using fluorescent microscopy. *N*, individual neurons from 3 distinct experiments: GFP = 34; GFP-SH2B1δ(WT) = 45; GFP-SH2B1δ(P90H) = 38; GFP-SH2B1δ(P322S) = 39; GFP-SH2B1δ(A484T) = 38; GFP-SH2B1δ(T546A) = 43; GFP-SH2B1δ(R680C) = 39. **(E)** Sholl analysis was performed on neuron images used in **B-D**. Inset: subset of data in **E**, distances of 0-130 μm from soma. Data are means ± SEM. **Statistics: B-D**, one-way ANOVA followed by Dunnett's multiple comparisons test; **E, inset**, two-way repeated measures ANOVA followed by Dunnett's multiple comparisons test, significance indicated by thick lines above graph. * $P < 0.05$.

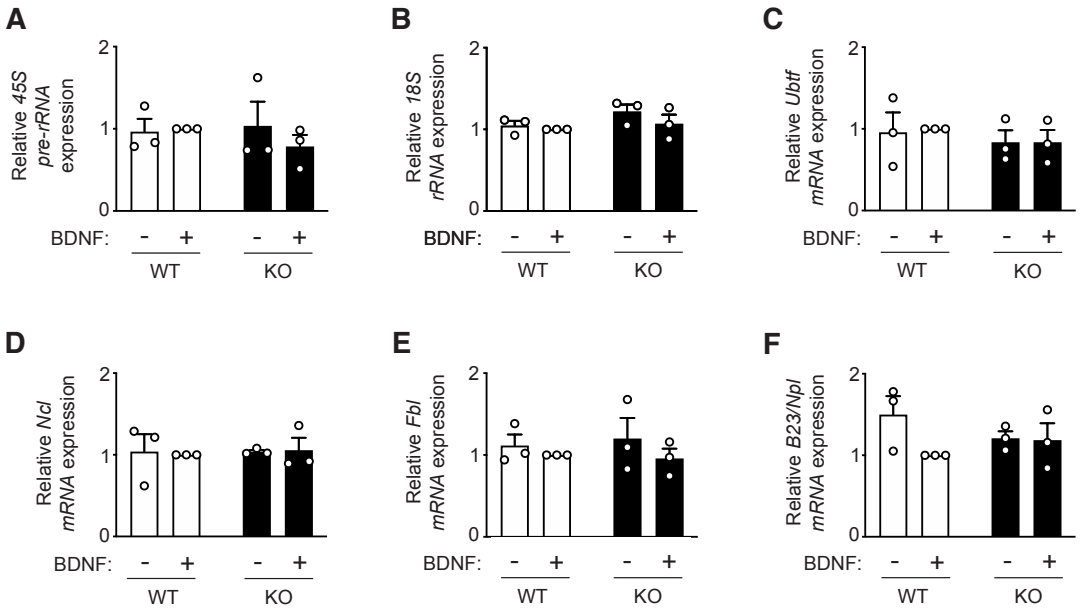

Figure 3.10. Deletion of SH2B1 isoforms does not appear to influence expression of genes associated with ribosomal biogenesis

Primary hippocampal neuron cultures from WT or KO mice were treated on DIV 5 with or without BDNF (50 ng/mL for 1 hour). RNA was isolated and relative expression levels of **(A)** *45S pre-rRNA*, **(B)** *18S rRNA*, **(C)** *Ubtf*, **(D)** *Ncl*, **(E)** *Fbl*, and **(F)** *B23/Npl* were measured by qPCR. Expression of the genes of interest was normalized to the geometric mean of the expression of reference genes *36b4*, *Gapdh*, and *Tbp*. Data were normalized to values obtained for WT cells treated with BDNF. *N*, biological replicates = 3. Data are means ± SEM. **Statistics**: **A-F**, no significant differences by repeated measures one-way ANOVA followed by Tukey's multiple comparisons test.

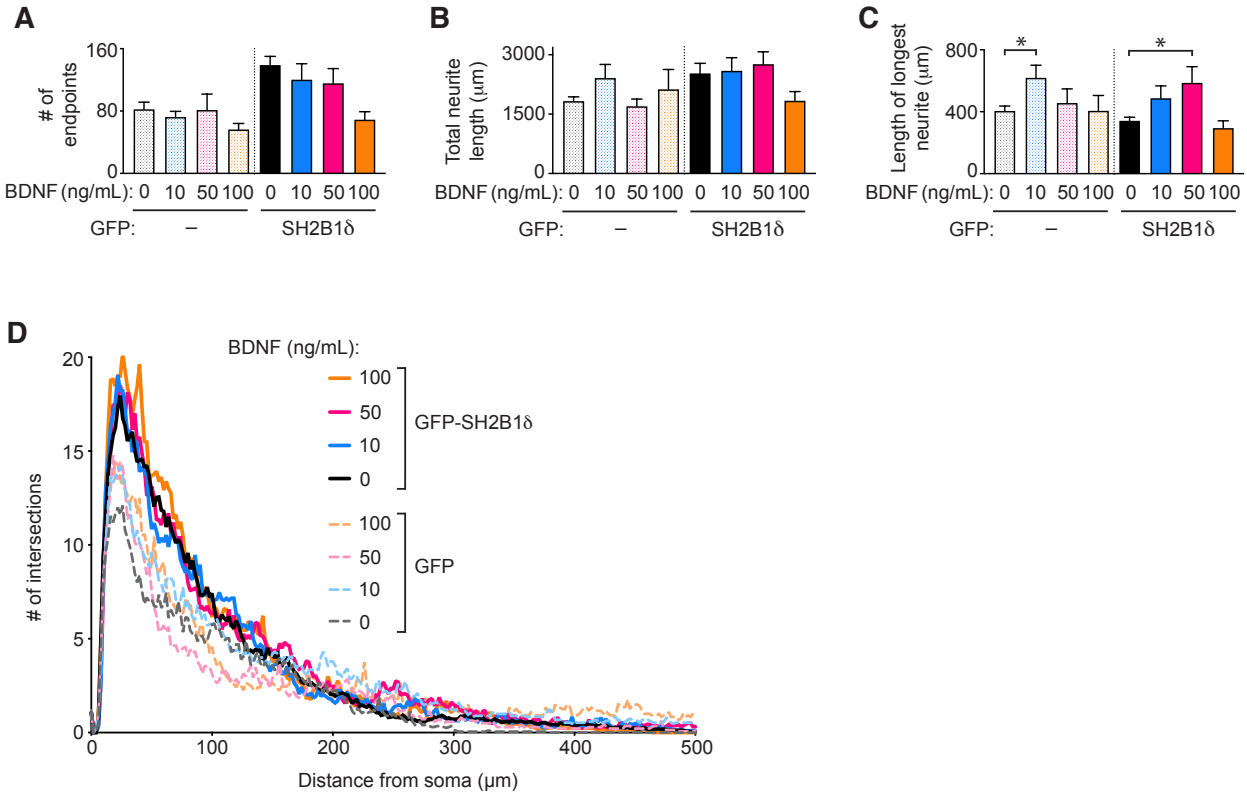

Figure 3.11. BDNF treatment does not appear to influence the ability of SH2B1δ to increase neurite complexity

(A-C) Indicated parameters were measured using Simple Neurite Tracer on images of primary hippocampal neurons from KO mice that were transiently expressing GFP or GFP-SH2B1δ. Neurons were transfected on DIV 4, treated with or without BDNF (0, 10, 50, or 100 ng/mL) overnight, and imaged on DIV 5 using fluorescent microscopy. *N*, individual neurons: GFP with 0 ng/mL BDNF = 10, 10 ng/mL = 20; 50 ng/mL = 15; 100 ng/mL = 12; GFP-SH2B1δ with 0 ng/mL BDNF = 10, 10 ng/mL = 20, 50 ng/mL = 16, 100 ng/mL = 13. **(D)** Sholl analysis was performed on neuron images used in **A-C**. Data are means ± SEM. **Statistics: A-C**, one-way ANOVA (GFP and GFP-SH2B1δ datasets analyzed separately) followed by Dunnett's multiple comparisons test. * $P < 0.05$.

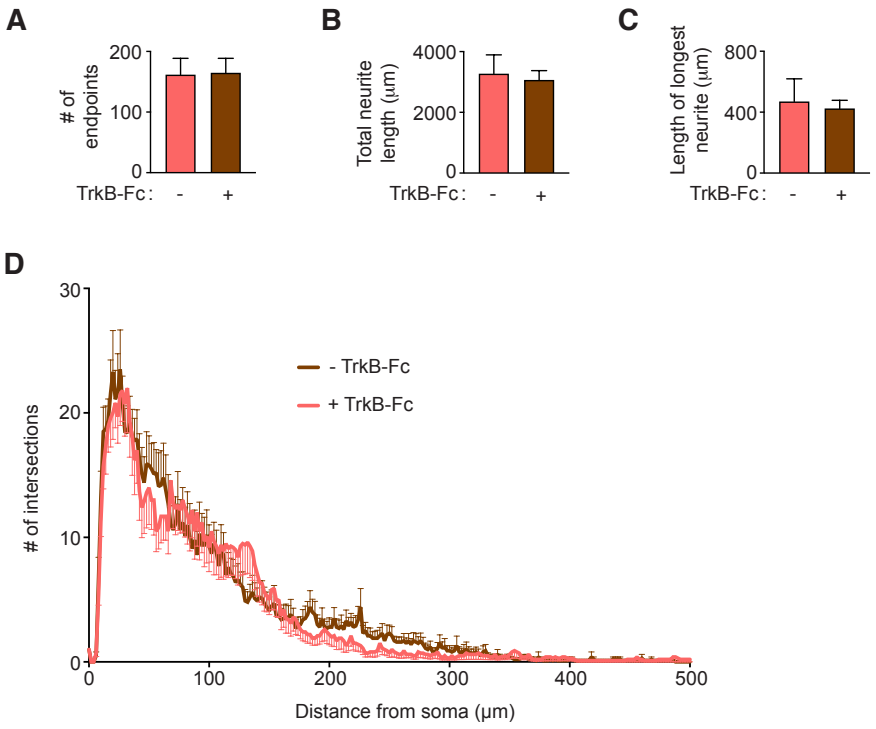

Figure 3.12. Scavenging endogenous BDNF with fusion protein TrkB-Fc does not appear to influence the ability of SH2B1δ to increase neurite complexity

(A-C) Indicated parameters were measured using Simple Neurite Tracer on images of primary hippocampal neurons from KO mice that were transiently expressing GFP-SH2B1δ. Neurons were transfected on DIV 4, treated with or without TrkB-Fc (1 μg/mL) overnight, and imaged on DIV 5 using fluorescent microscopy. *N*, individual neurons: GFP-SH2B1δ with 0 μg/mL = 10, 1 μg/mL = 10. **(D)** Sholl analysis was performed on neuron images used in **A-C**. Data are means ± SEM. **Statistics: A-C**, unpaired, one-tailed Student's t test; **D**, two-way repeated measures ANOVA followed by Dunnett's multiple comparisons test. No significant differences observed.

References

1. Huang, E.J. & Reichardt, L.F. Neurotrophins: roles in neuronal development and function. *Annu. Rev. Neurosci.* **24**, 677-736 (2001).
2. Snider, W.D. Functions of the neurotrophins during nervous system development: what the knockouts are teaching us. *Cell* **77**, 627-638 (1994).
3. Schlessinger, J. & Ullrich, A. Growth factor signaling by receptor tyrosine kinases. *Neuron* **9**, 383-391 (1992).
4. Huang, E.J. & Reichardt, L.F. Trk receptors: roles in neuronal signal transduction. *Ann. Rev. Biochem.* **72**, 609-642 (2003).
5. Rui, L. SH2B1 regulation of energy balance, body weight, and glucose metabolism. *World J Diabetes* **5**, 511-526 (2014).
6. Wang, X., Chen, L., Maures, T.J., Herrington, J. & Carter-Su, C. SH2-B is a positive regulator of nerve growth factor-mediated activation of the Akt/Forkhead pathway in PC12 cells. *J. Biol. Chem.* **279**, 133-141 (2004).
7. Wang, T.C., Chiu, H., Chang, Y.J., Hsu, T.Y., Chiu, I.M. & Chen, L. The adaptor protein SH2B3 (Lnk) negatively regulates neurite outgrowth of PC12 cells and cortical neurons. *PloS one* **6**, e26433 (2011).
8. Joe, R.M., Flores, A., Doche, M.E., Cline, J.M., Clutter, E.S., Vander, P.B., . . . Carter-Su, C. Phosphorylation of the Unique C-terminal Tail of the Alpha Isoform of the Scaffold Protein SH2B1 Controls the Ability of SH2B1alpha to Enhance Nerve Growth Factor Function. *Mol Cell Biol* (2017).
9. Shih, C.H., Chen, C.J. & Chen, L. New function of the adaptor protein SH2B1 in brain-derived neurotrophic factor-induced neurite outgrowth. *PloS one* **8**, e79619 (2013).
10. Chen, L., Maures, T.J., Jin, H., Huo, J.S., Rabbani, S.A., Schwartz, J. & Carter-Su, C. SH2B1β (SH2-Bβ) enhances expression of a subset of nerve growth factor-regulated genes important for neuronal differentiation including genes encoding uPAR and MMP3/10. *Mol. Endocrinol.* **22**, 454-476 (2008).
11. Maures, T.J., Chen, L. & Carter-Su, C. Nucleocytoplasmic shuttling of the adapter protein SH2B1β (SH2-Bβ) is required for nerve growth factor (NGF)-dependent neurite outgrowth and enhancement of expression of a subset of NGF-responsive genes. *Mol. Endocrinol.* **23**, 1077-1091 (2009).
12. Rider, L., Tao, J., Snyder, S., Brinley, B., Lu, J. & Diakonova, M. Adapter protein SH2B1β cross-links actin filaments and regulates actin cytoskeleton. *Mol. Endocrinol.* **23**, 1065-1076 (2009).
13. Diakonova, M., Gunter, D.R., Herrington, J. & Carter-Su, C. SH2-Bβ is a Rac-binding protein that regulates cell motility. *J. Biol. Chem.* **277**, 10669-10677 (2002).
14. Chen, C.J., Shih, C.H., Chang, Y.J., Hong, S.J., Li, T.N., Wang, L.H. & Chen, L. SH2B1 and IRSp53 proteins promote the formation of dendrites and dendritic branches. *J Biol Chem* **290**, 6010-6021 (2015).
15. Rider, L. & Diakonova, M. Adapter protein SH2B1β binds filamin A to regulate prolactin-dependent cytoskeletal reorganization and cell motility. *Mol. Endocrinol.* **25**, 1231-1243 (2011).

16. Lanning, N.J., Su, H.W., Argetsinger, L.S. & Carter-Su, C. Identification of SH2B1β as a focal adhesion protein that regulates focal adhesion size and number. *J. Cell Sci.* **124**, 3095-3105 (2011).
17. Doche, M.D., Bochukova, E.G., Su, H.W., Pearce, L., Keogh, J.M., Henning, E., . . . Farooqi, I.S. *SH2B1* mutations are associated with maladaptive behavior and obesity. *J. Clin. Invest.* **122**, 4732-4736 (2012).
18. Pearce, L.R., Joe, R., Doche, M.D., Su, H.W., Keogh, J.M., Henning, E., . . . Carter-Su, C. Functional characterisation of obesity-associated variants involving the alpha and beta isoforms of human SH2B1. *Endocrinology* **9**, 3219-3226 (2014).
19. Flores, A., Argetsinger, L.S., Stadler, L.K.J., Malaga, A.E., Vander, P.B., DeSantis, L.C., . . . Carter-Su, C. Crucial Role of the SH2B1 PH Domain for the Control of Energy Balance. *Diabetes* **68**, 2049-2062 (2019).
20. Ren, D., Li, M., Duan, C. & Rui, L. Identification of SH2-B as a key regulator of leptin sensitivity, energy balance and body weight in mice. *Cell Metab.* **2**, 95-104 (2005).
21. Duan, C., Yang, H., White, M.F. & Rui, L. Disruption of SH2-B causes age-dependent insulin resistance and glucose intolerance. *Mol. Cell. Biol.* **24**, 7435-7443 (2004).
22. Jiang, L., Su, H., Keogh, J.M., Chen, Z., Henning, E., Wilkinson, P., . . . Rui, L. Neural deletion of Sh2b1 results in brain growth retardation and reactive aggression. *FASEB J* **32**, 1830-1840 (2018).
23. Cote, J.L., Argetsinger, L.S., Flores, A., Rupp, A.C., Cline, J.M., DeSantis, L.C., . . . Carter-Su, C. Deletion of the Brain-Specific alpha and delta Isoforms of Adapter Protein SH2B1 Protects Mice From Obesity. *Diabetes* **70**, 15 (2021).
24. Jiang, L., Su, H., Wu, X., Shen, H., Kim, M.-H., Li, Y., . . . Rui, L. Leptin receptor-expressing neuron Sh2b1 supports sympathetic nervous system and protects against obesity and metabolic disease. *Nature communications* **11**, 1-13 (2020).
25. Rios, M. BDNF and the central control of feeding: accidental bystander or essential player? *Trends Neurosci.* **36**, 83-90 (2013).
26. Nelms, K., O'Neill, T.J., Li, S., Hubbard, S.R., Gustafson, T.A. & Paul, W.E. Alternative splicing, gene localization, and binding of SH2-B to the insulin receptor kinase domain. *Mammalian Genome* **10**, 1160-1167 (1999).
27. Yousaf, N., Deng, Y., Kang, Y. & Riedel, H. Four PSM/SH2-B alternative splice variants and their differential roles in mitogenesis. *J. Biol. Chem.* **276**, 40940-40948 (2001).
28. Chen, L. & Carter-Su, C. Adapter protein SH2-Bβ undergoes nucleocytoplasmic shuttling: implications for nerve growth factor induction of neuronal differentiation. *Mol. Cell. Biol.* **24**, 3633-3647 (2004).
29. Rui, L., Herrington, J. & Carter-Su, C. SH2-B is required for nerve growth factor-induced neuronal differentiation. *J. Biol. Chem.* **274**, 10590-10594 (1999).
30. Qian, X., Riccio, A., Zhang, Y. & Ginty, D.D. Identification and characterization of novel substrates of Trk receptors in developing neurons. *Neuron* **21**, 1017-1029 (1998).
31. Zhang, Y., Zhu, W., Wang, Y.G., Liu, X.J., Jiao, L., Liu, X., . . . He, C. Interaction of SH2-Bβ with RET is involved in signaling of GDNF-induced neurite outgrowth. *J. Cell. Sci.* **119**, 1666-1676 (2006).

32. Ren, D., Zhou, Y., Morris, D., Li, M., Li, Z. & Rui, L. Neuronal SH2B1 is essential for controlling energy and glucose homeostasis. *J. Clin. Invest.* **117**, 397-406 (2007).
33. Herrington, J., Diakonova, M., Rui, L., Gunter, D.R. & Carter-Su, C. SH2-B is required for growth hormone-induced actin reorganization. *J. Biol. Chem.* **275**, 13126-13133 (2000).
34. Vandesompele, J., De Preter, K., Pattyn, F., Poppe, B., Van Roy, N., De Paepe, A. & Speleman, F. Accurate normalization of real-time quantitative RT-PCR data by geometric averaging of multiple internal control genes. *Genome Biol* **3**, research0034.0031-0034.0011 (2002).
35. Maures, T.J., Su, H.-W., Argetsinger, L.S., Grinstein, S. & Carter-Su, C. Phosphorylation controls a dual function polybasic NLS in the adapter protein SH2B1β to regulate its cellular function and distribution between the plasma membrane, cytoplasm and nucleus. *J. Cell Sci.* **124**, 1542-1552 (2011).
36. Rui, L., Mathews, L.S., Hotta, K., Gustafson, T.A. & Carter-Su, C. Identification of SH2-Bβ as a substrate of the tyrosine kinase JAK2 involved in growth hormone signaling. *Mol. Cell. Biol.* **17**, 6633-6644 (1997).
37. Inagaki, N., Thoenen, H. & Lindholm, D. TrkA tyrosine residues involved in NGF-induced neurite outgrowth of PC12 cells. *Eur J Neurosci* **7**, 1125-1133 (1995).
38. Kumar, V., Zhang, M.X., Swank, M.W., Kunz, J. & Wu, G.Y. Regulation of dendritic morphogenesis by Ras-PI3K-Akt-mTOR and Ras-MAPK signaling pathways. *J Neurosci* **25**, 11288-11299 (2005).
39. Jaworski, J., Spangler, S., Seeburg, D.P., Hoogenraad, C.C. & Sheng, M. Control of dendritic arborization by the phosphoinositide-3'-kinase-Akt-mammalian target of rapamycin pathway. *J Neurosci* **25**, 11300-11312 (2005).
40. Atwal, J.K., Massie, B., Miller, F.D. & Kaplan, D.R. The TrkB-Shc site signals neuronal survival and local axon growth via MEK and P13-kinase. *Neuron* **27**, 265-277 (2000).
41. Wang, T.C., Li, Y.H., Chen, K.W., Chen, C.J., Wu, C.L., Teng, N.Y. & Chen, L. SH2B1β regulates N-cadherin levels, cell-cell adhesion and nerve growth factor-induced neurite initiation. *J. Cell. Physiol.* **226**, 2063-2074 (2011).
42. Farias-Eisner, R., Vician, L., Silver, A., Reddy, S., Rabbani, S.A. & Herschman, H.R. The urokinase plasminogen activator receptor (UPAR) is preferentially induced by nerve growth factor in PC12 pheochromocytoma cells and is required for NGF-driven differentiation. *J. Neurosci.* **20**, 230-239 (2000).
43. Hayden, S.M. & Seeds, N.W. Modulated expression of plasminogen activator system components in cultured cells from dissociated mouse dorsal root ganglia. *J. Neurosci.* **16**, 2307-2317 (1996).
44. Powell, E.M., Mars, W.M. & Levitt, P. Hepatocyte growth factor/scatter factor is a motogen for interneurons migrating from the ventral to dorsal telencephalon. *Neuron* **30**, 79-89 (2001).
45. McFarlane, S. Metalloproteases: carving out a role in axon guidance. *Neuron* **37**, 559-562 (2003).
46. Basbaum, C.B. & Werb, Z. Focalized proteolysis: spatial and temporal regulation of extracellular matrix degradation at the cell surface. *Curr. Opin. Cell Biol.* **8**, 731-738 (1996).

47. Ossowski, L. & Aguirre-Ghiso, J.A. Urokinase receptor and integrin partnership: coordination of signaling for cell adhesion, migration and growth. *Curr. Opin. Cell Biol.* **12**, 613-620 (2000).
48. Yap, E.L. & Greenberg, M.E. Activity-Regulated Transcription: Bridging the Gap between Neural Activity and Behavior. *Neuron* **100**, 330-348 (2018).
49. West, A.E. & Greenberg, M.E. Neuronal activity-regulated gene transcription in synapse development and cognitive function. *Cold Spring Harb Perspect Biol* **3**(2011).
50. Biosystems, A. Amplification Efficiency of TaqMan Gene Expression Assays. *Application Note*, 1-6 (2006).
51. Yoshihara, Y., De Roo, M. & Muller, D. Dendritic spine formation and stabilization. *Curr Opin Neurobiol* **19**, 146-153 (2009).
52. Scott, M.S., Troshin, P.V. & Barton, G.J. NoD: a Nucleolar localization sequence detector for eukaryotic and viral proteins. *BMC Bioinformatics* **12**, 317 (2011).
53. Schmidt-Zachmann, M.S. & Nigg, E.A. Protein localization to the nucleolus: a search for targeting domains in nucleolin. *J. Cell Sci.* **105 (Pt 3)**, 799-806 (1993).
54. Nishimura, Y., Ohkubo, T., Furuichi, Y. & Umekawa, H. Tryptophans 286 and 288 in the C-terminal region of protein B23.1 are important for its nucleolar localization. *Biosci Biotechnol Biochem* **66**, 2239-2242 (2002).
55. Grummitt, C.G., Townsley, F.M., Johnson, C.M., Warren, A.J. & Bycroft, M. Structural consequences of nucleophosmin mutations in acute myeloid leukemia. *J Biol Chem* **283**, 23326-23332 (2008).
56. Rui, L., Herrington, J. & Carter-Su, C. SH2-B, a membrane-associated adapter, is phosphorylated on multiple serines/threonines in response to nerve growth factor by kinases within the MEK/ERK cascade. *J. Biol. Chem.* **274**, 26485-26492 (1999).
57. Gomes, C., Smith, S.C., Youssef, M.N., Zheng, J.J., Hagg, T. & Hetman, M. RNA polymerase 1-driven transcription as a mediator of BDNF-induced neurite outgrowth. *J Biol Chem* **286**, 4357-4363 (2011).
58. Slomnicki, L.P., Pietrzak, M., Vashishta, A., Jones, J., Lynch, N., Elliot, S., . . . Hetman, M. Requirement of Neuronal Ribosome Synthesis for Growth and Maintenance of the Dendritic Tree. *J Biol Chem* **291**, 5721-5739 (2016).
59. Boisvert, F.M., van Koningsbruggen, S., Navascues, J. & Lamond, A.I. The multifunctional nucleolus. *Nat. Rev. Mol. Cell. Biol.* **8**, 574-585 (2007).
60. Raska, I., Shaw, P.J. & Cmarko, D. New insights into nucleolar architecture and activity. *Int Rev Cytol* **255**, 177-235 (2006).
61. Duclot, F. & Kabbaj, M. The Role of Early Growth Response 1 (EGR1) in Brain Plasticity and Neuropsychiatric Disorders. *Front Behav Neurosci* **11**, 1-20 (2017).
62. Minatohara, K., Akiyoshi, M. & Okuno, H. Role of Immediate-Early Genes in Synaptic Plasticity and Neuronal Ensembles Underlying the Memory Trace. *Front Mol Neurosci* **8**, 78 (2015).
63. Yin, Y., Edelman, G.M. & Vanderklish, P.W. The brain-derived neurotrophic factor enhances synthesis of Arc in synaptoneurosomes. *Proc Natl Acad Sci U S A* **99**, 2368-2373 (2002).
64. Ying, S.W., Futter, M., Rosenblum, K., Webber, M.J., Hunt, S.P., Bliss, T.V. & Bramham, C.R. Brain-derived neurotrophic factor induces long-term potentiation

in intact adult hippocampus: requirement for ERK activation coupled to CREB and upregulation of Arc synthesis. *J Neurosci* **22**, 1532-1540 (2002).
65. Alder, J., Thakker-Varia, S., Bangasser, D.A., Kuroiwa, M., Plummer, M.R., Shors, T.J. & Black, I.B. Brain-derived neurotrophic factor-induced gene expression reveals novel actions of VGF in hippocampal synaptic plasticity. *J Neurosci* **23**, 10800-10808 (2003).
66. Thul, P.J., Akesson, L., Wiking, M., Mahdessian, D., Geladaki, A., Ait Blal, H., . . . Lundberg, E. A subcellular map of the human proteome. *Science* **356**(2017).
67. Human Protein Atlas. Vol. 2021.
68. Zhang, M., Deng, Y. & Riedel, H. PSM/SH2B1 splice variants: critical role in src catalytic activation and the resulting STAT3s-mediated mitogenic response. *J. Cell. Biochem.* **104**, 105-118 (2008).
69. Zhang, M., Deng, Y., Tandon, R., Bai, C. & Riedel, H. Essential role of PSM/SH2-B variants in insulin receptor catalytic activation and the resulting cellular responses. *J. Cell. Biochem.* **103**, 162-181 (2008).
70. Nagappan-Chettiar, S., Johnson-Venkatesh, E.M. & Umemori, H. Activity-dependent proteolytic cleavage of cell adhesion molecules regulates excitatory synaptic development and function. *Neurosci Res* **116**, 60-69 (2017).
71. Sonderegger, P. & Matsumoto-Miyai, K. Activity-controlled proteolytic cleavage at the synapse. *Trends in neurosciences* **37**, 413-423 (2014).
72. Wiera, G., Lebida, K., Lech, A.M., Brzdak, P., Van Hove, I., De Groef, L., . . . Mozrzymas, J.W. Long-term plasticity of inhibitory synapses in the hippocampus and spatial learning depends on matrix metalloproteinase 3. *Cell Mol Life Sci* (2020).
73. Li, L., Carter, J., Gao, X., Whitehead, J. & Tourtellotte, W.G. The neuroplasticity-associated arc gene is a direct transcriptional target of early growth response (Egr) transcription factors. *Mol. Cell. Biol.* **25**, 10286-10300 (2005).
74. Wallace, C.S., Lyford, G.L., Worley, P.F. & Steward, O. Differential intracellular sorting of immediate early gene mRNAs depends on signals in the mRNA sequence. *J Neurosci* **18**, 26-35 (1998).
75. Guzowski, J.F., McNaughton, B.L., Barnes, C.A. & Worley, P.F. Environment-specific expression of the immediate-early gene Arc in hippocampal neuronal ensembles. *Nat Neurosci* **2**, 1120-1124 (1999).
76. Steward, O., Wallace, C.S., Lyford, G.L. & Worley, P.F. Synaptic activation causes the mRNA for the IEG Arc to localize selectively near activated postsynaptic sites on dendrites. *Neuron* **21**, 741-751 (1998).
77. Moga, D.E., Calhoun, M.E., Chowdhury, A., Worley, P., Morrison, J.H. & Shapiro, M.L. Activity-regulated cytoskeletal-associated protein is localized to recently activated excitatory synapses. *Neuroscience* **125**, 7-11 (2004).
78. Messaoudi, E., Kanhema, T., Soule, J., Tiron, A., Dagyte, G., da Silva, B. & Bramham, C.R. Sustained Arc/Arg3.1 synthesis controls long-term potentiation consolidation through regulation of local actin polymerization in the dentate gyrus in vivo. *J Neurosci* **27**, 10445-10455 (2007).
79. Chowdhury, S., Shepherd, J.D., Okuno, H., Lyford, G., Petralia, R.S., Plath, N., . . . Worley, P.F. Arc/Arg3.1 interacts with the endocytic machinery to regulate AMPA receptor trafficking. *Neuron* **52**, 445-459 (2006).

80. Shepherd, J.D., Rumbaugh, G., Wu, J., Chowdhury, S., Plath, N., Kuhl, D., . . . Worley, P.F. Arc/Arg3.1 mediates homeostatic synaptic scaling of AMPA receptors. *Neuron* **52**, 475-484 (2006).
81. Gavalda, N., Gutierrez, H. & Davies, A.M. Developmental switch in NF-kappaB signalling required for neurite growth. *Development* **136**, 3405-3412 (2009).
82. Iarovaia, O.V., Minina, E.P., Sheval, E.V., Onichtchouk, D., Dokudovskaya, S., Razin, S.V. & Vassetzky, Y.S. Nucleolus: A Central Hub for Nuclear Functions. *Trends Cell Biol* **29**, 647-659 (2019).
83. Hetman, M. & Pietrzak, M. Emerging roles of the neuronal nucleolus. *Trends Neurosci.* **35**, 305-314 (2012).
84. Brun, S., Abella, N., Berciano, M.T., Tapia, O., Jaumot, M., Freire, R., . . . Agell, N. SUMO regulates p21Cip1 intracellular distribution and with p21Cip1 facilitates multiprotein complex formation in the nucleolus upon DNA damage. *PLoS One* **12**, e0178925 (2017).

Chapter 4:

Conclusions and Future Directions

Chapter Summary

The overarching goal of my dissertation was to investigate how the brain-specific alternatively spliced isoforms of SH2B1, α and δ, regulate the brain at the whole body and cellular levels. In Chapter 2, I demonstrated that deletion of SH2B1α and δ reduces body weight in mice. Because previous work showed that deletion of all SH2B1 isoforms increases body weight [1,2], these results suggested that the different alternatively spliced SH2B1 isoforms perform different functions *in vivo.* In Chapter 3, I demonstrated that the brain-specific δ isoform of SH2B1 has the ability to increase neurite outgrowth and complexity in primary hippocampal neurons to a greater extent than the other three isoforms. I also showed that SH2B1δ localized to the nucleolus, which was required for SH2B1δ to maximally increase neurite complexity. Thus, I provided ample evidence that different isoforms of SH2B1 perform different functions *in vivo* and *in vitro*. Below, I reemphasize pertinent conclusions from Chapters 2 and 3 and present new questions and considerations that my experiments have inspired. I also discuss some preliminary and ongoing experiments and propose additional strategies for future work.

Conclusions and Future Directions

How do SH2B1 isoforms regulate BDNF/TrkB activity in neurons?

Multiple observations in Chapters 2 and 3 suggested that SH2B1α and/or δ promote weight gain and SH2B1 isoforms increase neurite complexity by, at least in part, enhancing BDNF/TrkB activity. Our most convincing observation in this category was that the BDNF-induced expression of neuronal immediate early genes *Arc* and *Egr1* was partially dependent on SH2B1 activity (Fig. 3.8). We now have multiple questions regarding the relationship between SH2B1 isoforms and BDNF/TrkB activity, some of which are addressed below.

Does deletion of specific SH2B1 isoforms affect TrkB-expressing neurons?

Because SH2B1 is known to modulate leptin signaling and SH2B1α/δ expression is largely restricted to the brain, the site of leptin action on energy balance and food intake, we initially hypothesized that increased leptin signaling might underlie the leanness of αδKO mice. However, multiple observations in Chapter 2 suggested that deletion of SH2B1α/δ does not alter cellular responses to leptin (Figs. 2.7 and 2.8). One possibility is that the deletion of SH2B1α/δ increases leptin sensitivity but our assays did not detect this change. Another possibility is as follows: based on work generated by our lab and others, including observations that BDNF and TrkB are critical regulators of energy balance [3] and that SH2B1 enhances BDNF-induced neurite outgrowth [4], the αδKO phenotype could be a consequence, at least in part, of increased signaling in TrkB-

expressing neurons. One way to test this hypothesis would be to delete SH2B1α/δ specifically from TrkB-expressing cells. A phenotype of the resulting animal that was similar to that of the original αδKO mouse would support our hypothesis. Unfortunately, when we made our mouse model (2014), there was no feasible way to introduce loxP sites flanking (e.g., "flox") only the α/δ transcripts to allow us to delete these isoforms from specific cell types using the Cre-lox system. We were also discouraged from trying to use FLP-FRT recombination as a strategy to target specific cell types because of the size of the insert (~3000 nucleotides) that would be required to "flip" between the WT and αδKO sequence. However, I am optimistic that the precision and flexibility of relevant gene-editing technologies will improve enough to eventually allow me to delete SH2B1α/δ from specific cell types. For example, if I were able to devise a strategy to flox the sequence specific for SH2B1α/δ, perhaps by deleting intron 9 with CRISPR/Cas9 and floxing the sequence that contains the α and δ stop codons, then I could delete SH2B1α/δ specifically from TrkB-expressing cells by crossing αδHET mice with $TrkB^{Cre}$ mice. Additionally, if I used $TrkB^{Cre}$ mice with a fluorescently-tagged L10 ribosomal subunit ($TrkB^{Cre\text{-}eGFP\text{-}L10}$ mice), I could assess the transcriptional profile of TrkB-expressing cells lacking SH2B1α/δ, in the hypothalamus and other brain regions, using TRAP-seq. Also, in parallel with the above experiments, I could cross SH2B1 floxed mice, which we already have in our mouse colony, with $TrkB^{Cre\text{-}eGFP\text{-}L10}$ mice to assess the effect of deleting all SH2B1 isoforms from TrkB-expressing cells on metabolic phenotypes and the transcriptome.

To gain further insight, I could assess projections of TrkB-expressing neurons in WT vs. KO vs. αδKO mice. I could start by focusing on neurons in the paraventricular

hypothalamus and ventromedial hypothalamus, both of which have been identified as areas that express BDNF to suppress food intake and promote energy expenditure [5-7]. Because TrkB antibodies do not mark cell bodies well in brain sections, I could cross our mouse models with Ntrk2$^{CreER/+}$;Ai9 mice in which a mutant estrogen receptor (ER) ligand binding domain is fused to the C-terminus of Cre such that, upon application of the estrogen receptor ligand tamoxifen, TrkB neurons are genetically labeled with TdTomato. I would then be able to immunostain fixed brain sections for TdTomato to visualize TrkB-expressing neuronal cell bodies and projections. See recent work by An and colleagues for an example of this strategy [8]. As a bonus, use of tamoxifen would offer temporal control, allowing me to examine the effect of SH2B1 isoforms at different stages of development, or even compare animal phenotypes or cellular functions before and after isoform deletion in the same mouse.

Does the SH2B1δ-induced increase in neurite complexity of primary hippocampal neurons arise, at least in part, from increased BDNF/TrkB activity?

Based on our findings in Chapter 3 and previous work from our lab and others, we hypothesized that the SH2B1δ-induced increase in neurite complexity in primary hippocampal neurons resulted, at least in part, from increased activity of BDNF/TrkB. Our preliminary experiments did not support this hypothesis (Supplementary Material Figs. 3.11 and 3.12). Nevertheless, it is possible that BDNF regulates the ability of SH2B1δ to increase neurite complexity but our assays did not detect the regulatory relationship. Indeed, because we were limited by time and resources, we only tested a small set of experimental conditions. In the future, it would be valuable to test the same hypothesis

using different experimental parameters. For example, I could dissect hippocampi from embryonic rather than postnatal mice to compare neurite outgrowth and complexity in KO neurons expressing different SH2B1 isoforms (WT and mutant/variant forms). This suggestion is inspired by work from Gavalda and colleagues, who demonstrated that embryonic nodose neurons were much more responsive to BDNF activity than postnatal nodose neurons by multiple measures including neurite complexity [9]. Second, I could experiment with gradual, prolonged BDNF treatment of hippocampal neuron cultures, as opposed to the acute treatment that we used during our preliminary assays. Indeed, previous results have demonstrated differential effects in cellular responses, including neurite outgrowth patterns and phosphorylation of signaling proteins, from transient and sustained activation of BDNF/TrkB signaling [10]. Finally, to assess the impact of different isoforms on cellular activity following BDNF treatment, I could measure signaling activity downstream of TrkB by highly expressing different SH2B1 isoforms (WT and mutant/variant forms) in KO primary cultured neurons via lentivirus transduction and detecting levels of phosphorylated S6 kinase using western blotting of neuron lysates and/or immunocytochemistry of fixed cells.

What is the nucleolar function of SH2B1δ in neurons?

In Chapter 3, we demonstrated that SH2B1δ localizes to the nucleolus in PC12 cells (Fig. 3.1) and primary hippocampal neurons (Fig. 3.5). Because SH2B1δ localization to nucleoli appears to be required for SH2B1δ to increase neurite complexity (Fig. 3.7), we hypothesized that SH2B1δ enhances neurite complexity, at least in part, by mediating ribosomal biogenesis. However, our measurement of the relative expression of genes associated with ribosomal biogenesis including *45S pre-rRNA*, *Ubtf*, *Ncl*, *Fbl*, and *B23/Npl* in primary hippocampal neuron cultures from WT or *Sh2b1* KO mice in the presence or absence of BDNF suggested that SH2B1 does not regulate ribosomal biogenesis in neurons with or without neurotrophin stimulation (Fig. 3.10). Thus, we continue to be uncertain about the nucleolar function of SH2B1δ in neurons. It is possible that the particular experimental conditions we used did not detect any SH2B1 regulation of ribosomal biogenesis but others (e.g., different concentration and/or timing of BDNF treatment) might. It is also possible that the changes are so subtle such that we did not detect any following deletion of all endogenous isoforms, whereas we might detect changes following exogenous expression of individual SH2B1 isoforms. Preliminary data suggest that stable expression of GFP-SH2B1β or GFP-SH2B1δ in PC12 cells does not affect ribosomal biogenesis, measured by expression of *45S pre-rRNA* (Fig. 4.1), although, again, we only ran this experiment using one set of conditions and two time points.

While ribosomal biogenesis has historically been touted as the major functional role of nucleoli, more recent work has illuminated several other roles for these subnuclear structures [11-13]. For example, nucleoli have been shown to serve as neuronal stress

sensors, thereby regulating apoptosis, and structures to sequester proteins. Interestingly, preliminary data demonstrated that SH2B1δ is capable of bringing SH2B1β but not SH2B1α or γ to nucleoli in PC12 cells (P. Vander, T. Maures, J. Cote, C. Carter-Su, unpublished data). Preliminary data also demonstrated that SH2B1δ brings a cytosolic version of the SH2B1 binding partner β-spectrin to nucleoli (L. Mancour and C. Carter-Su, unpublished data). These results suggest that SH2B1δ may serve, at least in part, to transport SH2B1β, and most likely other cytoplasmic proteins, into nucleoli. In the future, I could further assess the ability of SH2B1δ to bring SH2B1β, and potentially other proteins, into nucleoli using continuous monitoring live-cell confocal microscopy of neurons co-transfected with SH2B1δ and other proteins under a variety of different treatments. I could also investigate the potential for SH2B1δ to regulate neuronal stress responses by measuring markers of apoptosis in primary neuron lysates or cultures highly expressing individual SH2B1 isoforms via lentivirus transduction.

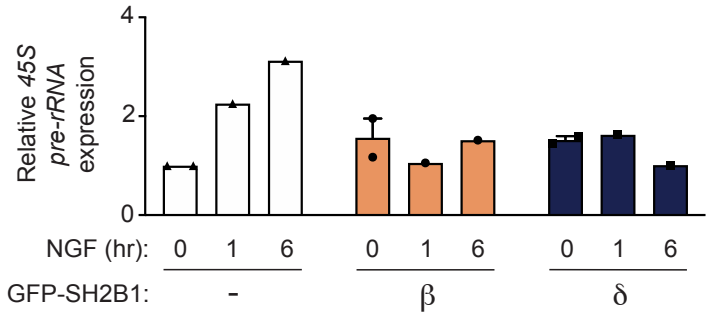

Figure 4.1. SH2B1β or δ do not appear to influence gene expression associated with ribosomal biogenesis in PC12 cells

PC12 cells stably expressing GFP (-) or GFP-tagged SH2B1β or SH2B1δ were treated with or without NGF (100 ng/mL for 1 or 6 hours). RNA was isolated and relative expression levels of *45S pre-rRNA* were normalized the expression levels of reference gene *Cyclophilin A* or the geometric mean of the expression levels of reference genes *Cyclophilin A*, *Hprt*, and *36b4* (primers listed in Table 4.1). Data were normalized to values obtained for GFP-expressing cells without NGF treatment. Means are from 1 or 2 separate experiments, each using distinct biological samples. Data are means ± SEM.

Table 4.1. Primers for qPCR using SYBR chemistry

Primer	**Direction**	**Sequence (5' → 3')**
45S pre-rRNA	Forward	GTGTGTCCCGCCTTTCCGT
45S pre-rRNA	Reverse	GAAACGAAACGGCACACGTAAG
Cyclophilin A (reference)	Forward	AACTTTCGTGCTCTGAGC
Cyclophilin A (reference)	Reverse	ATGGCGTGTGAAGTCACC
Hprt (reference)	Forward	CTCATGGACTGATTATGGACAGGAC
Hprt (reference)	Reverse	GCAGGTCAGCAAAGAACTTATAGCC
36b4 (reference)	Forward	GAAACTGCTGCCTCACATCCG
36b4 (reference)	Reverse	GCTGGCACAGTGACCTCACACG

How do SH2B1 isoforms regulate neuronal synapses?

In Chapter 2, our RNA-seq analysis presented the possibility that deletion of SH2B1α/δ altered gene expression associated with synaptic function in the hypothalamus (Fig. 2.12). In Chapter 3, we presented evidence that SH2B1 isoforms regulate neurotrophic factor-induced gene expression associated with the function of synapses in PC12 cells (Fig. 3.3) and primary hippocampal neurons (Fig. 3.8). Furthermore, previous findings have demonstrated that SH2B1 regulates the actin cytoskeleton including the formation of dendritic filopodia in primary cultured neurons [14-18]. Thus, we speculate that SH2B1 isoforms may serve to collectively fine-tune appetite-regulating neuronal synapses by mediating cytoskeletal rearrangement within dendritic spines.

Moving forward, I would first determine whether SH2B1 isoforms localize to synapses. Our images of hippocampal neurons transiently expressing individual SH2B1 isoforms suggested that all known SH2B1 isoforms localize to dendritic filopodia in young neurons (Fig. 3.5B). Additionally, previous work demonstrated that SH2B1 interacts with actin-binding protein IRSp53 to regulate the formation of dendritic filopodia in primary neurons [14]. These results suggest that SH2B1 isoforms may localize to dendritic spines, which emerge from dendritic filopodia to serve as post-synaptic compartments of synapses in mature neurons [19]. If I find that particular isoforms localize in spines, it would be helpful to know whether this localization is constant or transient depending on neuronal activity or other stimuli. One simple approach to determine whether any SH2B1 isoform localizes at synapses is to immunostain fixed primary hippocampal cultures for colocalization of SH2B1 and PSD-95. Another more sophisticated approach to determine whether (and which) SH2B1 isoforms are integrated at mature synapses would be to

perform continuous monitoring imaging using correlative three-dimensional super-resolution fluorescence and block-face electron microscopy [20]. This technique would allow me to observe localization of transiently expressed SH2B1 isoforms (WT and mutant/variant forms) in mature KO neurons, before and after action potentials or other environmental stimuli, at extremely high resolution. Additionally, comparing such images, and the subsequently rendered three-dimensional models, from WT vs. KO vs. αδKO neurons would provide valuable insight into the role of SH2B1 isoforms in synapse structure and function.

It would also be useful to expand upon our discovery that SH2B1 isoforms regulate neurotrophic factor-induced gene expression associated with synaptic function. While intriguing, the conclusions we can draw from this observation are limited because we were unable to distinguish the specific impact of individual isoforms on this gene expression. Preliminary results suggested that neither SH2B1β nor δ increased *Egr1* expression after 1 or 6 hours of NGF treatment (Fig. 4.2). Preliminary results also suggested that SH2B1δ may increase *Arc* expression after 1 and 6 hours of NGF treatment, and SH2B1β may increase *Arc* expression after 6 hours of NGF treatment, although these effects did not achieve statistical significance (Fig. 4.2). However, we ran this experiment using RNA samples that were over a year old. Indeed, the microarray dataset published by our lab in 2008 [21] indicated that SH2B1β enhanced the expression of *Egr1* and *Arc* by 2 and ~3.5 fold, respectively, following 6 hours of NGF treatment. Thus, “fresh” RNA samples may give more robust results. We also recognize that PC12 cells may give different results than hippocampal neurons. We have therefore begun to analyze the impact of individual isoforms on BDNF-induced expression of *Egr1* and *Arc*

in primary hippocampal neurons using two different experimental approaches. First, we are developing lentivirus constructs to highly express individual SH2B1 isoforms in KO neurons, which will allow us to test the impact of each isoform on gene expression in primary hippocampal neurons. We are also measuring expression of ARC protein by transiently expressing the SH2B1 isoforms individually in primary hippocampal neuron cultures via transfection, treating the cultures with or without BDNF, fixing the cells, and immunostaining for ARC.

In Chapter 3, we demonstrated that hippocampal neuron cultures lacking SH2B1 isoforms exhibit decreased expression, albeit not to a statistically significant extent, of key synaptic protein PSD-95 (Fig. 3.4). We suspect that the difference in expression between WT and KO cultures would become significant with additional experimental replicates. There are at least two explanations for a decrease in PSD-95 expression in KO cultures: One is that the deletion of SH2B1 reduces the abundance of PSD-95 proteins in some or all individual neurons. Another is that the deletion of SH2B1 reduces the overall abundance of synapses in the neuron culture. Or perhaps there is some combination thereof. The lack of clarity around this observation requires follow-up experiments. One way to gain further insight would be to perform immunocytochemistry experiments to detect PSD-95, and other synaptic proteins, in individual neurons in WT vs. KO vs. $\alpha\delta$KO primary hippocampal cultures to quantify the abundance of synaptic proteins in individual neurons and the number of synapses present overall. Furthermore, it will be important to understand how the individual SH2B1 isoforms, particularly SH2B1δ, in WT and mutant/variant forms, influence synaptic protein expression and function. To this end, I

could highly express individual SH2B1 isoforms in KO neurons via lentivirus transduction and proceed with the technique outlined above.

Finally, it would be worthwhile to investigate how SH2B1 isoforms impact synaptic plasticity. This would be particularly relevant given that *Egr1* and *Arc* are both considered critical regulators of synaptic plasticity. Synaptic plasticity could be assessed in the different primary neuron cultures described above using a variety of assays including single-cell electrophysiological recordings of miniature excitatory and inhibitory postsynaptic currents [22]. Paired with observations resulting from the experiments proposed in the previous paragraphs, these results would offer helpful insight into the effects of individual SH2B1 isoforms on neuronal synapses.

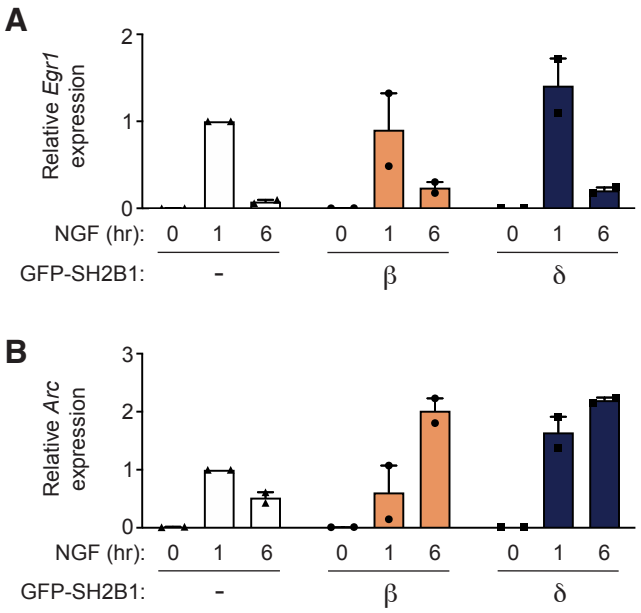

Figure 4.2. SH2B1β or SH2B1δ do not significantly alter NGF-stimulated gene expression of *Egr1* or *Arc* in PC12 cells

PC12 cells stably expressing GFP or GFP-tagged SH2B1β or SH2B1δ were treated with or without NGF (100 ng/mL for 1 or 6 hours). RNA was isolated and relative expression levels of **(A)** *Egr1* or **(B)** *Arc* were measured by qPCR (primers listed in Table 4.2). Expression of the genes of interest was normalized to the geometric mean of the expression levels of reference genes *Gapdh* or *Tbp.* Data were normalized to values obtained for GFP-expressing cells treated with NGF for 1 hour. Means are from 2 separate experiments, each using distinct biological samples. Data are means ± SEM. **Statistics**: **A-B**, repeated measures one-way ANOVA on NGF-treated samples followed by Holm-Sidak's multiple comparison's test. No significant differences detected.

Table 4.2. TaqMan Gene Expression Assays from Applied Biosystems

Gene	Species	TaqMan Gene Expression Assay
Arc	Rat	Rn00571208_g1
Egr1	Rat	Rn00561138_m1
Gapdh (reference gene)	Rat	Rn01775763_g1
Tbp (reference gene)	Rat	Rn01455646_m1

Do SH2B1 isoforms regulate other functions of primary hippocampal neurons?

Because the expansion of the actin cytoskeleton is a major determinant of neurite outgrowth and complexity, it seems essential to clarify precisely how different SH2B1 isoforms regulate the actin cytoskeleton in the context of neurite expansion and arborization. Previous work has demonstrated that SH2B1 regulates the actin cytoskeleton [14-17,23]. For example, SH2B1β enhances GH- and PDGF-induced membrane ruffling [18] and cross-links actin filaments [15]. However, this work focused solely on the β isoform, and much of it was performed in immortalized cell lines, not primary neurons. One approach to investigate the effect of individual SH2B1 isoforms on the neuronal actin cytoskeleton would be to compare actin cytoskeleton-related gene expression in WT vs. KO vs. αδKO neurons at multiple time points during neuronal development in culture (e.g., DIV 4, 7, 10, 14, 21) using RNA-seq. The same approach could be used to assess cultures highly expressing individual SH2B1 isoforms (WT and mutant/variant forms) via lentivirus transduction.

I am also interested in investigating whether SH2B1 isoforms influence electrophysiological properties in neurons. For example, I could compare the speed with which electrical signals are propagated along dendrites and axons in WT vs. KO vs. αδKO neurons, and KO neurons highly expressing individual SH2B1 isoforms (WT and mutant/variant forms) via lentivirus transduction, by measuring their capacitance.

Do SH2B1 isoforms regulate multiple neuron populations?

Does deletion of specific SH2B1 isoforms affect the function of multiple neuronal populations?

Whether or not SH2B1 isoforms are confirmed to regulate BDNF/TrkB activity at the whole animal and/or cellular level (see above), SH2B1 isoforms may regulate other neuronal populations. The aforementioned approach to investigate potential contributions of TrkB-expressing neurons in the αδKO and KO mouse models could be modified to target other neuronal populations of interest such as those expressing the GFRα1/RET complex and/or the GFRα-like (GFRAL)/RET complex. Intriguingly, the latter population, which is a target for growth differentiation factor (GDF) 15, has been shown to regulate food intake and body weight through its actions in the central nervous system [24]. Additionally, I could perform single-cell RNA-seq on the hypothalamus, hippocampus, cortex, and other brain regions in WT vs. KO vs. αδKO mice to determine how deletion of all SH2B1 isoforms, and specifically SH2B1α/δ, affects gene expression within specific cell types.

Relatedly, our lab recently used TRAP-seq to investigate whether deletion of all SH2B1 isoforms specifically from LepRb-expressing cells would alter the hypothalamic transcriptome. Surprisingly, our results indicated that this targeted deletion induced statistically significant differential expression of only one gene: *Kalrn* (M. Ellis, J. Cote, A. Rupp, M. Myers, C. Carter-Su, unpublished data). *Kalrn* encodes Kalirin, a Rho guanine-nucleotide exchange factor that is critical for neurite outgrowth, dendritic spine development, and synaptic structure and function, presumably through its regulation of

the actin cytoskeleton [25-29]. In agreement with data presented in Chapters 2 and 3 of my dissertation, these results provide evidence that SH2B1 regulates synaptic function and likely contributes to the regulation of energy balance via leptin-independent pathways.

How applicable are our findings from hippocampal neurons to other neurons?

Our assessment of the effect of SH2B1 activity on the morphology and function of primary mouse hippocampal neurons (Chapter 3) provides valuable insight into how SH2B1 isoforms regulate hippocampal neurons. However, neurons differ across brain regions. It would be worthwhile to assess the universality of our findings among neurons from other brain regions. Given our strong interest in understanding how SH2B1 regulates feeding behavior and energy balance, I would ideally next investigate how SH2B1 regulates the morphology and function of hypothalamic neurons. Unfortunately, primary hypothalamic neurons are difficult to culture and typically yield variable results. Furthermore, the cells that I would be most interested in analyzing (e.g., LepRb- and TrkB-expressing neurons within the leptin-melanocortin pathway) make up only a small portion of all hypothalamic cells. For reference, there are only ~3000 POMC neurons in the mouse arcuate nucleus [30], and only some of these (50-80%) express LepR [31]. This small number of relevant neurons would preclude meaningful biochemical assays. Nevertheless, if I observed that the effects of SH2B1 isoforms on cultured neurons were similar across neurons dissected from multiple brain regions, I might predict that SH2B1 will affect most neuronal populations, including the most relevant cells in the hypothalamus, in a similar way.

On a related note, preliminary results (Fig. 4.3) demonstrated that endogenous SH2B1 localizes in primary cerebellar granule neurons as predicted based on the

subcellular localization of GFP-tagged isoforms of SH2B1 in PC12 cells (Fig. 3.1) and primary hippocampal neurons (Fig. 3.5). Indeed, SH2B1 localizes to the plasma membrane, cytoplasm, and nucleoli in the soma and also localizes throughout neurites (Fig. 4.3). It is worth noting, however, that the nucleolar and plasma membrane localizations of endogenous SH2B1 are extremely pronounced in cerebellar granule cells, more so than in hippocampal neurons (Fig. 4.10). These images suggest that SH2B1 isoform expression is relatively consistent between brain regions, yet some differences may exist regarding their relative abundance and/or subcellular localizations, which may translate into meaningful differences in their functionality. As an aside, it would also be extremely useful to develop antibodies specific to individual SH2B1 isoforms. In the context of the experiment described above, they would allow us to identify which endogenous SH2B1 isoforms are localizing to, and most highly expressed in, specific subcellular compartments in different neuron cultures. These antibodies would also be exceptionally useful for myriad other experiments.

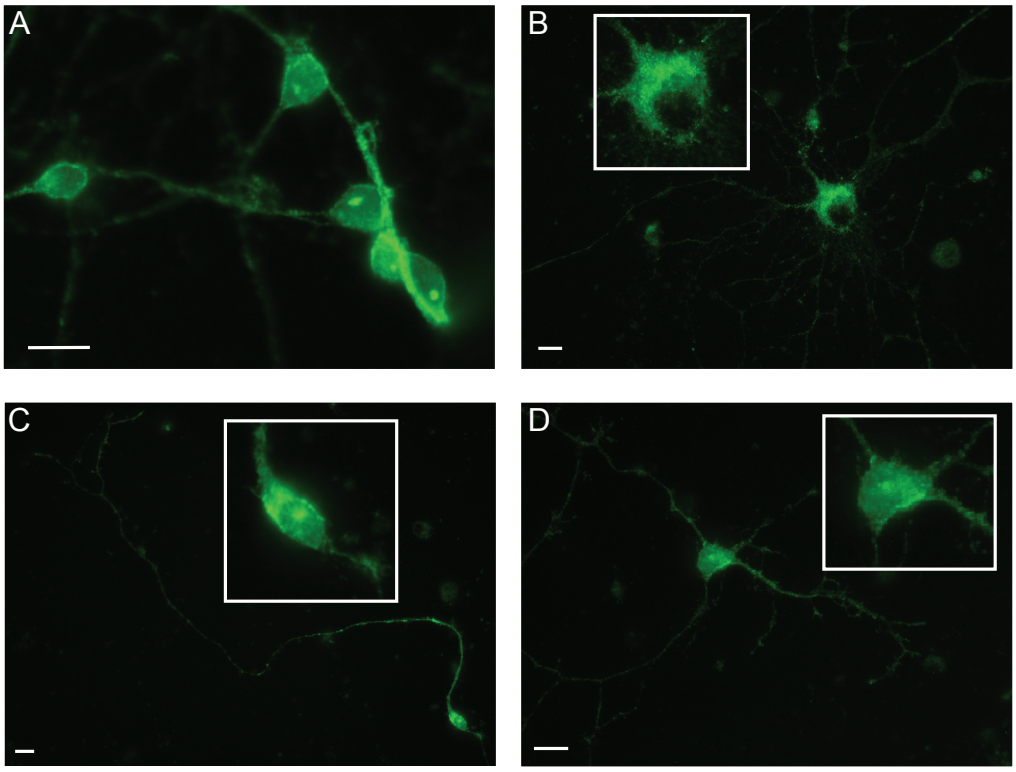

Figure 4.3. Endogenous SH2B1 localizes to the cytoplasm, plasma membrane, and nucleolus in cerebellar granule neurons

Representative images of cultured cerebellar granule neurons. Cells were fixed on DIV 7, stained with antibody to SH2B1, and imaged using confocal microscopy (Zeiss Axio Observer D1, University of Edinburgh). Scale bar = 10 μm. Bordered insets show enlarged somas.

How do SH2B1 isoforms affect specific neuronal populations?

In Chapter 3, we took a close look at the impact of SH2B1 isoforms on morphology and function of hippocampal neurons. We acknowledge that these cultures included a heterogenous population of neurons. Indeed, the hippocampus contains many types of neurons that can be classified in a variety of ways such as excitatory vs. inhibitory, pyramidal vs. non-pyramidal, originating in different regions of the hippocampus (e.g., CA1 vs. CA3 regions), and expressing particular proteins. Even among CA1 pyramidal neurons, previous studies have observed diverse firing patterns and dendritic arborizations [32,33]. We attempted to categorize our imaged neurons "by eye", identifying them as pyramidal or not. But due to their immaturity (~DIV 5), it was difficult to do so. Thus, it would be useful to investigate further whether our findings apply to all hippocampal neurons, or only a subset of them. I could do this by fixing WT vs. KO cultures and KO cultures expressing individual SH2B1 isoforms (WT and mutant/variant forms), performing immunocytochemistry for indicative protein markers such as glutamatergic neuron marker vesicular glutamate transporter 1 (vGluT1) or GABAergic neuron marker glutamic acid decarboxylase 65 (GAD65), and performing morphological analyses on different neuron types.

To assess the distribution of individual SH2B1 isoforms in specific subsets of neurons, we have begun analyzing single-cell RNA-seq datasets prepared from mouse brain. Until recently, this strategy was flawed because single-cell RNA-seq libraries are typically 3' biased, capturing only ~150 nucleotides starting from the 3' end, and SH2B1 isoforms share the most 3' exon (exon 10). However, in their recent publication, Joglekar and colleagues [34] prepared full-length cDNA libraries from multiple cell types in young

(P7) mouse hippocampus and prefrontal cortex. Their novel sample preparation has allowed us to measure the abundance of individual SH2B1 isoforms in specific neuron types. Our preliminary analysis is intriguing: SH2B1α and δ appear to be very highly expressed in both excitatory and inhibitory neurons in the hippocampus and cortex. Both isoforms have relatively similar levels of expression in inhibitory neurons, yet the δ isoform is consistently more highly expressed than the α isoform in excitatory neurons (Fig. 4.4). In contrast, SH2B1β and γ appear to be expressed at very low levels in both excitatory and inhibitory neurons in the hippocampus and cortex. All four isoforms appear to be expressed in dentate gyrus granule neuroblast clusters, although there is great variability in their expression levels between biological samples. If these results are accurate, they would immensely impact our understanding of SH2B1 activity in the central nervous system. We are currently running additional analyses on these datasets to gather more information.

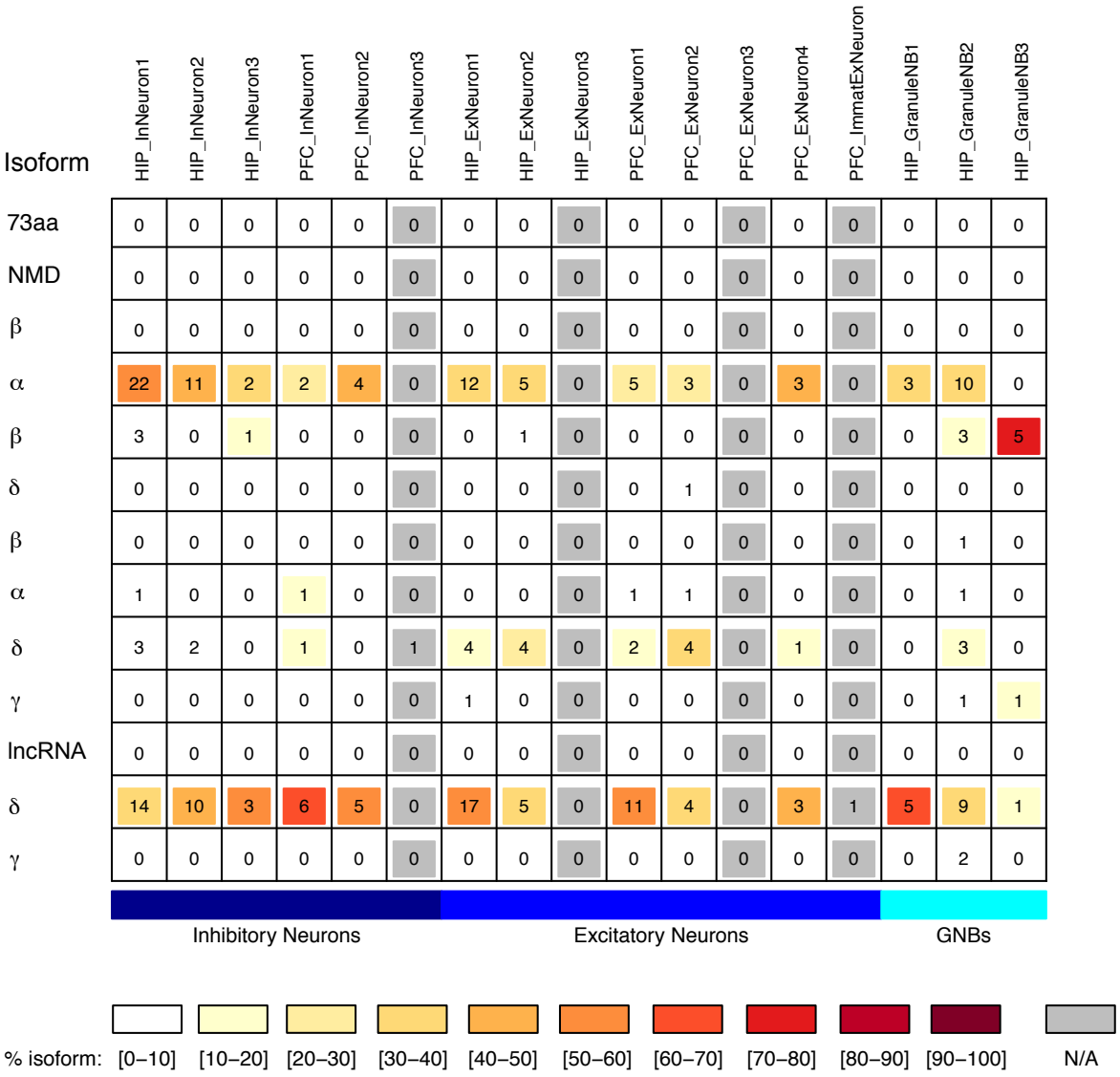

Figure 4.4. Cell-type specific expression of SH2B1 isoforms in neurons in P7 mouse hippocampus and prefrontal cortex

SH2B1 isoforms are indicated on the left. Each isoform appears more than once in the list because there are multiple mRNA transcripts that encode each isoform. Numbers in boxes represent the number of unique molecules identified. % isoform color gradient indicates the percentage of each isoform among a particular cell type such that each column adds up to 100%. Gray boxes (labeled “N/A”) indicate that there were very low reads across the entire cell type. 73aa, 73 amino acid variant; NMD, nonsense-mediated decay; lncRNA, long noncoding RNA; HIP, hippocampus; PFC, prefrontal cortex; InNeuron, inhibitory neuron; ExNeuron, excitatory neuron; Immat, immature; GranuleNB, dentate gyrus granule neuroblast clusters. See Joglekar et al., 2021 for experimental details.

Do SH2B1 isoforms regulate activity of non-neuronal brain cells?

Do SH2B1 isoforms directly regulate microglia function?

In Chapter 2, we discovered that deletion of SH2B1α/δ resulted in hypothalamic transcriptional changes associated with microglia function (Fig. 2.12). This finding is intriguing and raises multiple questions. For example, did deletion of SH2B1α/δ affect microglia function indirectly, perhaps via neuronal activity, or directly, through microglial activity? Thus, we wondered if SH2B1 isoforms are expressed in microglia. Preliminary analysis of a previously published RNA-seq dataset [35], whose samples were prepared from FACS-sorted cells, suggests that all SH2B1 isoforms are expressed in microglia in young (P7) mouse cortex (Fig. 4.5). Interestingly, SH2B1β/γ appeared to be more highly expressed in microglia than SH2B1α/δ, although statistical significance was not achieved, likely due to the small sample size. However, analysis of the previously mentioned single-cell RNA-seq experiment [34] indicated that no SH2B1 transcripts were identified in microglia in the prefrontal cortex, and only two molecules of one β-encoding variant were identified in microglia in the hippocampus (data not shown). Thus, additional experimental and/or bioinformatic work will be required to more precisely determine SH2B1 isoform expression in microglia throughout the central nervous system. For example, to directly test the contributions of SH2B1 to microglia function, I could delete SH2B1 isoforms (all or specifically α/δ) from microglia using the Cre-lox system mentioned previously.

Because most of the microglia-related genes within our significantly differentially regulated gene set in αδKO mice (Fig. 2.12B and Table 2.4) have been identified as contributors to complement-mediated synaptic pruning, we speculated that the deletion

of SH2B1α/δ disrupted appetite-regulating neuronal synapses, at least in part, by regulating the complement-mediated synaptic pruning carried out by microglia. To gain insight into this possibility, I could prepare sections of different brain regions from perfused WT, KO, and $\alpha\delta$KO mice and perform immunohistochemistry to detect expression of complement proteins, like C1q and C3, colocalizing with synaptic markers such as PSD-95. I could also assess synaptic stability/pruning by culturing primary neurons from WT, KO, and $\alpha\delta$KO mice and continuously monitoring multiple synapses over time with super-resolution electron microscopy.

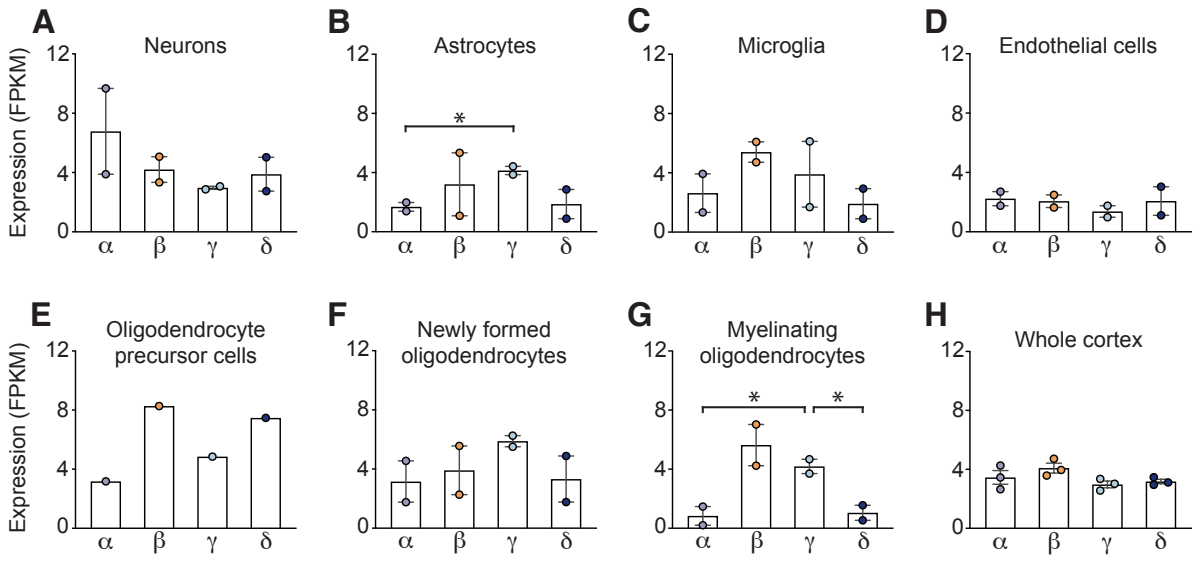

Figure 4.5. Cell-type specific expression of SH2B1 isoforms in P7 mouse cortex

(A-H) Cell type-specific expression, displayed as Fragment Per Kilobase Million (FPKM), of SH2B1 isoforms in the indicated cell types of mouse cortex. RNA-seq experimental protocols and source data are available in Zhang et al., 2014. Data are means ± SEM. **Statistics: A-H**, repeated measures one-way ANOVA followed by Tukey's multiple comparisons test. * $P < 0.05$.

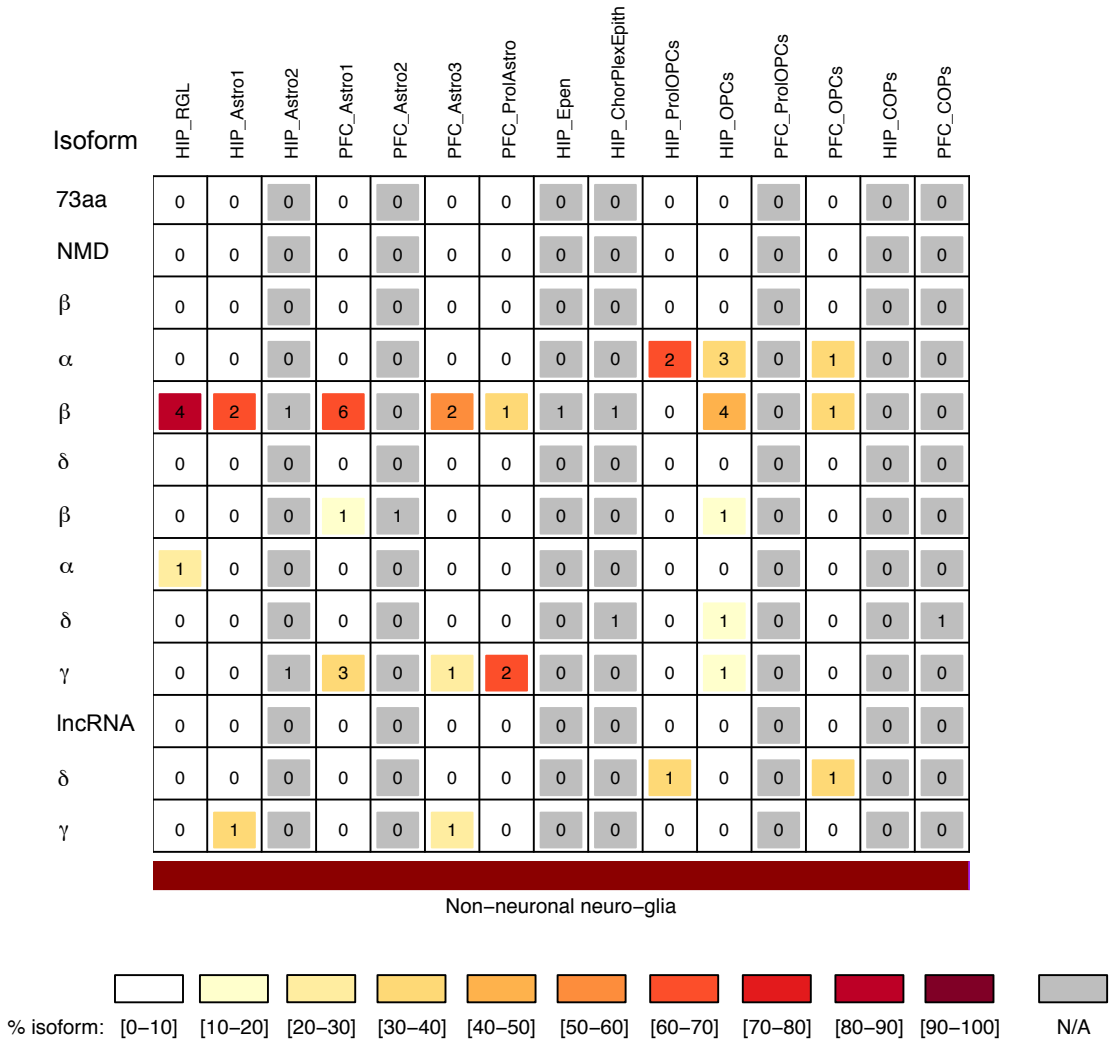

Figure 4.6. Cell-type specific expression of SH2B1 isoforms in glial cells in P7 mouse hippocampus and prefrontal cortex

SH2B1 isoforms are indicated on the left. Each isoform appears more than once in the list because there are multiple mRNA transcripts that encode each isoform. Numbers in boxes represent the number of unique molecules identified. % isoform color gradient indicates the distribution of each isoform among a particular cell type such that each column adds up to 100%. Gray boxes (labeled “N/A”) indicate that there were very low reads across the entire cell type. 73aa, 73 amino acid variant; NMD, nonsense-mediated decay; lncRNA, long noncoding RNA; HIP, hippocampus; PFC, prefrontal cortex; RGL, radial glia like cells; Astro, astrocyte; Epen, ependymal; ChorPlexEpith, choroid plexus epithelial cells; OPCs, oligodendrocyte precursor cells. See Joglekar et al., 2021 for experimental details.

Do SH2B1 isoforms directly regulate activity of other non-neuronal cell types?

In addition to microglia, the brain contains other non-neuronal cell types including astrocytes, oligodendrocytes, and endothelial cells. Because our preliminary analysis of previously published RNA-seq datasets (see above) suggested that SH2B1 isoforms are expressed in microglia, we wondered if SH2B1 isoforms may also be expressed in other non-neuronal cell types. Indeed, according to further analysis of the aforementioned RNA-seq dataset [35], SH2B1 isoforms appear to be expressed in astrocytes, oligodendrocytes, and epithelial cells (Fig. 4.5). Similar to the pattern observed in microglia, SH2B1β/γ appear to be more highly expressed than SH2B1α/δ in astrocytes and newly formed and myelinating oligodendrocytes, though only some of these differences achieved statistical significance, likely due to the small sample size. In concert with these findings, further analysis of the previously mentioned single-cell RNA-seq dataset [34] indicated that β and γ are the primary SH2B1 isoforms expressed in astrocytes in both hippocampus and prefrontal cortex (Fig. 4.6).

Moving forward, I could investigate the functional impact of SH2B1 isoforms in various brain cells by performing single-cell RNA-seq to compare gene expression of individual cells in WT vs. KO vs. $\alpha\delta$KO neuron cultures, and individual cells in KO cultures highly expressing individual SH2B1 isoforms (WT and mutant/variant forms) via lentivirus transduction. As mentioned above, I would need to create datasets with full-length cDNA libraries. In addition, I could delete SH2B1 isoforms (all or specifically α/δ) from specific cell types like astrocytes using the Cre-lox system mentioned previously.

Do primary cultured neurons from other SH2B1 mouse models exhibit altered morphology and function?

In Chapter 3, we focused our efforts on comparing the morphology and function of neurons from WT vs. KO mice. We also analyzed the morphology of KO neurons expressing individual SH2B1 isoforms. Because we observed robust differences within these comparisons, it would be worthwhile to investigate potential differences in morphology and function of neurons from other mouse models in which SH2B1 is manipulated in some way. For example, because αδKO mice exhibited a metabolic phenotype (Fig. 2.2) that was largely opposite that of mice lacking all SH2B1 isoforms [2], one might expect that neurons from αδKO mice would exhibit changes in their morphology and function that are largely opposite those observed in neurons from KO mice. Surprisingly, preliminary data suggested that the morphology of primary hippocampal neurons from αδKO mice is largely similar to that of neurons from WT mice (Fig. 4.7). However, few neurons were analyzed, only hippocampal neurons were assessed, and gene expression and other functional assays were not performed.

In the future, analysis of neurons from other mouse models like the SH2B1ΔPR mouse, which has a two amino acid deletion within its SH2B1 PH domain and exhibits obesity and insulin resistance and glucose intolerance [36], could provide other helpful clues regarding how SH2B1, and its specific domains, influences neurite outgrowth and complexity. These analyses may offer insight into whether SH2B1-dependent changes in morphology and function of primary cultured neurons is directly correlated with, and perhaps causative of, changes in the body's ability to regulate energy balance.

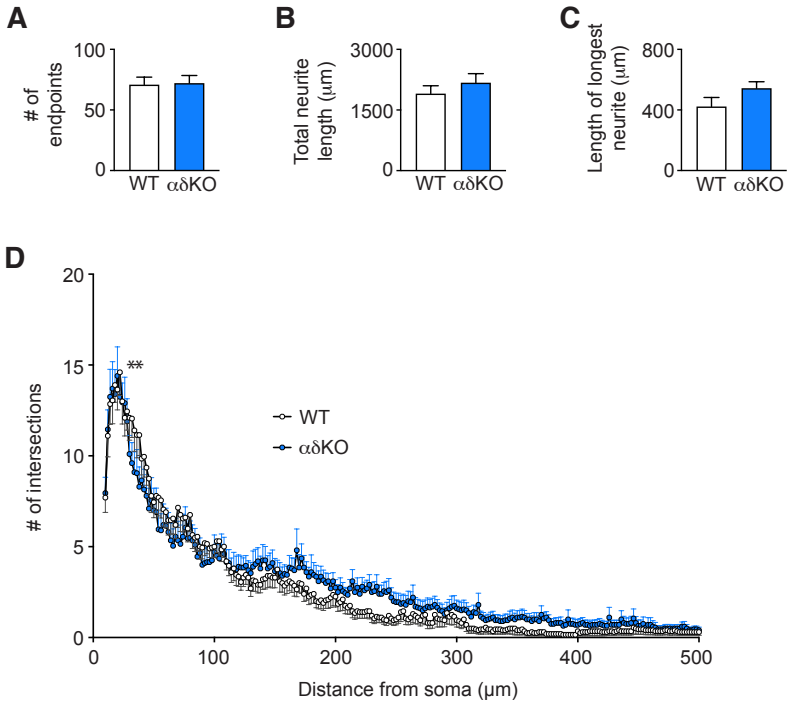

Figure 4.7. Morphology of primary hippocampal neurons from αδKO mice is largely similar to that of neurons from WT mice

(A-C) Indicated parameters were measured using Simple Neurite Tracer on images of WT or αδKO primary hippocampal neurons. Neurons were transfected with GFP to facilitate visualization on DIV 4 and imaged on DIV 5 using fluorescent microscopy. *N*, individual neurons from 1 experiment: WT = 20; αδKO = 20. **(D)** Sholl analysis was performed on neuron images used in **A-C**. Data are means ± SEM. **Statistics: A-C**, unpaired, two-tailed Student's t test; **D**, two-way repeated measures ANOVA followed by Sidak's multiple comparisons test. * P > 0.05.

Do physiological stressors and/or genetic mutations or variants regulate the SH2B1 isoform ratio?

Our findings in Chapter 2 suggested that the ratio of SH2B1 isoforms must be carefully titrated for the body to appropriate balance its energy. We considered that the body may alter the SH2B1 isoform ratio in response to physiological stressors such as starvation or overeating, yet preliminary findings suggested that the ratios of the various isoforms are not regulated under these conditions (Figs. 4.8 and 4.9). Nevertheless, it is possible that other physiological stressors and/or genetic mutations or variants could impact the SH2B1 isoform ratio and, as a consequence, energy balance. I could test this possibility by applying stressors such as chronic social stress to WT vs. $\alpha\delta$KO mice or examining mice expressing mutations or variants in SH2B1, and measuring isoform expression in brain homogenates by western blotting.

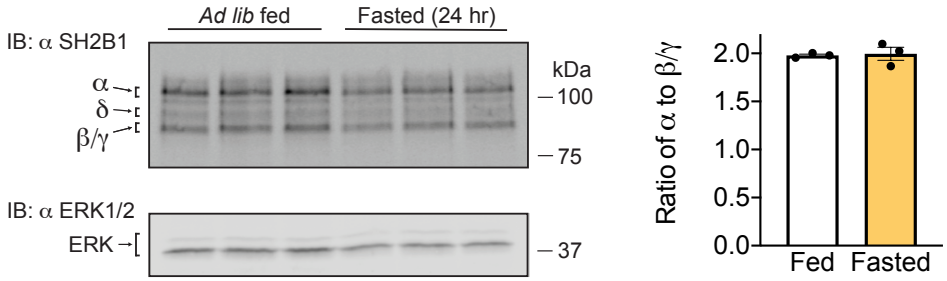

Figure 4.8. Ratio of SH2B1 isoforms is similar between fed and fasted mice

Proteins in whole brain lysates from 10-week-old C57BL6 male mice that were *ad lib* fed or fasted for 24 hours were immunoblotted with antibody to SH2B1 (α SH2B1) or to ERK1/2 (α ERK) (used as a loading control). The migration of molecular weight standards is shown on the right. The expected migration of the different SH2B1 isoforms is indicated on the left. Expression levels of SH2B1 isoforms were quantified using Li-Cor Image Studio Lite (version 5.2.5).

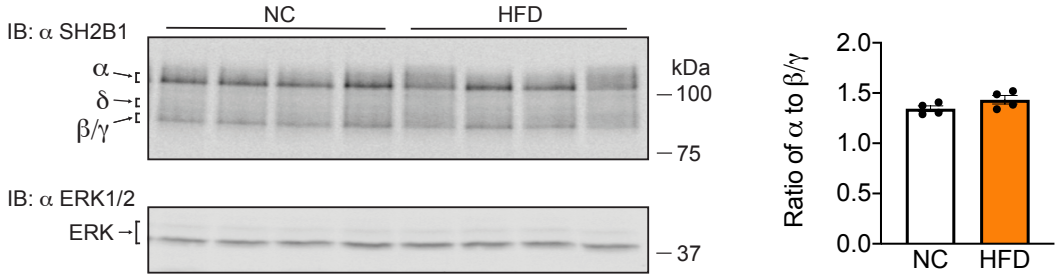

Figure 4.9. Ratio of SH2B1 isoforms is similar between mice fed a normal chow or a HFD

Proteins in whole brain lysates from C57BL6 adult male mice fed normal chow (NC) or a HFD were immunoblotted with antibody to SH2B1 (α SH2B1) or to ERK1/2 (α ERK) (used as a loading control). The migration of molecular weight standards is shown on the right. The expected migration of the different SH2B1 isoforms is indicated on the left. Expression levels of SH2B1 isoforms were quantified using Li-Cor Image Studio Lite (version 5.2.5).

Do external stimuli regulate the subcellular localization of SH2B1 isoforms?

In Chapter 3, we documented the subcellular localization of SH2B1 isoforms in primary hippocampal neurons (Fig. 3.5). Notably, we demonstrated that SH2B1δ exhibited a unique nucleolar localization. These neurons were imaged while in a steady state, not treated or stimulated by any agents. To expand upon these initial observations, it will be important to explore the possibility that different treatments or stimuli, such as those that trigger action potentials in neurons, may shift the subcellular localizations of SH2B1δ and/or other SH2B1 isoforms. Preliminary results suggested that BDNF treatment and/or depolarization with KCl does not result in any obvious changes in the subcellular localizations of SH2B1 isoforms in primary hippocampal neurons (Fig. 4.10). Nevertheless, to gain further insight into this possibility, I could perform live-cell confocal microscopy with neurons expressing GFP-tagged SH2B1 isoforms to monitor potential movement of the isoforms following the application of various agents such as NMDA or AMPA to activate their respective receptors. A potential stimulus-driven shift in SH2B1 subcellular localization would be interesting to document and explore, particularly when we consider, based on our findings regarding the δ isoform of SH2B1 in Chapter 3, how such a shift could impact SH2B1 regulation of neuronal structure and function.

If I did find a stimulus-driven shift in SH2B1 subcellular localization, this would be another instance in which isoform-specific antibodies, discussed above, would be particularly helpful. I could fix neurons at various time points under various conditions and perform immunocytochemistry with isoform-specific antibodies, which would allow us to understand which isoforms were changing localizations.

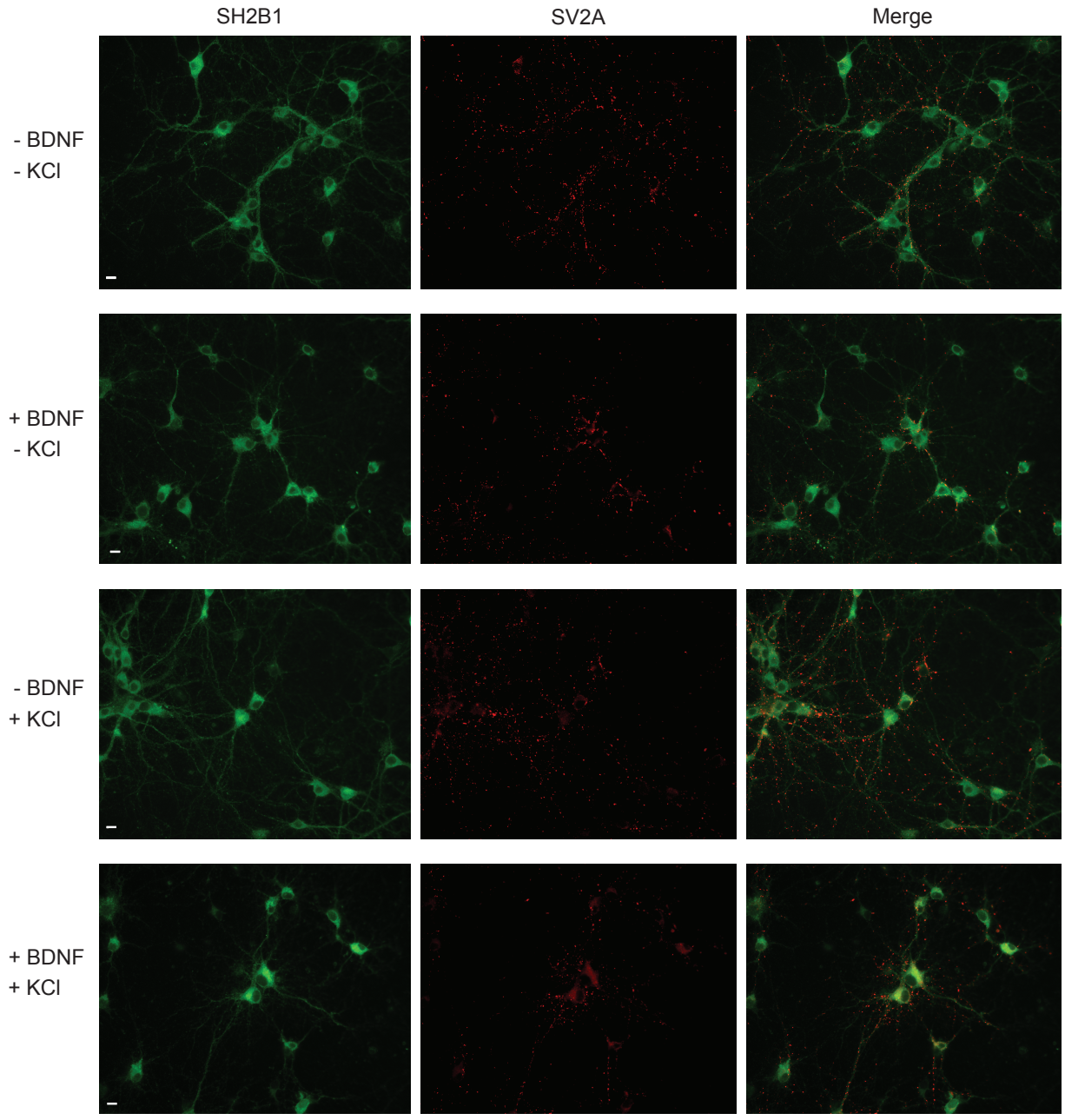

Figure 4.10. Subcellular localization of endogenous SH2B1 after BDNF treatment and/or depolarization

Representative images of cultured hippocampal neurons that were treated with or without BDNF and stimulated with or without KCl. Cells were fixed on DIV 14, stained with antibody to SH2B1 and synaptic vesicle glycoprotein 2A (SV2A), and imaged using confocal microscopy (Zeiss Axio Observer D1, University of Edinburgh). Scale bar = 10 μm.

Concluding Remarks

In Chapter 4, I elaborated on some of the most noteworthy findings presented in Chapters 2 and 3 by presenting preliminary results from newer experiments, discussing additional ongoing work, and suggesting strategies for future experiments. I hope that my results, interpretations, follow-up questions, and ideas for the future advance our understanding of the different isoforms of adapter protein SH2B1 and their differing abilities to regulate energy balance and neuronal morphology and function.

Acknowledgements

I thank Drs. Mike Cousin and Karen Smillie and members of the Cousin lab at the Centre for Discovery Brain Sciences at the University of Edinburgh for their interest in collaborating, and willingness to host and train me, during my visit in September 2018.

Collaborator Contributions

Alan C. Rupp performed the initial bioinformatic analysis of the RNA-seq data displayed in Fig. 4.5. Paul B. Vander performed imaging and analysis for Fig. 4.7.

References

1. Ren, D., Zhou, Y., Morris, D., Li, M., Li, Z. & Rui, L. Neuronal SH2B1 is essential for controlling energy and glucose homeostasis. *J. Clin. Invest.* **117**, 397-406 (2007).
2. Ren, D., Li, M., Duan, C. & Rui, L. Identification of SH2-B as a key regulator of leptin sensitivity, energy balance and body weight in mice. *Cell Metab.* **2**, 95-104 (2005).
3. Rios, M. BDNF and the central control of feeding: accidental bystander or essential player? *Trends Neurosci.* **36**, 83-90 (2013).
4. Shih, C.H., Chen, C.J. & Chen, L. New function of the adaptor protein SH2B1 in brain-derived neurotrophic factor-induced neurite outgrowth. *PloS one* **8**, e79619 (2013).
5. Unger, T.J., Calderon, G.A., Bradley, L.C., Sena-Esteves, M. & Rios, M. Selective deletion of *Bdnf* in the ventromedial and dorsomedial hypothalamus of adult mice results in hyperphagic behavior and obesity. *J. Neurosci.* **27**, 14265-14274 (2007).
6. An, J.J., Liao, G.Y., Kinney, C.E., Sahibzada, N. & Xu, B. Discrete BDNF Neurons in the Paraventricular Hypothalamus Control Feeding and Energy Expenditure. *Cell Metab* **22**, 175-188 (2015).
7. Yang, H., An, J.J., Sun, C. & Xu, B. Regulation of Energy Balance via BDNF Expressed in Nonparaventricular Hypothalamic Neurons. *Molecular endocrinology* **30**, 494-503 (2016).
8. An, J.J., Kinney, C.E., Tan, J.W., Liao, G.Y., Kremer, E.J. & Xu, B. TrkB-expressing paraventricular hypothalamic neurons suppress appetite through multiple neurocircuits. *Nature communications* **11**, 1729 (2020).
9. Gavalda, N., Gutierrez, H. & Davies, A.M. Developmental switch in NF-kappaB signalling required for neurite growth. *Development* **136**, 3405-3412 (2009).
10. Ji, Y., Lu, Y., Yang, F., Shen, W., Tang, T.T., Feng, L., . . . Lu, B. Acute and gradual increases in BDNF concentration elicit distinct signaling and functions in neurons. *Nat Neurosci* **13**, 302-309 (2010).
11. Boisvert, F.M., van Koningsbruggen, S., Navascues, J. & Lamond, A.I. The multifunctional nucleolus. *Nat. Rev. Mol. Cell. Biol.* **8**, 574-585 (2007).
12. Hetman, M. & Pietrzak, M. Emerging roles of the neuronal nucleolus. *Trends Neurosci.* **35**, 305-314 (2012).
13. Iarovaia, O.V., Minina, E.P., Sheval, E.V., Onichtchouk, D., Dokudovskaya, S., Razin, S.V. & Vassetzky, Y.S. Nucleolus: A Central Hub for Nuclear Functions. *Trends Cell Biol* **29**, 647-659 (2019).
14. Chen, C.J., Shih, C.H., Chang, Y.J., Hong, S.J., Li, T.N., Wang, L.H. & Chen, L. SH2B1 and IRSp53 proteins promote the formation of dendrites and dendritic branches. *J Biol Chem* **290**, 6010-6021 (2015).
15. Rider, L., Tao, J., Snyder, S., Brinley, B., Lu, J. & Diakonova, M. Adapter protein SH2B1β cross-links actin filaments and regulates actin cytoskeleton. *Mol. Endocrinol.* **23**, 1065-1076 (2009).
16. Diakonova, M., Gunter, D.R., Herrington, J. & Carter-Su, C. SH2-Bβ is a Rac-binding protein that regulates cell motility. *J. Biol. Chem.* **277**, 10669-10677 (2002).

17. Rider, L. & Diakonova, M. Adapter protein SH2B1β binds filamin A to regulate prolactin-dependent cytoskeletal reorganization and cell motility. *Mol. Endocrinol.* **25**, 1231-1243 (2011).
18. Herrington, J., Diakonova, M., Rui, L., Gunter, D.R. & Carter-Su, C. SH2-B is required for growth hormone-induced actin reorganization. *J. Biol. Chem.* **275**, 13126-13133 (2000).
19. Yoshihara, Y., De Roo, M. & Muller, D. Dendritic spine formation and stabilization. *Curr Opin Neurobiol* **19**, 146-153 (2009).
20. Hoffman, D.P., Shtengel, G., Xu, C.S., Campbell, K.R., Freeman, M., Wang, L., . . . Hess, H.F. Correlative three-dimensional super-resolution and block-face electron microscopy of whole vitreously frozen cells. *Science* **367**(2020).
21. Chen, L., Maures, T.J., Jin, H., Huo, J.S., Rabbani, S.A., Schwartz, J. & Carter-Su, C. SH2B1β (SH2-Bβ) enhances expression of a subset of nerve growth factor-regulated genes important for neuronal differentiation including genes encoding uPAR and MMP3/10. *Mol. Endocrinol.* **22**, 454-476 (2008).
22. Glasgow, S.D., McPhedrain, R., Madranges, J.F., Kennedy, T.E. & Ruthazer, E.S. Approaches and Limitations in the Investigation of Synaptic Transmission and Plasticity. *Front Synaptic Neurosci* **11**, 20 (2019).
23. Herrington, J., Rui, L. & Carter-Su, C. SH2-Bβ is required for growth hormone-induced regulation of the actin cytoskeleton. *Program and Abstracts, The Endocrine Society 81st Annual Meeting*, 387 (1999).
24. Emmerson, P.J., Wang, F., Du, Y., Liu, Q., Pickard, R.T., Gonciarz, M.D., . . . Wu, X. The metabolic effects of GDF15 are mediated by the orphan receptor GFRAL. *Nat Med* **23**, 1215-1219 (2017).
25. Penzes, P. & Jones, K.A. Dendritic spine dynamics--a key role for kalirin-7. *Trends in neurosciences* **31**, 419-427 (2008).
26. Ma, X.M., Kiraly, D.D., Gaier, E.D., Wang, Y., Kim, E.J., Levine, E.S., . . . Mains, R.E. Kalirin-7 is required for synaptic structure and function. *J Neurosci* **28**, 12368-12382 (2008).
27. Ma, X.M., Wang, Y., Ferraro, F., Mains, R.E. & Eipper, B.A. Kalirin-7 is an essential component of both shaft and spine excitatory synapses in hippocampal interneurons. *J Neurosci* **28**, 711-724 (2008).
28. Paskus, J.D., Herring, B.E. & Roche, K.W. Kalirin and Trio: RhoGEFs in Synaptic Transmission, Plasticity, and Complex Brain Disorders. *Trends in neurosciences* **43**, 505-518 (2020).
29. Herring, B.E. & Nicoll, R.A. Kalirin and Trio proteins serve critical roles in excitatory synaptic transmission and LTP. *Proc Natl Acad Sci U S A* **113**, 2264-2269 (2016).
30. Hentges, S.T., Nishiyama, M., Overstreet, L.S., Stenzel-Poore, M., Williams, J.T. & Low, M.J. GABA release from proopiomelanocortin neurons. *J. Neurosci.* **24**, 1578-1583 (2004).
31. Lam, D.D., Attard, C.A., Mercer, A.J., Myers, M.G., Jr., Rubinstein, M. & Low, M.J. Conditional expression of Pomc in the Lepr-positive subpopulation of POMC neurons is sufficient for normal energy homeostasis and metabolism. *Endocrinology* **156**, 1292-1302 (2015).
32. Spruston, N. Pyramidal neurons: dendritic structure and synaptic integration. *Nat Rev Neurosci* **9**, 206-221 (2008).

33. Mizuseki, K., Diba, K., Pastalkova, E. & Buzsaki, G. Hippocampal CA1 pyramidal cells form functionally distinct sublayers. *Nat Neurosci* **14**, 1174-1181 (2011).
34. Joglekar, A., Prjibelski, A., Mahfouz, A., Collier, P., Lin, S., Schlusche, A.K., . . . Tilgner, H.U. A spatially resolved brain region- and cell type-specific isoform atlas of the postnatal mouse brain. *Nature communications* **12**, 463 (2021).
35. Zhang, Y., Chen, K., Sloan, S.A., Bennett, M.L., Scholze, A.R., O'Keeffe, S., . . . Wu, J.Q. An RNA-sequencing transcriptome and splicing database of glia, neurons, and vascular cells of the cerebral cortex. *J Neurosci* **34**, 11929-11947 (2014).
36. Flores, A., Argetsinger, L.S., Stadler, L.K.J., Malaga, A.E., Vander, P.B., DeSantis, L.C., . . . Carter-Su, C. Crucial Role of the SH2B1 PH Domain for the Control of Energy Balance. *Diabetes* **68**, 2049-2062 (2019).